Studies on Hydrocarbon Fueled Dual Combustion Ramjet for High Speed Applications

A Thesis submitted in the partial fulfillment of the requirements for the award of the degree of

DOCTOR OF PHILOSOPHY

By

M. RAGHAVENDRA RAO

(ROLL NO: 701618)

Under the Supervision of

Dr. G. Amba Prasad Rao
Professor
National Institute of Technology

Dr. B.V.N Charyulu
Scientist 'G'
Defence Research and Development Laboratory

DEPARTMENT OF MECHANICAL ENGINEERING
NATIONAL INSTITUTE OF TECHNOLOGY
WARANGAL (T.S) INDIA 506 004

April 2022

Dedicated

to

my organization

and

my beloved family members

NATIONAL INSTITUTE OF TECHNOLOGY
WARANGAL (T.S) INDIA 506 004

DECLARATION

This is to certify that the work presented in the thesis entitled **"Studies on Hydrocarbon Fueled Dual Combustion Ramjet for High Speed Applications"** is a bonafide work done by me under the supervision of Prof. G. Amba Prasad Rao and Dr. B.V.N. Charyulu was not submitted elsewhere for the award of any degree.

I declare that this written submission represents my idea in my own words and where other's ideas or words have not been included. I have adequately cited and referenced the original sources. I also declare that I have adhered to all principles of academic honesty and integrity and have not misinterpreted or fabricated or falsified any idea/data/fact/source in my submission. I understand that any violation of the above will be a cause for disciplinary action by the Institute and can also evoke penal action from the sources which have thus not been properly cited or from whom proper permission has not taken when needed.

Date April'2022

Place: Warangal

(M. Raghavendra Rao)
Research Scholar
Roll No.701618

NATIONAL INSTITUTE OF TECHNOLOGY
WARANGAL (T.S) INDIA 506 004

CERTIFICATE

This is to certify that the thesis entitled **"Studies on Hydrocarbon Fueled Dual Combustion Ramjet for High Speed Applications"** that is being submitted by **Mr. M. Raghavendra Rao** in partial fulfillment for the award of Doctor of Philosophy (**Ph.D)** in the Department of Mechanical Engineering, National Institute of Technology, Warangal, is a record of bonafide work carried out by him under our guidance and supervision. The results of embodied in this thesis have not been submitted to any other Universities or Institutes for the award of any degree or diploma.

Dr. B.V.N. Charyulu
Scientist 'G'
Defence Research and Development Laboratory
Hyderabad

Dr. G. Amba Prasad Rao
Professor
Department of Mechanical Engineering
NIT- Warangal.

NOMENCLATURE

A	*Area*
A_{cell}	*Cell area*
A/F	*Air/Fuel ratio*
*C**	*Characteristic velocity*
C_p	*Specific heat capacity of air*
D	*Duct diameter*
D_k	*Mass diffusion coefficient for species k*
e	$Total\ energy\ per\ unit\ mass$
e_{i1}	*Error indicator*
E_r	*Activation energy for the reaction*
f	*Grid convergence parameter*
f_{st}	*Stoichiometric fuel to air ratio*
G_K	*Turbulent kinetic energy due to mean velocity gradient*
G_b	*Turbulent kinetic energy due to buoyancy*
h	$Enthalpy$
h_f	*Fuel enthalpy*
Isp	*Specific Impulse*
k_{ij}	*Reacting species*
k	*Specific heat ratio*
	Turbulent kinetic energy
m	*Mass*
$\dot{m}$	*Mass flow rate*
$\dot{m}_{air}$	*Mass flow rate of air*
$\dot{m}_f$	*Mass flow rate of fuel*
$(m_{CO_2})_x$	*CO_2 concentration in the combustor*
M	*Mach Number*
M_∞	*free stream Mach number*
M_2, M_{SI}	*Isolator inlet Mach number*
O/F	*Oxidizer/fuel ratio*
P	*Pressure*
Pc	*Chamber pressure*
Ps	*Static Pressure*
Po, Pt	*Total Pressure*
P_S/P_2	*Pressure Ratio*
phi, ϕ	$Equivalence\ ratio$
q_0	*Dynamic Pressure*

r	*Gradient volume weight*
R	*Gas constant*
$R_{e\theta}$	*Reynolds number*
R_k	*Net rate of production of chemical species k*
S	*Source term*
T	*Temperature*
Ts	*Static temperature*
To, Tt	*Total Temperature*
$\bar{u}_i$	*Mean velocity*
u'_i	*Fluctuating part of the velocity*
u	*Velocity*
u_τ	*Friction Velocity*
x	*Coordinate*
Y	*Species mass fraction*
Y_M	*Dilatation Dissipation Term*
y^+	*non-dimensional wall distance*
ε	*Rate of dissipation of kinetic energy*
ω	*Specific rate of dissipation*
ρ	*Density*
τ	*Stress*
τ_{ij}	*Reynolds stress term*
μ_t	*Turbulent viscosity*
δ_{ij}	*Knorker delta*
λ	*Thermal Conductivity*
θ	*Boundary layer momentum thickness*
η_{comb}	*Combustion efficiency*
$\eta_{KE_{AD}}$	*Adiabatic kinetic energy efficiency*
∇f	*Euclidean norm of the gradient of the desired field variable*

Subscript

0, ∞	*Free stream condition*
C	*Max. Capture station*
1	*Intake entry station*
3	*Isolator entry station/Intake exit location/Oblique shock train end location of GG*
4	*Isolator exit station/GG post normal shock location*
5	*After Burner station*
E	*Engine exit station*
SI	*Scram Inlet*
t	*Turbulent*
k	*Species*
gg	*Gas Generator*

ABSTRACT

Hypersonic air-breathing propulsion technology allows vehicles to fly at higher speeds exceeding Mach number 5 using Scramjet engine as its power plant. Worldwide, many countries have attempted Scramjet technology using hydrogen as fuel at fixed cruising altitude and few of them achieved partial/full success. The issues reported were mainly achieving ignition, sustained combustion in supersonic flow environment in the main combustor. For military applications, liquid hydrocarbon fuels are preferred due to handling/storage limitations of gaseous fuels. Ignition further becomes complex with liquid fuels as the injection, atomization processes involved require more residence time. The present work focuses on this aspect by considering an alternate propulsion system, Dual Combustion Ramjet (DCR). It is the innovative concept which mitigates the ignition issues of the Scramjet by embedding a fuel rich subsonic combustor in the propulsion system. This idea led to the development of propulsion system that can operate in a wider Mach number (M4 to M6) regime during the flight trajectory unlike conventional cruising hypersonic vehicles. However, it is posing challenges in terms of its sub-systems interdependency for varying flight Mach number conditions during its operation.

Many researchers have tried to study the thermodynamic cycle analysis of such systems, flow filed of the combustor and intake system, and its characterization for different operating conditions by experimental/numerical methods. Studies also revealed that DCR system is highly coupled with its configuration, fuels used, trajectory design, intake-combustor interactions especially in off design conditions and high heat flux environment in the combustor.

The present work is an effort to understand and analyze the hydrocarbon fueled DCR propulsion technology and its critical sub systems mainly by experimental methods. Numerical simulations carried out helped in finalizing the designs for the experiments. The study is initiated with a feasible full-scale propulsion system specification in view. DCR propulsion system design requirements, design goals and design constraints of each sub-system are defined based on the preliminary studies. Major elements such as gas generator, supersonic combustor, isolator and nozzle are studied for its performance, combustor flow field numerically and experimentally.

Extensive experimental work has been carried out to develop a fuel rich gas generator suitable for operation in the range of 4-6 flight Mach number. Connect pipe mode tests were carried for Mach 4 conditions with Jet-A fuel at different equivalence ratio and with suitable fuel injection in different combinations and stages to establish consistent ignition and sustained combustion. A One-dimensional mathematical model with NASA CEA interface has been

developed to predict and compare the test performance. Sustained ignition is achieved for fuel flow rates ranging from 0.4 kg/s to 0.8 kg/s and at an equivalence ratio of 0.8-0.9.

Computational/Numerical procedure is evolved for combustor-isolator interaction and the model is validated with experimental data from literature for isolator inlet Mach number. 1.79 and 2.23. Favre Averaged equations are solved using Commercial code–ANSYS FLUENT. Reactive flow is modelled using 7 species and 4 step chemistry. Numerical simulations have been carried out with various turbulence models namely k-ε (Standard), (RNG) k-ε, kω-Standard, kω-SST and combustor wall pressures were compared with experimental results. Error in estimation of starting location of Shock train, maximum pressure, average pressure in combustor is compared. RNG k-ε predicted shock train location with an error difference of 5% compared to k-ε (Standard). Further, effect on shock train position in isolator with change in gas generator equivalence ratio is also studied for free stream Mach numbers 4 and 5.

Numerical simulation of different combustor geometries (5 cases) was carried out by the validated methodology to arrive at the geometry. Variations include isolator angle, area ratios and divergence angle of the combustor. A parametric study was also conducted with the 14° isolator angle geometry. Influence of equivalence ratio was studied for flight Mach numbers of 4 and 6.

Connect pipe mode test facility is re-designed to meet the full scale DCR testing requirements. Facility components such as test bed nozzles, truncated intakes, isolator, injection mechanism are realized and integrated. Full scale DCR engine with truncated intake is tested in connect pipe mode at freestream Mach number. M6 conditions by simulating combustor entry conditions with the help of hydrogen vitiated heater. Non- Reactive and reactive flow conditions are simulated experimentally. Extensive instrumentation was done to capture the wall pressures along the combustor length, gas generator pressure rise and flow rates. It is concluded from experimental studies of DCR that Jet-A fuel ignition was achieved successfully at an equivalence ratio of 0.9 (global). Sustained combustion is achieved for a duration of 10 seconds. Fuel rich Gas generator has performed at an equivalence ratio of 3.6 with C* of 1041 m/sec. Pressure rise along the length of the combustor indicates the high speed combustion in the supersonic combustor.

Table of Contents

List of Figures

List of Tables

List of Abbreviations

A/F	Air/Fuel ratio
CEA	Chemical Equilibrium Applications
CFD	Computational Fluid Dynamics
CO	Carbon Monoxide
CO_2	Carbon Dioxide
C-SiC	Carbon Silicon Carbide
DCR	Dual Combustion Ramjet
DNS	Direct Numerical Simulations
DMRJ	Dual Mode RamJet
DMSJ	Dual Mode ScramJet
FC	Film Cooling
GG	Gas Generator
GCI	Grid Convergence Index
HCM	Hypersonic Cruise Missile
LDAM	Low Density Ablative Material
LES	Large Eddy Simulation
NASA	National Aeronautics and Space Administration
PCST	Pre-Combustion Shock Train
PT	Pressure Transducer
RANS	Reynold Average Navier Stokes
RNG	Re-Normalized Group
SC	Supersonic Combustor
SST	Shear Stress Transport
SERN	Single Expansion Ramp Nozzle
TKE	Turbulent Kinetic Energy
VAH	Vitiated Air Heater

Chapter 1

INTRODUCTION

Breaking the barrier of sound, the quest to fly faster and faster at speeds Mach number > 5 drives towards development of energetic and agile systems for numerous applications. Hypersonic vehicles have the potential for long range civil transportation, fast strike missile systems and space transportation. To propel such vehicles, hypersonic air-breathing propulsion is the most promising technology due to its high speeds and high specific impulse in comparison to chemical rocket systems. It allows efficient vehicle designs in terms of minimum lift off weight, precision strike capability, agility and survivability from interception. Innovative applications were visualized, conceptualized and some of them were tried by prominent researchers during the past few decades. Hypersonic propulsion has high potential in the respective areas, but the challenges are also equally interesting. Very high temperatures, understanding the aerothermal environment of the vehicles flying at 20-30km altitude in the stratosphere at M = 6-10 pose challenges to the structural vehicle designers. Energetic fuels, exotic materials/high temperature super alloys, huge and expensive test facilities, flying test beds, high speed computing techniques etc are the most essential resources needed to handle these kinds of system's design and development. Efforts are continuously on across the globe to address all the issues associated with this technology at academic institutes and space/defense industries.

Higher the speed of the vehicle in the atmosphere, higher will be the drag and the thrust needed to overcome this drag becomes critically important to ensure the flight in cruise/accelerating mode. In addition, higher speed of the vehicle results in shorter residence times of airflow and fuel in the engine, which is the crux of the combustion in these engines. Achieving ignition and flame holding becomes extremely difficult and generally achieved by shock-induced mechanisms or recirculation forms achieved through flow sheltering mechanisms. Design of suitable injection schemes and cavities play very critical role in scramjet combustor development.

A typical scramjet propulsion system comprises of the entire flow path, i.e., [fore body, Engine, Single Expansion Ramp Nozzle (SERN)], Fuel feed system and an engine-airframe attachment. The vehicle comprises of Cruise vehicle airframe, Scramjet Engine and engine airframe attachment. The fore body is the external compression intake of the vehicle which decelerates and compresses the incoming air with the help of oblique shocks. The scramjet engine comprises of an internal compression intake, isolator and Scramjet combustor. The internal compression intake further compresses and decelerates the ingested air to make combustion in the scramjet combustor conducive.

Fuel is injected through injection struts/wall injectors into the combustor for fuel distribution and flame holding mechanisms are employed. A fuel feed system is used to supply regulated fuel flow to the injection system. Combustion creates pressure rise in the combustor which results in thrust. This pressure rise and therefore thrust can be increased or decreased by changing the amount of fuel injected into the combustor (fuel ϕ). But higher-pressure rise can be detrimental to engine operation as it results in a pre-combustion shock train (PCST) which travels upstream and un-starts the intake. Intake un-start will result in sudden thrust loss and increased drag which could destabilize the vehicle. To minimize this intake-combustor interaction, an isolator is provided. The isolator is a small constant area duct in between the intake and combustor. This minimizes the severity of high pressure rise in combustor by providing extra length for the shock train. SERN produces additional thrust by accelerating the combustion products from the combustor.

1.1 Principle of operation of typical Scramjet engine

A scramjet propulsion system [1] is a hypersonic air-breathing engine in which heat addition (due to combustion of fuel and air) occurs in the flow that is supersonic relative to the engine. In a conventional ramjet engine, the incoming supersonic airflow is decelerated to subsonic speeds by means of a multi-shock intake system and diffusion process. Fuel is added to the subsonic airflow, the mixture combusts and then re-accelerates through a mechanical choke to supersonic speeds.

By contrast, the airflow in a pure scramjet remains supersonic throughout the combustion process and does not require a choking mechanism. The performance of an air-breathing engine, as measured by specific impulse (I_{sp}), is considerably higher than that of a rocket, and by the use of a scramjet, this advantage extends into the higher Mach number regime, as shown in Figure 1-1.

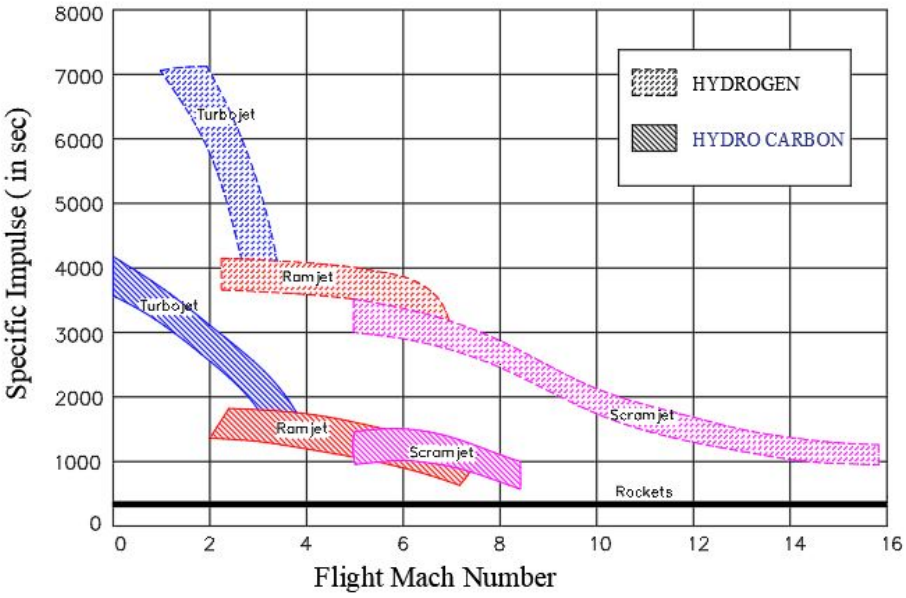

Figure 1-1 Variation of Specific Impulse (Isp) with flight Mach number [2]

Selection of engines for highspeed vehicles is dependent on the intended mission and the speed range of interest. Figure 1-2 shows a summary of various options as a function of Mach number.

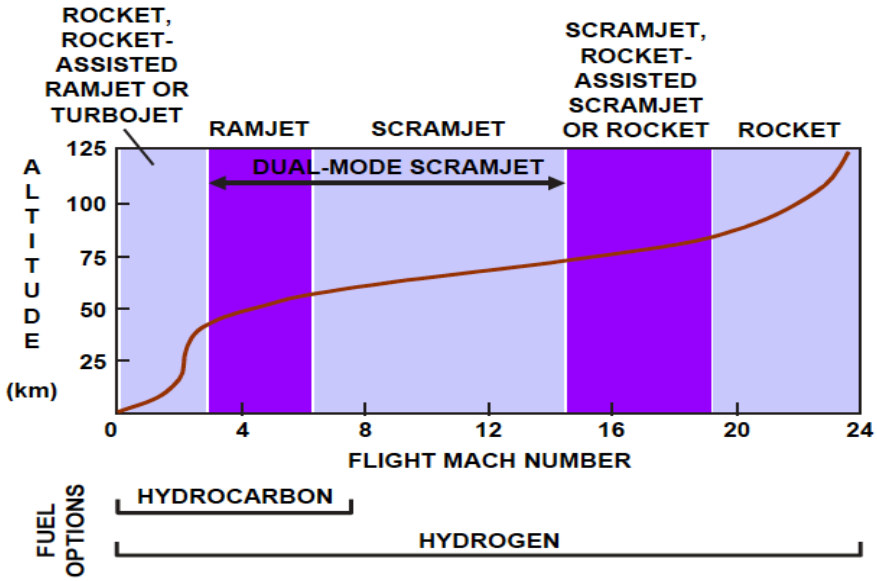

Figure 1-2 Engine options as a function of Mach number [2]

Hence, for hydrocarbon powered air breathing propelled flights, the upper limit for Mach number is around 7.0 – 7.5. Also, the best suited propulsion system would be dual-mode ramjet / scramjet. Pure scramjet powered missions may be feasible at higher Mach numbers and with fuels like Hydrogen.

Scramjet propulsion system consists of five major engine components namely Internal inlet, Isolator, Combustor, Internal nozzle, Fuel feed system. Scramjet Propulsion System also includes two vehicle components – namely,

a) The vehicle fore-body is an essential part of the air induction system and
b) The vehicle aft body is a critical part of the nozzle component.

These are described schematically in Figure 1-3

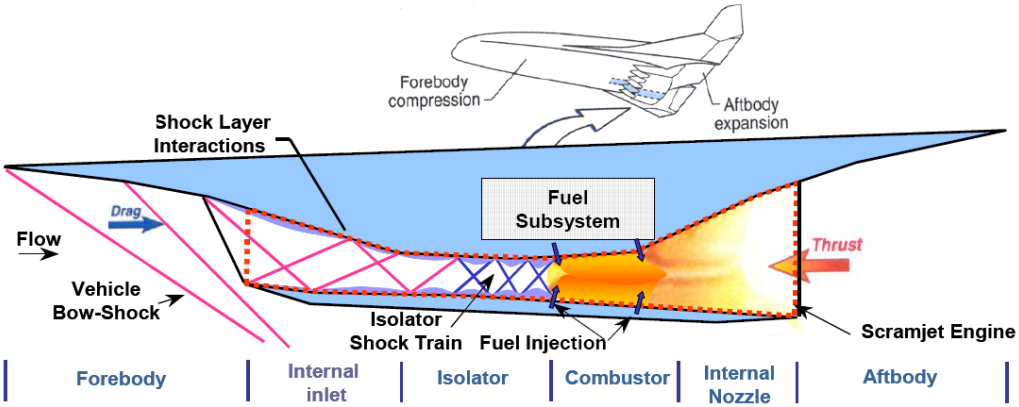

Figure 1-3 Representative Scramjet engine [1]

The primary purpose of the high-speed air induction system, comprised of the vehicle fore-body and internal inlet, is to capture and compress air for processing by the remaining components of the engine. The fore-body provides the initial external compression and contributes to the drag and moments of the vehicle. The internal inlet compression provides the final compression of the propulsion cycle. The fore-body along with the internal inlet is designed to provide the required mass capture and aerodynamic contraction ratio at maximum inlet efficiency. The air in the captured stream tube undergoes a reduction in Mach number with an attendant increase in pressure and temperature as it passes through the system of shock waves in the fore-body and internal inlet. It typically contains non-uniformities, due to oblique reflecting shock waves, which can influence the combustion process.

The isolator allows supersonic flow to adjust to a static backpressure higher than its inlet static pressure. The isolator cross-sectional area may be constant or slightly divergent to accommodate boundary layer separation. When the combustion process begins to separate the boundary layer, a Pre-Combustion Shock Train (PCST) forms (Figure 1-4). The shock structure or shock train allows the required pressure rise to occur over a finite distance, isolating the combustion process from the inlet compression process, thus acting to prevent inlet surge or un-start. The required length to capture the pressure rise is defined as the isolator length. The isolator in a dual mode (mixed flow supersonic and subsonic) ramjet and scramjet is a critical component that enables the combustor to achieve the required heat release profile and capture the induced combustor pressure rise without inlet unstart and ultimately facilitate the engine to complete transition to scramjet operation.

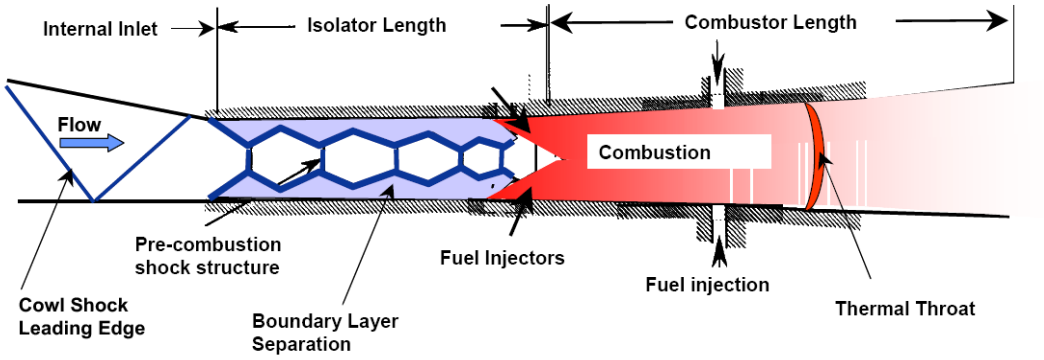

Figure 1-4 Isolator and combustor physics [1]

The combustor accepts the inlet/isolator airflow with variations in geometry inflow profiles and provides efficient fuel air mixing within the available combustor length as shown in Figure 1-4. The fuel feed system is required to deliver fuel to the flow path at appropriate locations with the desired physical properties. The combustor fuel is scheduled to stay within the engine operability limits while optimizing engine thrust potential.

The expansion system, consisting of the internal nozzle and vehicle aft-body, completes the propulsion flow path and controls the expansion of the high pressure and temperature gas mixture to produce net thrust. During the expansion process, the potential energy generated by the combustor is converted into kinetic energy. The design of the nozzle has a major effect on the efficiency of the propulsion system and the vehicle due to its ability to influence vehicle pitching moment and lift.

1.2 Modes of combustor operation

As the flight Mach number increases from 3 to 12, the engine operation undergoes three stage transition to pure scramjet operation. These stages are:

a. Dual-mode ramjet
b. Dual-mode scramjet / early scramjet
c. Pure scramjet

These modes are depicted in

Figure 1-5

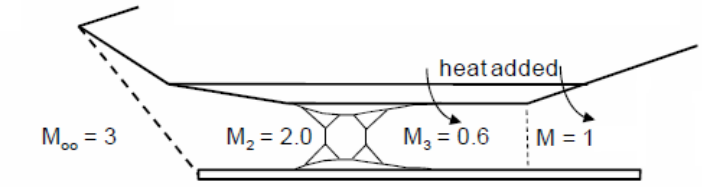

a) Dual-mode Ramjet: Strong PCST, no separation in combustor, thermally chocked

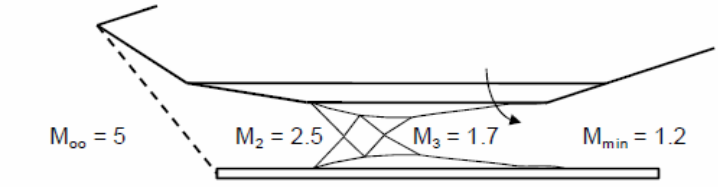

b) Dual-mode Scramjet: Weak PCST, separation in combustor, not chocked

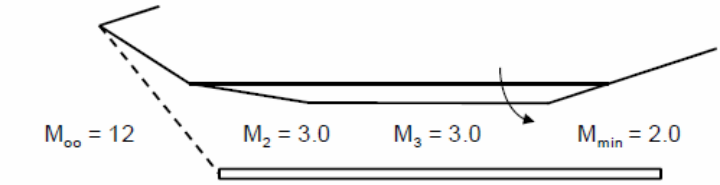

c) Pure Scramjet: No PCST, not chocked

Figure 1-5 Modes of combustor operation [4]

a) Dual-mode ramjet:

In this mode, isolator entrance Mach number is around 2.0 and strong PCST reduces the Mach number further to 0.6 leading to subsonic flow during heat addition. Due to heat addition, the flow gets thermally chocked and accelerates to supersonic flow in the divergent section. In this mode, the shock waves create an adverse pressure gradient in the isolator and cause the boundary layer to be separated. However, a favorable pressure gradient exists in the combustor since, in the flow direction – the Mach number increases and static pressure decreases. Therefore, the boundary layer will reattach at the end of isolator and remain attached in the combustor.

b) Dual-mode scramjet:

As the vehicle accelerates, the engine inlet Mach number and Total temperature increase, the flow Mach number remains supersonic in the entire engine flow path. The total temperature rise across the combustor begins to decrease along with the pressure rise produced by the combustion process. Consequently, a weaker pre-combustion system is required, and the pre-combustion shock is pulled back from the inlet throat towards the entrance to the combustor. Operation of a scramjet engine in this critical regime is generally referred to as dual-mode scramjet, implying mixed characteristics of both subsonic and supersonic flow or active transitioning between subsonic and supersonic combustion within the scramjet.

In the combustor, an adverse pressure gradient exists because in the x-direction the Mach number decreases, and the static pressure increases. Heiser and Pratt [3] explain that constant pressure combustion is expected to occur during the early scram mode because the separated boundary layer creates a new effective wall shape. As shown in the above figure, the separated boundary layer gets thinner in x-direction (increase in effective flow area), leading to reduction in static pressure. This decrease is offset by the increase in static pressure due to heat addition leading to the condition – 'constant pressure heat addition'. Thermal chocking condition no longer applies in the dual-mode scramjet.

c) Pure scramjet:

As the vehicle continues to accelerate beyond Mach number 7, the combustion process is unable to separate the flow and the engine operates in scramjet mode with a pre-combustion shock-free isolator. The inlet shocks propagate through the entire engine. The scramjet operational line and isolator physical phenomena during mode transition are illustrated in Figure 1-6.

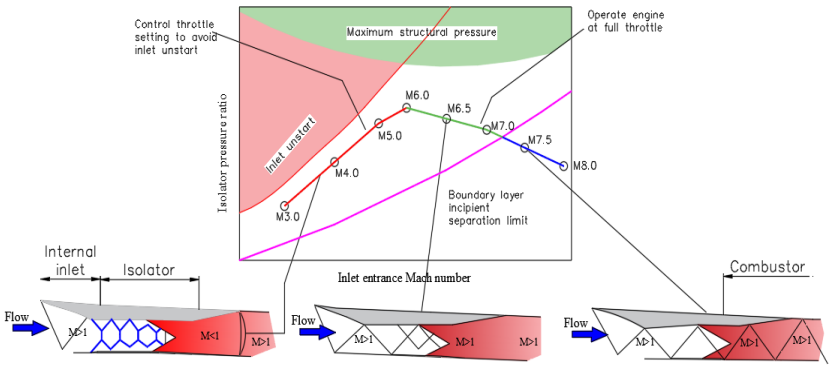

Figure 1-6 Different modes in Scramjet combustion [1]

Typical flight corridor for air breathing propulsion system

A typical Mach number–altitude air-breathing flight corridor is shown in Figure 1-7. The upper boundary is characterized as a region of low combustion efficiency and narrow fuel/air ratio ranges thereby establishing a combustion limit. The lower boundary is a region of high skin temperature and pressure loading thereby establishing design and material limits." The higher flight altitude for the same flight Mach number and 'angle of attack' may result in lower 'mass ingestion' and lower 'combustor static pressure'. Reduction in static pressure increases the fuel ignition delay and thereby reducing the combustion efficiency and engine performance. Hence, at a given flight Mach number, greater the flight altitude from the nominal, more issues related to ignition, flame holding and combustion efficiency are expected.

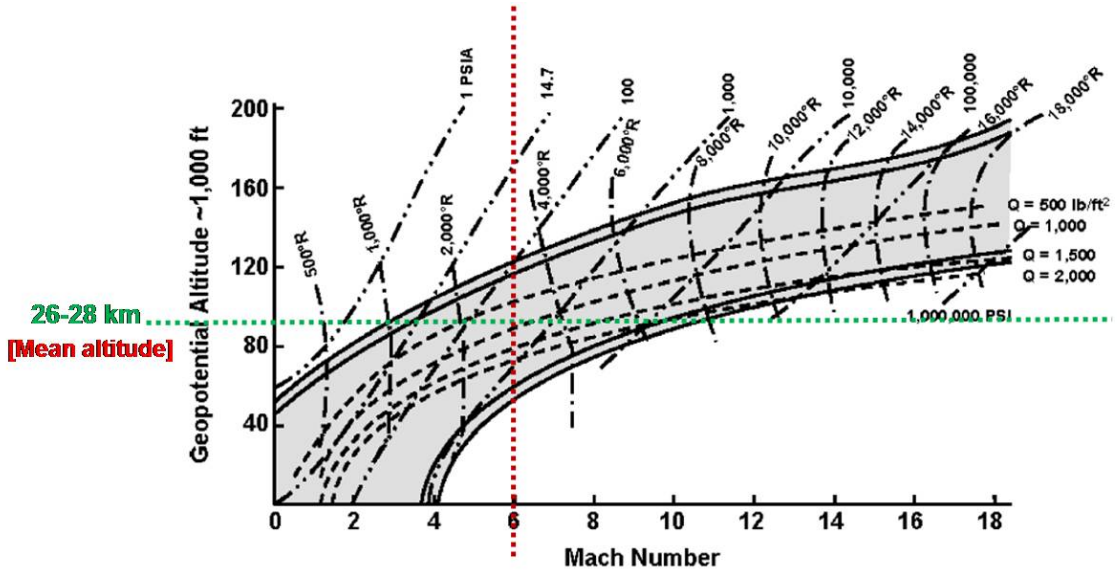

Figure 1-7 Typical air-breathing flight corridor [5]

1.3 Need of liquid hydrocarbon fuels for high-speed air breathing propulsion systems

Scramjet engine's high performance [6] is dictated by the fuel selection, its ignition and flame stabilization. With a residence time of 1 to 3 milliseconds, the fuel injected with the aid of instream fuel injectors or wall injectors and air mixture has to burn in a fixed length of combustor efficiently. Instream injectors like struts distribute the fuel but induces drag whereas aerodynamically shaped wall injectors are free from such problems. For single point operation missions i.e vehicles operating/cruising at the specified altitude and at specific Mach Number;

ignition of the scramjet engine is one of the mission critical events. Any lapse in ignition can lead to total mission failure and there will be no time or another chance for relighting the engine. Hydrogen is commonly used fuel for scramjet applications but when a storable weapon system is to be designed, many logistic points are to be considered. Storing/handling of hydrogen in gas mode or in cryogenic mode is a complex activity.

The highspeed tactical weapon systems are designed for

- Powered range to reach the target within few minutes
- High Ground impact Mach number (of the order of 1.2 km/s)
- Survivability against surface-to-air Attack and Compatibility with air-launched platforms
- High performance air breathing propulsion system with logistically suitable liquid hydrocarbon fuels
- Capacity for at least 10 years of storage

Systems designed for such military applications or volume limited weapon systems have to be configured with high density liquid hydrocarbon fuels such as Jet-A, RJ-4, RJ-5, JP-7, JP-8, JP-10 or specially designed endothermic fuels. Ignition delay of these liquid hydrocarbon fuels is 1-2 order higher compared to hydrogen fuel and poses extreme challenges in ignition/autoignition to the combustor designers. Long burn duration engines used for few minutes of cruising during the mission require adequate cooling of the combustor walls actively by fuels. Hydrocarbon fuels offer mainly the advantages of:

- Higher density (better packaging efficiency/minimum volume)
- storability and stability for long periods (needed for military weapon systems)
- better cooling properties for long duration operation of the engine
- fuel heat sink capacity / endothermicity (ability to absorb heat and crack into products, which can further participate in combustion)

The major disadvantages are:

- higher ignition delays (time taken for the liquid hydrocarbon to first vaporize, then penetrate into the airstream and finally mix with the air to form the combustion fuel and less energy compared to hydrogen gas

- Physical and chemical properties of the hydrocarbon fuels are evaluated before they are chosen for the intended application. Main Properties include density, volatility, vapor pressure, viscosity, freezing point and other miscellaneous properties to be ensured are heat of combustion, thermal stability, corrosivity, particulates, gum content, electrical conductivity etc.

1.4 Scramjet based weapon concepts

Hypersonic air breathing missile systems are designed using scramjet engine as the power source, but they are to be boosted to the specified altitude with the aid of solid rocket boosters, if launched from surface. The other version which is more flexible compared to ground launched version is is air launched hypersonic missile.

The two Candidate propulsion system concepts for weaponizing hypersonic tactical missiles are:

- A wave rider is a vehicle having a high lift-to-drag ratio with a 2-D rectangular engine and integrated to the belly of the flight vehicle, utilizing the underside compression for the inlet. The intake feeds the combustor air that allow burning of a hydrocarbon fuel in a supersonic combustor. The combustor is actively cooled using the liquid hydrocarbon fuel preferably an endothermic fuel. The aft portion of the vehicle acts as a nozzle called SERN. The cruise vehicle is usually boosted to the Mach number at which the air-breathing engine takes over from the rocket booster. The size of such rocket boosters is very large, and their operation requires prepared test sites, which are stationary. Such systems may be easily detected and targeted by the adversaries.
- The second missile concept is based on dual-combustor ramjet (DCR) technology with a suitable aircraft used as launch platform. The DCR powered Hypersonic cruise missile is boosted to its air-breathing take-over Mach number (~M4) with the help of a solid booster. At M4, the solid booster is separated, and air-breathing mode takes over. The vehicle then accelerates and climbs to the pre-designed cruising Mach number (~M6) and altitude (~28km), cruises for long duration and then dives towards the target with a high impact velocity. Hence, it is obvious that DCR based weapons have wider operating Mach number regime. Such weapons can be used in forward areas as precision strike force.

It is to be noted that DCR is different from dual mode scramjet (DMSJ), in which the combustor operates in ramjet mode for one phase of the trajectory and slow transition takes place from ram to scram to continue in scram mode in the cruise phase of the trajectory. The dual-mode Scramjet is capable of having both subsonic and supersonic combustion velocities inside its combustion chamber. Thermal throat at the combustor exit allows to accelerate subsonic flows to supersonic speeds before entering the diverging nozzle of the engine. A constant area isolator captures the pressure rise due to combustion in the form of oblique shock waves during scramjet mode; during ramjet mode a normal shock exists at the end of the isolator before the combustor. Perturbations in the combustion process change the location of this normal shock inside a constant area isolator and thus affects thermal choking and can lead to unstart of the inlet. Ignition of fuel is equally difficult in DMSJ as that of Scramjet. Whereas DCR has been proven versatile in this aspect as the air entering the gas generator is decelerated to subsonic speeds and made conducive for ignition by simple ignition devices.

1.5 Dual Combustion Ramjet (DCR) and its Significance

Dual combustion ramjet (DCR) was first proposed by Billig *et al.* [7] of John Hopkins university in1970. DCR is mainly composed of a subsonic gas generator and a supersonic combustor. Because it is difficult to ignite liquid kerosene in supersonic flow, the subsonic gas generator is used to preheat the liquid kerosene and to crack it into small-molecular species such as ethylene, carbon monoxide or hydrogen. The high-temperature fuel-rich gas from the gas generator is then mixed with the peripheral air entering from multiple supersonic intakes. In comparison with scramjet, DCR combines the best features of a ramjet and scramjet and has several merits:

- axisymmetric in configuration
- wider range of operating Mach number M3.0 -M6.0 or M4.0-M8.0
- easier ignition and more stable combustion (main problem of ignition and sustained combustion in conventional scramjet engine's supersonic flow regime is mitigated with the predigested fuel rich hot fuel)
- higher performance at low Mach number
- less severe thermal loads on the engine wall, more convenient cooling of the wall

A generic schematic of the DCR engine is shown in Figure 1-8

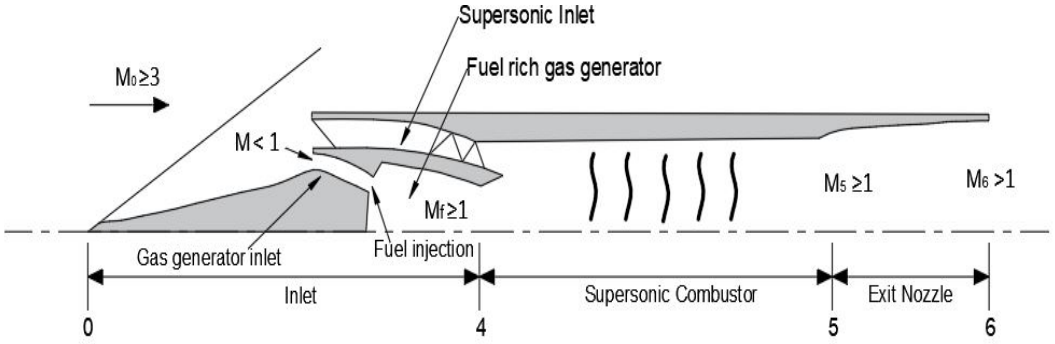

Figure 1-8 Schematic of Dual Combustion Ramjet [7]

DCR has a fuel-rich subsonic dump combustor where complete fuel is partially cracked into smaller molecular species by mixing with air from subsonic intake and this partially cracked fuel subsequently mixes and burns efficiently with the peripheral air from supersonic intake in main combustor. Such a dual propulsion system employs the best features of both ramjet and scramjet in order to achieve stable combustion, higher performance at low Mach numbers and more convenient cooling of the wall. The major components are supersonic and subsonic intake, fuel rich gas generator/dump combustor, supersonic combustor and exit nozzle. Typically, one-fourth of total captured air is diffused through a subsonic inlet to dump combustor. The fuel rich exhaust gases enter the supersonic combustor where it undergoes secondary combustion in supersonic flow. The dump combustor aids in easier ignition and more stable combustion, higher performance at low Mach number. It helps in achieving a wider range of operating flight Mach number (typically 3.5 – 7) with hydrocarbon-based fuel system. The upper limit is due to energy consumption by dissociating and ionizing species at elevated temperature, which cannot be compensated for by additional fuel as in the case of a diatomic gas such as hydrogen. The DCR propulsion system shown in
Figure 1-9 mainly consists of:

1) External compression cone
2) Internal compression intakes (subsonic and Supersonic) and feed system
3) Gas generator
4) Supersonic combustor
5) Nozzle

The view of a typical hypersonic missile based on dual combustor ramjet engine and the various sub-systems involved are also shown in the

Figure 1-9. and Figure 1-10. respectively.

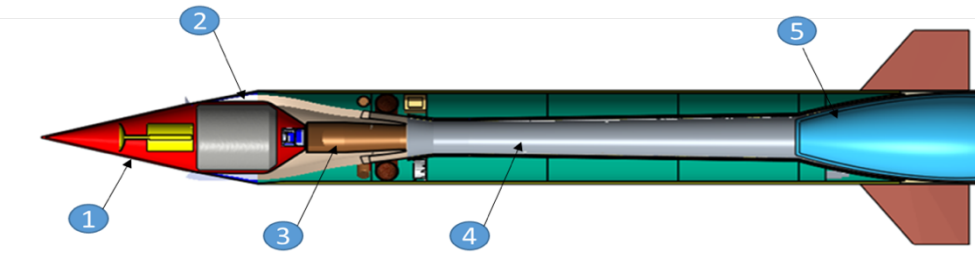

Figure 1-9 A view of Hypersonic Cruise missile based on DCR Engine

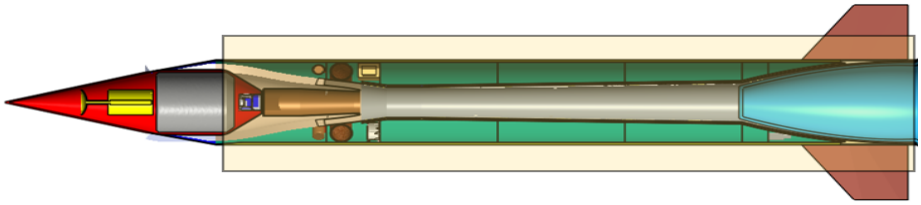

Figure 1-10 A View of DCR Propulsion system in the vehicle

1.6 Critical areas of the DCR propulsion system research

DCR propulsion system performance is highly coupled with the following four critical sub-systems:

- Intake system performance
- Gas generator ignition, sustained combustion at high equivalence ratio and its allowable pressure rise limit
- Annular isolator performance
- Supersonic combustor performance

and the other critical aspects are

- Thermal management with active/endothermic cooling by using liquid hydrocarbon fuels
- Freejet /Connect pipe mode testing with advanced diagnostic tools

1.7 Objectives of the current research work

The aim of the research work is to investigate liquid hydrocarbon fueled “Dual Combustion Ramjet” propulsion system numerically and experimentally over a variable Mach number range between 4 to 6 for highspeed applications

Mixing of reactants, ignition, flame stability and completion of combustion, with hydrocarbon (kerosene) fuel are the challenging problems associated with supersonic combustion. Embedding a dump combustor / gas generator in a supersonic combustor with multiple intake system mitigates these problems and makes the system more flexible and simpler.

DCR technology has very high potential in developing long-range high-speed air breathing tactical weapon system with a capability to launch from multiple platforms. Information on such technologies is very less published and it is always denied. Available information is mostly theoretical/analytical. Experimental data is very scarce and validation with experiments is also less attempted.

Objectives of the current investigations are:

a) Understanding the DCR technology and identifying the challenges through literature survey

b) DCR design methodology considering the requirements and constraints

c) Gas generator characterization
   - Experimental characterization with multiple tests
   - Development of 1-D Model and its validation

d) Numerical studies on combustor flow field
   - Numerical studies on combustor- annular Isolator interactions in axisymmetric liquid hydrocarbon fueled DCR
   - Various turbulence models comparison
   - Validation with available experimental data
   - Combustor geometry Parametric studies
   - Numerical simulations for critical parameters for Mach Number 4 and Mach Number 6 flight conditions for the full-scale geometry

e) Full scale DCR proto testing and Evolving design methodology
   - Fabrication of the combustor Proto hardware for testing
   - Test facility modifications and characterization
   - Connect pipe mode testing of integrated “Gas generator” and “Supersonic combustor” of DCR engine for freestream condition at Mach Number 6
   - Discussion of the test data

1.8 Organization of the thesis

In order to arrive at the scope for the present work, an extensive review of the research work reported so far on DCR based vehicles and DCR Propulsion system design, analysis and experimental work is presented under Chapter-2. Current investigations covering the DCR design requirements and design calculations, characterization of fuel rich gas generator and its experimental data validation with the 1-D model, numerical analysis of combustor - isolator flow field for axisymmetric DCR engine and its validation with published literature, numerical studies on DCR combustor geometry, Full scale DCR testing methodology in connect pipe mode facility, its configuration, instrumentation, test data are presented are described in Chapter-3. Chapter-4 deals with a discussion on the results obtained from the experimental and numerical studies. Conclusions drawn from the present investigation are listed out in Chapter-5. Recommendations for the future work are presented in Chapter 6 and a list of references are presented at the end.

Chapter 2

LITERATURE REVIEW

Hypersonic propulsion is the most promising technology for futuristic military and space vehicles. Worldwide, relentless efforts are going on by many researchers to establish this technology. Ram/Scramjet propulsion is the key research area specific to the long-range cruise missile systems, where the engine must perform for long burn duration with suitable hydrocarbon fuels capable of cooling the engine/structures throughout the mission. The potential of air breathing propulsion can be efficiently utilized when the missile is designed as an air launched weapon, boosted with a small booster up to lower Mach numbers and allowed to accelerate till the cruise altitude to achieve hypersonic speeds for further cruising towards the target. Dual Combustion Ramjet (DCR) /Dual Mode Scramjet (DMSJ) propulsion systems can be adopted for such missions. DCR consists of a subsonic combustor embedded in the engine to generate fuel-rich hot gases for further combustion in the supersonic combustor in tandem mode. It has an edge over the rest of the options as it gives advantages of both ramjet and scramjet by allowing wider flight corridor and also mitigates critical issues like fuel ignition compared to conventional scramjet engines.

Very limited information is published in DCR technology even though it has matured and successfully flight tested in some of the missions. In this chapter, it is attempted to present the overall view of this technology by highlighting few interesting works carried out by various

researchers very specific to DCR propulsion system. Modeling work of DCR propulsion system; numerical works carried out on flame structures, flow and flame dynamics, combustor-isolator interactions; free jet testing/direct-connect testing experimental works on characterization of DCR and its combustor-isolator interactions are studied in detail and presented. Necessary facilities needed for testing of DCR propulsion systems and improvements needed in critical areas of ground testing, simulation, fuels are also highlighted.

2.1 DCR concepts and preliminary analysis literature

Dual Combustion Ramjet (DCR) based propulsion concept was conceptualized first by Billig as follows:

James Keirsey of Johns Hopkins University/Applied Physics Laboratory (JHU/APL) invented the DCR cycle in the early 1970s. Billig, *et al.* [7] proposed a new propulsion concept for hypersonic ramjet missile using hydrocarbon fuels over the complete trajectory. The new design was evolved by embedding a "dump-type" subsonic combustion ramjet within the main supersonic combustion ramjet (scramjet) system to generate fuel-rich hot gases from hydrocarbon fuels. This innovative idea had drastically reduced the volume/envelope of the vehicle.

Intake of this concept was axisymmetric but compartmentalized to supply air flow both to gas generator and supersonic combustor through suitably designed cross sectional ducts. Small portion of the air flow ~25% is allowed to the subsonic gas generator through the intake which is operated supercritically. The cross section of the intake increases in the stream direction ensures stable throttling and normal shock position. In supersonic combustor intake, remaining air flow ~75% is turned towards supersonic combustor axis compressing supersonically by the outer cowl surface. The outer annular duct houses isolator section which is designed to avoid combustion induced disturbances and interactions with the intake.

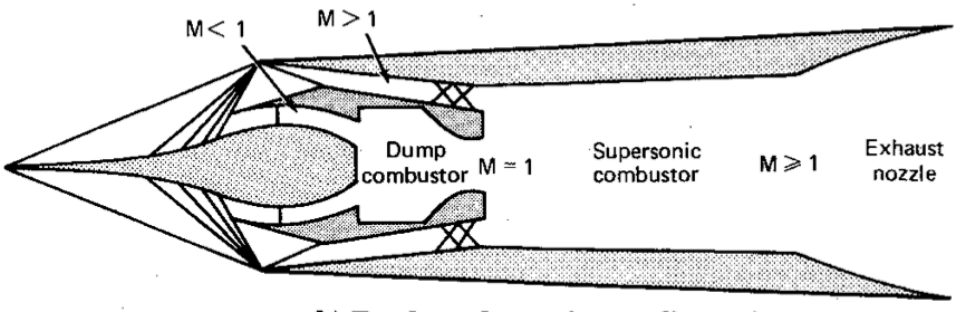

Figure 2-1 Schematic of integral-rocket dual-combustion ramjet [7]

Figure 2-1 shows Integral Rocket Dual Combustion Ramjet (IRDCR) proposed by Billig, *et al.* was a combination of two ramjet cycles, as subsonic fuel rich gas generator and scramjet with hydrocarbon fuel leading to a performance falling within the range of that of a single cycle ramjet of two types. The gas generator design, supersonic combustor analysis and engine performance were explained for the chosen mission. Analysis was carried out for a fixed geometry of the engine operating with zero angle of attack over the Mach number range of 4 - 7 and between equivalence ratios from 0.25 to 1.0 respectively for cruise and accelerating portions of the trajectory. Fuel rich gas generator design with hydrocarbon fuel was studied for discrete Mach numbers 4, 5, 6 and 7 and equivalence ratio between 1 and 4. At all flight conditions and equivalence ratios, inlet is allowed to operate near critical keeping the influence of gas generator on inlet in view. For a fixed geometry configuration, the inlet's critical pressure recovery limit is achieved by sizing the sonic area with margins. It was also ensured that all intakes operate supercritically over the entire range of equivalence ratios between 1 and 4.

Combustion Analysis of the supersonic combustor was done by considering three regions of the flow fields, namely shock expansion zone, a nonuniform 2D-3D combustion zone and 1D equivalent combustion zone as shown in Figure 2-2. It was mentioned that in the shock-expansion zone, shock-combustion model pressure matches with the pressure resulted from the mixing of flow from the gas generator and the supersonic air inlet. In another study, prediction of combustion wall pressures in scramjet engines was studied and local separation distance (So) in the flow in annular duct compression field from the exit of the gas generator and the extension distance (Sd) of the shock expansion region were determined.

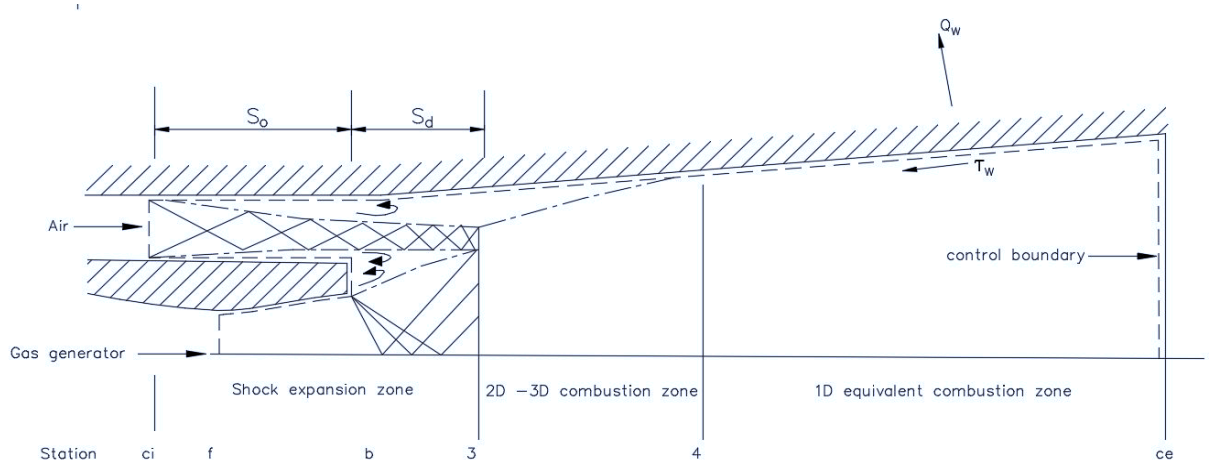

Figure 2-2 Billig's theoretical model for combustion analysis [7]

Billig, *et al.* [7] emphasized the mutual influence of inlet, gas generator and supersonic combustor in this concept. It is to be noted that the study carried out with arbitrary inlets did not consider viscous effects, angle of attack variations. Hence it is to be understood that the critical parameters like air capture, pressure recovery, drag and characteristics at design Mach number are highly configuration dependent. The primary outcome of this innovative study was to provide a flexible engine cycle adaptable for air breathing, wider speed range variable mission and intelligently avoiding the fundamental combustion limitation of scramjet.

Paul J Waltrup [8] of Johns Hopkins University has done extensive research on liquid fueled supersonic combustion ramjets technology and highlighted its strength, shortcomings and opportunities. A comparison of SCRAMJET and DCR combustors and their flow fields was explained as shown in Figure 2-3 in very elaborative manner. Advantages of DCR especially in fuel injection, ease of ignition and avoiding the combustor/inlet instabilities were highlighted. In scramjets fuel penetration and vaporization is a primary concern but in DCR mixing and combustion process is controlled by the shear layer emanating from region of air and fuel rich partially cracked streams. The control boundary needed to model the combustor flow field in both the cases was defined as shown in Figure 2-4 considering the pre-combustion shock train region, non-uniform mixing and combustion region and pseudo one dimensional zone.

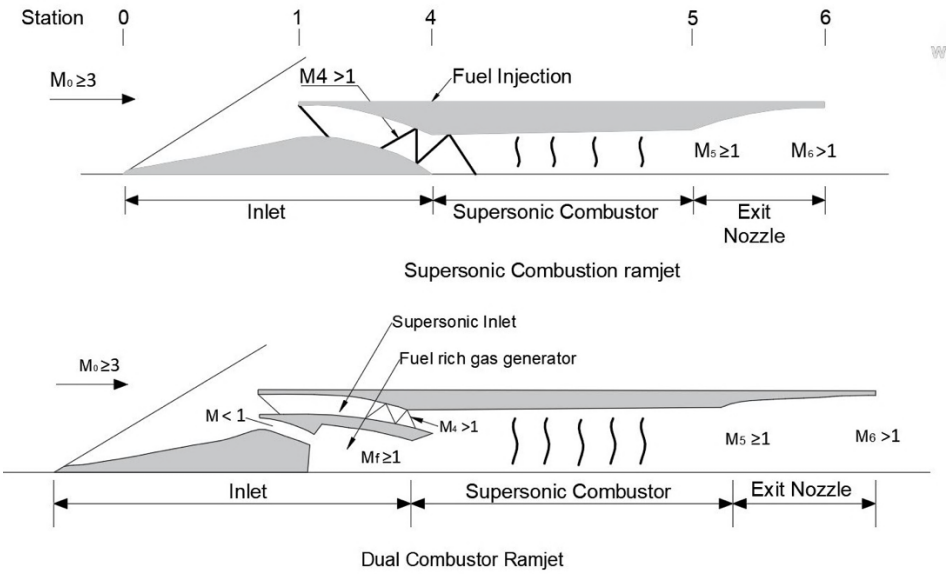

Figure 2-3 Schematic of generic SCRAMJET and DCR [8]

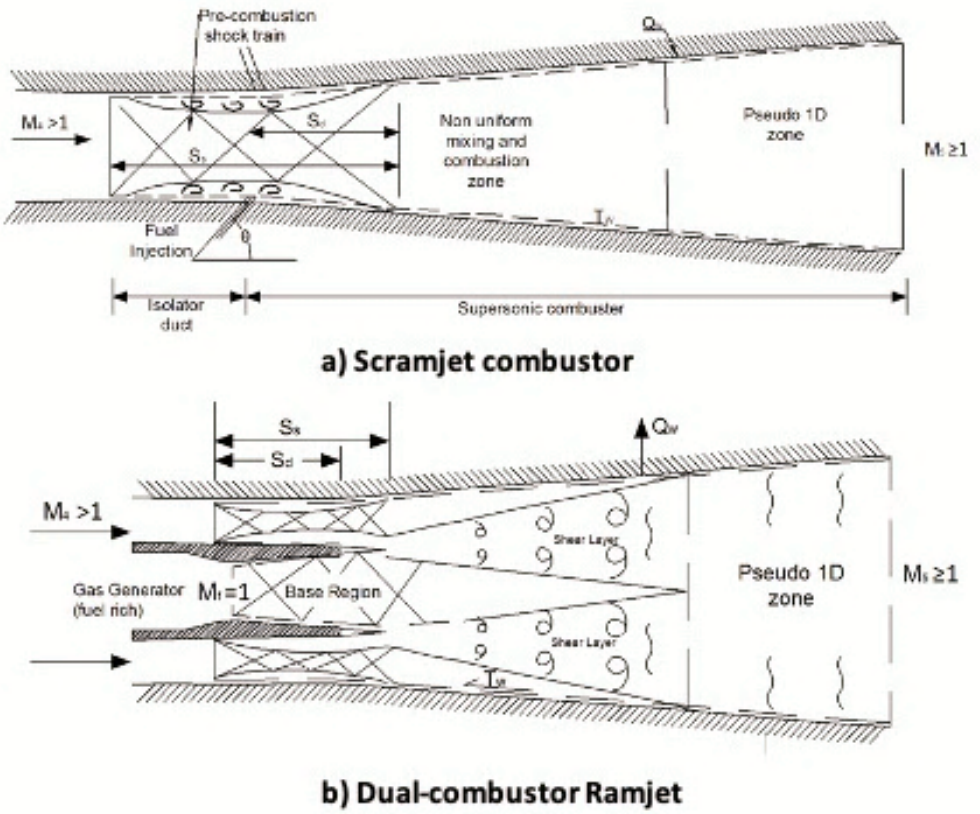

Figure 2-4 Schematic of SCRAMJET and DCR combustion process [8]

Fundamental areas of research and issues associated with each of the engine components Inlet, isolator, injector, combustor exit nozzle were listed as follows by P J Waltrup:

Inlets: Air capture capability, pressure recovery, flow parameters, Understanding of growth and interaction of laminar, transition, turbulent viscous layers with strong and weak expansion /compression fields, separation and reattachment mechanisms

Fuel: Desirable properties of fuel, vaporization, ignition energies and chemical kinetics

Fuel Injectors: Penetration, atomization, ignition characteristics, free shear layer growth process, transport properties, influence of external ignition aid on the basic ignition and chemical kinetic process

Supersonic combustor: Maximizing the heat release with minimum total pressure loss for a given combustor length, supersonic mixing and combustion process.

In addition to the above, the methodology to be adopted for modeling of the supersonic combustor was discussed highlighting the need aspects of engineering tools such as integral analyses, solutions to full Navier-Stokes equations considering viscosity and chemistry. The necessity of nonintrusive measurement techniques in the experimental work for accurate measurement of particulate size, velocity, temperature, density and species was mentioned. Special discussion was made on the isolator and the pre-combustion shock system of DCR propulsion system. Effect of mass flow ration variation on DCR pre-combustion compression field wall pressure distribution at M4 = 2.4 was studied as shown in Figure 2-5 and the deficiency of not considering the fundamental mechanisms of turbulent transport and dissipation was mentioned as the future research requirement.

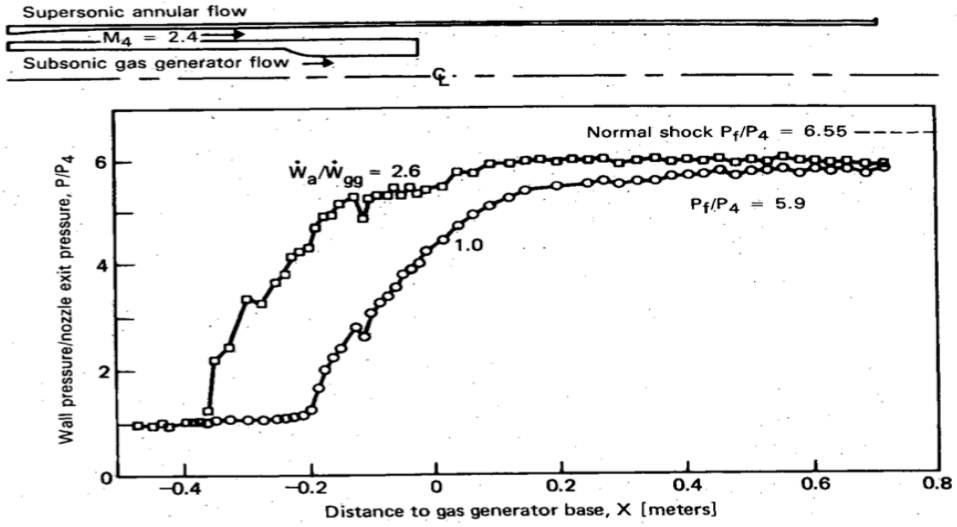

Figure 2-5 Effect of mass flow ration variation on DCR pre-combustion compression field wall pressure distribution [8]

A review of past and current research in liquid fueled supersonic combustors has also been provided by Waltrup [8] who also emphasized the need of DCR and the role it would play in future. Paul J Waltrup [9] proposed versatile propulsion system for hypersonic tactical missile application based on DCR technology. It was proposed to use DCR as sustainer engine with liquid fuel for hypersonic mission application. The use of heavy hydrocarbon fuel for supersonic combustion can be made possible if they are prepared to exceed minimum enthalpy requirement prior to injection. This preparation leads to heating and cracking the fuel to light gaseous species before entering the injector. To achieve this, an integral energy source in the form of subsonic gas generator was opted as part of the engine cycle. Design methodology of DCR engine giving the design criterion of inlet design Mach number, air flow split and contraction ratio, gas generator sizing and supersonic combustor area ratio were presented.

The methodology needed to design and maximize the performance of dual combustor ramjet engines was presented. Based on the results of these design studies and subsequent comparisons of the ramjet, scramjet and DCR powered vehicles, Waltrup has made the conclusions and recommendations regarding the following parameters:

- In flight regime of Mach number 4 to 8, DCR performs better at the lower flight Mach numbers and scramjet performs better at higher Mach numbers
- optimum inlet design Mach number needed for the required flying Mach number range
- optimum DCR supersonic combustor area ratio for the specified the flight Mach number regime
- Larger portion of air ingestion is better for better performance of DCR's supersonic combustor.
- Between DCR and ramjet powered vehicles, the DCR exhibits better performance at and near cruise at the highest flight Mach number if both are designed to have the same maximum net thrust at Mach number 3 for Mach number 3 to 6 flight.

2.2 DCR based systems literature

Moerel, *et al.* [10] integrated engineering methods of aerodynamic and propulsion as a system engineering tool and studied the performance of both axisymmetric and wave raider configurations. Analytical formulae that can yield first order accuracy were used to model aerodynamic and propulsion to study over a wide range of mission parameters namely cruise speed and altitude, size of the vehicle. Simple analytical relations were used to observe trends on the full vehicle and again to trace back subsystem level performance behavior.

White, *et al.* [11] studied on precision strike long range hypersonic air breathing missiles to attack time-critical targets. Integration of this technology with global positioning system and lethal kinetic energy penetrators was suggested and numerous factors required to completely develop a precision strike weapon system in terms of performance goals and technology challenges were highlighted. DCR based propulsion system's utility in such missions was shown as a viable option and the criticalities of this approach were listed as follows:

- Affordable materials for withstanding high temperatures for long durations in gas generator, supersonic combustor, inlet ducts and nozzle
- Complex fabrication technology involved in intake system
- Efficient packaging of the missile with maximum fuel carrying capacity and effective warhead.

Systems developed based on DCR propulsion technology:

Many countries like U.S, China, Korea and Russia have made significant research both experimentally and numerically in DCR technology. But in open literature U.S researchers have shared their configurations. Especially, U.S Navy has led in this field and made valuable contributions in multiple missions, ground testing and development of design tools for DCR technology. Between 1975-1986, as a successor to SCRAM concept, U.S focused on integration of scramjet engines and their components on hypersonic vehicle designs and the hydrocarbon-fueled Dual Combustor Ramjet (DCR*).* The U.S. Navy developed missiles of the Mach 4-6 Hypersonic Wide Area Defense Missile HyWADM in 1977 employing a DCR propulsion system (Figure 2-6).

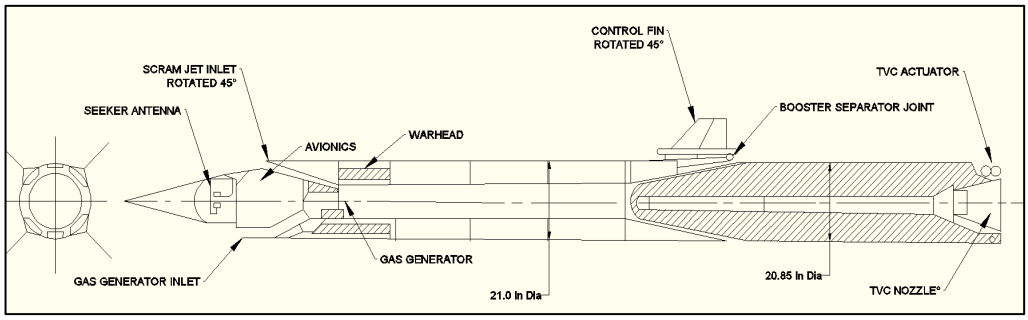

Figure 2-6 HyWADM Component Tested Missile [5]

U.S. Navy scramjet research established very useful database in the areas of design tools, test facilities and test methodologies, data analysis and computational fluid dynamics along with verification of analytical and computational methods. Cycle analysis methods established were useful for calculating the shear and thermal loads of the combustor wall, fuel mixing and finite-rate chemistry effects on combustion.

The U.S. Navy and DARPA have successfully developed and flight demonstrated the HyFly with DCR scramjet propulsion technology (Figure 2-7) in early 2002, for its application as hypersonic long-range missiles. Initially, direct connect combustor tests were done at Mach 3-6.5 and later Free-jet tests at Mach 6-6.5 conditions were successfully completed in 2002 using JP-10 as fuel. Further, full scale flight configuration engines were direct-connect and wind tunnel tested. Using flying test bed, ballistic flights of the engine were also carried out simulating Mach 4 and Mach 6 cruise flight tests till 2006 followed by successful flight-testing simulating above Mach 6 conditions. USA's HyFly is one of the well proven missiles using DCR technology. It was an air launched weapon system which is boosted to Mach number. M4 by a solid rocket booster; accelerated in air breathing mode from M4 to M6 and then cruises for intended duration and dives towards the target with high impact velocity.

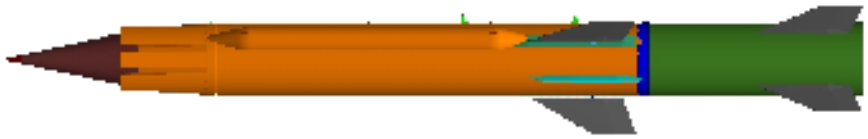

Figure 2-7 HyFly Flight Demonstration Vehicle [5]

Ronald S. Fry [2],[5] has compiled and presented lot of information on ramjet propulsion and its technological developments from subsonic to hypersonic flight speeds from the early 1900s to current times regarding ramjet, scramjet, and mixed-cycle engine types, and their operation. History of this technology, major contributions and flight demonstrations were summarized. Challenges, future research areas of the critical areas were identified as follows:

- Fixed/variable geometry intake system technology
- Combustor technology in terms of thermal management, insulators and materials
- High energy Ramjet/Scramjet fuels with endothermicity
- Fuel management systems for efficient injection, mixing
- Propulsion/airframe integration, materials and thermal management CFD code analysis and validation methodologies
- Thermochemical modeling and simulation development
- Ground test methodologies of Direct-connect/ Semi-free jet / free jet tests

2.3 Literature on Studies on Design, Modeling and Analysis of DCR propulsion system

Performance analysis of DCR was studied by Korean researchers Jong-Ryul Byun, *et al.* [12] based on gas dynamics and thermodynamics relations. A preliminary design and determination of geometry of the gas generator and supersonic combustor was presented. Wesley, *et.al* [13] have carried out a preliminary analysis of kerosene fueled DCR at different altitudes, velocities and equivalence ratios and studied critical performance parameters such as thrust, specific impulse and efficiency for a Mach number. range of 3 to 7 by developing a Matlab program. Following conclusions were drawn based on the study:

- Less Inlet pressure recovery of the engine at high Mach numbers
- High area requirements for scram and ram inlets for high Mach number. operation
- For a given equivalence ratio and altitude, higher thrust is generated for higher Mach number.
- Specific impulse is maximum at higher Mach number and higher equivalence ratio.

Waltrup [9] has presented the design methodology of DCR engines specifically for their application in tactical missiles. The critical parameters needed for the design of DCR are inlet

design Mach number, inlet air flow split ratio, Inlet area contraction ratio, gas generator throat size and supersonic combustor area ratio. Total pressure modulation is needed to keep the ramjet throat in choked condition for equivalence ratios less than one. Design criticalities of the most important four elements of DCR are Supersonic intake, gas generator intake, gas generator and supersonic combustor were explained as follows:

Intake's design requirement:

For inlet's compression performance, empirically derived correlation of supersonic inlet kinetic energy efficiency, as a function of diffuser throat (or) exit-to-free stream Mach number ratio, M_2/M_o,

$$\eta_{KE} = 1 - 0.4\left(1 - \frac{M_2}{M_0}\right)^4$$

…Eq(2.1)

was rearranged to express the total pressure recovery of the supersonic inlet, P_{t2}/P_{t0}, as a function of effective inlet contraction area ratio, A_o/A_2.

$$\eta_{pr} = \frac{P_{t2}}{P_{t0}} = \left[1 + (1 - \eta_{KE})\frac{\gamma - 1}{2} M_0^2\right]^{\frac{\gamma}{\gamma - 1}}$$

..Eq(2.2)

Supersonic Inlet kinetic energy efficiency as a function of diffuse exit-to-free stream Mach Number ratio and Supersonic Inlet total pressure recovery as a function of effective area contraction ratio are shown in Figure 2-8 and Figure 2-9 respectively.

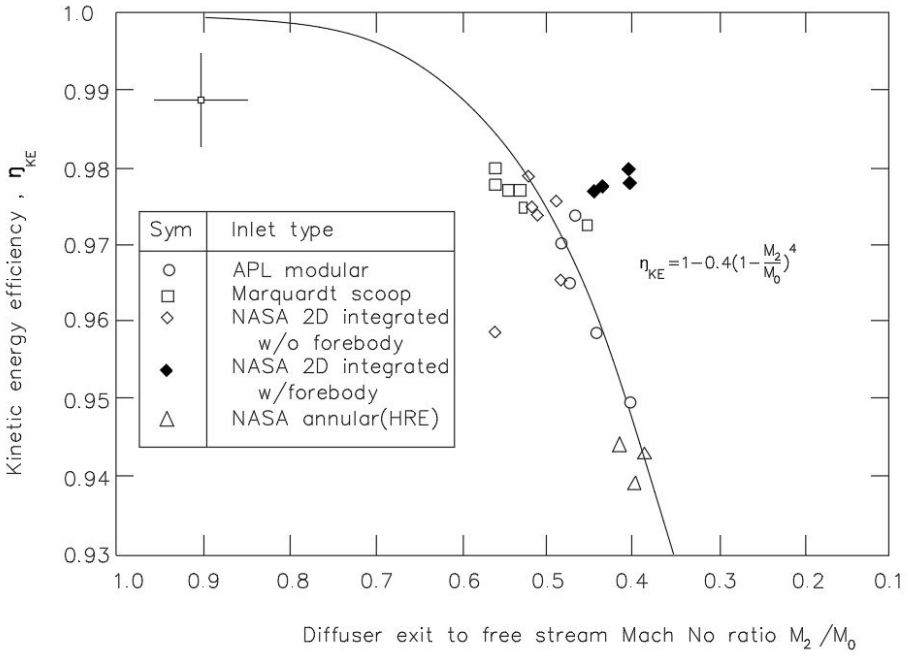

Figure 2-8 Supersonic Inlet kinetic energy efficiency as a function of diffuse exit-to-free stream Mach Number ratio [9]

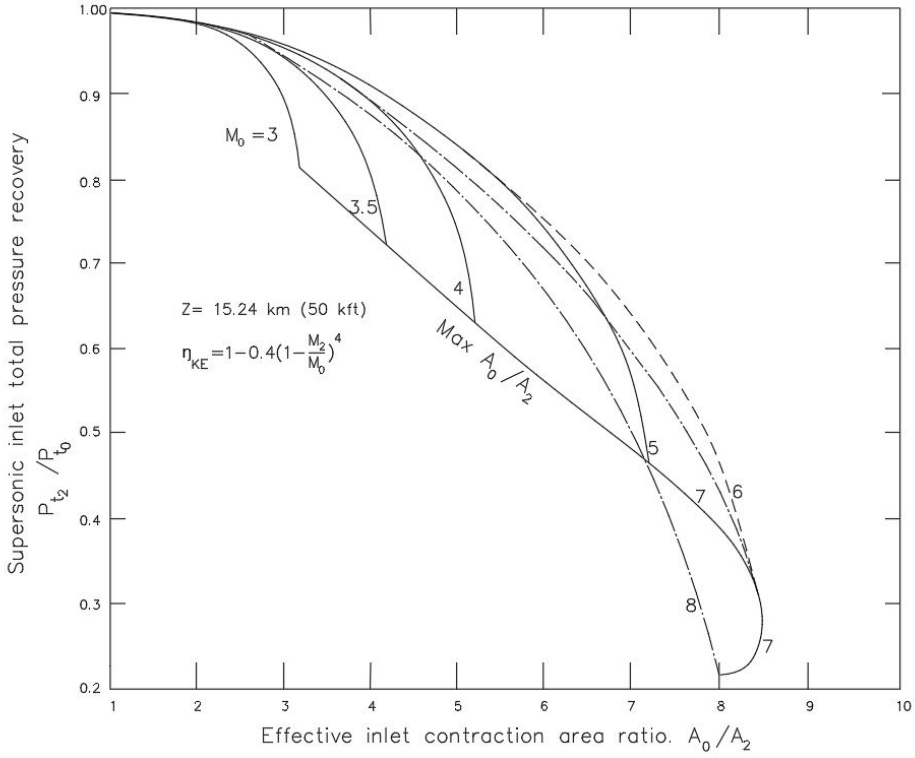

Figure 2-9 Supersonic Inlet total pressure recovery as a function of effective area contraction ratio [9]

Gas generator's design requirements:

Gas generator generates fuel rich hot gas products and accelerates the gas through a fixed throat. Its minimum throat area size is determined from conservation of mass using maximum critical total pressure recoveries. Since the air capture varies with altitude, it is to be designed for lower altitudes where larger air capture is possible. Gas generator shall be designed for lowest flight number. The other important parameter that dictates the gas generator's design is the difference between the gas generator's exit pressure and the precombustion shock static pressure. It is always desirable to have air intake's static pressure less than that of static pressure of gas generator. If it exceeds, it can lead to unstart of the gas generator's intake and further affects the complete DCR engine performance.

Supersonic combustor's design requirements:

Fuel injection into the supersonic combustor is in the form of products of fuel rich combustion from large sized throat of gas generator. The base area between the air intake duct and the exit of the gas generator and the area ratio between the exit of the supersonic combustor to inlet area greatly influence the mixing and combustion in the supersonic combustor in addition to the other operating parameters.

Waltrup has also compared the DCR and SCRAMJET powered vehicles and concluded that the performance was better for DCR based vehicles accelerating at lower Mach numbers and SCRAMJET was better for higher Mach number operations. When DCR was compared with RAMJET, DCR was found better at higher Mach numbers and comparable performance at lower Mach number.

Integrated DCR engine modeling and simulation were attempted for design analysis by Wadwankar, *et al.* [14]. A low order integrated model was evolved from the individual one-dimensional models of the sub-systems - intake, isolator, ram diffuser and gas generator, supersonic combustor and nozzle. Individual components were modeled with high fidelity by analytical or CFD methods and these high-fidelity models were integrated and used as mission analysis tool for studying DCR's performance at Mach 7 at 27.5km altitude. It was deduced from these studies that the equivalence ratio should be below the stoichiometric and intake total the pressure recovery had an influence on the DCR engine performance. The flow chart of the model is shown below Figure 2-10:

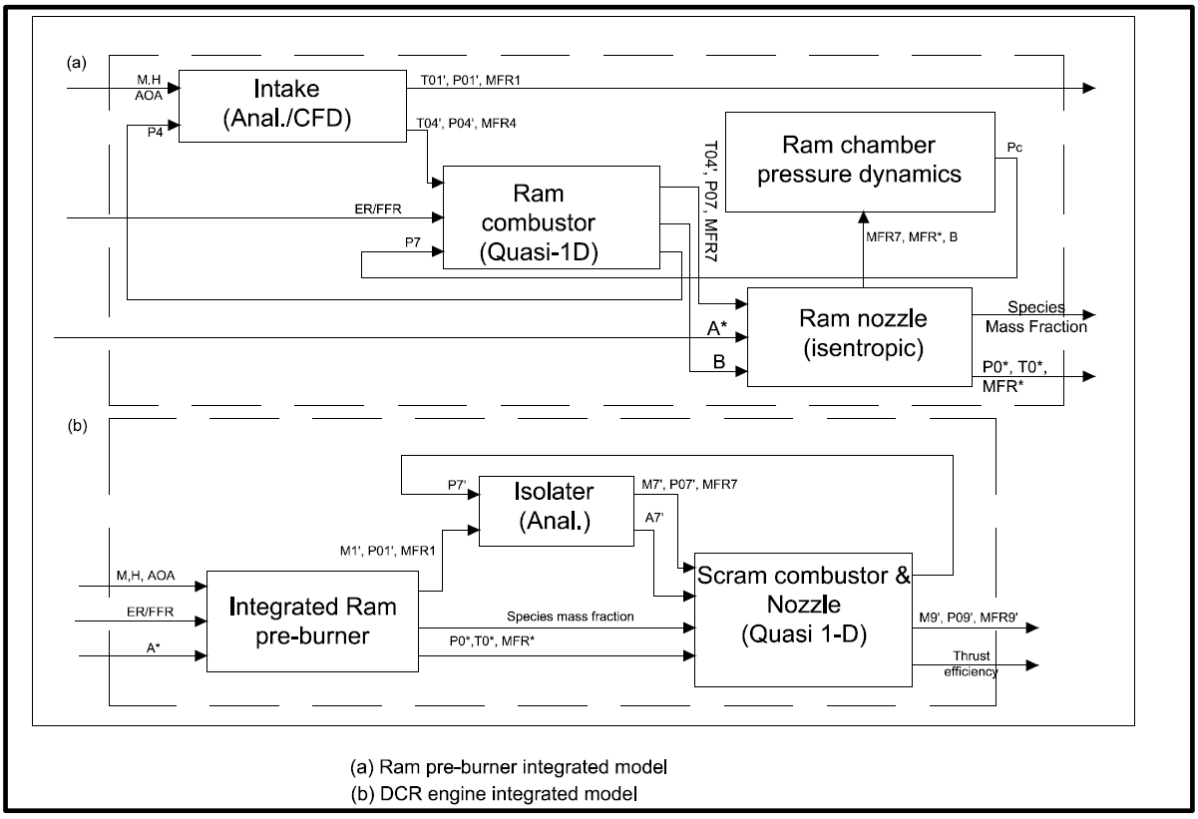

Figure 2-10 (a) ram pre-burner integrated model and (b)DCR engine integrated model [14]

Multi-Disciplinary Optimization (MDO) methodology is the most demanding design tool for complex air-breathing vehicles-based mission designs and these kinds of models become part of such tools.

2.3.1 Fuel rich gas combustion in supersonic combustor

Analysis procedure / computer code of turbulent mixing and combustion the scramjet combustor with a co-axial fuel jet was developed by Schetz, *et al.* [15]. Important physical and chemical processes, effects of heat release on the upstream pressure field were modeled. Mixing model, turbulent transport model and chemistry of DCR were presented. It was reported that a length of ~ 2 m DCR combustor is needed to ensure complete heat release for a Mach number range of M4 to M7.

For mixing calculations, boundary layer form of equations of motion for an axisymmetric flow involving the momentum equation, the work equation reformulated in terms of Stagnation enthalpy, species mass fractions were solved by finite difference procedure.

Turbulent transport model was proposed by use of equation for conservation of turbulent kinetic energy (TKE), k, to calculate eddy viscosity as a function of streamwise distance. Since estimation of the properties of fluid such as local molecular composition, temperature and density in the combustion chamber flow field is difficult, diffusion equations were simplified by replacing the molecular mass fractions with element mass fractions, which enabled to solve the diffusion equations numerically as that of frozen mixing problems.

In gas generator, liquid fuel injection into heated air stream, mixture formation, ignition and combustion need adequate modeling of evaporation. Combustion of mostly widespread hydrocarbon fuels takes place in a gas-phase regime. Thus, evaporation of fuel from the surface of droplets is one of the limiting factors for non-uniform reacting mixtures. Betelin and Smirnov, *et al.* [16],[17] have carried out modeling and simulation on evaporation and ignition of droplets in heated atmosphere of combustion chambers. They have done extensive investigation of process of non-equilibrium evaporation of small droplets with streaming flows. The lifetime for single evaporating droplet could be several times longer under non-equilibrium conditions as compared with equilibrium ones. They distinguished two scenarios for droplet heating and evaporation in a heated air flow i.e. small droplets undergo successively heating, then cooling due to heat losses for evaporation, and then rapid heating till the end of their lifetime while larger droplets could directly be heated up to a critical temperature and then evaporate rapidly. Thus, atomization affects droplet lifetime. They also concluded that fuel spray injection and self-ignition in a heated air flow has three characteristic stages. At the first stage of jet injection, droplets evaporate rapidly thus cooling the gas at injection point, the liquid jet is very short and changes for a vapor jet. At second stage liquid jet is becoming longer, because evaporation rate decreases due to decrease of temperature. But combustion of fuel vapor begins which brings to increase of heat flux to droplets and accelerates evaporation. The length of the liquid jet decreases again and remains constant slightly oscillating.

Nickolay N. Smirnov, *et al.* [18] have also done theoretical investigations of combustion and detonation initiation in heterogeneous polydispersed mixtures using deterministic methods of continuous mechanics of multiphase flows to determine the mean values of parameters of the gaseous phase and stochastic methods to describe the evolution of polydispersed particles in it and fluctuations of parameters. They have carried out numerical investigations of detonation initiation in dispersed hydrocarbon fuel–air mixtures after mild ignition via DDT and by shock waves of different intensities were performed in tubes of cylindrical geometry.

Several geometrical and flow parameters could influence the efficiency and the thrust produced by the ducted rocket. These include the dome height, angle of side arms, and location of the fuel injector, fuel-air ratio, combustor pressure and dimension.

Stull and Craig [19] investigated dual inlet side dump combustor using liquid fuel injection. The combustion performance at different dome height (varying from 0" to 4"), inlet angles (30°, 45°and 60°) and inlet air temperature were studied. They also investigated the effect of pressure oscillations in combustor on its performance.

Vanka, *et al.* [20] studied and made calculations to examine the effect of mixing, chemical reaction and flow field development in reacting flow. They observed that with increase of dome length, the combustion efficiency increases. Also, steeping the inlet arm increases the mixing. The location of the fuel injector also affects the combustion efficiency. The eccentrically placed fuel injector system gave better results than the one with concentric fuel injector.

Brophy and Hawk [21] conducted experiments on flow visualization of four inlet configuration ducted rocket engine. The complex mixing patterns within the dome head region of the combustors exhibited a strong dependence on dome height, momentum ratios and inlet flow angles. Six combustors have been evaluated. Three of the combustors had the inlet flow inlets at the same axial station. The remaining three had one inlet staggered 1.5 inlet diameters downstream of the upstream inlet flow. All were investigated up to a Reynolds number of 5.5×10^5. The mass flow ratio and momentum ratio were varied between 10 to 60 and 4.58 to 2.58 respectively.

An analytical model with NASA CEA [22] interface has been developed to predict the combustor performance for the given combustor size and flow rates. NASA Chemical Equilibrium with Applications (CEA) is a computer program for calculation of chemical equilibrium compositions and properties of complex mixtures developed by Gordon and McBride. Governing equations are developed using conservation of mass, momentum and energy [23]-[25].

The mechanism of liquid film evaporation and boiling is different and has been studied extensively by Tyurenkova, *et al.* [26] and [27]. They have assumed fuel gasification and gas phase chemical reacting in a diffusion flame. Regression rate of the material surface in the turbulent and laminar flow regimes has been carried out for a hybrid rocket motor.

An analytical model of film cooling for liquid rocket engine [28] can also be used to study the wall cooling mechanism. This model has been used for preliminary work.

2.3.2 DCR combustion, flow field and Injection studies

Behavior of supersonic turbulent combustion in DCR was examined by Jeong-Yeol CHOI, *et al.* [29] by numerical analysis. Fuel-air mixing at the turbulent shear layer is very important in DCR combustion process. Flame structures in DCR are represented below Figure 2-11:

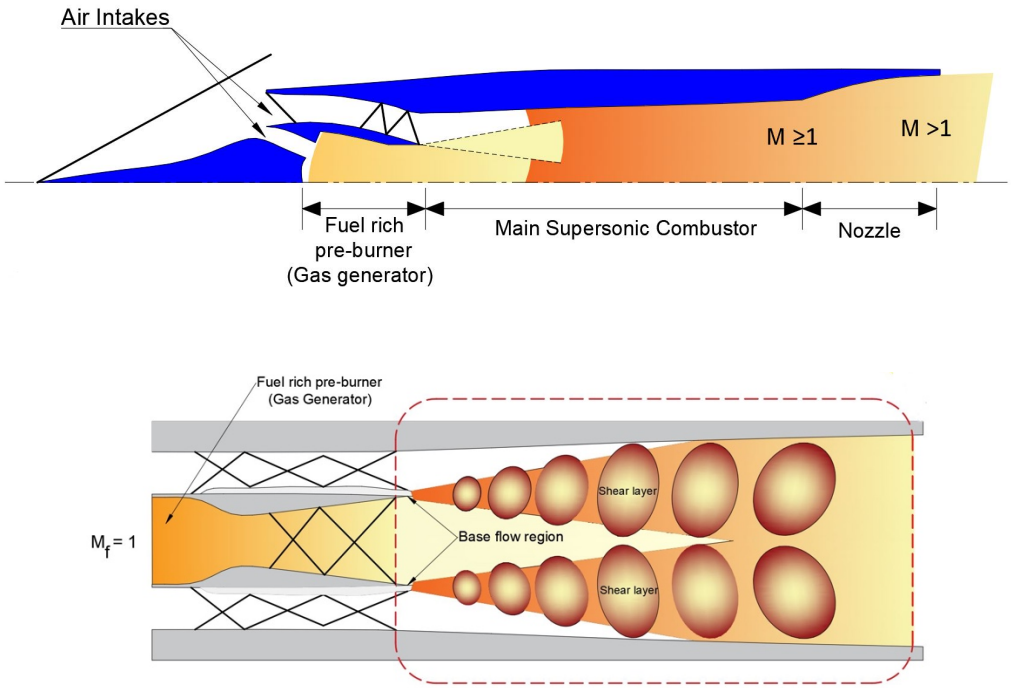

Figure 2-11 A view of DCR flame structures [29]

Numerical experiments were carried out for different divergence angles and lengths of the constant area of DCR combustor, the variation in combustion modes was observed based on the Mach reflection as shown in Figure 2-12

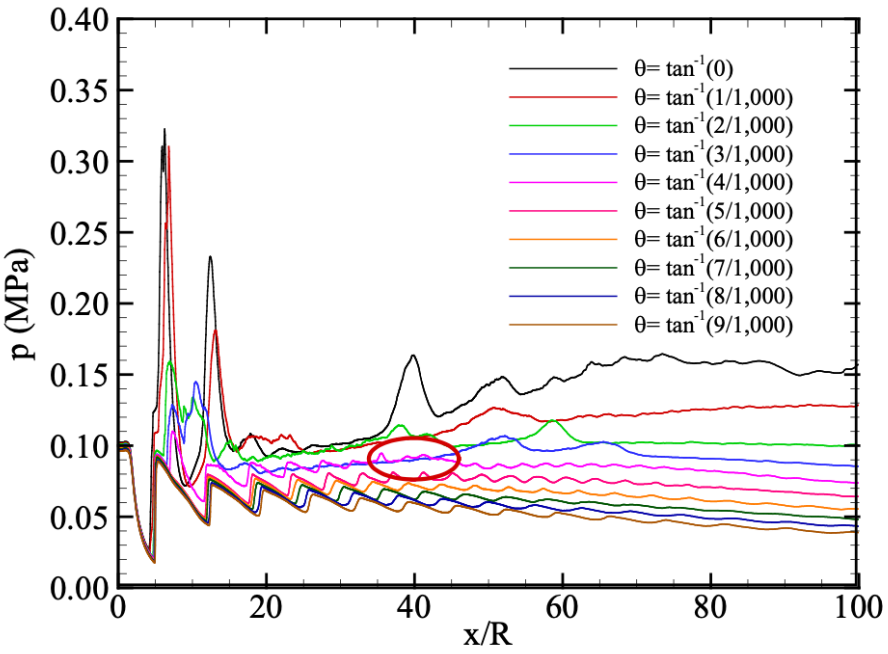

Figure 2-12 Time-averaged wall pressure distributions for DCR combustors with various divergence angles [29]

It was proved numerically that combustion mode changes to local thermal choking at divergence angle $\theta = \tan^{-1}(4/1{,}000)$ and the primary pressure peak becomes stronger as the θ becomes smaller.

Relation between the turbulent combustion, Scalar dissipation rate (SDR), and formation of Mach reflection was studied. Coupling between the compressibility effects and the turbulent combustion was analyzed and their effects on the changes of modes of combustion to thermal choking were presented. Numerical modeling of DCR turbulent combustion was carried out by solving fully coupled equations of energy conservation, momentum and species with a RANS turbulence model and combustion was modeled with eight reacting species (CO, CO_2, O, O_2, H, H_2, OH, H_2O). From the results it was found that the DCR has a turbulent lifted flame and the lifting distance becomes longer with increase in the divergence angle.

DCR flow and flame dynamics studies:

Zhang, *et al.* [30] have studied the flow and flame dynamics of hydrocarbon fueled DCR engine. Flow field and the shock structures appeared immediately downstream of the gas generator exit were studied; interaction of the gas generator hot gases and airflow from the isolator and their effect of creating expansion fans in the supersonic combustor were predicted. A shock train was observed between the inner and secondary shear layers. Numerical simulations are performed under both chemically frozen and reacting conditions. The

composition and temperature of the hot reactive mixture from the subsonic gas generator are determined at three fuel equivalence ratios, 1.0, 2.0, and 3.0. The numerical methods, the system configuration, operation conditions, computational grids, boundary conditions, results of non-reacting and reacting cases were presented in detail. Numerical methodology used for modeling the flame dynamics and the flow was as follows:

- Favre-averaged conservation equations of mass, momentum, energy, and species concentration for chemically reacting systems.
- Fick's law was used to approximate the species diffusion in a multicomponent mixture
- Menter's shear-stress transport model augmented with a detached eddy simulation extension for turbulence closure
- chemical reactions by the two-step global kinetics scheme for Jet-A fuel
- Finite volume method for solving the governing equations and associated boundary conditions
- Roe's flux-differencing splitting method derived for multispecies reacting flows for evaluating convective fluxes

Percentages of unburnt carbon and hydrogen were used as two measurable parameters to assess the combustion performance of DCR and evaluated as below:

$$R_C = \frac{\frac{12}{16}\times\dot{m}_{CH4} + \frac{12}{28}\times\dot{m}_{CO}}{\frac{12}{16}\times\dot{m}_{CH4} + \frac{12}{28}\times\dot{m}_{CO} + \frac{12}{44}\times\dot{m}_{CO2} + \epsilon}$$

$$R_H = \frac{\frac{4}{16}\times\dot{m}_{CH4}}{\frac{4}{16}\times\dot{m}_{CH4} + \frac{2}{18}\times\dot{m}_{H2O} + \epsilon}$$

…Eq(2,3)

The pilot flame with low molecular products and enriched radicals enhances ignition and sustained combustion capability in supersonic flow as compared to direct injection of heavy [31], [32]. J.A.Schetz, *et al.* [33] has evolved a modular approach to carryout calculations for DCR. Double flame sheet model with chemical equilibrium was adopted in this approach. Liwei Zhang, *et al.* [34] has studied coaxial flow and used LES code to study the effect of splitter plate thickness on flame stabilization and mixing in dual combustion ramjet. According to the research, higher plate thickness leads to better combustion.

2.4 Literature on Experimental /Numerical investigations on DCR

Since the flow fields of ram/scramjet propulsion systems is very complex and coupled in nature with multiple subsystems, it is not possible to understand the physics involved only by theoretical studies or by experimental studies. Each of them has its own limitations and not fully sufficient to explain the complex flow filed/combustion in ram/scramjet propulsion. Even though recent CFD techniques and high-end computers have improved a lot and able to capture well maximum information in reactive flow field; some of the critical phenomenon like chemical kinetics, ignition modeling, liquid droplet/atomization modeling etc. cannot be integrated easily by all the researchers in this field. Hence, it is customary to carry out numerical/CFD studies by experts and validate them with experimental studies. The correlation between CFD data and experimental data brings out the gaps of understanding and enable us to finetune the models/experiments wherever it is necessary. In many published articles also, it can be observed that many researchers have tried to explain their findings by using both these methods. Some of those findings are presented in the following parts of this chapter.

2.4.1 Direct connect pipe mode experimental work on DCR

Tan, *et al.* [35] have investigated on the flow fields and the performance of full size DCR at M4 and M7 conditions of the flight through direct connected experiments and numerical analysis. Schematic of the DCR with multiple axi-symmetric intakes and the Ram/Scram combustor is shown in Figure 2-13. Geometrical parameters of the DCR were as per Table 2-1. Main findings of this study were:

- In M4 condition, subsonic flow field is established in front portion of the combustor and there is a thermally choked region
- In M6 condition, central flow is subsonic and lower static temperature is resulted due to the peripheral supersonic airflow.
- Thrust increases with increase in equivalence ratio upto a value of 0.9, there after it leads to unstart of the supersonic intake
- Specific impulse is high at M4 condition (~1330 N-s/kg) and at M6 condition it is of the order of 800 N.s/kg.

National University of Defense Technology in China has investigated scramjet and DCR for a decade on development of practical propulsion systems for hypersonic vehicles. Direct-connected experimental systems and high temperature wind tunnels were built. Many critical investigations were undertaken in the areas of hypersonic flow control, supersonic combustion characteristics, performance optimization and regenerative cooling by using supercritical kerosene. A special experimental set up built to simulate the full scale DCR with intakes, gas generator, supersonic combustor and nozzle.

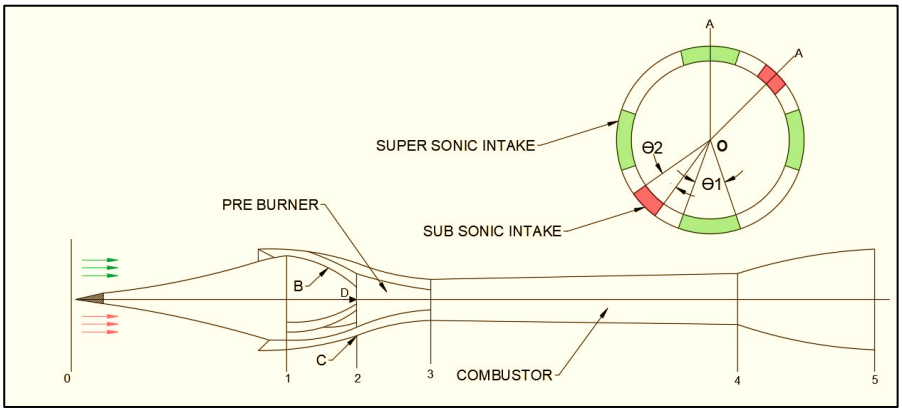

Figure 2-13 Schematics of the dual combustion ramjet [35]

Table 2-1 Main Geometrical Parameters [35]

Item	Unit	Value
Diameter of the OCR	mm	500
Diameter of the combustor inlet (3)	mm	215
Total angle of the intakes	Deg	190
Total length of the DCR (1-5)	m	4.52
Length of the combustor (3-4)	m	1.97

Flight conditions of Mach number, pressures and flow rates were simulated and achieved on ground by Vitiated air heater (Air, oxygen, ethanol fueled) with appropriately designed nozzles. Using liquid kerosene as fuel and multiple injection locations in the intakes, core of the gas generator and periphery of the gas generator, hot partially cracked gases were generated and allowed to mix with the air from supersonic intakes.

Reactive flow field in DCR was investigated numerically by Navier-Stokes equations and chemistry reaction models. Lab scale combustors were analyzed by Large Eddy Simulation (LES) methods, however for a full size DCR, as the Reynolds number is extremely high (1.0x 10^7) LES could not be applied. Reynold average Navier stokes (RANS), RNG k-ε turbulence

model, finite rate chemistry model were adopted. Both experimental results and numerical analysis were compared and validated.

In another study, Situ, *et al.* [36] investigated on combustion of hydrocarbon fuel rich hot gas in supersonic air stream by injecting the fuel rich hot gas generated from a subsonic burner parallel to the free stream. Ignition was reliably proven between total temperature 880k and 1700k. Experimental studies were carried out in a two-dimensional wind tunnel to study the effect of fuel air equivalence ratio on combustion efficiency and pressure recovery by investigating the effect of heat release on mixing process. Wall pressures rise location in both reacting and non-reacting flow conditions was experimentally determined., combustion efficiency for different equivalence ratio was reported as 0.5 to 0.68.

A two dimensional direct connect wind tunnel was used to conduct the experiments; fuel rich hot gas generated from a subsonic dump combustor was injected supersonically to achieve supersonic ignition and flame spreading in shear layer. Wall pressures and the effect of shocks in mixing of two streams were computed and confirmed that the interaction between the mixing region and oblique shocks enhance the hot gas air mixing in the shear layer.

2.4.2 Freejet mode experimental work on DCR

Tan, *et al.* [38] carried out freejet experimental studies of a full-size DCR, focusing on thrust and specific impulse. The DCR studied in these tests was a robust and practical system which can be investigated as an option for its use as power plant for a missile. The outcome of this study was:

- A DCR with cavity is proposed, for efficient operation in a range of Mach 4 to Mach 6.5.
- Study of the performance of full scale DCR under various conditions of attack angle α, equivalence ratio φ, and flight Mach number.
- A cavity is applied to enhance mixing and combustion
- Unlike conventional DCR, it is not necessary to inject all the fuel in the preburner (for decomposition), some of the fuel injected into the combustor can also burn efficiently.
- Combustion is efficient due to boundary layer induced by the cavity rather than on the free shear layer between peripheral air and central fuel-rich gas
- Bleeding holes are applied in the intakes to increase the capability of total pressure recovery.

The DCR model considered for freejet testing for this study and its geometrical parameters of the test article are shown in Figure 2-14 and Table 2-2

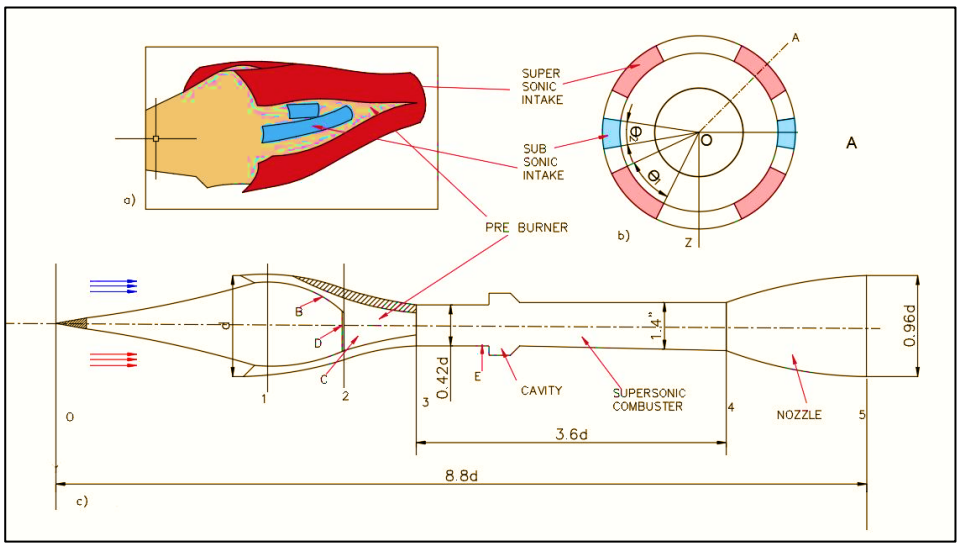

Figure 2-14 DCR model considered for freejet testing and its geometry [37]

Table 2-2 Geometrical Parameters of the DCR [37]

Item	Unit	Value
Diameter of the missile	mm	d
Diameter of the combustor inlet (3)	mm	0.42d
Diameter of the nozzle exit	mm	0.96d
Divergent angle of the combustor	deg	1.4
Ratio of windward area	null	0.50
Area ratio of subsonic intakes to supersonic ones	null	0.25
Total length of the DCR (sections 1-5)	mm	8.8d
Length of the combustor (sections 3-4)	mm	3.6d
Depth of the cavity	mm	20
Length of the cavity	mm	120

During the freejet testing, DCR performance was evaluated in 3 stages. Initially flight drag was evaluated in stage 1, later in stage 2 only preburner was ignited and the thrust coefficient was evaluated and found to be negative and in the last stage supersonic combustor was ignited and positive thrust coefficient achieved is compared with stage 2 value. Pressure ratio distribution of supersonic intakes, combustor and subsonic intakes was evaluated, and a thorough characterization was done (shown in Figure 2-15 and Figure 2-16).

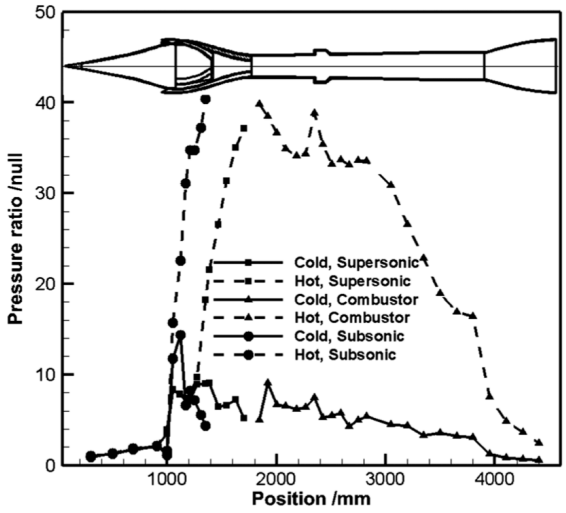

Figure 2-15 Distribution of pressure ratio of supersonic intakes, combustor, and subsonic intakes at Mach 4 flight condition [37]

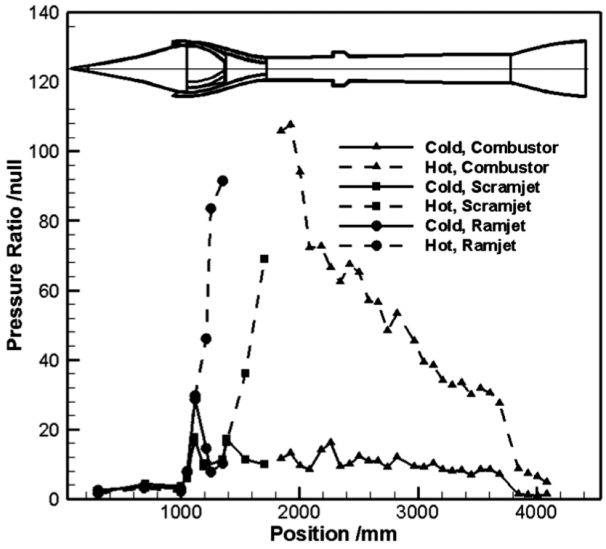

Figure 2-16 Distribution of pressure ratio of supersonic intakes, combustor, and subsonic intakes at Mach 6 flight condition [37]

In hot flow tests, the pressure along the streamwise direction increases sharply in the intakes and decreases in the supersonic combustor. The maximum pressure is located at the exit of the subsonic intake (for Mach 4) or the inlet of the combustor (for Mach 6) and the pressure ratio reaches the limit of the intake implying that the DCR reaches its maximum performance. The pressure distribution at Mach 6 is different from that at Mach 4. At Mach 4, isotonic pressure exists for a long distance which indicates that combustion is subsonic. At Mach 6, the pressure decreases rapidly within 0.2 m, and then it continually decreases at the exit of the combustor

indicating the flow is supersonic, and the total pressure loss is caused by heat release. Additionally,

- Effect of equivalence ratio on the DCR performance, corresponding thrust coefficients at M4, M6 and M6.5 conditions
- Specific impulse variation at M4, M6 and M6.5 conditions
- Effect of angle of attack in terms of maximum thrust coefficient

were studied and all the results were reported.

2.4.3 Studies on combustor-Isolator interactions in DCR

Combustor Intake interactions study is very important for design of Ramjet/Scramjet propulsion systems. High Combustion-induced backpressures make the shock train propagate upstream further and interfere the flow of inlet and the scramjet would unstart. The study has more relevance especially for the propulsion systems like Dual combustion Ramjet (DCR) due to its wider range operation of Shock train generates in the isolator to decelerate the supersonic flow with sufficient strength. If the combustion-induced backpressures were big enough to make the shock train propagate upstream further and interfere the flow of inlet, the scramjet would unstart which should be prevented, During the operation of scramjet, the shock train constantly varies its length and structure to match the upstream and downstream conditions. The quality of outflow at the isolator exit has great impact on the combustion performance since the violent oscillation of shock train may lead to flame oscillation or even flame out. Combustor Intake interactions knowledge is very important for design of Ramjet/Scramjet propulsion systems.

Isolator is a critical component which does not allow shock train to interact with combustion chamber. Worldwide many researchers have numerically studied isolator and shock train phenomena.

Jong-Ryul, *et al.* [38] carried out experiments to study isolator interaction with combustion chamber and evolved correlation for estimating wall static pressure. Experiments simulated flight Mach numbers from 4 to 5 , altitude from 20 to 25km . Isolator entry Mach number. are 1.8, 2.0, 2.23 for flight Mach number. 4, 4.5, 5 respectively. Liquid hydrocarbon fuel is injected in gas generator at different equivalence ratio varying from 0.0 to 3.0 for all above mentioned conditions. With change in equivalence ratio pressure increase in the

combustor and to match pressure combustor pressure, pre-combustion shock train is established in isolator. With increase in equivalence ratio shock train in isolator moves upstream. During study it is concluded that shock train is less affected by isolator inlet Mach number. Experimental work was also compared with existing empirical correlations of Waltrup and Billig's correlation and and Stockbridge's correlation. Correlations did not match with experiments for annular isolator. New correlation for DCR is proposed and additional term of equivalence ratio is introduced which was missing in previous correlations.

Zhang, *et al.* [39] numerically investigated and compared effect of isolator shock train with back pressure and combustion. It was found that shock train movement is due to back pressure but is also affected by high temperature which entrains through boundary layer. This temperature shrinks and stretches shock train.Wei Huang, *et al.* [40] studied three-dimensional scramjet isolator and position of shock train with varying back pressure and increase in divergence angle of isolator. With increase in divergence angle of isolator, it is observed that shock wave transition takes place from oblique shock to normal shock and back to oblique shock. Fei Xing, *et al.* [41] has proposed use of bleed slot for reducing load on isolator. This reduces total pressure loss but also has reducing effect on combustion efficiency.

Yubao He, *et al.* [42] has suggested reduction of subsonic region by ejecting cracked gas. This leads to increase on total momentum and suppresses pressure gradient.

Stockbridge, *et al.* [43] has carried out similar experiments to evaluate isolator wall pressure rise in annular duct with non-reacting setup. Back pressure is built by blockage of the exit.Numerical simulation was done by using Fluent to solve RANS equations and a two-equation shear stress transport (SST) k–ω model was used as turbulence simulation for predicting the wall pressure distribution of the transverse injection. It was observed that at lower equivalence ratio, weak combustion heat release led to absence of shock train in isolator and increase in static pressure of isolator entrance led to the whole pressure rise. But at higher equivalence ratio, a reverse trend was observed in the pressure variation in isolator and combustor. Lesser the incoming Mach number, shorter was length of the shock train and pressure peak lifted.

Detailed studies of the effect of backward oscillations are carried out by many researchers [44] to [46]. Wenxin Hou, *et al.* [44] investigated experimentally on shock train self-excited oscillation influenced by background waves occurring within an isolator in a direct-connect wind tunnel using high-speed schlieren technique and high-frequency pressure

measurements. Top-Large-Separation, Bottom-Large-Separation, and transition mode of shock train self-excited oscillations were studied. To understand the differences of shock train unsteady behaviors in different modes, the distributions of intermittent region and zero-crossing frequency were compared. For the shock train in a uniform incoming flow and for the shock train influenced by background waves, the Strouhal number range is predicted. It was found that the wall pressure gradient caused by background waves influences the unsteadiness of shock train self-excited oscillation.

Wen Shi, *et al.* [45] investigated the forced oscillations of shock train caused by sinusoidal backpressure perturbations with different amplitudes and frequencies in a hypersonic inlet equipped with translating cowl. Numerical simulations conducted with the application of dynamic mesh method reveal that under sinusoidal backpressure perturbations, the shock train oscillates and propagates upstream as the cowl moves downstream rather than crosses the shock-impact points abruptly with significant migration distance, compared to the result obtained under constant backpressure. Effect of back pressure perturbations on forced oscillations, number of shock impact points crossed by shock train in one cycle and there by the shock train structures variation was studied. In another study, Wen Shi, *et al.* [46] have carried out numerical investigations to study the path dependence characteristic of shock train with the application of dynamic mesh method. Based on the paths of shock train leading edges, it is discovered that the behavior of shock train is highly related to the variable background waves. The results also reveal that the path dependence characteristic embodies in the abrupt motions, average velocities of shock train, structures of shock train and oscillations. It is concluded that the discrepancies of critical internal contraction ratios that lead to the hysteresis loops in the paths of shock train leading edges; the structures and average velocities of shock train in opposite directions of translating cowl are different in each loop. The shock train would oscillate around the separation bubble, which intensifies the unsteadiness of shock train behavior.

In the flow path of the combustor which is supersonic in nature, shockwaves and boundary layer interaction when intensified, boundary layer thickens and tends to separate. If the pressure rise due to combustion is high enough precombustion shock train starts and separates the boundary layer and the flow pressure increases to a higher value in the combustor and leads to intake unstart. To achieve intake performance, an isolator must be provided with

a suitable length covering the entire operating range. In DCR similar shock structure exists in the annular duct and isolator should stabilize it to prevent the combustion induced disturbances.

Waltrup and Billig conducted experiments by using a nonreacting system simulated by throttling /overexpanded supersonic airflows in cylindrical ducts for the pre- combustion shock structure of the scramjet [47]-[49]. Combustor entry Mach numbers ranging from 1.53 to 2.72 were simulated in these tests and based on the test results, empirical correlations defining the length of the precombustion shock train and wall static pressure distribution as a function of Mach number, Reynolds number, Boundary layer momentum thickness and the combustor geometry were defined. But the overall length of the PCST predicted by the correlation was underestimated for a given pressure rise and the two empirical correlations by Waltrup and Billig; Stockbridge [49] were questioned.

The most interesting experimental study was from Jong-Ryul Byun, *et al.* [38] where it was experimentally investigated to study the combustor–isolator interactions in the DCR engine

- Experimentally generated database for the DCR combustor–isolator interactions
- Evaluated the validity of the existing empirical correlations by Waltrup and Billig

$$\frac{s_t(M_2^2-1)Re_\theta^{0.25}}{D^{0.5}\theta^{0.5}} = 50\left(\frac{P_s}{P_2}-1\right)+170\left(\frac{P_s}{P_2}-1\right)^2$$

…Eq(2.4)

Where P_S/P_2: Pressure Ratio

M_2: Isolator inlet Mach number,

Re_θ: Reynolds number,

D: Duct diameter and

θ: Boundary layer momentum thickness

- Proposed a new empirical correlation for the DCR isolator equipped with an annular airflow duct /cylindrical duct

Wall static pressures were measured for supersonic flows of annular isolator, supersonic combustor. For varying inlet Mach numbers and equivalence ratios of the supersonic combustor, the precombustion compression field is analyzed experimentally. The presented

results are compared with the existing empirical correlations. Modified empirical correlations and corresponding theoretical model applicable to the DCR combustor–isolator is presented and compared with the test results. Experimental setup and the simulated test conditions are shown in Figure 2-17 and Table 2-3 and Table 2-4.

.

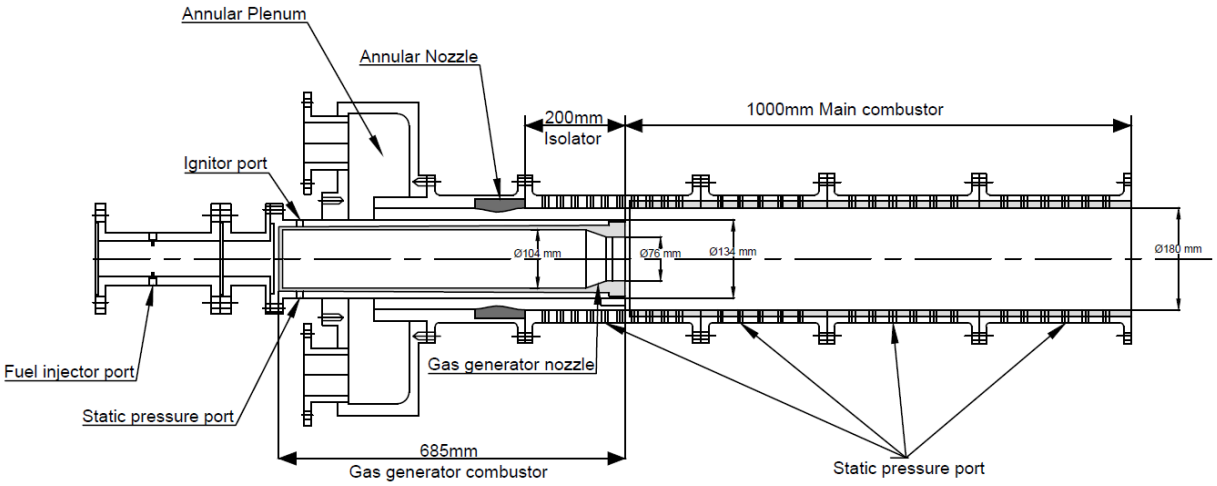

Figure 2-17 Schematic of experimental setup for DCR combustor [38]

Table 2-3 Test conditions of airflow [38]

Case	M_2	Air flow condition T_t ,K	P_t ,kPa	Total air mass, kg/s	Air split ratio
A	1.79	925 ± 7.5	555.9 ± 7.0	7.71 ± 0.3%	3.00
B	1.98	1105 ± 10.0	479.9 ± 8.0	5.20 ± 0.7%	2.96
C	2.23	1120 ± 11.0	610.1 ± 8.0	5.28 ± 0.7%	2.98

Table 2-4 Fuel equivalence ratios [38]

Case	Equivalence ratios $Ø_{gg}$	$Ø_t$
A	0.74-3.05	0.18-0.76
B	0.98-3.10	0.25-0.78
C	1.02-3.17	0.26-0.80

The length of the shock train estimated based on the time averaged wall pressure distribution data at different equivalence ratios was found nearly constant or decreasing trend. The lengths S_t and S_d referred in the flow field diagram shown below are largely influenced by combustor conditions and less influenced by isolator entry Mach number.

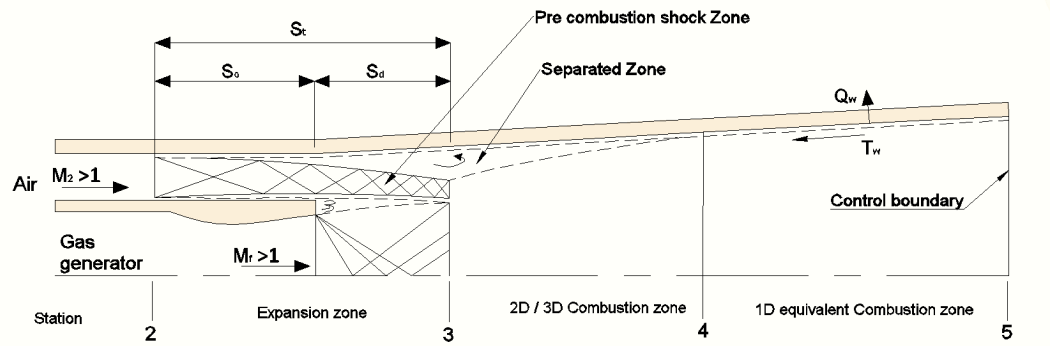

Figure 2-18 Schematic of flow field in supersonic combustor of a DCR [38]

New Empirical Correlation for overall Shock-Train Length was established by the following considerations based on the experimental data:

$$\phi_t^{0.52}\left(\frac{D_h}{s_t}\right)\left(\frac{M_2^2-1}{M_2^2}\right)Re_\theta^{0.25}\left(\frac{D_h}{\theta}\right)^{0.5} = \left(\frac{135}{100}\right)\left(\frac{P_s}{P_2}-1\right)+\left(\frac{145}{100}\right)\left(\frac{P_s}{P_2}-1\right)^2$$

..Eq(2.5)

1) In the new correlation, $(M_2^2 - 1) / M_2^2$ is adopted instead of $(M_2^2 - 1)$ used Billig's correlation as the overall length of the pre-combustion shock train was found to be less sensitive to the variation of the isolator entrance Mach number.
2) It is assumed that the shock-train length s_t varies inversely with the maximum pressure rise Ps/P_2
3) The pressure ratio should depend on the equivalence ratio and be proportional to the equivalence ratio. The form $\varphi^k t$ was introduced, and k = 0.52 was obtained from a regression analysis of the experimental data.
4) The Reynolds number Re_θ and the boundary-layer momentum thickness θ dependencies remain the same as in Waltrup and Billig's correlation [49].

2.5 Test facility requirements for DCR engine

Despite carrying out extensive CFD studies, final acceptance of any propulsion system is done by conducting experiments in an environment as close as possible to that of flight environment. The facilities for testing air breathing engines are very expensive, complex and requires heavy infrastructure. Hence very few countries could establish such facilities and most of them are

shared by all the researchers across the globe. It is clear from the literature or from the experience of any developing agency that the tests on ram/scramjet propulsion systems can be done in multiple stages with specific objectives in mind for each test matrix. Basically, two types of tests are essentially carried out, first in 'direct-connect" facility to prove the combustor performance and in second stage "freejet" tests are carried out to evaluate the complete engine/cruise vehicle. DCR /SCRAMJET propulsion systems are usually tested in two phases. The first and the most used facility is the Connect pipe mode facility, where the combustor along with full scale flow path, the fuel feed system can be tested for combustor performance, heat flux estimation, fuel ignition and injection studies by simulating the combustor entry conditions. The second method is freejet testing where the complete propulsion system, intake and the structure are tested in an integrated manner by simulating the flight conditions and burn durations to ensure the aero-propulsive performance.

2.5.1 Direct-connect test facility

A direct-connected test facility is equipped with a Vitiated Air Heater (VAH) and the DCR combustor (test article). Vitiated air heater uses Air, oxygen and hydrogen as fuels, and they are allowed to burn to generate vitiated air to simulate different flight altitude and flight combustor entry Mach number. The mass flow rates are controlled by using suitable flow capable pressure regulators to achieve the required conditions. The total pressure, the total temperature and the flow rate in the VAH are evaluated, and the mass flow fraction of oxygen in the combustion product is ensured as 23%. Concentration of water vapor and carbon dioxide in the products of VAH makes it different from pure air. The presence of these elements affects the combustion and makes it different from that of pure air. The test bed nozzles are designed to ensure the conditions Mach number and static parameters. In these tests 100% of the vitiated air is allowed to pass through the combustor flow path and sets the specified conditions near the inlet and the isolator region.

Both VAH and the DCR combustor are installed rigidly on a movable structure, and the structure is fixed to a bed with pliable plates that allows displacement. Feed system pipes from all the media systems and associated valves, filters, transmit the air, the oxygen, the hydrogen from high-pressure (up to 20 MPa) vessels to the VAH. Hydrocarbon fuel used is pumped upto the engine in pressure fed mode and injected into the DCR combustor at the specified timing for ignition. Nitrogen is used as pressurizing gas for liquid. Scheduling of supply of all

propellants is done as per the countdown sequence. A Programmable Logical Control system is used to control the pneumatic valves remotely and monitor the status of the system during the test.

2.5.2 Freejet Test Facility

In freejet testing, the engine and the inlet geometry of the flying vehicle are placed in the flow field to accurately measure the forebody and inlet distortion effects. For simulating a constant dynamic pressure trajectory, the total pressure to be simulated at multiple Mach numbers; very large power of the order of 500 to 1000MW is needed.

In free jet tests, the effect of oblique shocks on the forebody boundary layer, which in turn leads to local separation near isolator and increase in the boundary layer thickness in the flowpath along the wall result in decrease the maximum sustainable back pressure limit. In direct connect tests, these distortions cannot be captured.

Additionally, the static pressure at the exit of the expansion nozzle is influenced by operating altitude due to compressions emanating from the missile. These effects can be captured well in freejet tests equipped with suitable vacuum systems

The freejet test facility also consists of a vitiated air heater (VAH), a hot-gas ejector, and a test control system. The heater generated high-temperature gas simulates the stagnation conditions of the real freestream, total pressure, total temperature, and an oxygen concentration of 23%. The mass flow rates of the heater fuels are controlled according to required flight altitudes and flight Mach numbers. The mass flow rate of the air is used to control the total pressure, that of the hydrogen is used to control the total temperature, and that of the oxygen is used to keep the concentration of oxygen. A convergent–divergent nozzle installed ensures the gas supply into the test cabin with the same static pressure and Mach number as those of the freestream.

An ejector system is needed downstream to eject the gas into ambient atmosphere to maintain a low-pressure environment in the cabin. A hot-gas generator is needed to improve ejecting efficiency. The kinetic energy from the ejector is large enough to entrain the gas from the heater into the normal pressure ambience.

The procedure to run the freejet test is as follows: first, the ejector shall establish a low- pressure environment; second, the heater shall ignite and burns steadily, and the Mach number and the static pressure in the test cabin reach the predetermined values; and at this stage, after the stable flow field is established, the DCR ignition command is issued with the fuel injected on schedule.

Measurements of mass flow rate, pressure, and thrust are made by turbo flow meters, by independent piezoresistive pressure sensors and through a six-component strain-gauge balance respectively. The measurement error is to be taken into account, and the balance should be calibrated in situ.

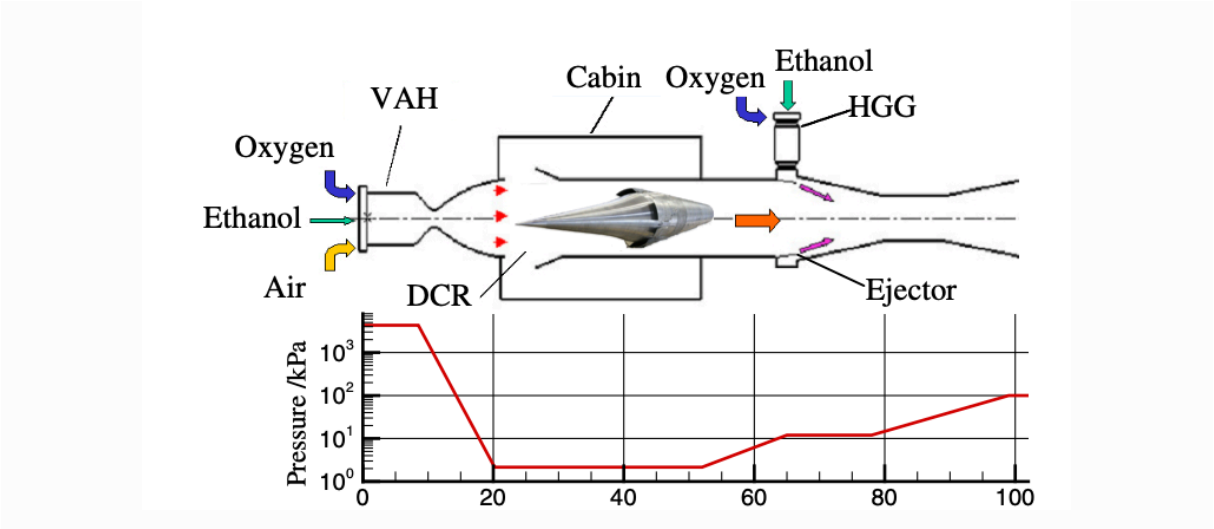

Figure 2-19 Schematic Layout of freejet test facility used for DCR testing and its test sequence [37]

2.6 Summary of the literature review

Dual combustion ramjet propulsion is one of the innovative ideas that is under investigation for achieving higher envelope of flight for hypersonic/supersonic flight weapon systems since 1980. Since it offers the advantages of both ramjet and scramjet in the same engine, this technology offers good flexibility in the design of long-range hypersonic weapons. Using liquid hydrocarbons is an obvious choice for long storable weapons due to its storability and stability properties in addition to the energetics. Popular Fuels like Jet-A, RJ-4, JP-7, JP-10 are the typical fuels being used in multiple air breathing propulsion systems.

Research was actively carried out in the fields of DCR cycle analysis, it's combustion processes, intake performance requirements, coupling effects of intake and the combustor, fuel

injection schemes. Countries like USA, Russia, China, S. Korea and France have contributed in this technology and few operational/developmental flight tests were also conducted by USA. The flight regime between M4 and M6 was thoroughly analyzed and the optimal requirements of the inlet design, combustor design were identified. Performance of the propulsion system in each phase of the trajectory at different flight Mach numbers was predicted and few correlations were evolved to understand the mission studies.

The advantage of an embedded fuel rich gas generator was captured well and the issues of ignition of a typical supersonic combustion were mitigated. Usage of high-density hydrocarbon fuels, partial cracking of the fuel in the gas generator and then allowing the cracked products to take part in supersonic combustion were studied theoretically and experimentally. Important physical and chemical processes, effects of heat release on the upstream pressure field were modeled. Mixing model, turbulent transport model and chemistry of DCR were presented.

Numerous studies on the numerical simulations of the complex flow field of the DCR propulsion system have been published. The methodology to be adopted for modeling of the supersonic combustor was discussed highlighting the need aspects of engineering tools such as integral analyses, solutions to full Navier-Stokes equations considering viscosity and chemistry. Numerical modeling of DCR turbulent combustion was carried out by solving fully coupled equations of energy conservation, momentum and species with a RANS turbulence model and combustion was modeled with eight reacting species. Flow and flame dynamics of hydrocarbon fueled DCR engine, the shock structures appeared immediately downstream of the gas generator exit were studied; interaction of the gas generator hot gases and airflow from the isolator and their effect of creating expansion fans in the supersonic combustor were predicted. Numerical simulations are performed under both chemically frozen and reacting conditions.

Connect pipe mode and freejet tests were conducted on the lab-scale/ full scale combustors and the validation studies, modification of few theoretical correlations were also attempted. Combustor -isolator interactions were studied experimentally and evolved correlation for estimating wall static pressure for various Mach numbers, altitude of flights and different equivalence ratios of O/F.

The necessity of nonintrusive measurement techniques in the experimental work for accurate measurement of particulate size, velocity, temperature, density and species were highlighted by researchers.

2.7 Observations from the Literature

The major advantages and findings associated with realizing DCR based propulsion system and its vehicle are detailed below:

1. DCR based engines perform without any ignition problems unlike pure scramjet engines.
2. DCR propulsion allows the vehicle designer to boost it to lower Mach numbers of the order of M3 or M4 condition and accelerate to higher altitudes in air breathing mode and cruises at hypersonic speeds at M6 for the remaining mission duration. This feature reduces the lift off weight of the vehicle drastically as it need not be boosted to higher altitudes using chemical propulsion rockets.
3. In flight regime of Mach 4 to 8, DCR performs better at the lower flight Mach numbers and scramjet performs better at higher Mach numbers
4. Between DCR and ramjet powered vehicles, the DCR exhibits better performance at and near cruise at the highest flight Mach number if both are designed to have the same maximum net thrust at Mach 3 for Mach 3 to 6 flight.
5. Specific impulse is maximum at higher Mach number and higher equivalence ratio.
6. Partial cracking of the fuel in the gas generator and using it as fuel for supersonic combustor mitigates the ignition problems of scramjet engine.
7. For fuel rich gas generator, ignition was reliably proven between total temperature 880K and 1700K.
8. Shock train generates in the isolator to decelerate the supersonic flow with sufficient strength. During the operation of scramjet, the shock train constantly varies its length and structure to match the upstream and downstream conditions. The quality of outflow at the isolator exit has great impacts on the combustion performance since the violent oscillation of shock train may lead to flame oscillation or even flame out. Combustor Intake interactions knowledge is very important for design of Ramjet/Scramjet propulsion systems.
9. Fuel-air mixing at the turbulent shear layer is very important in DCR combustion process.
10. Coupling between the compressibility effects and the turbulent combustion changes the modes of combustion to thermal choking; thermal choking location changes based on the divergence angle of the combustor.

11. Connect pipe tests revealed that in M4 condition, subsonic flow field is established in front portion of the combustor and there is a thermally choked region; in M6 condition, central flow is subsonic and lower static temperature is resulted due to the peripheral supersonic airflow.
12. With increase in equivalence ratio variations in shock train in the isolator were reported.
13. Combustor entry Mach numbers ranging from 1.53 to 2.72 were simulated in tests and empirical correlations defining the length of the precombustion shock train and wall static pressure distribution as a function of Mach number, Reynolds number, boundary layer momentum thickness were defined.
14. Numerical simulations are done by using turbulence model for predicting the wall pressure distribution. At lower equivalence ratio, weak combustion heat release led to absence of shock train in isolator and increase in static pressure of isolator entrance led to the whole pressure rise. But at higher equivalence ratio, a reverse trend was observed in the pressure variation in isolator and combustor.
15. Configuration, design, performance of DCR is a strong function of its size and hence each design becomes unique and needs extensive numerical and experimental studies.
16. Generating experimental/numerical data for a given configuration is essential and it is not possible to develop a DCR based system based on standard set of procedures as it is highly coupled to its flight conditions, intake-combustor interactions and many other parameters.
17. Combustion efficiency varies drastically depending upon the equivalence ratio, operating Mach numbers and the intake-combustor geometry.
18. Connect pipe mode tests and freejet tests are essential to understand the combustor performance, intake-combustor coupled system performance, ignition issues, thermal management of the system.

2.8 Gaps observed from the literature review

Being a potential technology for military applications, the critical aspects of the technology published in open literature gives generic details of the work and its results. Literature on DMRJ/DMSJ types of systems was abundantly available but that of DCR is less published especially in the field of experimental studies. Information on know-how of practical systems, its design, test methodologies is scarce. It is observed that the following areas, more so with

experimental studies and computational analysis, did not receive much attention of the researchers' in addressing the challenges associated with DCR propulsion system:

1. Design requirements and constraints for all sub-systems of DCR of any given configuration are to be evolved based on specific design/application. This knowledge is neither available in the form of standard design procedures nor in the form of standard codes.
2. Experimental studies on fuel rich gas generator and development of simple tools for their qualitative/quantitative validation for full scale working systems keeping a weapon system as an end application.
3. DCR based air-launched weapons are generally designed as axisymmetric and the configurations evolved usually demands for cylindrical shape for various reasons. Studies related to flow field of an axisymmetric ramjet/scramjet with annular isolator are less investigated especially in choosing the suitable turbulence model for this class of studies and very limited experimental data is available for comparison of the CFD/1-D code results.
4. Geometry parametric studies are not discussed in open literature. Combustor geometry needed to mitigate thermal choking is not discussed in detail.
5. Practical aspects of the propulsion system components, their integration, testing and performance evaluation of these systems is not available in detail.

2.9 Objective and Scope of Research Work

The aim of the research work is to investigate liquid hydrocarbon fueled "Dual Combustion Ramjet" propulsion system numerically and experimentally over a variable Mach number range between 4 to 6 for highspeed applications specific to propulsion system.
Major Objectives of the current investigations are:

1) **Evolving the design requirements for the intended application, identifying the constraints**

2) **Gas generator characterization**

   a. Experimental characterization with multiple tests for M4 condition
   b. Development of 1-D Model and its validation

3) **Numerical studies on combustor flow field**

   a. Numerical studies on combustor- annular Isolator interactions in axisymmetric liquid hydrocarbon fueled DCR
   b. Various turbulence models comparison
   c. Validation with experimental data
   d. Combustor geometry Parametric studies
   e. Numerical simulations for Prediction of performance for M4 and M6 conditions for the full-scale geometry

4) **Full scale DCR proto testing**

   a. Fabrication of the combustor Proto hardware for testing
   b. Test facility modifications and characterization
   c. Connect pipe mode testing of integrated “Gas generator” and “Supersonic combustor” of DCR engine at M6 condition
   d. Discussions on the numerical and experimental results

Chapter 3

METHODOLOGY – EXPERIMENTAL AND COMPUTATIONAL INVESTIGATIONS

After identifying the gaps in the literature related to present scope of work, to meet the objectives presented in the previous Chapter, the work is divided into the categories of both experimental and computational investigations.

To begin with, the work is sub-divided into 4 major tasks as detailed below:

1) **DCR design methodology**
    a. Design aspects of critical sub-systems viz: Intake, gas generator, supersonic combustor, nozzle etc.
    b. DCR Propulsion cycle analysis

2) **Gas generator characterization**
    a. Development of 1-D Model
    b. Experimental characterization with multiple tests and its qualitative validation with the 1-D model

3) **Numerical studies on combustor flow field**
    a. Numerical studies on combustor- annular Isolator interactions in axisymmetric liquid hydrocarbon fueled DCR
    b. Validation with experimental data of literature
    c. Numerical study of Combustor geometry Parametric studies
    d. Numerical simulations for critical parameters for M4 and M6 conditions for the full-scale geometry

4) **Full scale DCR proto realization and static testing**
    a. Fabrication of the combustor Proto hardware for testing
    b. Test facility modifications and characterization
    c. Connect pipe mode testing of integrated "Gas generator" and "Supersonic combustor" of DCR engine at M6 condition with truncated intakes
    d. Test data analysis

Methodology followed for both experimental and computational investigations is explained in this chapter. Results are discussed in the next chapter.

3.1 DCR Propulsion system design criterion

In this part, the design requirements, specifications, constraints of all critical sub-systems of DCR are discussed and the preliminary specifications of each sub-system are evolved based on few basic design studies. This exercise gives the information on design goals of DCR subsystems. Sizing of the DCR system depends on the vehicle needed (its size) and its performance requirements in the mission. Based on the vehicle frontal cross section area (assumed), drag data on the vehicle at different flight trajectories shall be used as an input data to start the design exercise. Assuming reasonable acceleration (assumed) requirements, the overall thrust requirement from the DCR propulsion system can be arrived at. With the available data of requirements and literature information, a broad propulsion specification was arrived at. Table 3-1 shows the broad propulsion system specifications.

Table 3-1 Typical DCR based Propulsion system Specifications for a highspeed application

Flight Mach number	M4 to M6
Operating Altitude	20 – 28 km*
Fuel options	Conventional Hydrocarbon fuel → Jet-A, RJ-4, JP-10, JP-7
Specific Impulse, I_{SP}	1200 – 1300* s @ M4 conditions (*from literature) 800 – 900* s @ M6 conditions (*from literature)
Thrust Requirement (depends on the mission)	~ 8000 N @ M4.0, 20 km ~ 4000 N @ M6.0, 28 km
Duration of operation	As needed by the mission (generally few minutes for long range missions)

The DCR propulsion system mainly consists of an

1) External compression cone
2) Internal compression intakes (subsonic and Supersonic)
3) Gas generator
4) Supersonic combustor and
5) Nozzle
6) Fuel feed system.

From the literature studies carried out, it was understood that for design and development of Dual Combustor Ramjet (DCR) based systems, Preliminary studies to be carried out on each of these sub-systems to arrive at the inputs, outputs and design goals for each system are identified and highlighted in Table 3-2.

It is very difficult to study a particular sub-system of the DCR as all sub-systems are highly coupled with each other. In the current investigations, gas generator, isolator, supersonic combustor and nozzle subsystems which form the DCR engine flow path are considered and others are not covered in the scope of current research work.

Table 3-2 Performance requirements of DCR

No	Sub system	Input	Output	Performance parameters
1	External compression cone	Dimensional constraints, M, Altitude, Ps, Ts, Alpha, Beta	Intake entry M, Ps, Mass ingested	Pressure recovery > 40% at all M Optimised performance for all M Alpha, Beta effects minimum Boundary Layer management – Bleed/divert
2a	GG intake	• Intake entry M, Ps, • Mass ingested	• GG entry M, Ps, Ts, • Passage design	• GG entry Mach number < 0.5 • Wider operational margin • Pressure rise control
2b	SC intake	• Intake entry M, Ps • Mass ingested	• SC entry M, Ps, Ts • Isolator design	• SC entry Mach number 1.5 – 2.3 • SC entry Pressure • PCST control (Annular Isolator performance)
3	Gas Generator	• Entry M,Ps,Ts • Fuel injection • Fuel equivalence ratio	• 1-D Model, • Pressure rise in GG • Temperature • Injector design • Throat Size • Gas composition	• Achieving ignition at high equivalence ratio, • Predicting the performance of gas generator, • C* efficiency • Fuel distribution scheme
4	Scramjet combustor	• Entry M, Ps, Ts • Gas composition, • Temperature	• Pressure distribution • Po, To @ exit • Thrust • Heat flux	• M, Ps, To Contours along the combustor • Combustion efficiency • Heat flux • Thrust @M6 ~4000N
5	Fuel feed system	Fuel flow rate, Injection pressure,	Feed system sizing, flow controller, Pressurisation system	Expulsion efficiency > 98%

3.1.1 Intake System

Intake system comprises of external compression by nose cone and internal compression by in both types of intakes of subsonic gas generator and supersonic combustor. Dual Combustor Ramjet engine has an axisymmetric configuration. For such configurations of the flight vehicles, the most suitable type of intake is either nose intake or a chin intake with streamline tracing design. As described before, DCR engine comprises of a gas generator/ ramjet combustor which digests the total fuel and the hot fuel rich gases generated in the GG is let into the supersonic combustor. This requires the combustors to be placed in tandem and hence increases the length of the missile. This affects the intake configuration due to limitations in the length.

3.1.1.1 External compression cone design criterion:

For the chosen vehicle configuration design, a nose intake is configured with separate sub-sonic and supersonic intake ducts. This configuration is more suitable taking into considerations the vehicle constraints. The important constraints are:

- Depending upon the chosen diameter of the vehicle and Length of the vehicle and due to the mounting configuration of the engine, the nose intake is more feasible. Hence, the intake ducts are configured around the nose cone which is essential for reducing aerodynamic drag and for packaging the sensors and other avionics modules.
- For the axisymmetric nose intakes, separate ducts are configured for the sub-sonic and the supersonic combustor. The dimensions or ratios of the intakes are based on the air flow through these combustors which is approximately 1:3 as per the reported configurations.

Intake configuration is a mixed compression type intake, where the external compression is due to the nose cone, where a conical shock compresses the incoming air. The internal compression is due to the converging ducts where the air gets diverted into the two combustors.

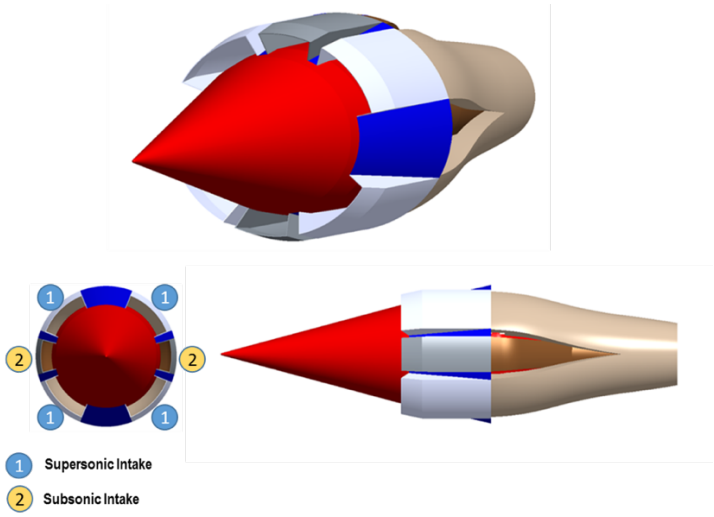

Figure 3-1 Intake configuration

Design approach of external compression cone

DCR (Dual Combustor Ramjet) is configured with six air intakes in which four are scramjet intakes and the other two are ramjet intakes, as shown in Figure 3-1. The objectives of the air intake design shall be:

- Capture the exact amount of air required by the engine
- Decelerate the flow to the required engine entry Mach number (~M2) with minimum total pressure loss
- Deliver the air with tolerable flow distortion and minimize the contribution to the internal drag of the system.

Design considerations depend on the overall system requirements and leads to specific inlet characteristics like cowl, duct, and compression region in the flow path. Design was carried out by designing a a straight cone with 15^0 half angle. The fore-body shall be designed in such way that the conical shock from the nose should hit the intake entry lip. In order to achieve this, the following dimensions for the cone are required:

- Cone length: Sufficient length from apex to intake entry (base point),
- Cone base diameter: 75% of vehicle diameter
- Intake should be attached to duct.

Preliminary simulations for this analysis are done using FLUENT and it was observed that a small separation bubble with about 20% blockage is formed in the intake ducts at the internal compression region on the cone body due to the impingement of the reflected shock from the cowl lip. Inlet (external + internal) design allows, in general, a safety margin for shock

ingestion and operates at the design point (M6). The air contained in the flow tube between the free-steam air captured by the engine and the entrance is spilled around the cowl, resulting in an additive drag that must be included in the overall drag accounting.

Air properties at different altitudes (28km and 20km), considered for this analysis are shown below:

Table 3-3 Flow properties at various altitudes

Air properties	**20km**	**28km**
Static pressure	0.056 bar	0.016 bar
Speed of sound	289.25 m/s	301.77 m/s
Static temperature	208 K	227 K
Density	0.094	0.0247
Flow properties	**M4 @ 20 km**	**M6 @ 28 km**
Total temperature	791 K	1654 K
Total Pressure	9.69 bar	34.2 bar

Initial conditions are based on two different conditions of Mach number (M4 andM6). The intake entry area is based on the mass flow rates capture which is required for the combustion in the combustor, at different Mach conditions. At M4 the global mass flow rate is 12.91 kg/s out of which 3.25 kg/s of flow rate is required in the subsonic intakes and 9.66 kg/s is required in the supersonic intake. At M6 the global flow rate is 6.5 kg/s out of which that 1.63 kg/s is required for subsonic intake and 4.87 kg/s for supersonic intake. The area ratio from inlet to outlet of the intake duct is 1.25, which will compress the supersonic flow to the required Mach number.

Design of the external compression cone was carried out for the cruise condition of M6. Since fixed geometry compression cones are employed, there is expected to be spillage of flow for off-design condition. The performance of the cone for M4 entry condition (20km altitude) is shown in Figure 3-2.

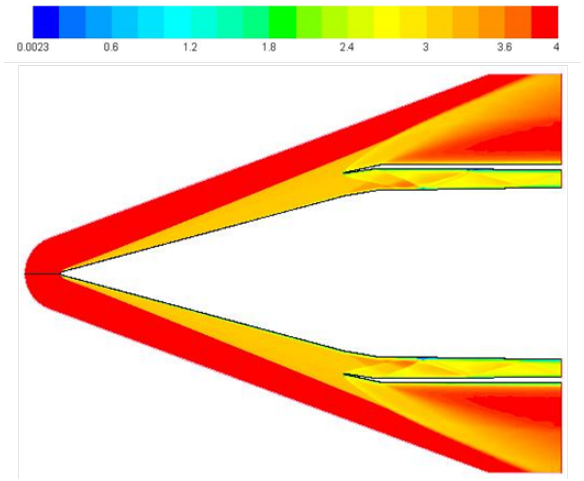

Figure 3-2 Mach contour for flight condition of M4 @ 20kms altitude

Flow conditions at the exit of the cone (entry to the intake) are shown below Table 3-4. The flow conditions are taken at a location 160mm downstream of the intake cowl. This is fed as input for the supersonic intake duct design. The configuration of the external compression is shown below in Figure 3-3.

Table 3-4 Flow conditions at cone exit

Parameter	**(M4 @ 20km)**	**Cone exit (M4) / Intake entry**	**M6 @ 28km**	**Cone exit (M6) / Intake entry**
Mach Number	4.0	2.64	6.0	3.48
Total Pressure	9.69 bar	4.83 bar	34.2 bar	10.95 bar
Ts	208 K	345K	227 K	531 K

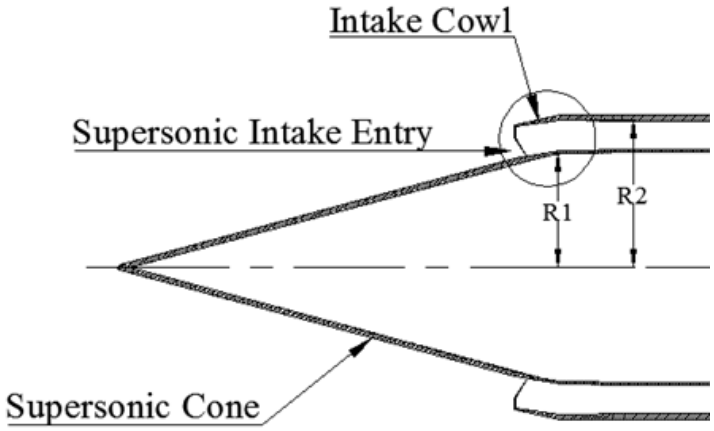

Figure 3-3 Configuration of External cone

3.1.1.2 Supersonic Intake design criterion:

DCR consists of six air intakes, four scramjet intakes and two ramjet intakes as shown in Figure 3-1. Figure 3-4 shows the contour of the intake duct along with the external cone. R1 and R2 of the intake entry is decided based on the external cone design. Sector angle of the intake is designed in such as way so as to ingest the required mass flow into the supersonic intake (4.87kg/s @ M6 for 4 intakes). This comes to be 45˚ for each supersonic intake. The design objective for supersonic intake is:

- Required mass flow rate of air is ingested into the intake.
- Isolator exit / Combustor entry Mach number should be > 2
- Pressure recovery should be higher
- Space for the passenger mounting and gas generator, which is located within the 4 supersonic intakes has to be considered.

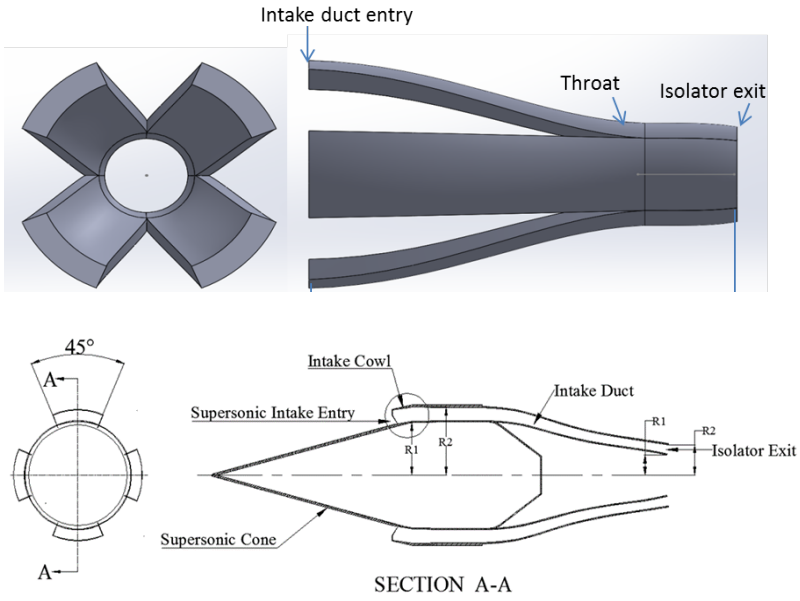

Figure 3-4 Supersonic duct with isolator

The inlet to throat area ratio is 3:1 (based on literature). It is likely that supersonic inlet will compress the incoming air using all its surfaces, thereby resulting in a complex 3D shock-wave system in the duct preceding the combustion chamber entrance. If variable geometry is provided in the intake duct, it will increase the pressure recovery over the entire flight regime of operation.

Isolator is designed to absorb the pressure difference between the intake exit and the combustion chamber, thereby isolating the respective sub-systems. As expected for highspeed flight, the scramjet combustor's inlet will operate with both external and internal compression. The flow path is curved with varied area similar to convergent-divergent nozzle where the flow compression contribution is from all of its surfaces.

Supersonic Intake Duct Configuration

Supersonic intake design is an iterative process and involves 2D/3D analysis. The flow properties at this location are considered as entry conditions for intake duct inlet. The length of intake duct is 842mm. This is arrived based on the gas generator length, which will dictate the supersonic combustor entry location. Supersonic intake duct entry flow properties **(**static and total pressures, Static and total temperature, Mach number) are taken from the 2D intake simulations. Final configuration shall be decided based on isolator exit Mach number of 2.2 and the required mass flow ingestion into the intake with higher pressure recovery.

The final configuration of the intake duct is shown in Figure 3-5. R2 (inner radius at inlet) remains constant from cone exit to intake duct entry. The flow properties (static and total pressures, Static and total temperature, Mach number, mass flow rates) at the end of the isolator exit for M4 and M6 conditions are taken from preliminary calculations.

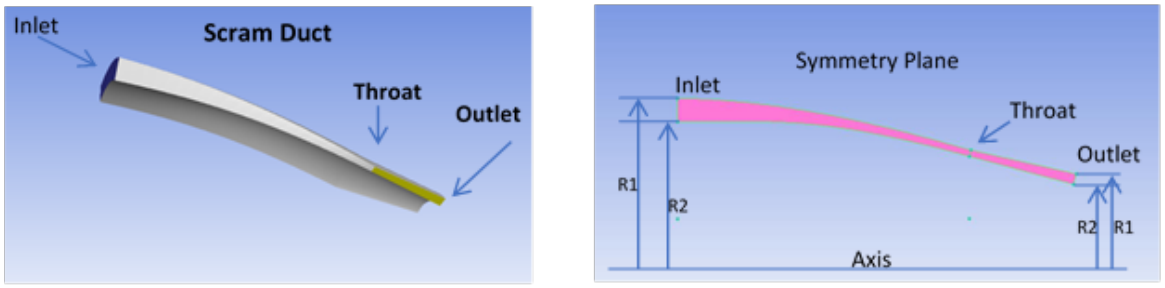

Figure 3-5 Supersonic intake duct configuration

3.1.1.3 Subsonic Intake:

Similarly, the design parameters (static and total pressures, Static and total temperature, Mach number, mass flow rates) for the subsonic intake for M4 and M6 flight conditions are evaluated.

3.1.2 Gas Generator (GG)

The main purpose of the gas generator is to generate fuel rich gases and feed to the supersonic combustor for further combustion. This involves fuel combustion at equivalence ratios greater than 1.0. Problems associated with fuel rich combustion is the ignition itself as the fuel – air mixture will be outside the flammability limit. It is understood from the literature that the fuel is injected into the GG at different locations and this should cater for the following

- Combustion (to raise the air temperature),
- Cooling the GG walls
- Rest of the fuel for cracking/decomposition.

The preliminary sizing and design of GG is explained below.

3.1.2.1 Design specifications of Gas Generator:

As the gas generator plays an important role in the functioning of the DCR engine, it is necessary to carefully design and evaluate before developing the full engine. Total air and fuel mass flow rates for the cruise conditions have been arrived at based on the thrust requirement of the vehicle. Following are the entry conditions to the gas generator shown in Table 3-5.

Table 3-5 Flow entry condition at GG

Parameter	**M6**	**M4**
Total Air mass flow rate (kg/s)	6.5 ± 0.3	12.9 ± 0.7
GG air mass flow rate (kg/s)	1.63±0.1	3.25±0.2
SC mass flow rate (kg/s)	4.87±0.2	9.66±0.5
Global Equivalence ratio	0.8 - 0.9	0.8 - 0.9
GG Fuel mass flow rate	~ 350 g/s	~ 800 g/s
GG equivalence ratio	3.0 to 3.66	3.0 to 3.66
Total temperature (K)	1682 ± 10	849±10

Even though only 25% of the intake air is ingested into the GG, the complete fuel mass is dumped in the GG. This results in higher equivalence ratio (~3.66). The complete combustion of this air with eq 1.0 fuel results in gas temperature greater than 2400K. This hot gas will heat the remaining fuel (corresponding to eq ratio: 2.66), which undergoes endothermic cracking, thereby reducing the temperature and pressure. Hence the objective in GG is to get lesser C* of ~1080, which indicates that cracking of fuel has taken place. This highly reactive fuel from GG is fed to the supersonic combustor for further combustion and thrust generation.

The following are the design objectives for the gas generator:

- Achieve combustor inlet conditions of 3.25 kg/s air flow rate at 800 K temperature for M4 condition
- Ignition and sustained combustion of fuel at highly fuel rich conditions (fuel $\phi > 3.5$)
- Achieve the required C* (1050 to1080 m/s) by varying the fuel injection scheme.
- Finalize GG chamber pressure limits (2.2 barA) determined by throat diameter, combustion / cracking efficiency. This chamber pressure will be input for subsonic intake design.

3.1.2.2 Design Constraints to be considered for Gas generator:

- Maximum back pressure that can be handled by subsonic intake is ~2.0. bar.
- This limits the maximum GG chamber pressure. Throat diameter has to be designed to achieve this. Effect of this variation on C* has to be studied.
- Fluctuations / Variations in pressure will affect the intake performance. Fuel injection sequence should be determined with this constraint in mind.
- Cracking of excess fuel leads to soot formation. Fuel injection scheme should be optimized to minimize soot, since soot formation directly affects the combustion efficiency.
- Cracking of excess fuel leads to reduction of chamber C*. Theoretical C* value for Jet A fuel combustion in air for an O/F ratio of 4.03 is 1028.6. Design optimization to be carried out to get close to this value (~ 1050-1080). Chamber C* and GG throat diameter will determine Chamber pressure. Higher C* will call for a larger throat diameter to keep the chamber pressure under limit. This may lead to undesired sizing to the overall engine.
- Gases like CO, H_2, C_2H_4 etc., are highly reactive. Effort should be made to achieve cracking to produce more of these gases.

3.1.2.3 Preliminary sizing and design of GG:

To understand the basic working of the DCR Gas generator, a hardware was developed with available understanding of a subsonic ramjet combustor. Methodology for preliminary sizing of the GG is mentioned below:

1) The DCR engine is being developed for a hypersonic vehicle of diameter 600mm. Vehicle drag and the acceleration requirements dictate the sizing of the engine. From preliminary calculations, it was understood that the DCR engine must produce a thrust of ~8000N at Mach 4 flight conditions and ~4000N at Mach 6 conditions.
2) With the frontal cross-section area known (Ø 600mm), the mass capture into the engine can be calculated. Of this, 52% of the mass is ingested into the engine to produce thrust. This number is taken from literature [35].

Frontal cross section area = $0.2826\ m^2 \times 0.52 = 0.1467\ m^2$

At M4 condition, there would be flow spillage since the intake are designed for M6. Considering the spillage efficiency of 81% (indicated by CFD)

Effective capture area, A_c = 0.1467 x 0.81 = 0.119 m^2

Mass capture, $\dot{m}_{air}$ = ρAcV

Flow condition for M4@20km corresponds to

Density, ρ = 0.0945 kg/m^3

Static temperature = 208.2 K

Velocity for M4 = 4 x 289.25 m/s = 1157 m/s

Mass capture, $\dot{m}_{air}$ = 13 kg/s

3) Specific impulse of a typical DCR engine is reported in the literature as ~1300s at M4 conditions and ~900s at M6 conditions. These values are taken for calculating the O/F ratios.

At M4 condition, thrust required F_c	= 950 kgf	
I_{sp}	= 1300 s	
Fuel flow rate, $\dot{m}_f$	= F_c / I_{sp} = 0.73 kg/s	
Hence O/F ratio	= $\dot{m}_{air}/\dot{m}_f$ =	= 17.8
Overall equivalence ratio, ϕ	= 14.7/(O/F)	= 0.83
Mass capture in GG, $\dot{m}_{air\ gg}$	= 0.258 x $\dot{m}_{air}$	= 3.25 kg/s
O/F ratio in GG	= 4.45	
Equivalence ratio in GG, ϕ_{gg}	= 14.7/4.45	= 3.3

4) 25% of all the air ingested is diverted to Gas generator [35]. All the fuel is injected into GG. NASA CEA code is used to calculate the C* value of the mixture. Chamber pressure is calculated by assuming a normal shock at the intake followed by a 10% 'dump loss' (loss due to dumping of air at an angle into the gg) and a 10% 'Rayleigh loss' (loss due to fuel combustion). As the mass flow rate, chamber pressure and C* are known, the throat area of the GG can be estimated. This comes to Ø 164mm.

Theoretical C* = 1080 m/s

Throat area to limit the chamber pressure, P_c to 2 bar = ($\dot{m}_{air\ gg}$ x C*) /P_c = 0.0176 m^2

Throat Diameter = 150mm

5) From the throat diameter, other dimensions can be empirically calculated; Chamber diameter is 1.5 times the throat area (Ø225mm), Minimum chamber length → 2 times the chamber diameter (450mm).
6) Fuel injection scheme for GG – one portion of fuel (local ϕ-1.0) will be injected into the intake tubes for early mixing and combustion. This ensures reliable ignition. One portion of fuel will be injected along the circumference of the GG walls. This is used as a coolant in film cooling of the GG and the rest of the fuel will be injected in the centre of the GG for partial cracking into smaller and reactive molecules (~ ϕ-1.0 at intake, ~100g/s for film cooling).
7) Significant amount of testing has to be carried out to understand the performance of the gas generator.

Design of fuel injection scheme for the gas generator:

Fuel injection is one of the critical processes in the combustion of the ramjets. In DCR, flow rates are different for different operating conditions. Hence the maximum and minimum flow rates are considered for M4 and M6 conditions respectively. The total quantity of the fuel required for is 800 g/s for M4 condition and 400 g/s for M6 condition. Multi staging fuel distribution scheme is designed to meet the different operating conditions The scheme is as follows:

a) For maximum flow condition of M4 case:

- Intake arm 1 : 100 g/s
- Intake arm 2 : 100 g/s
- Central Swirl Injector : 450 g/s
- Pilot Swirl Injector : 30g/s
- Wall cooling : 120g/s

b) Flow for condition of M6 case:

- Central Swirl Injector and Pilot Swirl Injector : 450 g/s to 400 g/s (to be finalized based on the further tests)

Central swirl Injector design calculations:

The function of the injector is to atomize the fuel, mix intensely with the incoming air to provide efficient ignition and combustion processes.

Fuel flow rate, $\dot{m}_f$: 450g/s

Pressure drop considered, Δpf : $9x10^5$ Pa

Spray Cone angle : $90° \pm 10$

Assumptions *:*

Discharge Coefficient : $C_d = 0.24$

No. of Tangential ports, n : 4

Swirl Number,Ns : 4

Swirl injector is designed based on the guidelines given by "Spray and Atomization by H Lefebvre".

Exit orifice diameter d_0 is calculated by $\sqrt{\left(4.\dot{m}_f\right) / \left(\pi.\mathrm{Cd}.\sqrt{2.\rho f.\Delta Pf}\right)}$

Summary of the results are:

Table 3-6 Swirler Injection elements design parameters

Dimension	Central Swirler	Pilot Swirler
Swirl chamber diameter	24mm	9mm
Swirl chamber length	21.6mm	8mm
Orifice Diameter	8mm	2.7mm
Length of the orifice	4mm	1.4mm
Tangential port size	3.5mm	1.2mm
Swirl number	4	4
Spray Angle	92°	108°

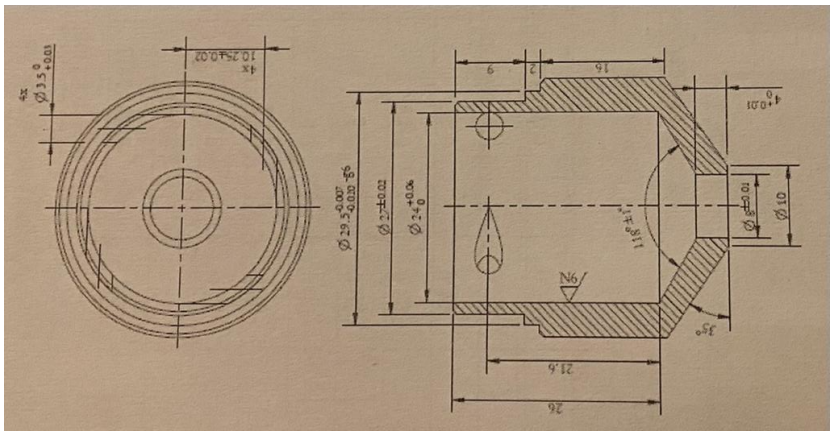

Figure 3-6 Central Swirler Configuration

3.1.3 Supersonic combustor

Fuel rich gases from the GG and air from supersonic intakes mixes and burns in the supersonic combustor. Sufficient length needs to be provided to ensure complete combustion of the fuel in the scramjet combustor. Fuel (gases from GG) will be flowing in the core of the combustor

and the oxidizer (air from supersonic intakes) will be flowing annularly around it. The Wall between the GG and scramjet isolator will act as flame holder for the supersonic combustor. This flame holder will also be used to generate axial vortices, which would improve the mixing between the fuel and oxidizer jets.

3.1.3.1 Design approach of Supersonic combustor

Scramjet combustor configuration design an iterative process with flow simulations. It was understood from the literature that

- the mixing of the two co-flowing jets will improve with the impinging angle of the scramjet intake flow ~ 140° intake angles was found to be optimal. Mixing improves with higher angles, but losses also increase.
- Flame holder thickness also affects mixing and combustion. A thickness of 15mm was selected. Length of the combustor was taken as 2100mm (literature). This length includes constant area mixing section and rest with marginal divergence to compensate for the pressure rise.
- During non-reacting flow simulations, to estimate the mixing performance in each of these iterations, 'spread-ratio' shall be considered. Spread ratio is a parameter which shows "Goodness of mixing" or "Degree of mixing". Spread ratio may be defined as ratio of mixing region length at axial location of 1000mm from the combustor entry and mixing region length at combustor entry. Mixing region is defined as the radial distance of lateral diffusion / mixing of Oxygen into the core fuel jet. Higher Spread-ratio means better mixing and therefore better combustor performance. It was also observed from reacting simulations that combustion efficiency improves with spread-ratio.

Table 3-7 Design parameters for supersonic combustor

Thrust	Thrust @M4 ~8000N (includes nozzle) Thrust @M6 ~40000N (includes nozzle)
Combustor wall Heat Flux	< 90 W/cm^2 (cold wall) and < 5 W/cm^2 (1800 K)
Combustion efficiency	~ 80%

Design of supersonic combustor and simulations are to be repeated for getting better efficiencies from combustor, by varying the flame holder design. Following is to be planned on the while developing the supersonic combustor:

- Simulations on various mixer/flame holder designs
- Identify ways to improve mixing and combustion efficiency

- Optimize fuel injection scheme and fuel equivalence ratios to achieve the above task
- Finalize Combustor configuration and fabricate the combustor for testing
- Testing of engine in truncated intake + combustor configuration.
- Carryout design modifications if any.

3.1.3.2 Design Constraints to be considered for supersonic combustor:

Design constraints for the supersonic combustor include the following:

- Maximum back pressure that can be handled by subsonic intake / Supersonic intake is ~2.0 – 2.5 bar. This limits the peak pressure in engine isolator.
- Fluctuations / Variations in pressure will affect the intake performance. Fuel injection sequence should be determined with this constraint in mind.
- Operating margins for the engine will be determined by thrust requirement on one end and Intake un-start on the other end. Fuel modulation and equivalence ratio will be determined by these two requirements.

3.1.4 Nozzle

Nozzle of the DCR engine is major thrust producing component. As the entry to the nozzle is always supersonic, a diverging area nozzle is needed. Contoured nozzle will be designed to achieve maximum thrust out of the engine with minimum losses. Simple parabolic contour nozzle was used along with combustor simulations. Constraints considered for the nozzle design are

1. Overall diameter of the proposed missile
2. Overall length of the missile.

With these constraints, the length of the nozzle comes to 950mm and exit diameter 570mm. Static testing of the nozzle was not attempted due to facility constraints.

3.1.5 Hydrocarbon Fuel Feed system

3.1.5.1 Hydrocarbon Fuel selection criteria

Following are the desired fuel properties for air breathing applications.

- High density : More volumetric energy
- Low Freezing point : High altitude conditions
- Low viscosity : Aid better fuel spray atomization

- High flash point : Safety during handling
- High Heat of combustion : Energy release during combustion / thrust
- Low Soot formation : Better combustion efficiency
- Oxidation stability : Fuel storage / Reduced gum formation
- High Thermal Stability : Higher boiling point / Reduced gum formation at elevated temperature
- Low corrosion : Better storage

Based on the above desired fuel properties, following fuel candidates have been identified for DCR

- RJ-4 : Endo- and Exo-tetra Hydro Di Methyl Di Cyclo Penta Diene (TH-MCPD)
- JP-10: Exo- tetra Hydro Di-Cyclo Penta Diene (TH-CPD)
- JP-7
- Jet A

Of the above five fuel candidates, RJ-4 and JP-10 are synthetic single component hydrocarbon molecules whereas the Jet A, JP-7 are multicomponent petroleum distillate fractions. The synthetic hydrocarbons RJ-4 and JP-10 have a correspondingly higher densities compared to petroleum distillate fractions Jet A/JP-7.

3.1.5.2 Comparison of the selected hydrocarbon fuels:

Table 3-8 Comparison of fuel properties

Property	**Jet A**	**JP-7**	**JP-10**	**RJ-4**
Density (kg/m^3)	0.81	0.79	0.94	0.915-0.93
Molecular formula	$C_{11}H_{21}$	$C_{12}H_{25}$	$C_{10}H_{16}$	$C_{12}H_{20}$
Viscosity@(-20°C)	8	8	10	20 max (-18 °C)
Boiling Range, °C	165-265	190-250	185	232 max
Flash point, °C	53	60	54 min	60-79
Aromatics, % vol	25	5	NIL	NIL
Sulphur, total, wt %	0.30	0.10	NIL	0.005
Freezing point, °C	-51	-44	-79 max	- 47 max
Net Heat of combustion (KJ/ kg)	43,140	43,895	42,100	42,260

3.1.5.3 Fuel Selection Methodology:

For Ramjet / Scramjet engine operation, the selected fuel must have a high density in order to have higher volumetric energy content. The fuel candidates shall be subjected to thermal decomposition studies in a bomb calorimeter to study their thermal stability and decomposition products. The fuel for static test shall be selected such that its performance matches with the performance |with MIL grade fuel apart from the meeting the other major criteria mentioned below:

- High density
- Fuel availability and cost

The following are the properties of the fuel that must be considered while selecting a fuel for ramjet/Scramjet application:

- Density: Min 0.90 g/cc @ 15 °C
- Freezing point: Max -43.3 °C
- Flash point: 60 °C (min)
- Viscosity at -20° C: 8 mm^2/s (max)
- Aromatic content: 5 % by volume (max)
- Sulphur, total: 0.1 % by mass (max)
- Net heat of combustion: 43.5 MJ/kg (min)
- Existent gum content: 5 mg/100 ml (max)

3.1.5.4 Fuel feed system specifications:

The DCR based propulsion system is being developed to propel a hypersonic cruise missile to a maximum range. A fuel feed system needs to be developed which will ensure supply of fuel at required flow rate and pressure to the DCR engine throughout the mission. The following are the specifications for the fuel feed system.

Table 3-9 Fuel flow specifications for DCR

S.No	Parameter	Value
1	Fuel Flow rate	~800 g/s @ M4 flight ~350 g/s @ M6 flight
2	Fuel Injection pressure	As per the system requirement
3	Total fuel required for the mission	Mission dependent
4	Fuel Pressurization method	Pneumatic / Electric pump
5	Fuel flow rate controller required	Yes based on mission's needs

3.1.6 Engine thermal management

Thermal management scheme for DCR engine comprises of combination of passive and active cooling techniques.

- Passive cooling is achieved by providing a suitable insulating material over the combustor wall. Silica based Low Density Ablative material is one of the candidates for passive insulation due to its low thermal conductivity and low density.
- Active cooling is achieved by means of the fuel flowing through micro channels in the engine outer wall, before being injected into the combustor.

3.1.6.1 Thermal loads on the supersonic combustor:

The temperatures in the flow path at gas generator, supersonic combustor and nozzle of DCR engine are shown in Figure 3-7.

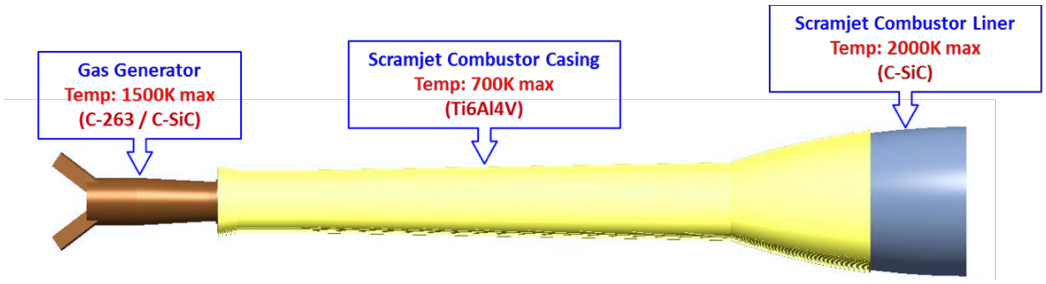

Figure 3-7 Maximum temperature regions on the DCR engine

The various sections of the vehicle, where thermal management is required, and the expected maximum temperature is given below:

Table 3-10 Predicted Maximum temperatures across engine sections

S.No	Vehicle section	Maximum Expected temperature (K)	Thermal management scheme options
1	Air intake leading edges	1800	Tungsten/C-SiC
2	Scramjet combustor casing	2000	C-SiC or C103 /LDAM/Ti
3	Gas generator	1500	C-SiC/C-263

C-SiC : Carbon Silicon Carbide
Ti : Titanium
C-103 : Niobium alloy grade C-103
LDAM : Low Density Ablative Material

It is observed that, if the combustor is operated at a design temperature of 1500 K, the maximum input heat flux is 25 W/cm^2. The maximum input heat flux for the combustor wall temperature of 1200 K is of the order of 50 W/cm^2. High temperature composite material such

as C-SiC can withstand temperature up to 2500 K. On the other hand, if a high temperature composite material C-SiC is selected for the combustor and operated at a higher design temperature of 1800 K, the maximum input heat flux faced by the combustor wall can be reduced to less than 6 W/cm^2. This reduces the load on the active cooling mechanism. Since the fuel tank is mounted over the engine, the maximum temperature on the engine wall should be limited to 700 K. Lesser the input heat flux to the combustor wall, lesser shall be rise in temperature of the fuel that flows through the micro channels. It is desirable to limit the maximum fuel temperature to 650 K, as higher temperature leads to cracking of the hydrocarbon fuel to gaseous cracked products that affects the heat transfer in the coolant channels. The other important aspect that must be considered is the fuel operating pressure. The hydrocarbon fuel must be pumped through the channels at a higher pressure if it is designed to operate at a higher temperature in order to avoid any phase change in the coolant passage.

The design constraints for thermal management have been listed:

3.1.6.2 Design constraints for Thermal management:

- For C-SiC, the maximum operating temperature < 2000 K
- For metals the maximum operating temperature < 1600 K
- Fuel temperature < 650 K
- Fuel operating pressure < 30 bar (TBD)
- Fuel mass flow rate: Limited by the equivalence ratio required for engine (800g/s @ M4 and 350g/s @ M6)
- Combustor casing outer wall temperature < 700K

3.1.6.3 Parameters to optimize/select for thermal management of combustor casing:

The following are the parameters that need to be optimized

- Thickness of the insulating material
- Thermal conductivity of the insulating material (material selection)
- Fuel flow rate through the channel and Fuel channel sizing: Channel Shape/Channel Size
- Engine casing material selection

3.2 DCR Design based on cycle analysis

DCR design calculation has been carried out for Mach 6 condition. The inputs for design calculation are given in the table below:

Table 3-11 Design inputs

SNo.	Parameters	Case1	Case2
1	Flight Mach number	6	4.5
2	Altitude of operation	28 km	22 km
3	Uninstalled Thrust (Nom.)	~4000N	~8000N
4	Gamma	1.4	1.4
5	Gas constant, R_{air}	287 J/kg	287 J/kg
6	Freestream conditions*		
	Static pressure	0.016 kg/cm^2	0.041 kg/cm^2
	Static temperature	224.53 K	218.57 K
	Total temperature	1841.1K	1103.8 K
	Total pressure	26.012 kg/cm^2	11.941 kg/cm^2
	Dynamic viscosity of air	1.4646x10^{-6} kg/m/s	1.4322x10^{-5} kg/m/s
	Thermal conductivity of air	0.0198 w/m/k	0.0198 w/m/k
7	Specific heat capacity of air	1252 J/kg/K (@ 2000K)	
8	Stoichiometric fuel-air ratio	0.068	0.068
9	Fuel enthalpy	42.81 MJ/kg	42.81MJ/kg

Freestream conditions are taken from standard US atmospheric data [24].

Notations specific to this section:
0: Free stream condition

C: Max. Capture station

1: Intake entry station

3: Isolator entry station/Intake exit location/Oblique shock train end location of GG

4: Isolator exit station/GG post normal shock location

5: After Burner station

e: Engine exit station

3.2.1 Supersonic Intake Pressure Recovery

Supersonic Intake of DCR is a mixed compression intake type i.e. part of compression is external and a part of it is internal. Total temperature remains same as total enthalpy remains constant across shock. Using stagnation temperature relationship maximum static temperature rise can be written as:

$$\frac{T_3}{T_0} = \frac{1 + \frac{k-1}{2} \cdot M_0^2}{1 + \frac{k-1}{2} \cdot M_3^2}$$

..Eq(3.1)

In extreme case when M3 = 0, maximum static temperature ratio can be given by

$$\frac{T_3}{T_0} = 1 + \frac{k-1}{2} \cdot M_0^2 = 8.2$$

For M = 6 flight condition, static temperature rise considered is 3.91, which gives static temperature at the entry to isolator as

$$T_3 = \left(\frac{T_3}{T_0}\right) \cdot T_0 = 877.9\ K$$

Isolator entry Mach number is calculated using following relation from Heiser and Pratt [3],

$$\frac{T_3}{T_0} = \left(\frac{1 + \frac{k-1}{2} \cdot M_0^2}{1 + \frac{k-1}{2} \cdot M_3^2}\right) \cdot \frac{T_{03}}{T_{00}}$$

$$M_3 = 2.1$$

Kinetic energy efficiency is the common parameter used to quantify the efficiency of supersonic intake. The usefulness of this parameter lies in that it can be used for nonideal gas processes and that its value is independent of flight Mach number for a class of inlets. It is defined as the ratio of kinetic energy the compressed flow would achieve if it is expanded isentropically to freestream pressure, relative to the kinetic energy of the freestream. The following two correlations developed is used for calculating the kinetic energy efficiency.

Using Smart [50] correlation, adiabatic kinetic energy efficiency is given by,

$$\eta_{KE_{AD}} = 1 - \left(\frac{9}{M_0}\right)^{0.7} \cdot \left[0.018 \cdot \left\{1 - \frac{M_3}{M_0}\right\} + 0.12 \cdot \left\{1 - \frac{M_3}{M_0}\right\}^4\right] = 0.9562$$

…Eq(3.2)

Using Heiser and Pratt [3] correlation, intake compression efficiency is given by,

$$\eta_c = 1 - \frac{k-1}{2} \cdot M_0^2 \cdot \left[\frac{1 - \eta_{KE_{AD}}}{\frac{T_3}{T_0} - 1} \right] = 0.892$$

..Eq(3.3)

Total pressure ratio across a supersonic intake is calculated by using relation given by Heiser and Pratt [3]

$$\eta_{KE_{AD}} = 1 - \frac{2}{(k-1) \cdot M_0^2} \cdot \left[\left(\frac{P_{00}}{P_{03}} \right)^{\frac{k-1}{k}} - 1 \right]$$

$$\frac{P_{03}}{P_{00}} = 0.383$$

$$P_{03} = P_{00} \cdot \left(\frac{P_{03}}{P_{00}} \right) = 9.971\ kg/sq.cm$$

Flow velocity at isolator entry is given by, $U_3 = \sqrt{2 \cdot C_p \cdot (T_{00} - T_3)} = 1553.0\ m/s$

..Eq(3.4)

3.2.2 Supersonic Combustor Calculation

Maximum temperature rise for a given fuel-air ratio at a given flight Mach number and assuming constant heat capacities and assuming adiabatic flow in the inlet and nozzle can be expressed as

$$T_{05\_max} = \left[\frac{f_{st} \cdot \frac{h_f}{C_p \cdot T_0}}{1 + f_{st}} \cdot \frac{1}{1 + \frac{k-1}{2} \cdot M_0^2} + \frac{1}{1 + f_{st}} \right] \cdot T_{00} = 3901\ K$$

..Eq(3.5)

Where,

f_{st}: Stoichiometric fuel to air ratio ; C_p: Specific heat capacity of air @ 2000K.

h_f: Fuel enthalpy (J/kg)

Assuming a combustion efficiency (η_{comb}) of 0.9, the total temperature rise across combustor is given as

$$T_{05} = \left[\frac{f_{st} \cdot \frac{\eta_{comb} \cdot h_f}{C_p \cdot T_0}}{1 + f_{st}} \cdot \frac{1}{1 + \frac{k-1}{2} \cdot M_0^2} + \frac{1}{1 + f_{st}} \right] \cdot T_{00} = 3683.3\ K$$

Mach number of the flow post combustion is an input for the design calculation and it should be such that flow is supersonic as well as it is low enough to allow sufficient residence time in order to achieve efficient combustion. To start with, it is taken as 1.4. However, actual number can be decided based on experimental data.

$$M_5 = 1.4$$

Static temperature after combustion is then given as

$$T_5 = \left(\frac{T_{05}}{1 + \frac{k-1}{2} \cdot M_5^2} \right) = 2646\ K$$

..Eq(3.6)

From enthalpy balance with constant Cp assumption, fuel-air ratio is given as

$$f = \frac{\frac{T_{05}}{T_{00}} - 1}{\frac{h_f}{C_p \cdot T_0} - \frac{T_{05}}{T_{00}}} = 0.0604$$

..Eq(3.7)

Equivalence ratio is then given as

$$\emptyset = \frac{f}{f_{st}} = 0.888$$

..Eq(3.8)

As a general guideline given in Heiser andPratt [3], equivalence ratio must be in the range of 0.2 – 2.0 for combustion to occur within a useful timescale and burner combustion pressure vary from 0.5 to 10 atm. Stagnation pressure post heat addition can be then calculated using Rayleigh line equations for a perfect gas [24] as

$$P_{05} = P_{03} \cdot \left(\frac{1 + k \cdot M_3^2}{1 + k \cdot M_5^2} \right) \cdot \left(\frac{1 + \frac{k-1}{2} \cdot M_5^2}{1 + \frac{k-1}{2} \cdot M_3^2} \right)^{\frac{k}{k-1}} = 6.616$$

..Eq(3.9)

And static pressure post heat addition from stagnation condition relation is given as

$$P_5 = \frac{P_{05}}{\left(1 + \frac{k-1}{2} \cdot M_5^2\right)^{\frac{k}{k-1}}} = 2.079 kg/sq.cm$$

..Eq(3.10)

3.2.3 DCR Nozzle Exit Conditions

Total pressure and temperature in the nozzle remain the same as after combustion if nozzle flow is assumed isentropic i.e.

$$P_{0e} = P_{05} \quad \text{and} \quad T_{0e} = T_{05}$$

Static pr ratio between DCR inlet to its nozzle exit is taken as 62.5 i.e.

$$\frac{P_e}{P_0} = 62.5$$

DCR nozzle exit flow Mach number and static temperature is then given as

$$M_e = \sqrt{\frac{\left(\frac{P_{0e}}{P_e}\right)^{\frac{k-1}{k}} - 1}{\frac{k-1}{2}}} = 1.873$$

..Eq(3.11)

$$T_e = \left(\frac{T_{0e}}{1 + \frac{k-1}{2} \cdot M_e^2}\right) = 2164.7\ K$$

..Eq(3.12)

Flow velocity ratio across DCR and exit flow velocity is given as

$$\frac{U_e}{U_0} = \frac{M_e}{M_0} \cdot \sqrt{\frac{T_e}{T_0}} = 0.969$$

..Eq(3.13)

$$U_e = U_0 \cdot \frac{U_e}{U_0} = 1745.7\ m/s$$

Post combustion flow velocity is given as

$$U_5 = M_5 \cdot \sqrt{k \cdot R_{air} \cdot T_5} = 1442.8\ m/s$$

Mass flow rate of air required to achieve the given uninstalled thrust requirement at flight Mach condition 6 is given as

$$\dot{m}_a = \frac{T}{(U_e - U_0) + f \cdot U_e} = 7.011\ kg/s$$

..Eq(3.14)

Mass flow rate of fuel and total flow rate is given as

$$\dot{m}_f = f \cdot \dot{m}_a = 0.423\ kg/s$$

$$\dot{m}_{tot} = \dot{m}_a + \dot{m}_f = 8.473\ kg/s$$

Intake total flow capture using continuity equation is calculated as

$$A_0 = \frac{\dot{m}_a}{\rho_0 \cdot U_0} = 0.155\ m^2$$

Supersonic intake flow capture area as 75% of the flow only passes through it is given as

$$A_{0SI} = \frac{0.75 \cdot \dot{m}_a}{\rho_0 \cdot U_0} = 0.116\ m^2$$

Equivalent capture diameter is given as

$$D_{oSI} = \sqrt{\frac{4 \cdot A_{0SI}}{\pi}} \cdot 1000 = 384.7\ mm$$

Flight dynamic pressure force for hypersonic flight lies between 20-90kPa. For this case it is calculated as

$$q_0 = \frac{k \cdot P_0 \cdot M_0^2}{2} = 40.7\ kPa$$

..Eq(3.15)

Thrust coefficient is given as

$$C_f = \frac{T}{q_0 \cdot A_0} = 0.544$$

..Eq(3.16)

Uninstalled thrust equation for an airbreathing engine is given using mass and momentum conservation as

$$T = \dot{m}_a \cdot (U_e - U_0) + (P_e - P_0) \cdot A_e + \dot{m}_f \cdot U_e$$

..Eq(3.17)

The thrust equation can be written in dimensionless forms by normalizing it by P_0A_0 which compares thrust to a force equal to the ambient pressure multiplied by the capture area. And it is essential that this number in order to overcome drag be considerably larger than 1. Therefore, dimensionless form of thrust is given as

$$\frac{T}{P_0 \cdot A_0} = k \cdot M_0^2 \left((1 + f) \cdot \frac{U_e}{U_0} - 1 \right) + \frac{A_e}{A_0} \cdot \left(\frac{P_e}{P_0} - 1 \right)$$

..Eq(3.18)

For a given thrust, exit to entry area ratio using above equation is calculated as

$$\frac{A_e}{A_0} = 0.2$$

Therefore, exit area and diameter is

$$A_e = A_0 \cdot \frac{A_e}{A_0} = 0.031$$

$$D_e = \sqrt{\frac{4 \cdot A_e}{\pi}} \cdot 1000 = 198.7\ mm$$

Using mass conservation, combustor area is estimated as

$$A_5 = \frac{\dot{m}_{tot}}{\frac{P_5}{R_{air} \cdot T_5} \cdot \left(M_5 \cdot \sqrt{k \cdot R_{air} \cdot T_5}\right)} = 0.019\, m^2$$

..Eq(3.19)

$$D_5 = \sqrt{\frac{4 \cdot A_5}{\pi}} \cdot 1000 = 156.2\, mm$$

Intake flow area calculation is done using 1-D mass flow conservation in terms of the stagnation pressure and temperature which is given as

$$\dot{m} = \left(\frac{P_t \cdot A}{\sqrt{k \cdot R_{air} \cdot T_t}}\right) \cdot f(M) \cdot \left(\frac{k}{\left(\frac{k+1}{2}\right)^{\frac{k+1}{2 \cdot (k-1)}}}\right)$$

..Eq(3.20)

Where,

$$f(M) = \left(\frac{k+1}{2}\right)^{\frac{k+1}{2 \cdot (k-1)}} \cdot \frac{M}{\left(1 + \frac{k-1}{2} \cdot M^2\right)^{\frac{k+1}{2 \cdot (k-1)}}}$$

This gives a direct connection between the local flow area and Mach number for adiabatic, isentropic flow of a calorically perfect gas along a duct. Using the above relation between intake entry and exit, intake exit area is calculated as

$$A_3 = \left(\frac{\frac{P_{00} \cdot f(0)}{\sqrt{T_{00}}}}{\frac{P_{03} \cdot f(3)}{\sqrt{T_{03}}}}\right) \cdot A_{0SI} = 0.01\, m^2$$

..Eq(3.21)

Equivalent intake exit diameter is the given as

$$D_{3eqv} = \sqrt{\frac{4 \cdot A_3}{\pi}} \cdot 1000 = 112.8\, mm$$

Similar calculation has been carried out for Flight Mach number condition of 4.5 at 22 km. The design calculation is summarized in table below.

Table 3-12 Flow rates (kg/s)

S No.	Parameters	Case1	Case2
1	Equivalence ratio	0.888	0.836
2	Air mass flow rate	7.011	14.148
3	Fuel mass flow rate	0.423	0.804
4	Total flow rate	7.434	14.953

Table 3-13 Flow Mach number

SNo.	Parameters	Case1	Case2
1	M_0	6.00	4.50
2	M_3	2.10	1.00
3	M_5	1.40	1.30
4	M_e	1.87	1.46

Table 3-14 Flow Velocity (m/s)

SNo.	Parameters	Case1	Case2
1	U_0	1801.2	1332.8
2	U_3	1553.0	1091.7
3	U_5	1442.8	1209.1
4	U_e	1745.7	1314.6

Table 3-15 Static temperature (K)

SNo.	Parameters	Case1	Case2
1	T_0	224.5	218.57
2	T_3	877.9	688.50
3	T_5	2646.0	2155.50
4	T_e	2164.7	2022.85

Table 3-16 Total temperature (K)

SNo.	Parameters	Case1	Case2
1	T_{00}	1841.1	1103.8
2	T_{03}	1657.0	827.8
3	T_{05}	3683.3	2884.0
4	T_{0e}	3683.3	2884.0

Table 3-17 Static pressure (kg/cm^2)

SNo.	Parameters	Case1	Case2
1	P_0	0.016	0.041
2	P_3	1.079	2.035
3	P_5	2.079	1.461
4	P_e	1.030	1.170

Table 3-18 Total pressure (kg/cm^2)

SNo.	Parameters	Case1	Case2
1	P_{00}	26.012	11.941
2	P_{03}	9.971	3.878
3	P_{05}	6.616	4.048
4	P_{0e}	6.616	4.048

Table 3-19 Flow diameter (mm)

SNo.	Parameters	Case1	Case2
1	D_0	444.3	457.4
2	$D_{3eqv.}$	112.8	183.5
3	D_5	156.2	260.5
4	D_e	198.7	284.7

The DCR Sizing has been carried out with Case 2 i.e., M 4.5 condition as flow rate requirements are higher for this case.

3.3 Gas Generator characterization

Dual combustion ramjet technology based high speed vehicle uses subsonic gas generator where it dumps all its fuel and its combustion with incoming rammed air coming from subsonic intake takes place in such a manner that partially cracked fuel is generated. These fuel rich gases then enter supersonic combustor as core flow for mixing and combustion with the annular rammed air coming from supersonic inlet. As all the fuel gets dumped into subsonic gas generator before entering the supersonic combustor, it's also called sometimes as dump combustor. Typically, one-fourth of total captured air is diffused through a subsonic inlet to dump combustor. The fuel rich exhaust gases enter the supersonic combustor where it undergoes secondary combustion in supersonic flow. The dump combustor aids in easier ignition and more stable combustion, higher performance at low Mach number. It helps in achieving a wider range of operating flight Mach number (typically 3.5 – 7) with hydrocarbon-based fuel system. The upper limit is due to energy consumption by dissociating and ionizing species at elevated temperature, which cannot be compensated for by additional fuel as in the case of a diatomic gas such as hydrogen.

In gas generator, liquid fuel injection into heated air stream, mixture formation, ignition and combustion need adequate modeling of evaporation. Combustion of mostly widespread hydrocarbon fuels takes place in a gas-phase regime. Thus, evaporation of fuel from the surface of droplets is one of the limiting factors for non-uniform reacting mixtures. Gas generator configuration is shown in

Figure 3-8. The major components of gas generators are:

1. Subsonic Intake side arm
2. Head end dome height
3. Fuel distribution scheme
4. Combustor

Subsonic intake side arm is used to supply rammed air from subsonic intake to gas generator. It can vary from 2 to 4. Head end dome height purpose is to provide the recirculation region for flame holding. Fuel distribution scheme is used to supply required mass flow rate with good atomization and mixing in the combustor. And combustor role is to provide sufficient time for mixing of fuel with rammed air and generation of partially cracked fuel and its supply to main supersonic combustor.

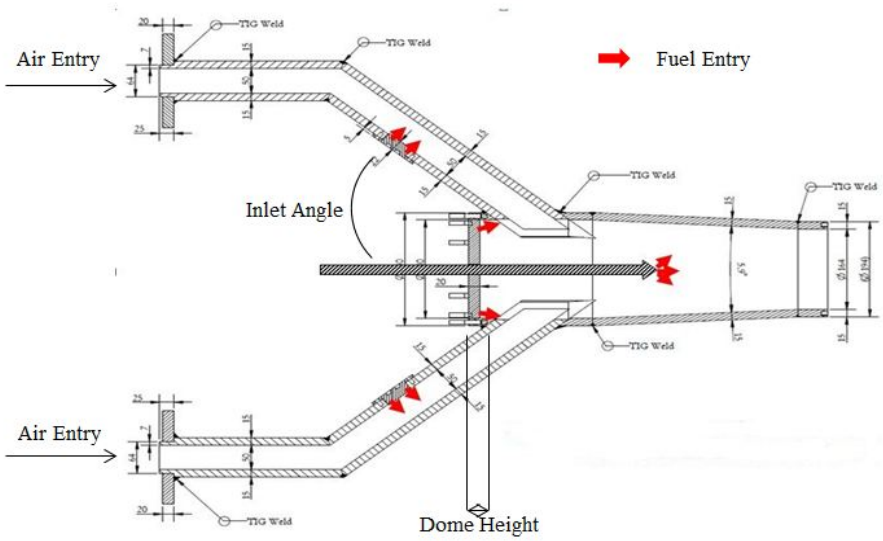

Figure 3-8 Gas Generator configuration [Present research]

Gas generator does not contain conventional combustion liners and flame holders. Therefore, the performance parameters depend on recirculation regimes formed during mixing and flame holding. Mixing and flame holding depends on following parameters:

1. Inlet flow angle
2. Head end dome height
3. Momentum ratio

Effect of Inlet flow angle: Inlet flow is the angle that rammed air coming from subsonic intake makes with the gas generator flow axis. It varies usually from 30° to 90°. Higher the inlet flow

angle the better is the recirculation, mixing and flame holding i.e., 90°>60°>45°>30° [19]. With increase in inlet flow angle recirculation size decreases but recirculation strength increases. Recirculation zone provides greater residence time for fuel to react with air in combustor in order to maintain sustained flame for its complete burn duration. When the fuel and air is mixed, two different recirculation regimes can be observed – passive and impinging regime.

Passive Regime: The passive regime is found to exist at high air/fuel momentum ratios when the off-axis fuel jets were observed to "bend back" and passively follow the incoming air stream as shown in the Figure 3-9.

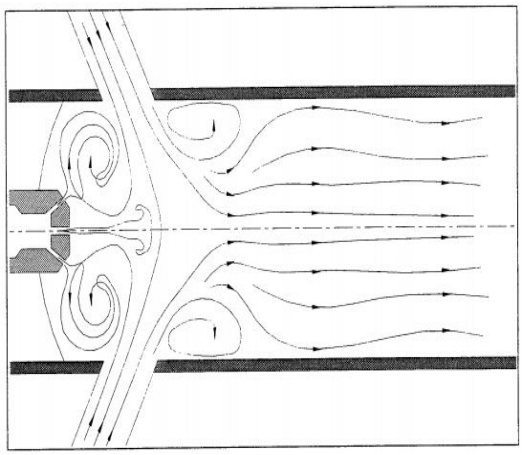

Figure 3-9 Passive Recirculation Regime [21]

Impinging Regime: The impinging regime exists at low air/fuel momentum ratios where the off-axis fuel jets dominated the flowfield and impinged on the incoming air stream as shown in the Figure 3-10.

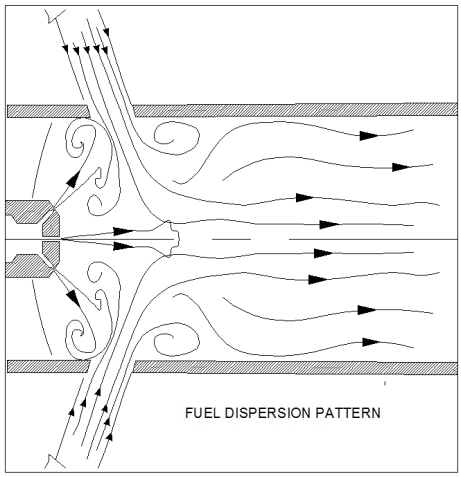

Figure 3-10 Impinging Recirculation Regime [21]

Also, with increase in intake angle, the size of gas generator increases which requires larger space in the vehicle. Hence, considering all these parameters, the two-inlet configuration with an inlet angle of 40 deg has been used for current study.

Effect of dome height: Dome height is defined as is the axial distance between the dome plate and the inlet arm entry. The preferred dome height is that which minimizes the fluctuation between passive and impinging regime and avoids wall impingement of fuel jet. For a given inlet flow angle, effect of dome height on combustion efficiency is negligible.

Effect of Momentum Ratio: It is defined as is the ratio of momentum of air to the momentum of fuel. For high momentum ratio, the flow fields follow a passive recirculation regime whereas for low momentum ratio, the fuel jet partially penetrates the inlet flow column and bifurcate into 2 branches. One deflects towards the wall and the other towards the stagnation point of the inlet jets. Brophy and Hawk [21] conducted experiments on flow visualization. They varied the mass flow ratio and momentum ratio between 10 to 60 and 4.58 to 2.58 respectively.

3.3.1 Gas Generator Analytical Model

To understand the physics of complex systems, it is necessary to predict its performance qualitatively in the early stages of design. This enables the development of concept into reality. A **"One-dimensional model**" developed with experimentally established correlations and reasonable assumptions from basic laws can be highly useful. One-Dimensional model has been developed to predict the performance of gas generator. The control volume considered for the model is shown in Figure 3-11 and Figure 3-12 Fuel is injected in two steps i.e.in intake arms and in the combustor as shown for proper mixing of fuel and air and to generate partially

cracked fuel rich gas products. For model, intake arm equivalent cross-section area is taken for analysis. The equivalent model for the control volume considered is shown in Figure 3-13.

Here the location descriptions are as follows:

Station1: Intake exit location

Station1': Combustor entry location

Station 2: Injector head location

Station 3: Location after central swirl

Station 4: Upstream of Throat location

A fraction of fuel is injected in the intake arm as a cross flow to incoming compressed air. The premixed fuel with air enters the combustion chamber where ignition is achieved using spark plug and using pyro cartridge charge. The remaining fuel is injected at combustor head end and through single swirler.

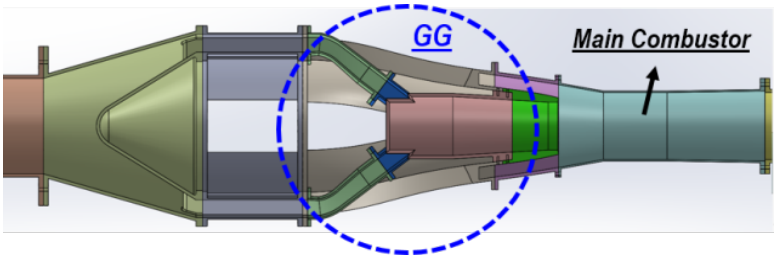

Figure 3-11 Gas Generator location in DCR

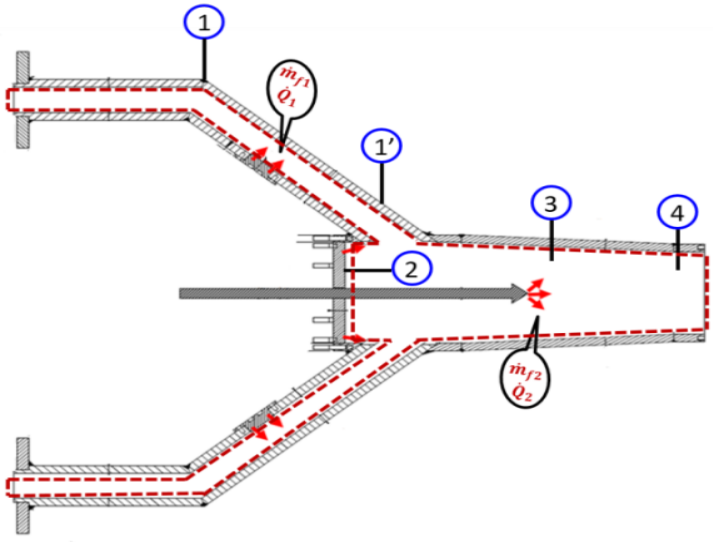

Figure 3-12 Gas Generator control volume

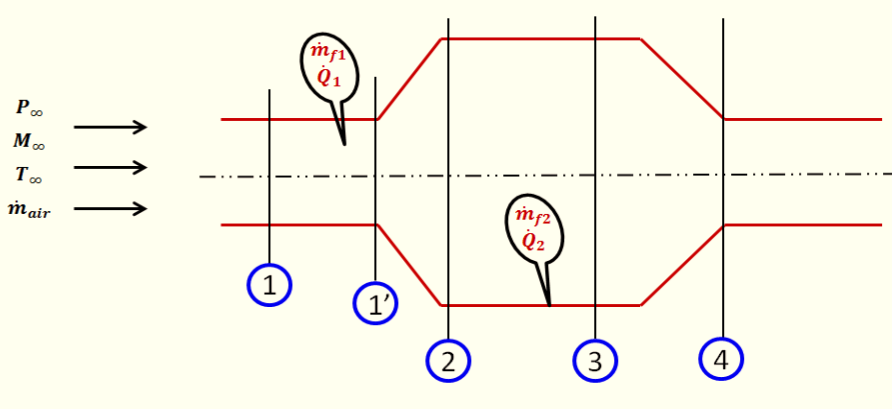

Figure 3-13 Equivalent control volume for model analysis [Present research]

Governing equations are obtained using the concepts of law of conservation of mass, momentum and energy. The heat addition is assumed as a point heat addition and chemical reactions between Fuel and air are calculated using NASA CEA [22] with some assumptions.

NASA Chemical Equilibrium with Applications (CEA) is a computer program for calculation of chemical equilibrium compositions and properties of complex mixtures developed by Gordon and Mcbride [22] at NASA Glenn Research center. CEA is used for a wide variety of problems by chemical engineering, aerodynamics and thermodynamics community. The program was written in ANSI standard FORTRAN.

CEA is a standard for detailed analysis of problems involving combustion; shock detonation and calculation of theoretical rocket performance with over 2000 species are contained in the thermodynamic database. The state of a thermodynamic system consisting of a multispecies compressible gas in equilibrium can be described by the overall chemical composition and two independent thermodynamic variables, such as (temperature, pressure) or (enthalpy, pressure). The choice of which two independent variables to be held constant is determined by the problem to be solved. An example is adiabatic combustion at constant pressure. Chemical Equilibrium is solved through minimization of free energy formulation. CEA can be used from the command prompt. It reads in a text file input and outputs the result into a text file. An online program CEARUN is available to facilitate the use of the NASA chemical equilibrium code CES (open access software). Equilibrium combustion is considered for the current model. Chemical species obtained from step1 heat addition is used as Oxidizer for step2 fuel addition. The two main processes involved are Rayleigh flow and flow with area change. It can be observed that the heat addition takes place in Rayleigh flow.

3.3.1.1 Rayleigh heat addition:

Rayleigh flow is a frictionless, one-dimensional flow in a constant area in which there is only heat interaction. Hence the Rayleigh flow is a diabatic or non-adiabatic flow with the following assumptions:

- The area of the flow passage or duct is constant
- The flow is steady and one dimensional.
- There is no work; body forces and the effect of friction are negligible.
- Heat transfer is the only driving potential.

$$dA = \delta W = dz = \delta f = \delta D = 0 \text{ and } \delta Q \neq 0$$

Because of the above assumptions, the changes in stagnation enthalpy of the fluid are entirely due to heat transfer. Basic characteristic of simple diabatic flow is that stream thrust per unit area remains constant. In view of the above assumptions, considering only the effects of dynamic states for the fluid, the flow conditions may be represented diagrammatically as shown in Figure 3-14.

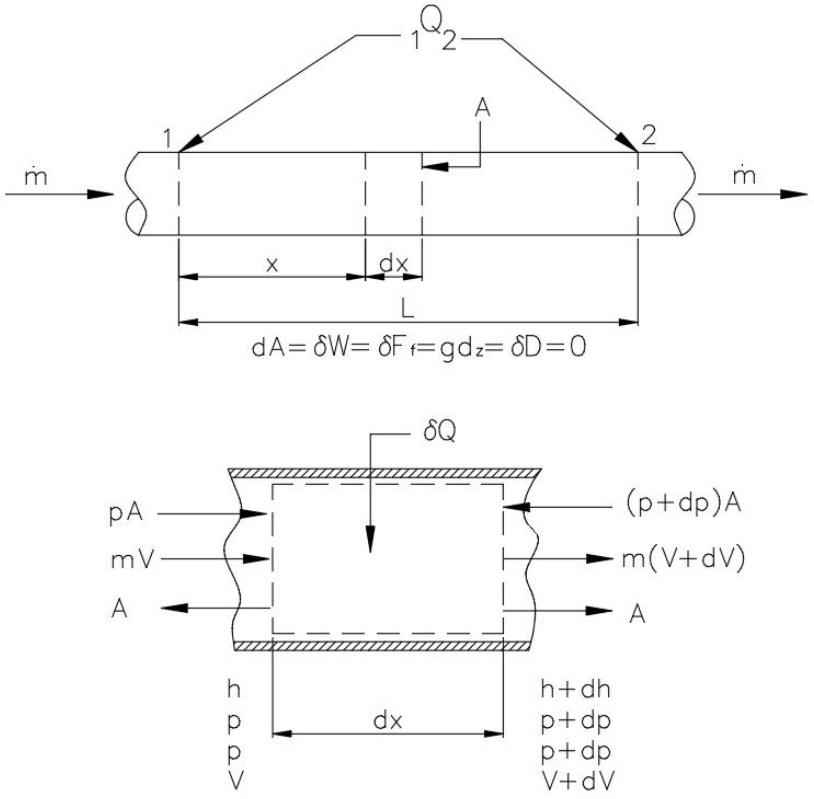

Figure 3-14 Steady 1-D flow in a constant area duct [23]

Referring to the above diagram, the equations of continuity and momentum are as follows

$$dp + \rho V dV = 0 \qquad \text{..Eq(3.22)}$$

$$G = \frac{\dot{m}}{A} = \rho V = \frac{V}{v} = mass\ flux = constant \qquad \text{..Eq(3.13)}$$

From the above two equations, and integrating equation between states 1 and 2,

$$p_1 + G^2 v_1 = p_2 + G^2 v_2 = constant \qquad \text{..Eq(3.24)}$$

The above equation is also known as **Rayleigh line equation.** A curve obtained by applying equation (3.24) is called Rayleigh line or R-line.

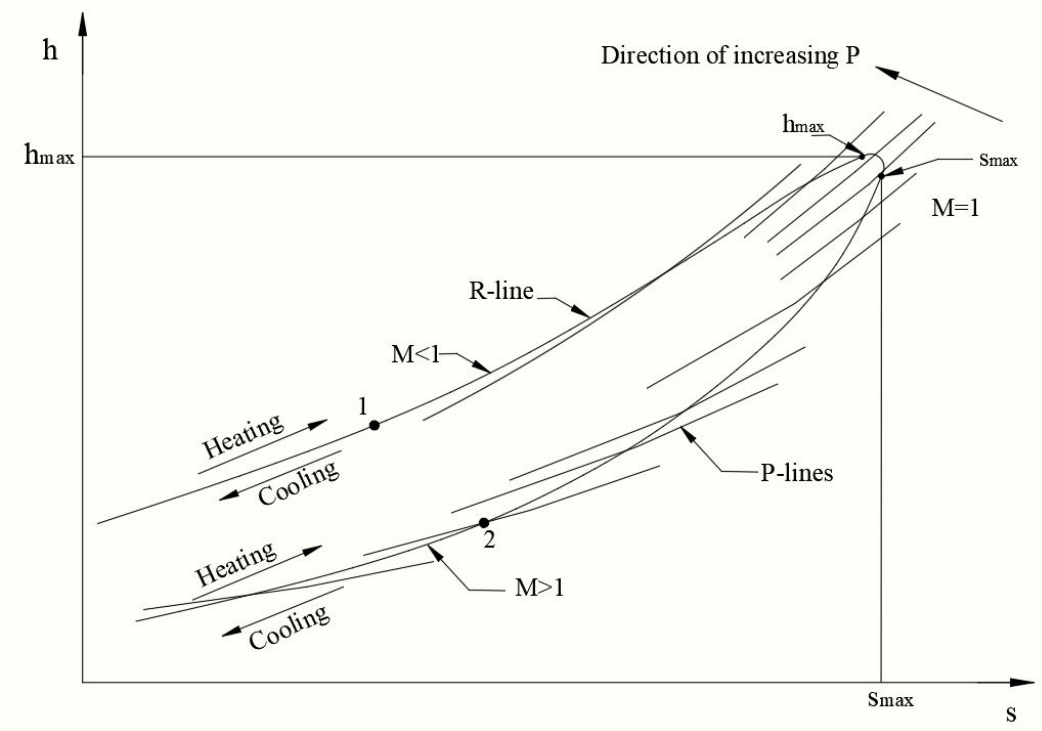

Figure 3-15 Rayleigh line plotted on h-s plane (constant-area duct) [23]

From Figure 3-15, the effect of heat addition is to accelerate a subsonic flow towards sonic condition and to decelerate a supersonic flow to sonic condition as a limit. If the mass flow rate is held constant, raising the enthalpy of the fluid by heat addition causes its static pressure to fall and its specific volume to increase.

Effect of area change on flow properties: Considering a steady, one-dimensional and isentropic flow, from the equations of state and momentum, by taking differential and logarithms and rearranging, we obtain

$$\frac{dA}{A} = (1 - M^2)\frac{dV}{V}$$

$$\frac{dA}{A} = (1 - M^2)\left(\frac{p}{\rho V^2}\right)\frac{dp}{p}$$

..Eq(3.25)

The following table gives the idea and physical interpretation of the equations given above.

Table 3-20 Effect of area change on the flow Mach number

dA	M	
	Less than 1.0	Greater than 1.0
dA < 0	dM > 0	dM < 0
dA > 0	dM < 0	dM > 0

Therefore, the effect of area change in the combustor is in such a way that when flow enters a diverging passage, subsonic flow decelerates towards zero velocity and supersonic flow accelerates towards maximum isentropic speed.

3.3.1.2 Estimation of flow properties:

Flow properties between 1and1' are estimated using Rayleigh heat addition relation. The equations used are:

For Rayleigh heat addition process, Stream thrust per unit area is given by,

$$P_1.A_1 \cdot \left(1 + \gamma \cdot {M_1}^2\right) = P_{1p}.A_{1p} \cdot \left(1 + \gamma_1 \cdot {M_{1p}}^2\right)$$

..Eq(3.26)

Here, area is constant i.e $A_1 = A_{1p}$

This reduces the equation to

$$P_1 \cdot \left(1 + \gamma \cdot {M_1}^2\right) = P_{1p} \cdot \left(1 + \gamma_1 \cdot {M_{1p}}^2\right)$$

..Eq(3.27)

Continuity equation for the flow of a perfect gas in a duct is given by,

$$\dot{m} = \rho \cdot A \cdot V = A \cdot p \cdot M\left(\frac{\gamma}{R \cdot t}\right)^{\frac{1}{2}}$$

..Eq(3.28)

For a constant area duct, equation reduces to,

$$\frac{p_1.M_1}{\sqrt{t_1}} = \frac{p_{1p}.M_{1p}}{\sqrt{t_{1p}}}$$

..Eq(3.29)

Total temperature change in a Rayleigh heat addition is given by using stagnation state relation,

$$\frac{T_{01}}{T_{01p}} = \frac{t_1 \cdot \left(1 + \frac{\gamma - 1}{2} \cdot {M_1}^2\right)}{t_{1p} \cdot \left(1 + \frac{\gamma_1 - 1}{2} \cdot {M_{1p}}^2\right)}$$

..Eq(3.30)

This equation can be modified using continuity relation in terms of Mach number and temperature as given below,

$$\frac{T_{01}}{T_{01p}} = \frac{{M_1}^2 \cdot \left(1 + \gamma_1 \cdot {M_{1p}}^2\right)^2 \cdot \left(1 + \frac{\gamma - 1}{2} \cdot {M_1}^2\right)}{{M_{1p}}^2 \cdot \left(1 + \gamma \cdot {M_1}^2\right)^2 \cdot \left(1 + \frac{\gamma_1 - 1}{2} \cdot {M_{1p}}^2\right)}$$

..Eq(3.31)

The above relation is used to find flow Mach number after heat addition process is completed at location 1p. For a fixed inlet flow condition, Mach number variation due to heat addition and temperature rise for a subsonic flow can never exceed sonic value i.e.

$$\frac{T_{01}}{T^*} = \frac{2 \cdot {M_1}^2 \cdot (1 + \gamma_1) \cdot \left(1 + \frac{\gamma - 1}{2} \cdot {M_1}^2\right)}{\left(1 + \gamma \cdot {M_1}^2\right)^2} \leq 1$$

..Eq(3.32)

If the value becomes 1, Flow Mach number will be equal to 1.

At station 1p,

$$\frac{T_{0P}}{T^*} = \frac{T_{01}}{T^*} \cdot \frac{T_{01p}}{T_{01}}$$

..Eq(3.33)

Once flow Mach number is known, properties are calculated using stagnation state relations.

Between station 1' and 2, effect of area change is considered for flow parameters estimation. Continuity equation between 1' and 2 is given by,

$$\rho_{1p} \cdot U_{1p} \cdot A_{1p} = \rho_2 \cdot U_2 \cdot A_2 \qquad \text{..Eq(3.34)}$$

Stream thrust relation using momentum conservation between 1' and 2 is given by,

$$A_{1p} \cdot \left(P_{1p} + \rho_{1p} \cdot {U_{1p}}^2\right) + P_{1p} \cdot \left(A_2 - A_{1p}\right) = A_2 \cdot \left(P_2 + \rho_2 \cdot {U_2}^2\right)$$

..Eq(3.35)

Stagnation temperature relation for station2,

$$T_{02} = T_2 + \frac{{U_2}^2}{2 \cdot C_p}$$

..Eq(3.36)

Total temperature is assumed to be constant as flow is considered to be inviscid

i.e. T01p = T02.

Ideal gas relation is given by,

$$P_2 = \rho_2 \cdot R_1 \cdot T_2$$

..Eq(3.37)

Using the above four relations, properties at station 2 are calculated.

Between station 2 and 3, flow properties are estimated using the similar relations used for station 1 and 1'. Between station 3 and 4, flow properties are estimated using similar relations used for station 1'and 2. The model flow chart is shown in Figure 3-16.

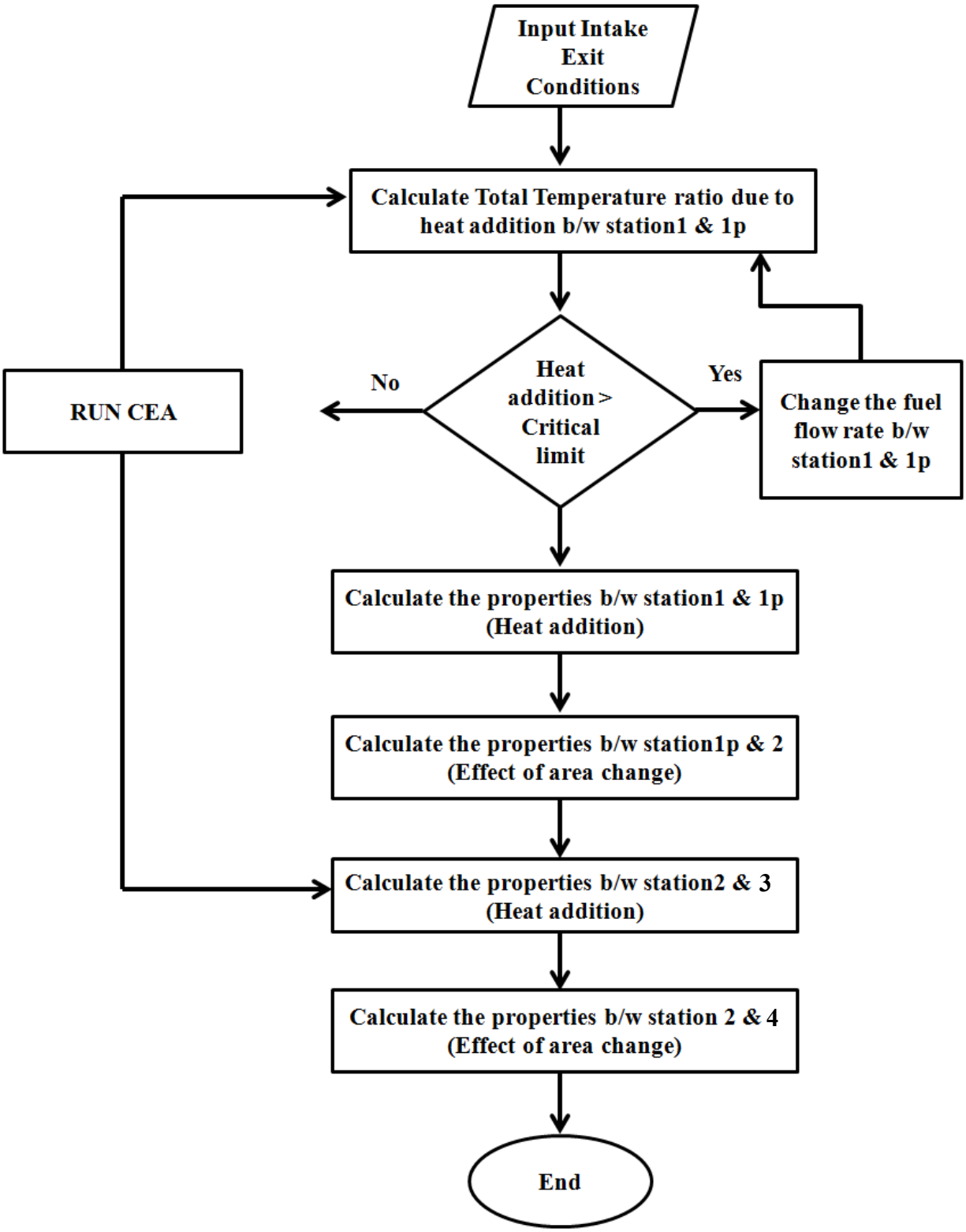

Figure 3-16 Flow chart of Gas generator 1-Dimensional Model

The model input for one of the simulated cases is given in Table 3-21 and model output is plotted in Figure 3-17 to Figure 3-18. Entry air temperature is 806 K. From the Figure 3-17, it

can be observed that first rise in temperature occurs due to combustion in intake arm. Second rise in temperature occurs because of combustion between injected fuel in step 2 and gas products coming from intake arm. Total temperature remains constant after that and Static temperature falls because of flow acceleration in the converging duct. From the Figure 3-18, it can be observed that pressure is constant in intake arm. First rise in pressure occurs because of step increase in area at the entry of main combustor. After combustion in second step, pressure starts falling because of decreasing area. From the Figure 3-19, it can be observed that flow Mach number decreases at entry to main combustor due to step rise in duct flow area. And it starts rising, when duct area starts converging and reaches sonic value at the throat. This is exactly what happens when flow is subsonic. Flow accelerates in converging area.

Table 3-21 Model inputs

SNo.	Parameters	Value
1	Air flow rate	3.536 kg/s
2	Fuel flow rate	0.836 kg/s
	Step1	0.204 kg/s
	Step2	0.632 kg/s
3	Fuel initial temperature	298 K
4	Gama	1.4
5	R	287 kJ/kg
6	Intake exit conditions	
	Total pressure	3.8 bar
	Static pressure	3.6 bar
	Static temperature	806K

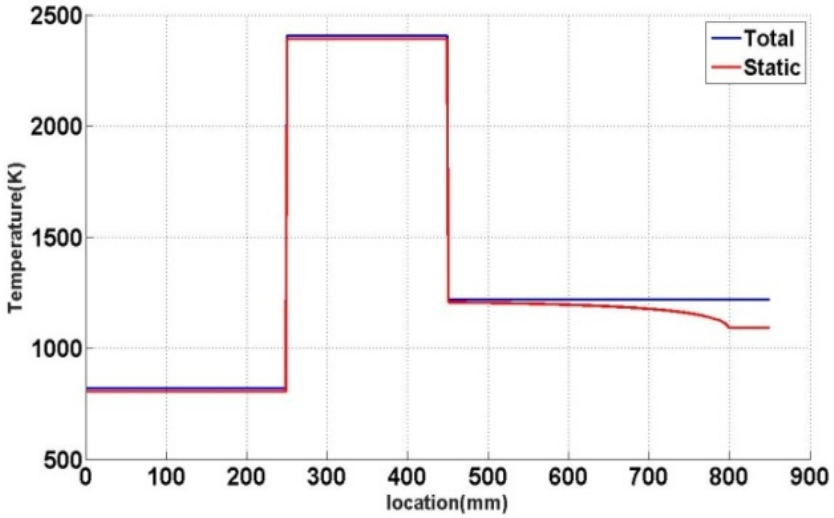

Figure 3-17 Predicted axial variation of total and static temperature in dump combustor

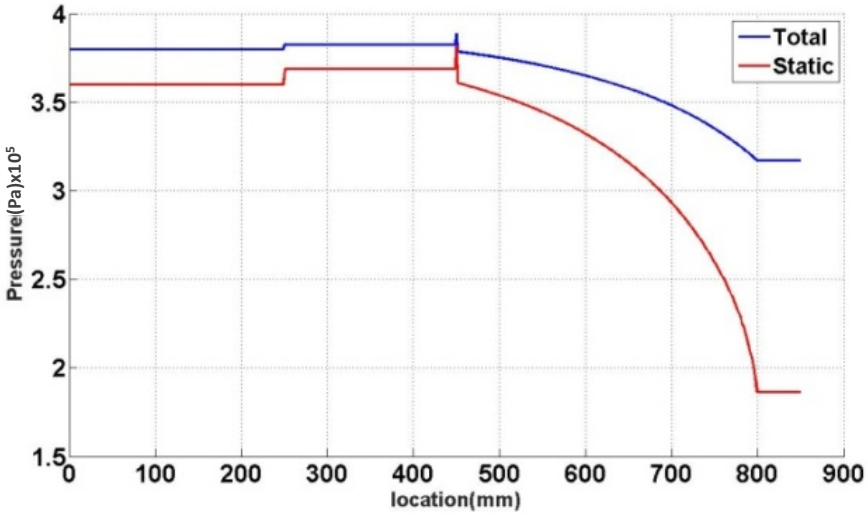

Figure 3-18 Predicted axial variation of total and static pressure in dump combustor

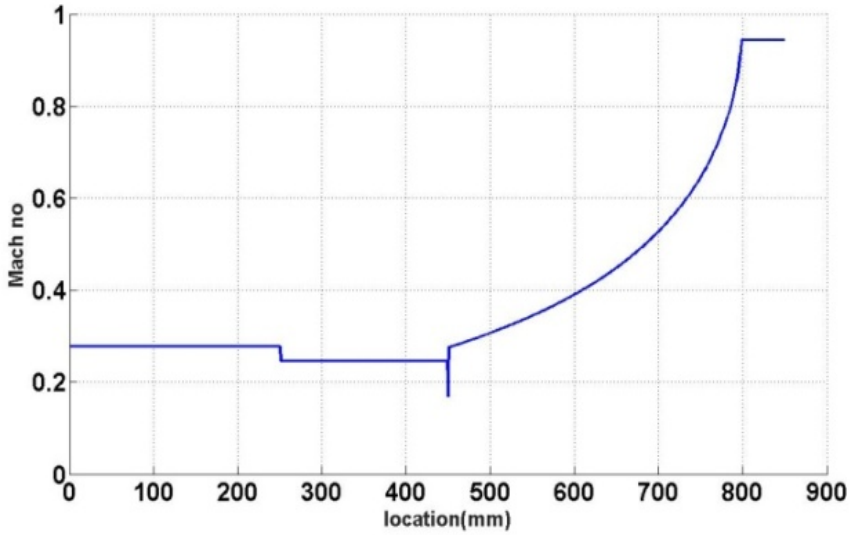

Figure 3-19 Predicted axial variation of flow Mach number in dump combustor

3.3.2 Experimental Studies on Gas Generator

Experimental studies have been carried out in connect pipe mode to establish the sustained ignition condition, to understand the combustion in gas generator and to arrive at final configuration of gas generator to achieve its intended performance in dual combustion ramjet engine.

The test setup is shown in Figure 3-20 and Figure 3-21. Fuel is supplied through fuel feed system. Combustor entry air flow condition is simulated using vitiated air heater. The heater employed for heating the incoming air to the gas generator is of combustion driven heater based on hydrogen. The hydrogen gas fed into the heater undergoes exothermic combustion reaction with the incoming air and heat released during the combustion is used to heat the air to the desired temperature. The concentration of oxygen in the gas stream decreases as some amount is consumed in undergoing combustion reaction with hydrogen. To maintain same amount of oxygen as in the atmospheric air, oxygen gas is added downstream of the heater section.

Heated air flows through two intake arms and gets dumped in GG. There are 3 sets of injectors in the gas generator. Two sets of similar type plain orifice injectors are located in the intake arm and the second set of single swirl type is located in gas generator. The location of injectors is shown in Figure 3-22. The test firing sequence in unit of second is given in Table 3-22. Ignition is initiated using spark igniter and pyro igniter firing. Instrumentation details are shown in Figure 3-23 and details are given in Table 3-23.

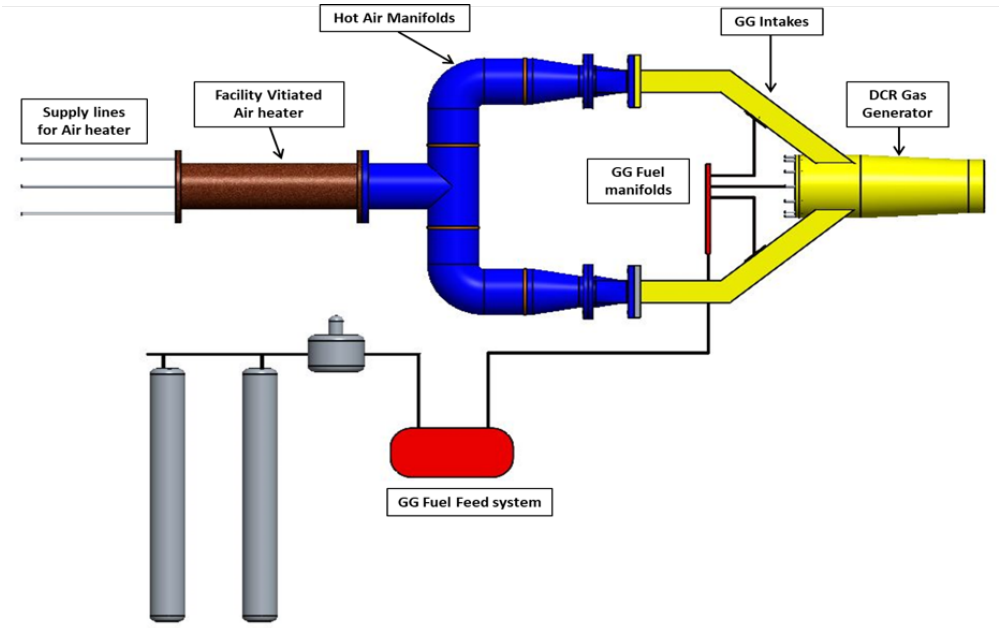

Figure 3-20 Test set up for gas generator testing [Present research]

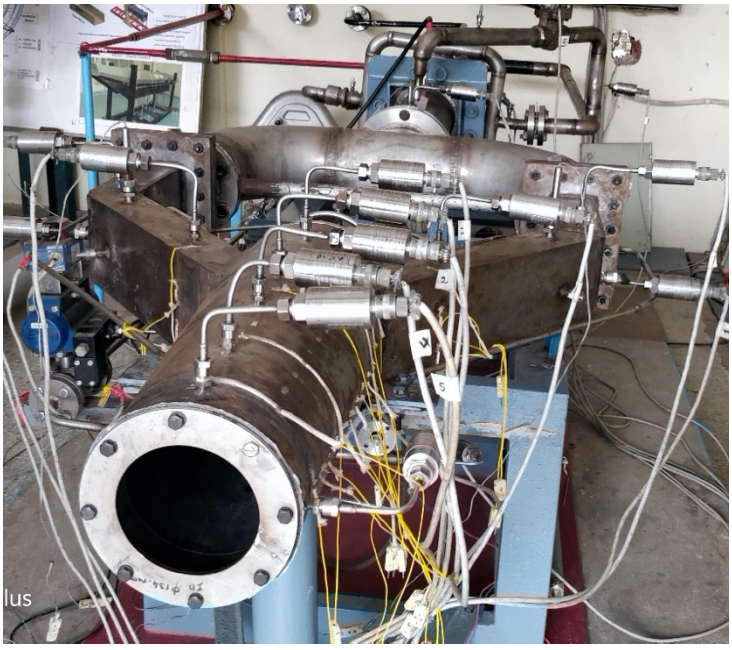

Figure 3-21 GG Instrumented Hardware [Present research]

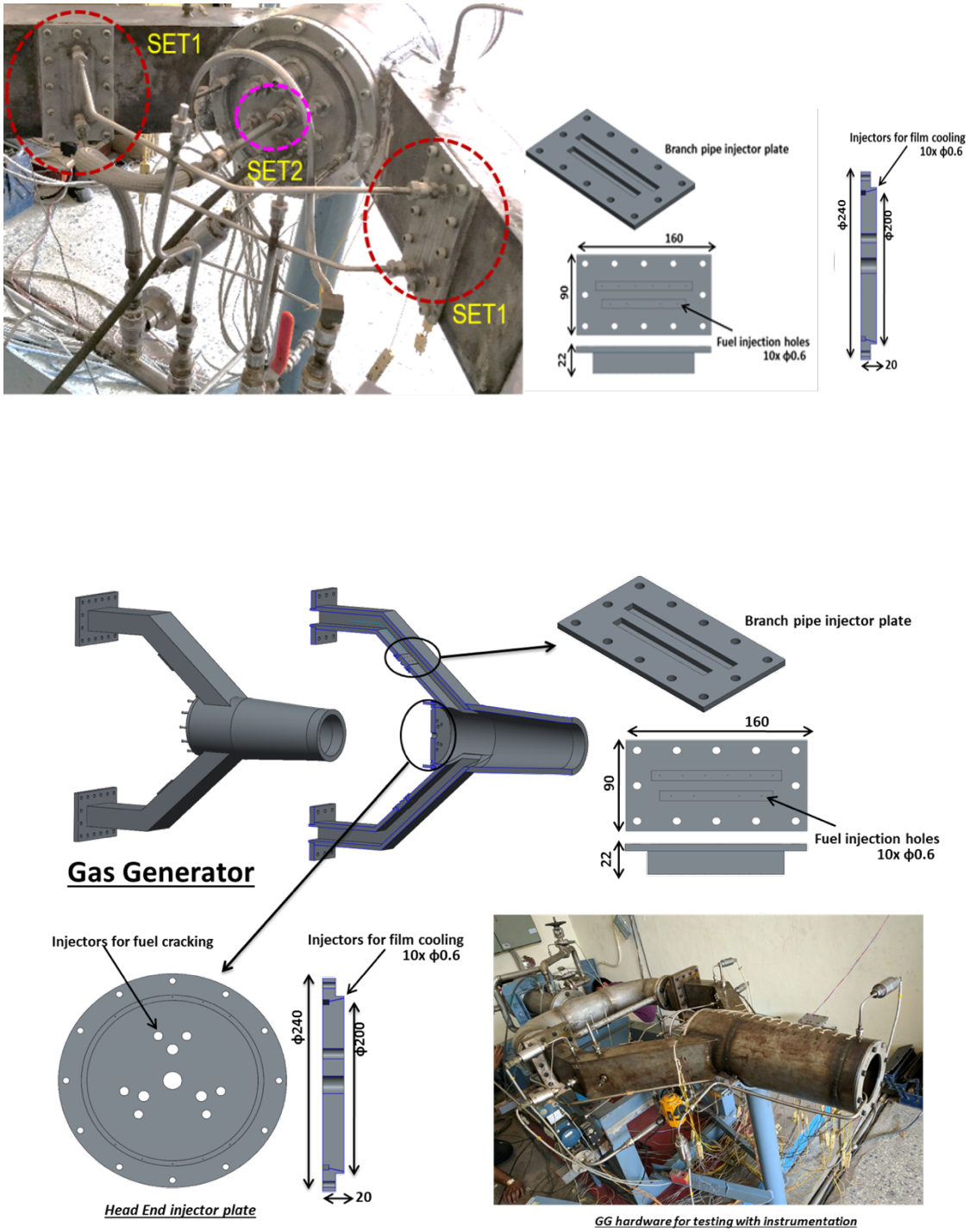

Figure 3-22 GG Injector details [Present research]

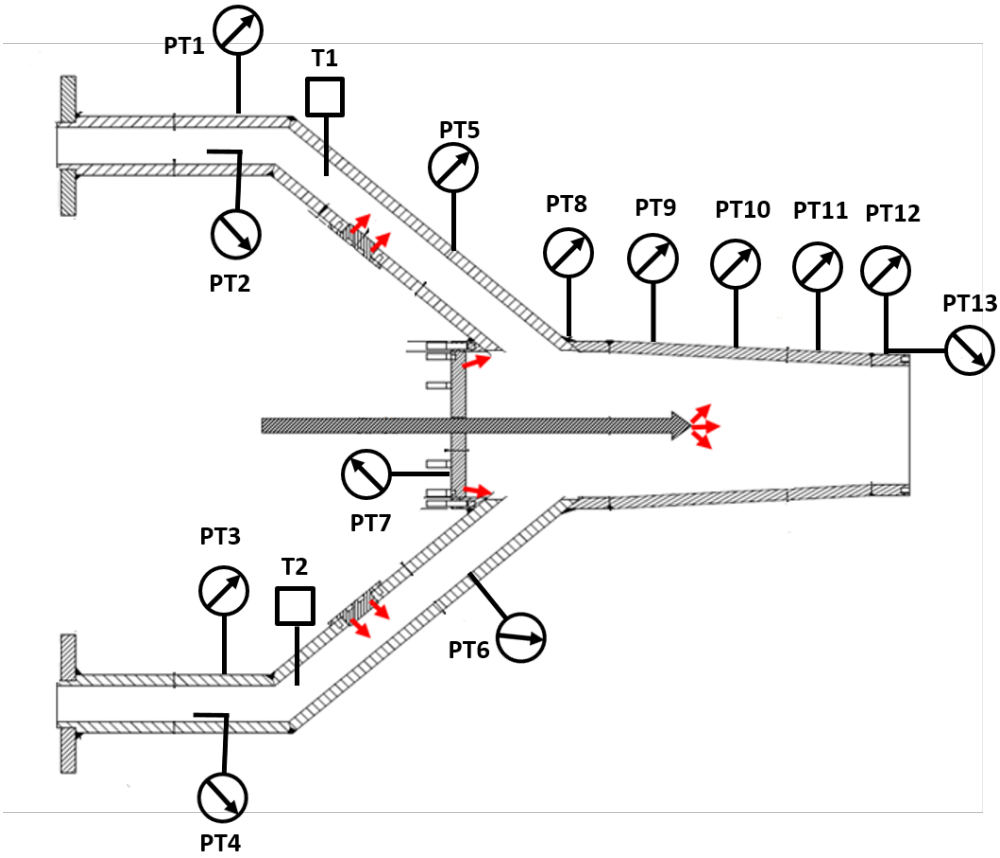

Figure 3-23 Gas generator pressure and temperature sensor locations

Table 3-22 Test firing sequence (Time in Seconds)

	System	ON	OFF
1	Air	0	40
2	Oxygen	4	18
3	Heater Spark igniter	5	9
4	Main Hydrogen	7	18
5	Fuel	9	18
6	GG Spark igniter	11	16
7	GG Pyro (Manual)	13	16

Table 3-23 Instrumentation description

S No	Instrumentation Details
1	Air Inlet1 Entry Static Pr. (PT1)
2	Air Inlet1 Entry Total Pr. (PT2)
3	Air Inlet2 Entry Static Pr. (PT3)
4	Air Inlet2 Entry Total Pr. (PT4)
5	Air Exit1 Static Pr. (PT5)
6	Air Exit2 Static Pr. (PT6)
7	Injector Head Pr. (PT7)
8	GG1 Pr. (PT8)
9	GG2 Pr. (PT9)
10	GG3 Pr. (PT10)
11	GG4 Pr. (PT11)
12	Noz1 and Noz 2 Pr.(PT12 and PT13)
13	Intake Air Temperatures (T1 and T2)
14	Turbine flow meter

Data sampling rate was 2 kHz and bandwidth was 1kHz. The uncertainties in instrumentation measurement are given in Table 3-24. Each type sensors are pre-calibrated before each test. End to end calibration is carried out before each test using dry runs and following a standard operating procedure to ensure accuracy and correctness of measure data.

Table 3-24 Instrumentation specifications and uncertainties

	Sensors	Type	Make	Uncertainty (± % of full scale)
1	Pressure sensor	Resistance type strain gauge sensors	Sensotech/Honeywell	± 0.2524
2	Temperature sensor	B – type for 600K to 1800 K K – type for RT to 1200 K	Omega	± 1
3	Flow rate sensor	Turbine flow meters	Flow Technologies	± 0.5
4	Data acquisition system	---	National Instruments	± 0.07
5	Signal conditioning unit	---	---	± 0.01

Test matrix is tabulated in Table 3-25.

In run1, fuel was injected from intake as well as central swirl simultaneously. Total fuel flow rate simulated was 700 g/s approximately. However, there was no ignition.

In 2nd run, H_2 from heater was allowed to enter combustion chamber unburnt and heater combustion was initiated once the ignition in combustor was sustained. Sustained ignition was achieved.

In 3rd run, fuel injection in intake arms alone was switched on first and later pyro was fired. Sustained ignition was achieved with an equivalence ratio of 1.

In 4th run, staged fuel injection was carried out. Injectors in intake arm were switched on first and then pyro was fired. After achieving ignition, central swirl was switched ON and ignition sustained in the combustor.

Run 1 to 4 was carried out with total fuel flow rate of ~700 g/s (except run3 which was with ~ 360 g/s mass flow rate of fuel).

Run 5 and 6 were carried out with total fuel flow rate of ~ 800g/s. However, no ignition occurred in combustor when the equivalence ratio in intake was ~ 1.2.

So, next set of tests were planned with lower equivalence ratio of the order of 0.8-0.9 in the intake arm. Fuel feed system was recalibrated to achieve the desired equivalence ratio and fuel flow rate in the system.

In run 7, staged fuel injection was carried out with equivalence ratio of ~ 0.85 in the intake arm and total fuel flow rate of ~ 800 g/s. Central swirl was switched on after ensuring ignition occurrence in the GG.

Run 8 and 9 were carried out with simultaneous fuel injection from intake arm as well as central swirl. Pyro was fired next and sustained ignition was achieved in the combustor.

Results are analyzed and discussed in the next chapter.

Table 3-25 Gas Generator Test matrix

S NO.	Configuration
RUN1	Fuel injection simultaneously (~ 700 g/s) 1. Intake injection (~ 220 g/s) 2. Film cooling injection(~120 g/s) 3. Central swirl injection(~360 g/s) 4. 100 DQ pyro for ignition initiation
RUN2	Fuel injection simultaneously (~ 700 g/s) 1. Intake injection and Film cooling injection 2. Central swirl injection 3. 100 DQ pyro for ignition initiation 4. Heater ignition after 3 sec pyro firing
RUN3	Staged fuel injection (~ 360 g/s) 1. Intake + Film cooling injection 2. 100 DQ pyro for ignition initiation 3. No – Central swirl injection
RUN4	Staged fuel injection (~ 700 g/s) 1. Intake + Film cooling injection 2. 100 DQ pyro for ignition initiation 3. Central swirl injection
RUN5and6	Staged fuel injection (~ 800 g/s) 1. Intake + Film cooling injection 2. 100 DQ pyro for ignition initiation 3. Central swirl injection
RUN7	Staged fuel injection (~ 800 g/s) 1. Intake + Film cooling injection 2. 100 DQ pyro for ignition initiation 3. Central swirl injection
RUN8and9	Combined fuel injection (~ 800 g/s) 1. Intake + Film cooling inj. + Central swirl inj. 2. 100 DQ pyro for ignition initiation

3.4 Numerical Studies on DCR Combustor design and modelling

3.4.1 CFD methodology

The study was carried out in two parts. In the first part, existing engine geometry with experimental data is taken from the literature and studied to evolve a CFD procedure for combustor-isolator modelling. Various turbulence models and combustion modelling techniques were tried and compared with experimental data to find the best suitable procedure. In the second part of the study the chosen CFD procedure is adopted to develop a new combustor design, based on the current requirement.

3.4.1.1 Numerical Method:

Numerical simulations were carried out in commercial CFD software ANSYS fluent. A steady state simulation with Density based solver with an 2nd order implicit Roe- FDS scheme is used; 2D axisymmetric simulations were carried out for all configurations. Supersonic flow consists of large density gradients hence Favre averaged Navier stokes equations, wherein the mean quantity of flow variables is considered while the fluctuating quantities are ignored. For combustion simulations species transport equations are solved considering volumetric reactions, modelled with Finite-rate/eddy dissipation model.

Fluent uses finite volume based discretized Navier-stokes equation for computing the flow variables. The Navier-stokes equation consists of continuity, momentum and energy equations. In addition to that species transport equations are also solved for each gas in the flow. The time averaged Navier-stokes equation also results in Reynold's stress terms, which requires additional equations to be solved for closure.

Navier stokes equations are given as follows.

I. Continuity

The continuity equation gives the net mass flux of a control volume which is zero. The compressible form of continuity equation can be written as follows.

$$\frac{\partial}{\partial t}(\rho) + \frac{\partial}{\partial x_i}(\rho u_i) = 0 \qquad \text{..Eq(3.38)}$$

II. Momentum

Momentum equation is based on the Newton's second law which states that the force is directly proportional to the change in momentum. The equation equates the forces to the

time rate of change of momentum. The forces include the pressure term, along with viscous forces (Reynolds stress term) and any other body forces.

$$\frac{\partial}{\partial t}(\rho u_i) + \frac{\partial}{\partial x_i}\left(\rho u_i u_j\right) = -\frac{\partial P}{\partial x_i} + \frac{\partial}{\partial x_i}(\tau_{ij}) \quad \text{..Eq(3.39)}$$

Where, τ_{ij} is the Reynolds stress term, which requires additional turbulence model for the closure of Navier stokes equations.

III. Energy

The energy conservation equation relates the energy added to the fluid, to the rate of work done on the fluid to the rate of change in total energy of the fluid in the control volume. It includes effects of temperature change in the flow, which is very large in case of supersonic reacting flows.

$$\frac{\partial}{\partial t}(\rho e_{total}) + \frac{\partial}{\partial x_i}\left(\rho h_{total} u_j\right) = -\frac{\partial}{\partial x_i}(\tau_{ij} u_i - q_i)$$

…Eq(3.40)

$$\tau_{ij} \; is \; the \; stress \; tensor, q_i \; is \; the \; heat \; flux$$

$$\tau_{ij} = (\mu + \mu_t)\left[\frac{\partial u_i}{\partial x_j} + \frac{\partial u_j}{\partial x_i} - \frac{2}{3}\delta_{ij}\frac{\partial u_k}{\partial x_k}\right] - \frac{2}{3}\rho k \delta_{ij}$$

..Eq(3.41)

IV. Species Transport equation

For each of the chemical species in the flow, additional transport equation is solved for local mass fractions (Y_k) for each of the species involved. If N number of species are involved in the reactions then, this equation will be solved for (N-1) species. The mass fraction of N^{th} species will be obtained by subtracting the sum of mass fractions of all other species with one. The N^{th} species is the one with the largest mass fraction.

$$\frac{\partial(\rho Y_k)}{\partial t} + \frac{\partial}{\partial x_i}(\rho u_i Y_k) = -\frac{\partial}{\partial x_i}\left(\rho D_k \frac{\partial Y_k}{\partial x_i}\right) + R_k$$

..Eq(3.42)

Where, k - *1,2...*N are the Reacting species

R_k – is the net rate of production of chemical species *k*, which is described in combustor modelling.

D_k – Mass diffusion coefficient for species k.

3.4.1.2 Turbulence modelling

For the governing equations to be closed Reynolds stress term ($\tau_{ij} = -\rho\overline{u'_\iota u'_J}$) in equations (3.39) and (3.40) which takes into account the turbulence effects must be solved. Turbulence closure is achieved by considering Reynold shear stress related to average velocity gradient by turbulent viscosity, a property of flow. All the turbulence models that are considered uses Boussinesq model which suggest that like Newton's law of viscosity (Shear stress is proportional to shear strain), Reynolds stresses are proportional to mean deformation rate given by

$$\tau_{ij} = -\rho\overline{u'_\iota u'_J} = \mu_t\left(\frac{\partial \bar{u}_i}{\partial x_j} + \frac{\partial \bar{u}_j}{\partial x_i}\right) - \frac{2}{3}\rho k\delta_{ij}$$

..Eq(3.43)

$$k = \frac{1}{2}\left(\overline{u'^2} + \overline{v'^2} + \overline{w'^2}\right) \quad \text{. . Eq(3.44)}$$

There are different models which can be used for evaluating turbulent viscosity. Here two- equation turbulence models are considered. The common assumption of these models is that the turbulence to be isotropic. For Turbulence closures various models such as k-ε, k-ω SST and, k-ε RNG is applied. Turbulence models considered for present analysis are k-ε (Standard wall function) [51], RNG k-ε [52], k-ω (Standard) [53], k-ω-SST [54].

a) **k-ε**

The standard two equation model is developed by Launder and Spalding (1974). It is a widely used two – equation model in industrial flows due to its robustness and reasonable accuracy. Two equations are solved for k and ε. k is defined as turbulent kinetic energy and ε is dissipation rate. The transport equations for k and ε are,

$$\frac{\partial(\rho k)}{\partial t} + \frac{\partial}{\partial \mathrm{x_i}}(\rho k \mathrm{u_i}) = \frac{\partial}{\partial x_j}\left[\left(\mu + \frac{\mu_t}{\sigma_k}\right)\frac{\partial k}{\partial x_j}\right] + G_k + G_b - \rho\varepsilon - Y_M + S_k$$

…Eq(3.45)

$$\frac{\partial(\rho \varepsilon)}{\partial t} + \frac{\partial}{\partial \mathrm{x_i}}(\rho \varepsilon \mathrm{u_i}) = \frac{\partial}{\partial x_j}\left[\left(\mu + \frac{\mu_t}{\sigma_k}\right)\frac{\partial \varepsilon}{\partial x_j}\right] + C_{1\varepsilon}\frac{\varepsilon}{k}(G_k + C_{3\varepsilon}G_b) - C_{2\varepsilon}\rho\frac{\varepsilon^2}{k} + S_\varepsilon$$

…Eq(3.46)

Where,

G_K, G_b represents generation of turbulent kinetic energy due to mean velocity gradient and buoyancy respectively.

Y_M is Dilatation Dissipation Term to account for compressibility effects in the flow.

S_k, S_ε are user defined Source terms.

$C_\mu, \sigma_k, \sigma_\varepsilon, C_{1\varepsilon}, C_{2\varepsilon}$ are empirical constants.

Turbulent viscosity (μ_t) is computed from k and ε by $\mu_t = \frac{\rho C_\mu k^2}{\varepsilon}$ ..Eq(3.47)

b) **RNG k-ε**

The RNG procedure removes small scales of motion by expressing their effect in terms of large-scale motions and modified viscosity.

$$\frac{\partial(\rho k)}{\partial t} + \frac{\partial}{\partial \mathrm{x_i}}(\rho k \mathrm{u_i}) = \frac{\partial}{\partial x_j}\left[(\mu_{eff})\alpha_k \frac{\partial k}{\partial x_j}\right] + G_k + G_b - \rho\varepsilon - Y_M + S_k$$

..Eq(3.48)

$$\frac{\partial(\rho\varepsilon)}{\partial t} + \frac{\partial}{\partial \mathrm{x_i}}(\rho \varepsilon \mathrm{u_i}) = \frac{\partial}{\partial x_j}\left[(\mu_{eff})\alpha_\varepsilon \frac{\partial \varepsilon}{\partial x_j}\right] + C_{1\varepsilon}\frac{\varepsilon}{k}(G_k + C_{3\varepsilon}G_b) - C_{2\varepsilon}\rho\frac{\varepsilon^2}{k} - R_\varepsilon + S_\varepsilon$$

..Eq(3.49)

$\mu_{eff} = \frac{\rho C_\mu k^2}{\varepsilon}$, $C_\mu, C_{1\varepsilon}, C_{2\varepsilon}$ *are emperical constants*

Following are the major differences between RNG k-ε and k-ε standard turbulence model:

1. α_ε, α_k are evaluated using analytical equations
2. Dissipation rate Equation in standard k-ε model is considered to be reason for poor results in large deformation flows. R_ε is added as an additional term in dissipation equation. For weak and moderate strained flows R_ε term is positive. The net numerical result obtained by using RNG is same as standard k-ε. But for large strained flows R_ε is negative which increases dissipation rate and reduces turbulent kinetic energy, Hence reduction in turbulent viscosity.

c) **k-ω**

To evaluate dynamic turbulent viscosity, one velocity scale and one length scale is required**.** In the previous discussion of k-ε model, velocity scale is $\sqrt{k}$ and length scale is $k^{\frac{3}{2}}/\varepsilon$. In k-ω model velocity scale is $\sqrt{k}$ whereas for length scale another variable ω, which is the frequency of turbulence is considered

$$\frac{\partial(\rho k)}{\partial t} + \frac{\partial}{\partial \mathrm{x_i}}(\rho k \mathrm{u_i}) = \frac{\partial}{\partial x_j}\left(\Gamma_k \frac{\partial k}{\partial x_j}\right) + G_k - Y_k + S_k$$

..Eq(3.50)

$$\frac{\partial(\rho k)}{\partial t} + \frac{\partial}{\partial \mathrm{x_i}}(\rho k \mathrm{u_i}) = \frac{\partial}{\partial x_j}\left(\Gamma_\omega \frac{\partial k}{\partial x_j}\right) + G_\omega - Y_\omega + S_\omega$$

..Eq(3.51)

G_k, G_ω are generation due to velocity gradient. Y_k, Y_ω are dissipation terms and S_k, S_ω are source terms for k and ω.

The turbulence viscosity (μ_t) is computed by

$$\mu_t = \frac{\rho k}{\omega} \quad \text{. . Eq(3.52)}$$

d) k-ω(SST)

Menters [54] SST model is blend of k-ε model and kω model. k-ω model performs well near the wall but poor away from wall. It also gets affected by free stream variations. On the other hand, k-ε model is not accurate with adverse pressure gradient boundary condition but gives good results away from wall. A blending function is used to have smooth transition of models.

Production limiter is an important feature of SST model, which avoids building up of turbulent kinetic energy in stagnation region. With production limiter results are better in wake region and adverse pressure gradient.

e) Standard wall function

For high Reynolds number the standard k-ε model does not need to be solved up to the wall boundary. The universal behavior of flow near wall can be considered. For y+ between 30 to 500 log law is valid and given by

$$u^+ = \frac{U}{u_\tau} = \frac{1}{\kappa}\ln(EY^+) \quad \text{..Eq(3.53)}$$

Where, $\mathrm{u_\tau}$ is friction velocity given by $\sqrt{\tau_w/\rho}$; Von Karman's constantκ = 0.41, and wall roughness parameter is E=9.8

3.4.1.3 Solver procedure:

ANSYS provides two solvers, density and pressure based. In both methods it solves the conservation of mass, momentum, energy and other scalar equations such as species transport and turbulence based on control volume approach. Density based solver takes into account the compressibility effects and is used for supersonic compressible flow. Hence, density-based solver is used for all simulations in this study. In this method the velocity field is obtained from the momentum equations. The density field is arrived from the continuity equation, while the pressure field is determined from the equation of state.

The solver consists of the following steps:

1. First the flow properties are updates, if the solution has just started; the properties are updated from the initialization.
2. The continuity, momentum, energy and species transport equations are all solved simultaneously.
3. The turbulence transport equations are solved from updates values.
4. The calculated solution is checked for convergence, if the convergence criteria is satisfied then the solution is stopped if not the whole procedure is iterated again until convergence criteria is satisfied.

Convergence criteria: Convergence is monitored by residuals, i.e. the error between the current time step/iteration flow field variable and the previous one. When the error is below 0.001, convergence is met, until then the loop iterates. Mass convergence is also observed to be with 5% of net mass flow.

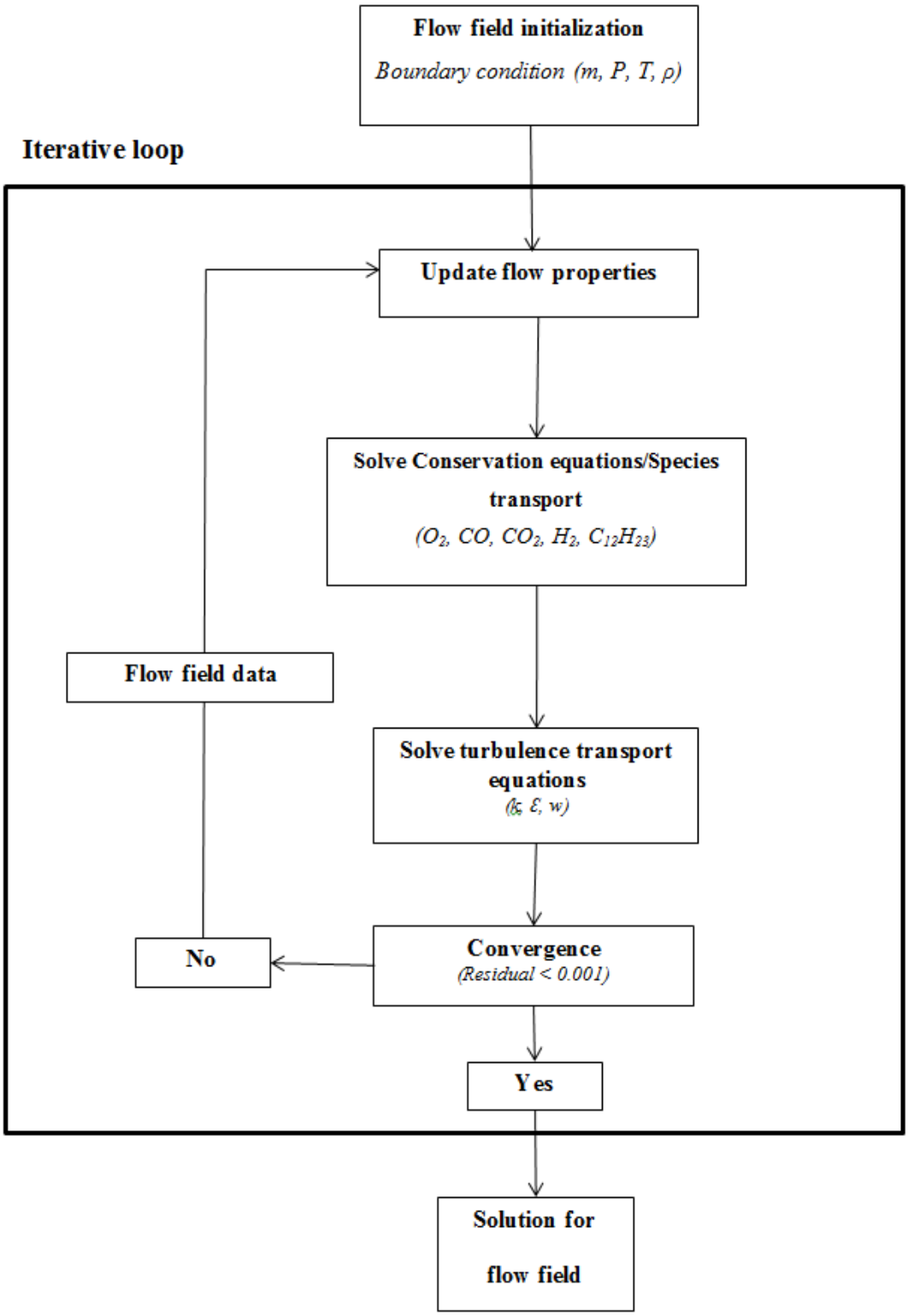

Figure 3-24 Solver methodology

3.4.1.4 Combustor / Chemistry modelling:

A reduced order kerosene/air reaction is used since a complete chemical reaction mechanism is not possible computationally. For combustion a 7 species and 4 step reaction model is used

$$C_{12}H_{23} + 6O_2 \rightarrow 12CO + 11.5\,H_2 \quad \text{(R1)}$$
$$H_2 + 0.5O_2 \rightarrow H_2O \quad \text{(R2)}$$
$$CO + 0.5O_2 \rightarrow CO_2 \quad \text{(R3)}$$
$$CO + H_2O \rightarrow CO_2 + H_2 \quad \text{(R4)}$$

Finite rate model computes the net rate of production term (R_k) in species transport equation by Arrhenius expressions. It does not consider the effects of turbulence; it is based upon the chemical kinetics. It is suitable for slow chemistry reactions, wherein the effect of turbulence is negligible, and the reaction is predominantly driven by kinetics rather than by turbulent mixing. The limiting factor here is the kinetics.

The species source term is given by,

$$R_k = M_{w,k} \sum_{r=1}^{N_R} \hat{R}_{k,r} \quad \text{. . Eq(3.54)}$$

Where,

$M_{w,k}$ - is the molecular weight of species k

$\hat{R}_{k,r}$ - is the Arrhenius molar rate of creation/destruction of species k in reaction r .

$\hat{R}_{k,r}$ for non- reversible reactions is given by

$$\hat{R}_{k,r} = (v''_{k,r} - v'_{k,r}) \left[K_{f,r} \prod_{j=1}^{N} (C_{j,r})^{(\eta'_{j,r} + \eta''_{j,r})}\right] \quad \text{. . Eq(3.55)}$$

Where,

$C_{j,r}$ – is the molar concentration of species j in reaction r (kmol/m^3)

$\eta'_{j,r}$ – is the rate exponent of the reactant species j in the reaction r.

$\eta''_{j,r}$ – is the rate exponent of the product species j in the reaction r.

$K_{f,r}$ is the forward rate constant for reaction r, which is calculated by Arrhenius expression,

$$K_{f,r} = A_r T^{\beta_r} e^{-E_r/RT} \quad \text{..Eq(3.56)}$$

Where,

A_r is the pre-exponential factor

β_r- temperature constant

E_r – activation energy for the reaction

R - Gas constant

In eddy dissipation model the chemical kinetics effect on the flame is not considered, turbulence has the major effect on the combustion. This model can be used where in the chemical reactions are fast and the overall reaction depends upon the mixing of the reactants due to turbulence. The limiting factor here is the turbulence.

The species source is computed least of the two equations,

$$R_{k,r} = v'_{k,r} M_{w,k} A \rho \frac{\varepsilon}{k} min_R \left(\frac{Y_R}{V'_{R,r} M_{w,R}} \right)$$

..Eq(3.57)

$$R_{k,r} = v'_{k,r} M_{w,k} AB \rho \frac{\varepsilon}{k} \frac{\sum_P Y_P}{\sum_j^N v''_{j,r} M_{w,j}}$$

..Eq(3.58)

Where,

Y_P– is the mass fraction of any product species, P

Y_R – is the mass fraction of a particular reactant, R

A –Empirical constant equal to 0.4

B– an empirical constant equal to 4.0

In case of supersonic combustion, the residence time of fuel inside the engine is in order of few milliseconds, hence chemical kinetics plays a major role in the reactions and turbulence is to be considered as the shear/mixing layer between the gas generator and isolator flow streams play a major role in mixing of fuel rich gas generator flow and air from isolator, hence one cannot ignore the effect of turbulence on the reactions. Finite rate/Eddy dissipation model considers both the turbulence and chemical kinetics. It solves both eddy dissipation equation and Arrhenius reactions rates are calculated. The net reaction rate is taken as the minimum of these two rates, i.e. if turbulence is low, then mixing is low so it becomes the limiting factor. If the kinetics are slow but turbulence is faster, then the kinetics becomes the limiting factor.

3.4.1.5 Experimental setup description:

For the validation study the static experiment performed by Jong – Ryun Byun, *et al.* [38] is taken from open literature. In this, DCR experimental set-up was designed with a gas generator, an isolator, and a supersonic combustor. Experiments were conducted in a connected pipe facility. The air was supplied from pressurized storage tanks, compressed to 1.0 MPa .Air is heated by a Vitiated heater using CH4 and air. Additional oxygen is added to maintain 0.21 mole fraction of O_2 in vitiated air. Heated air is split into two streams, one is directed towards the gas generator and the other stream to an annular plenum. The air which enters the plenum is passed trhough an annular convergent- divergent nozzle, which accelerates the air to supersonic speeds. The annular nozzle can be changed with different nozzle expansion ratios, to change the isolator entry Mach number (M_{SI}) . The accelerated air now flows to the annular isolator at supersonic speeds and then to supersonic combustor.

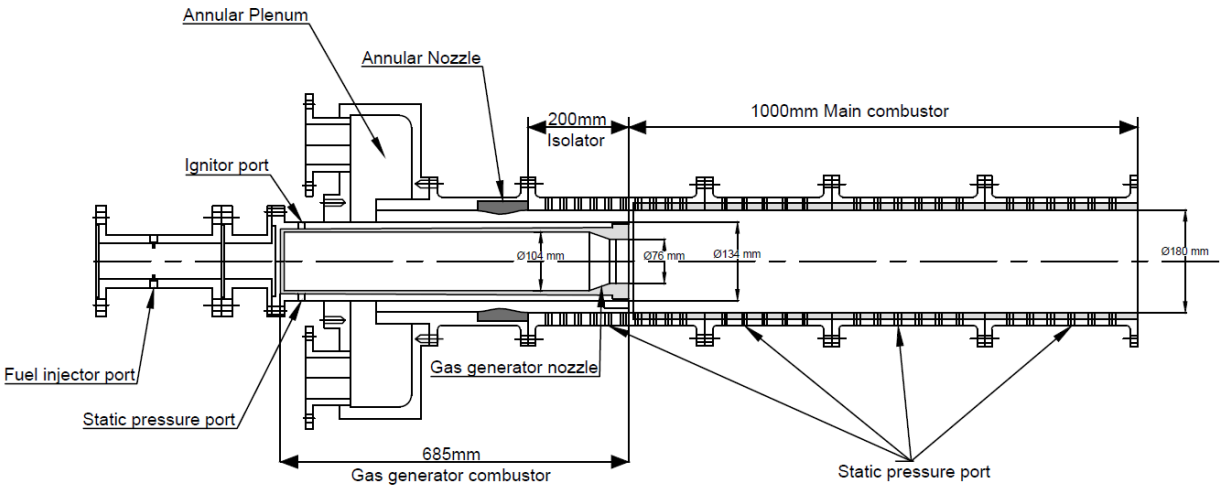

Figure 3-25 DCR test setup Schematic [38]

In the gas generator , liquid hydrocarbon fuel is added through a fuel collector , with circular orifices. The fuel is mixed with air and is ignited by a gas torch system at the inlet section of the gas-generator.A convergent – divergent nozzle is placed in the gas generator exit which accelerates the exhaust to supersonic speeds. The exit diameter of the nozzle is 84mm with an expansion ratio of 1.22.The calculated Mach number sat the nozzle exit was in range of 1.53 to 1.55. The supersonic combustor is an constant area duct of length 1000mm.The whole setup is made up of stainless steel.Composite silica- phenolic is used as insulators for both the gas generator and the supersonic combustor. The gas generator nozzle was madeup of graphite.

Experiments were conducted for free stream mach numbers (M_∞) 4, 4.5, 5 for flight altitudes of 20km to 25km. The isolator entry mach number studied are 1.8,2.0,2.25. The air flow is split in the ratio of 3:1 between the isolator and gas-generator.The tests are run multiple times and the experiemental data is an average of these runs. Various equivalence ratios for gas generator was also run.The experiemental conditions are as in the table below.

Table 3-26 Experimental conditions

Condition	M_∞	M_{SI}	T_t,K	P_t, kPa	Total Mass flow rate(kg/s)	Air split ratio
1	4	1.79	925	556	7.71	3
2	4.5	1.98	1105	479.9	5.2	2.96
3	5	2.23	1120	610	5.28	2.98

Table 3-27 Experimental Conditions-Gas generator Equivalence ratios (ϕ_{gg})

Condition	M_∞	M_{SI}	ϕ_{gg}
1	4	1.79	0.74-3.05
2	4.5	1.98	0.98-3.10
3	5	2.23	1.02-3.17

3.4.1.6 Boundary conditions and Grid structure

Boundary conditions:

From the literature two conditions were considered with equivalence ratios. At gas generator inlet and scramjet inlet, mass flow boundary condition as given in Figure 3-26; Table 3-28 and

Table 3-29 is applied to maintain the achieved air split ratio for simulation. Total temperature, mass fraction of species is specified. Mixing and evaporation is not accounted in this paper. Premixed mixture is assumed to enter gas generator. All surfaces are assumed to be adiabatic. Vitiation effect is not considered and therefore only air is assumed to enter from scram inlet. For simulating different Mach number conditions, scram inlet nozzle expansion ratio is changed.

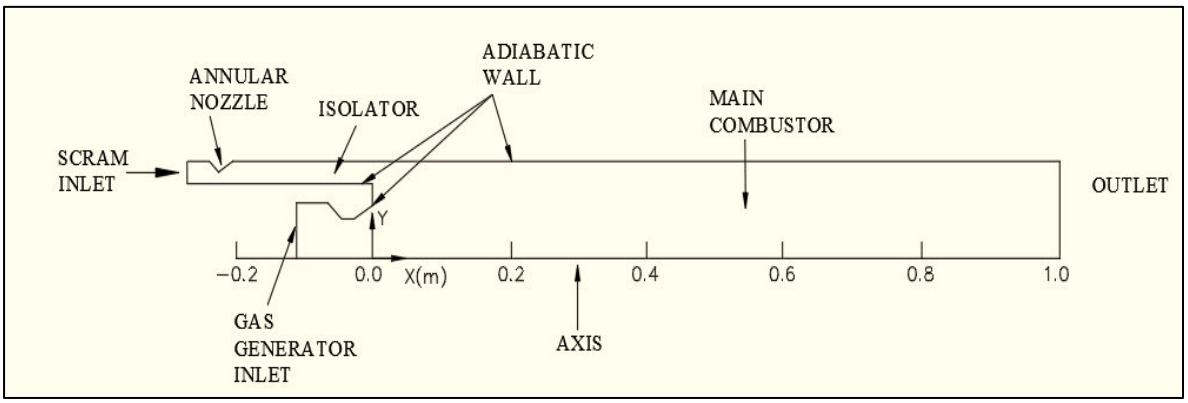

Figure 3-26 Domain boundaries

Grid Structure:

Simulations were carried out in a structured mesh generated in ANSYS ICEM CFD. Wall spacing was maintained at 0.1mm throughout. The y+ value along the mesh is shown is Figure 3-28**.** Mesh independence study was carried out in two stages in the first stage the overall mesh was refined and in the second stage an adaptive grid was generated and studied. Grid independence study is carried out for reacting flow at M_{SI}=1.79,ϕ_{gg}=2.84. The grid in the isolator region, Gas generator outlet and mixing region was refined while the wall spacing is maintained constant. Three grids with a ratio of 1:2:4 is studied. The coarse, medium and fine grid consisted

of 0.1 million, 0.2 million, 0.4 million nodes respectively. Grid convergence index as suggested by Roache [56],

$$GCI = \frac{F_s\left|\frac{(f_2 - f_1)}{f_1}\right|}{r^p - 1} \quad \text{..Eq(3.59)}$$

Where, f is the parameter that is considered for convergence, subscripts 1,2 corresponds to fine and moderate grids. The values for F_s, r, p are 1.25, 2 and 2 respectively as suggested by Roache. Figure 3-29 shows the wall static pressure distributions for coarse, medium and fine meshes. The error between the moderate and fine mesh was 2.5%. Hence, the solution produced is independent of mesh size. The medium mesh with 0.2million nodes is used for all the simulations here on.

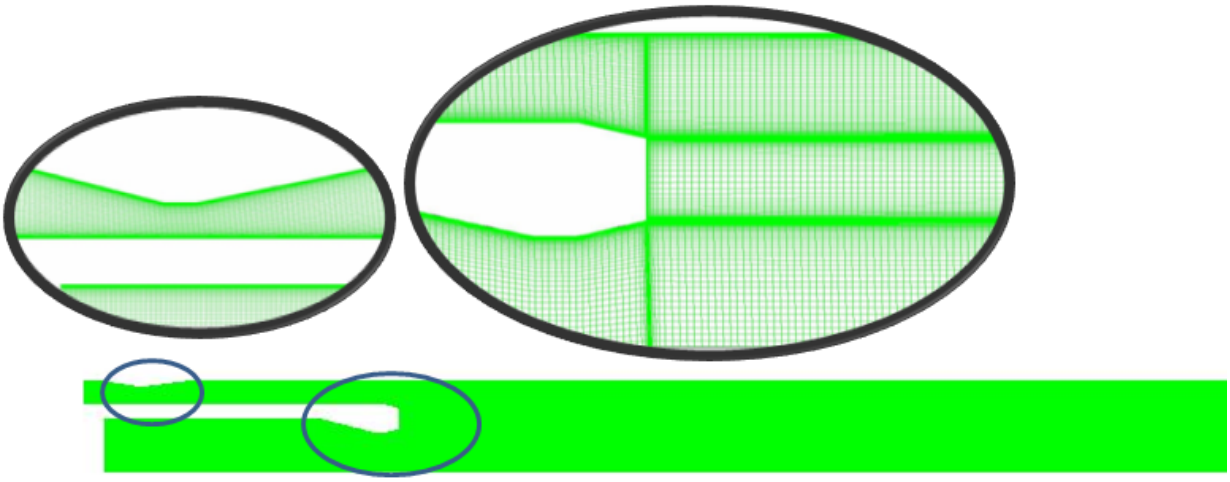

Figure 3-27 Grid structure of DCR: Mesh near nozzle regions

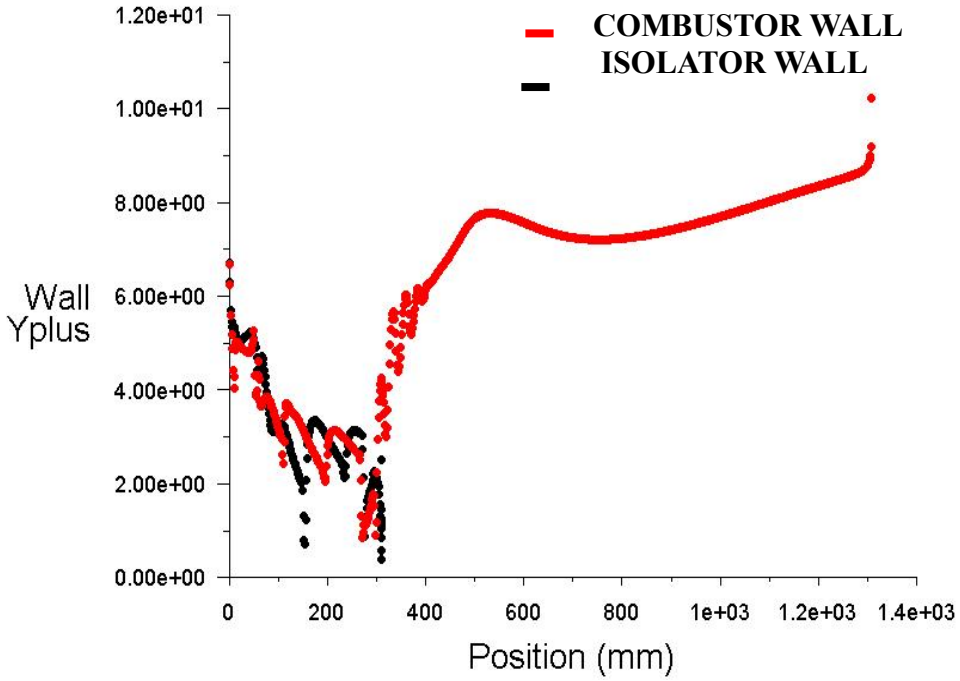

Figure 3-28 Y^+ distribution along the wall

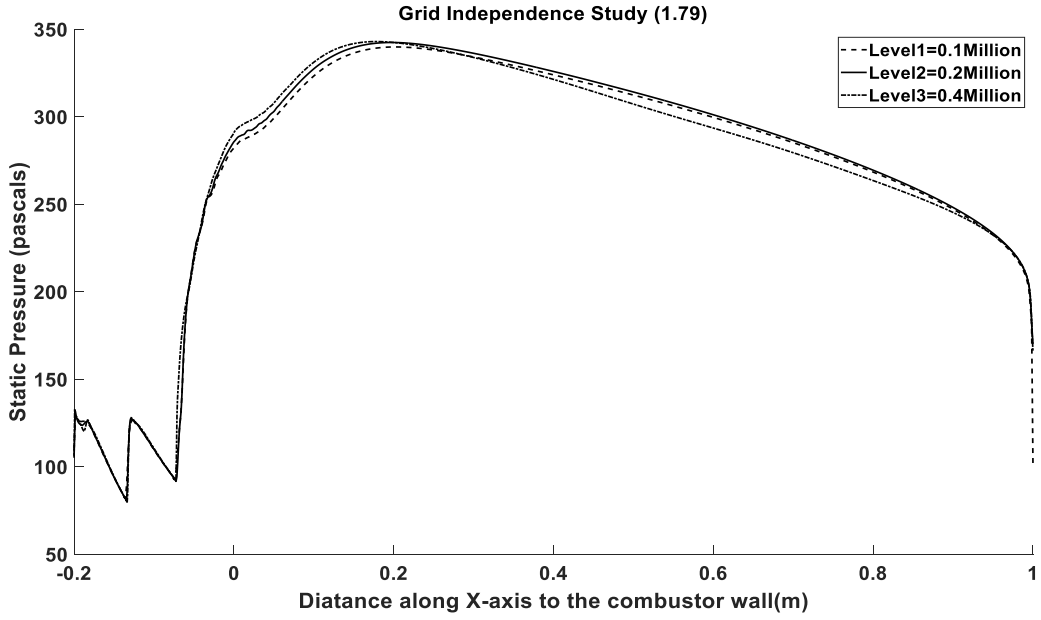

Figure 3-29 Grid convergence - Wall pressure along the combustor for various gird sizes (M_{SI} =1.79, ∅ =2.84)

Adaptive grid:

In the second stage of grid independence study, adaptive grid is studied. ANSYS offers a variety of grid adaptation methodologies, which refines/coarsens the grid at appropriate regions based on the geometry/solution data produced. Supersonic flow consists of shock waves which produce high, flow gradients. Gradient adaption methodology adapts the mesh based upon the gradient in the solution data. This methodology is based on the assumption that the highest error occurs where there is a higher flow gradient, hence the mesh at the region of high gradient is further refined to reduce the error. For a 2D grid the error is given by

$$|e_{i1}| = (A_{cell})^{\frac{r}{2}} |\nabla f| \quad \text{…Eq(3.60)}$$

Where,

e_{i1} - is the error indicator,

A_{cell}- is the cell area,

r - is the gradient volume weight,

∇f - is the euclidean norm of the gradient of the desired field variable

The solution data of static pressure is taken as the desired field for this study. The mesh is refined in two levels with 0.4 million nodes in level 1 and 0.8 million nodes in level 2 up from 0.2 million nodes in the base mesh (moderate mesh). The wall static pressure distribution of the two levels and the base case is in Figure 3-30, the refined meshes and corresponding flow field contours of static pressure is shown in Figure 3-31. The mesh adaption has refined the mesh along the high pressure gradients, along the shock waves. The shock waves formed in the refined meshes are more refined in that they are thinner than the unrefined base mesh. However, the wall static pressure distributions of base case and refined meshes show no significant changes. Hence, non- adaptive grid with 0.2 million nodes is taken for all further simulations.

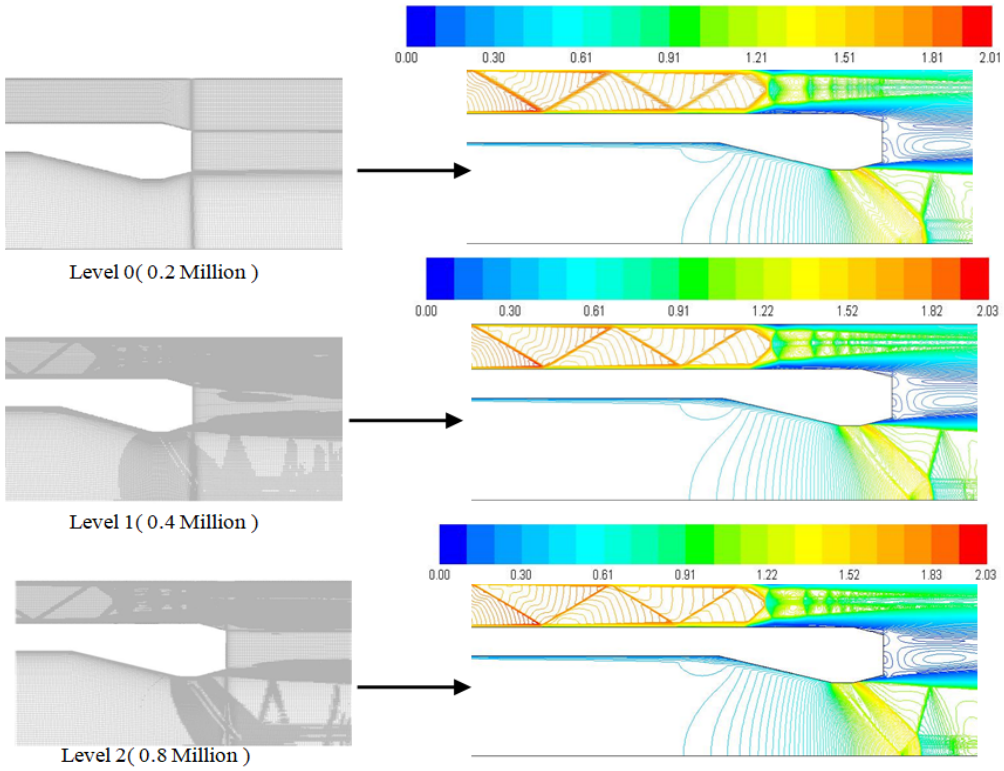

Figure 3-30 Left : Three levels of mesh refinements and Right: Mach contour

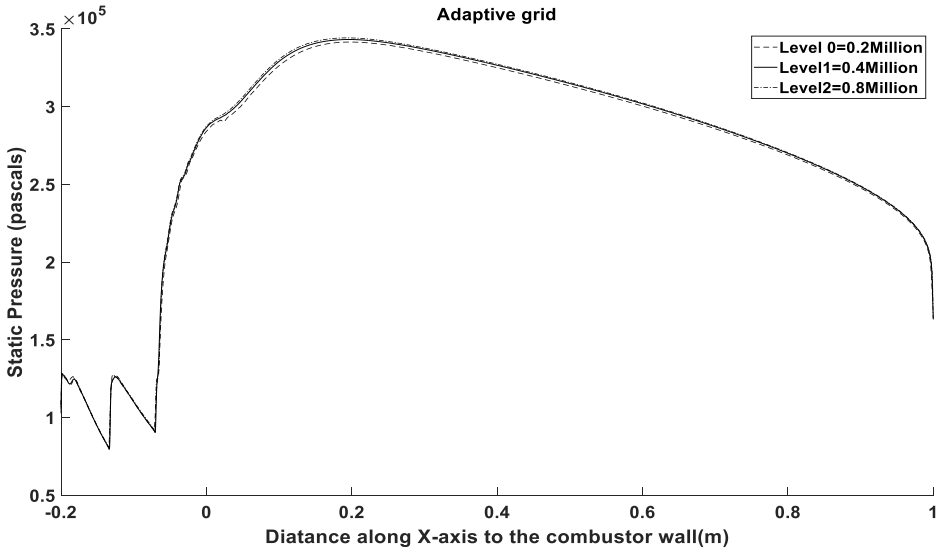

Figure 3-31 Adaptive grid convergence- Static wall pressure along the combustor for various levels

3.4.2 Turbulence model Validation

A turbulence study was carried out, turbulence models listed above are studied and compared with experimental data to find out the model which simulated the flow with high accuracy. The simulation is carried for two cases one at Mach 4 free stream condition with isolator entry Mach number, M_{SI} = 1.79 and Mach 5 free stream condition with isolator entry Mach number, M_{SI} = 2.23. Gas generator equivalence ratio (φ_{gg}) of M4 condition is 2.84 and of M5 condition is 2.64. Both reactive and non- reactive flow is simulated.

Table 3-28 Test conditions considered for numerical study

Condition	M_∞	M_{SI}	T_t, K	P_t, kPa	Total Mass flow rate(kg/s)	Air split ratio
1	4	1.79	925	556	7.71	3
2	5	2.23	1120	610	5.28	2.98

Table 3-29 Gas generator equivalence ratios (ϕ_{gg}) considered for numerical study

Condition	M_∞	M_{SI}	ϕ_{gg}
1	4	1.79	0.74, 1.24, 2.84
2	5	2.23	1.44, 1.60, 2.64

Figure 3-32 shows the wall static pressure distribution for non-reactive flow with experimental data. All the turbulence models over predict the static pressure distribution. The pressure oscillations seen in the graph is due to formation of oblique shock train in the duct. Figure 3-33 shows the static pressure contours and the Mach contours. The oblique shock train is clearly visible in the isolator.The pressure drop due to expansion wave downstream of the gas generator is clearly captured by the simulation as seen in the Figure 3-32.

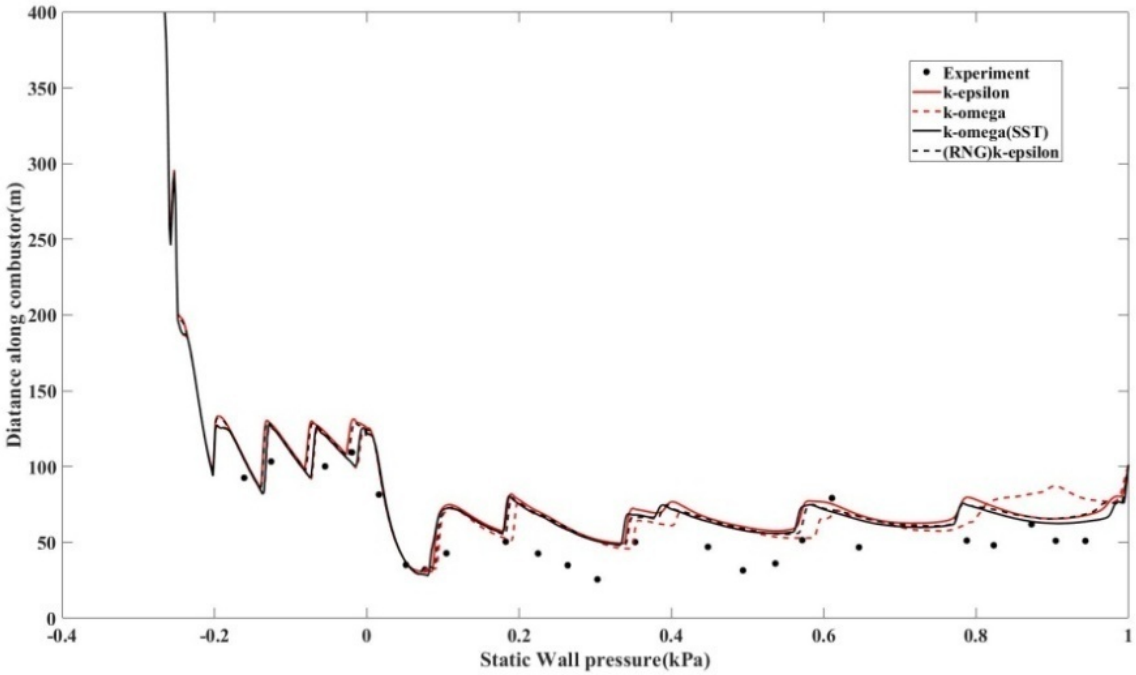

Figure 3-32 Non-reactive flow wall pressure CFD vs. Experiment

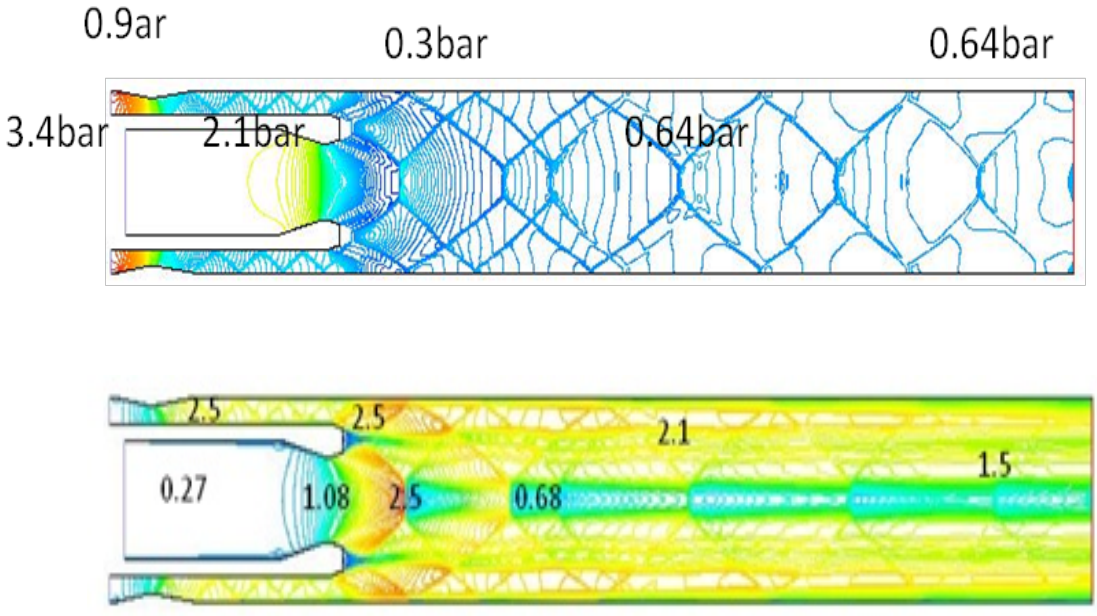

Figure 3-33 Non-reactive flow contours: Top: Static pressure and Bottom: Mach Number

Further reactive flow simulations for all the turbulence models for both the flow conditions were conducted. The reactive flow field was used for turbulence model comparison. The parameters used for comparison are

a) Wall static Pressure,
b) Shock train location, length and static pressure along shock train centre
c) Combustion efficiency
d) Velocity profile
e) Effect of equivalence ratio

a) Wall static pressure comparison:

Wall static distribution is representation of experimental flow field.

Figure 3-34 shows comparison of wall static pressure distributions with experiments for different turbulence models for condition 1(ϕ_{gg}=2.84) and condition 2(ϕ_{gg}=2.64) respectively. RNG, SST and k-ε are able to predict the pressure distribution of experimental flow field with a significant accuracy for the conditions simulated. Whereas wall pressure obtained from kω does not match with experimental data. For both conditions error in predicted wall pressure is computed along the length of combustor. Error in simulated wall static pressure with respect to experiment along length is plotted in

Figure 3-35 and Figure 3-37. The shock starting position is not accurately predicted by any of the models, subsequently the error in first three points is high but the error reduces to further downstream well within 10%.

RNG has captured the pressure rise part much better as compared to other models upto 0.3 m length. For pressure rise RNG predictions are better as compared to other models. SST and kε (standard) has larger error in the beginning but the error reduces downstream of the combustor. For both the conditions RNG captures flow accurately than other models. k-ω predictions are well away from the experimental flow field and does not match with experimental values. Simulation of Flow condition 2 shows large shock pressure oscillation in the beginning. These pressure oscillations are usually observed at the centre line but when flow separates and attaches back to wall, these oscillations are observed. Experiment measurements might have not

captured this phenomenon due to low no. of pressure measurement points and time averaging of data.

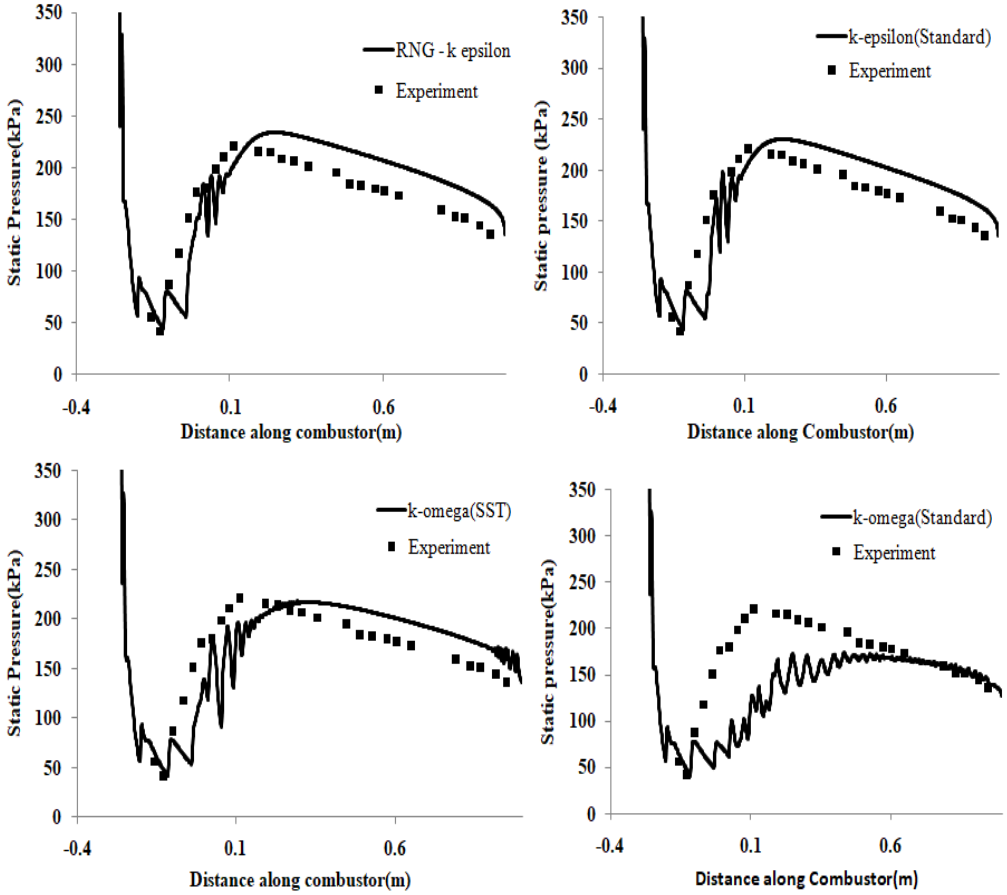

Figure 3-34 Wall static pressure compassion with experiments for various turbulence models (conditon1)(M_{SI}=1.79,ϕ_{gg}=2.84)

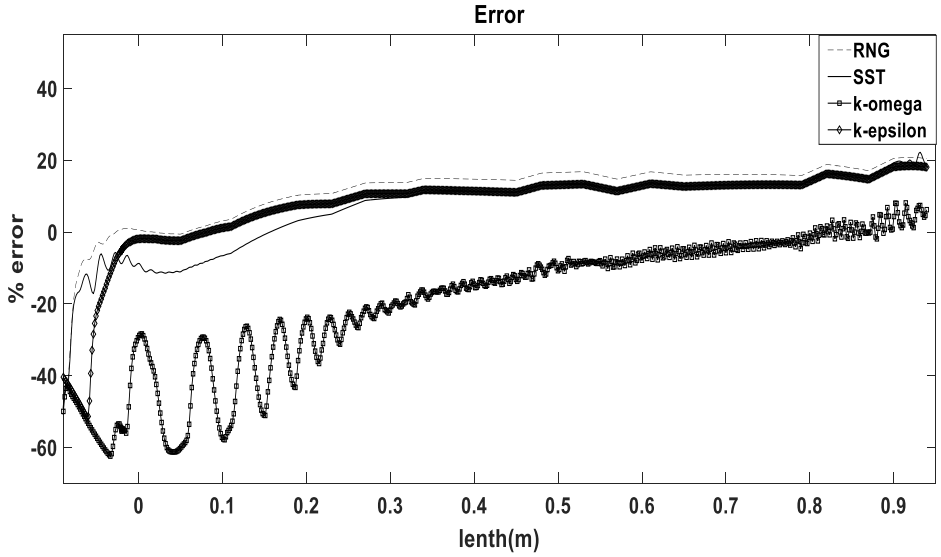

Figure 3-35 Estimated error along the length of the combustor (Condition -1)

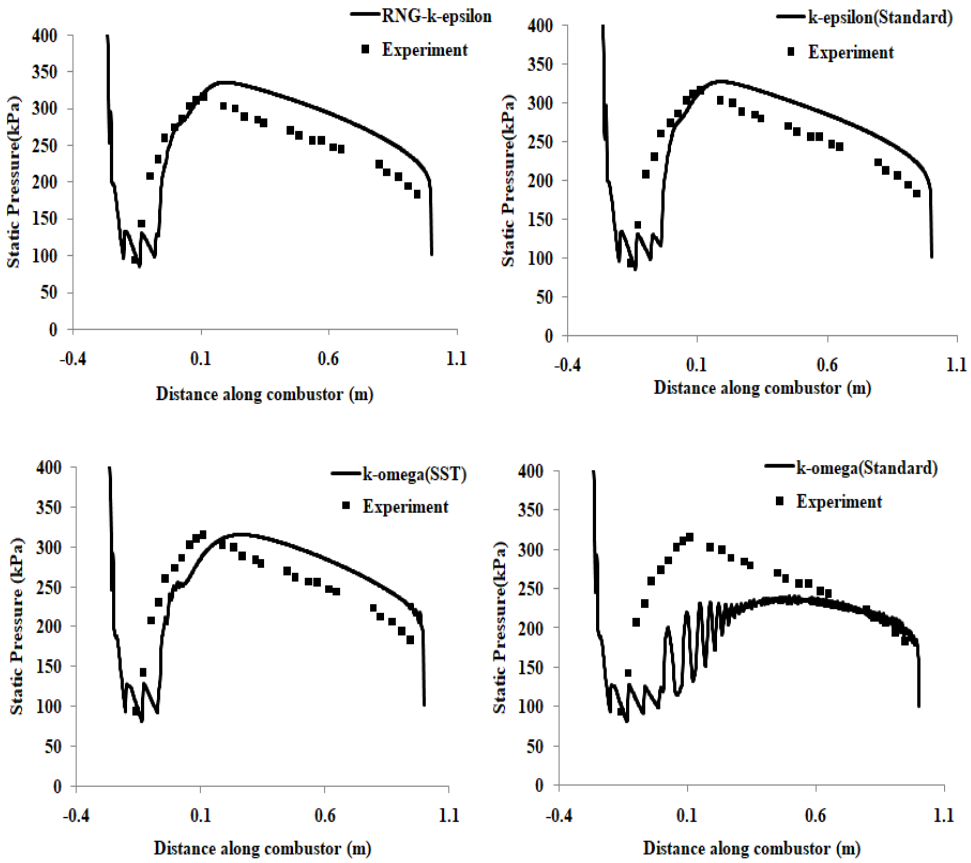

Figure 3-36 Wall static pressure compassion with experiments for various turbulence models for Condition 2 (M_{∞}=5,M_{SI}=2.23)

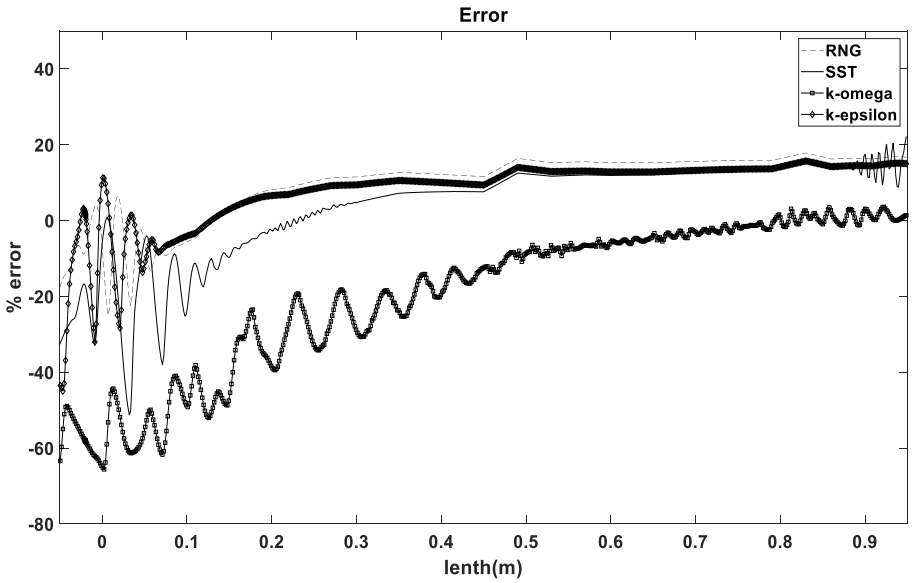

Figure 3-37 Estimated error along the length of the combustor (Condition -2)

b) Pre -combustion shock train (PCST):

The length of the isolator is crucial in that an insufficient isolator length will lead to an inlet unstart due to back pressure from the combustor, a longer isolator length will lead to extra weight. It is very important to predict accurate point of shock train as it decides the length of Isolator, to design isolator with optimum length. Four parameters are compared i.e. Average wall static pressure, shock train length (St), Shock train length inside isolator (So), Shock train length inside main combustor (Sd), which are given in Table 3-30 and Table 3-31.

Simulations could not accurately predict the shock train beginning in the isolator, the error in prediction is 80 mm and 87 mm for conditions 1 and 2 respectively. Average static pressure error is low for SST model in both the conditions. Shock train length is predicted with less error by RNG. Even though shock train length is captured accurately but still stating location has error more than acceptable.

Figure 3-40 shows Mach number contours of different turbulent models. Other than k-ω standard remaining have similar flow pattern. k-ω standard predicts very poor mixing and therefore largestretched recirculation zone is observed. Normal shock train is clearly visible with RNG, k-ε and SST. SST has captured the shock train formed at center of combustor much better as compared to other models. Difference is starting positi-on for each model is clearly visible in the Mach contours. Normal shock train is formed. For RNG, k-ε flow does not reattach to boundary, whereas flow simulated by SST model shows reattachment. Therefore, pressure rise by SST model shows oscillations.

Figure 3-38 shows shock train along line AA. For condition 1 shock train starting point is same but beyond x = 0.25 m both data start diverging. It is observed that shock train region is high when predicted by SST as compared to RNG, k-ε.

Table 3-30 Average wall pressure and shock stating length for Condition 1 (Msi = 1.79, ∅ =2.84)

Parameter	Experiment	RNG k-ε (Error)	k-ε (Error)	SST (Error)	k-ω (Error)
Avg Static Pressure(kPa)	248	274(+10.48)	263(+6%)	261.58(+5.5%)	196.2(-20.8%)
Shock Train (St)	0.27	0.258 (5%)	0.23 (-15%)	0.304 (+12%)	0.371 (28%)
So	0.16	0.08	0.041	0.074	0.013
Sd	0.117	0.178	0.19	0.23	0.35

Table 3-31 Average wall pressure and shock stating length for Condition 2 (Msi = 2.23, ∅ =2.64)

Parameters	Experiment	RNG k-ε (Error)	k-ε (Error)	SST (Error)	k-ω (Error)
Avg Static pressure(kPa)	166.6	185.8 (+11%)	183.0 (+10%)	174.3 (+4%)	134.0 (-19%)
St(m)	0.24	0.263 (+9%)	0.28 (+16%)	0.34 (+41%)	0.451 (+87%)
So(m)	0.13	0.043	0.038	0.04	0
Sd	0.11	0.22	0.24	0.3	0.451

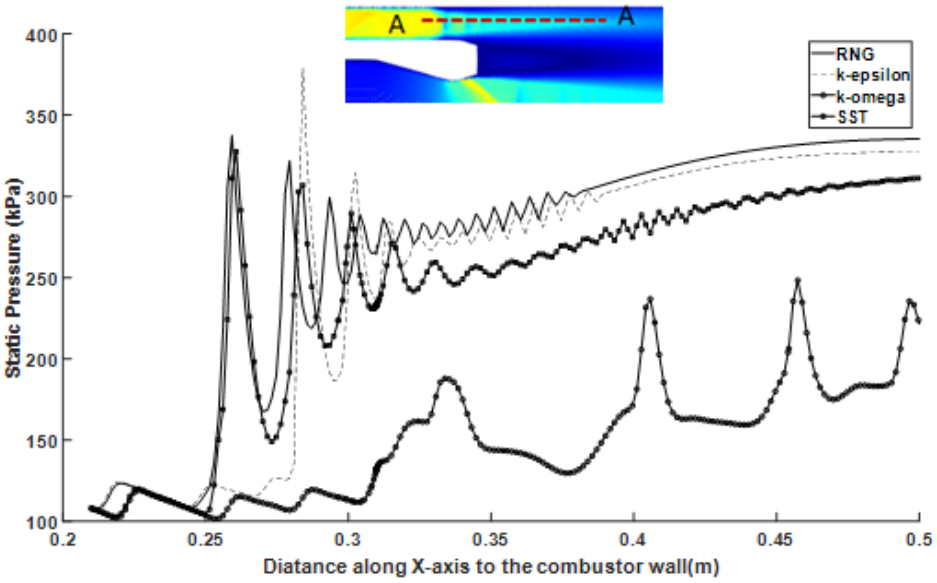

Figure 3-38 Static pressure along line 'A-A' for various turbulence models (Condition-1)

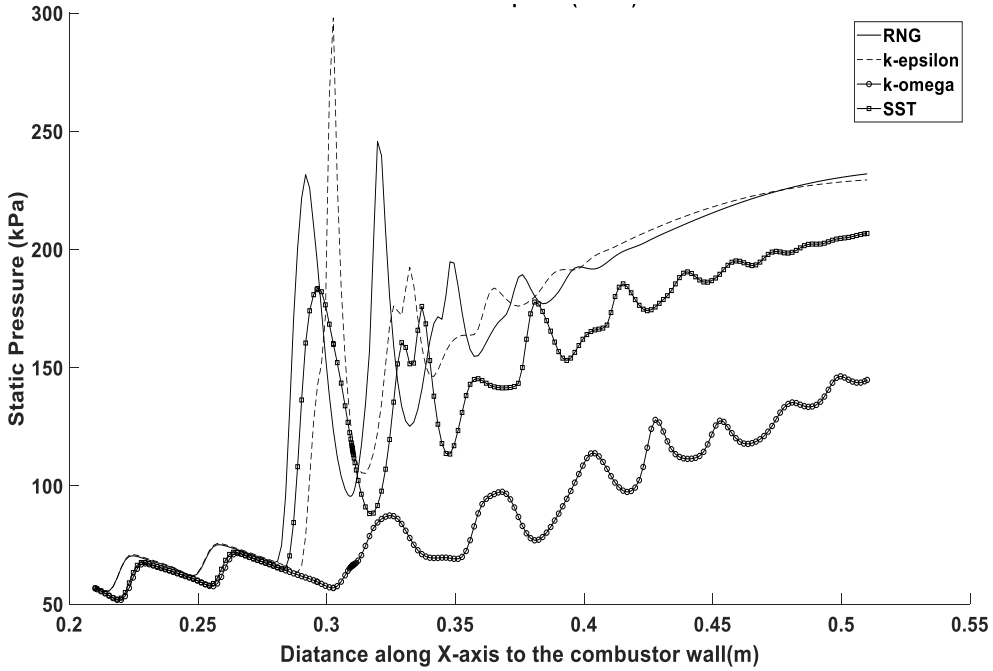

Figure 3-39 Static pressure along line 'A-A' for various turbulence models (Condition-2)

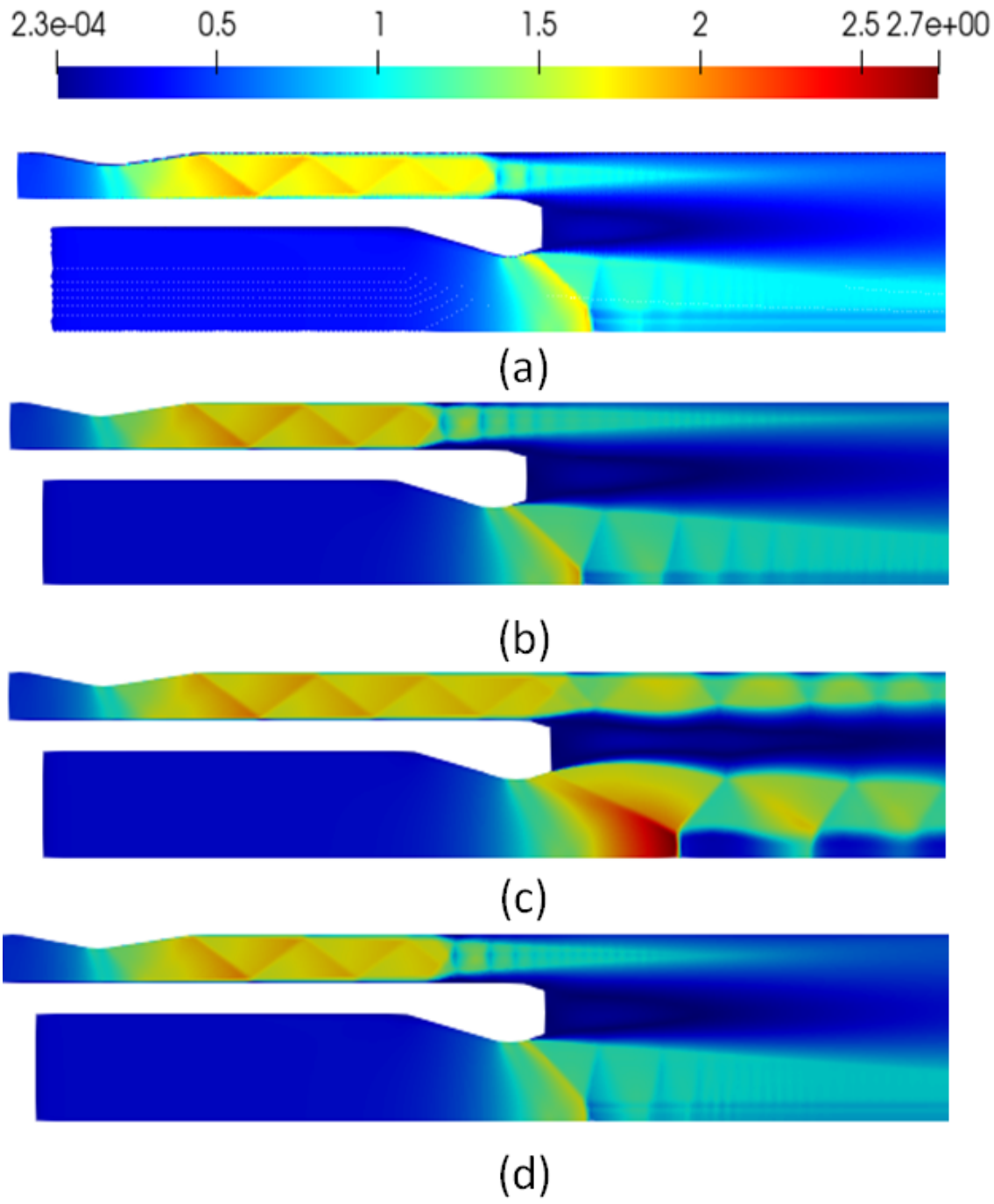

Figure 3-40 Static pressure along line 'A-A' for various turbulence models for Conditon-1

a)RNG, b) k-ε, c)k-ω, d) k-ω(SST)

c) **Combustion efficiency:**

Combustion simulation is assessed through total temperature contours and combustion efficiency. Combustion efficiency is the ratio of actual concentration of CO_2 ($m_{CO_2,x}$) to ideal CO_2 concentration (m_{CO_2ideal}) [35]. The ideal concentration of CO_2 is determined by NASA CEA code using inlet conditions.

$$Combustion\ effeciency(\eta_c) = \frac{m_{CO_2,x}}{m_{CO_2ideal}} \quad \text{..Eq(3.61)}$$

Figure 3-41 and Figure 3-42 gives combustion efficiency arrived from simulations using different Turbulence models for Conditions 1 and 2. Combustion efficiency increases upstream of the combustor, which shows mixing of fuel rich gas generator exhaust with supersonic air stream and subsequent combustion. K–ε RNG predicts highest combustion efficiency. The effect of high combustion efficiency can also be observed in static pressure plot where RNG predicted Maximum wall static pressure more than other models. The combustion efficiency at the exit of the combustor is still increasing and has not plateaued, this indicates incomplete combustion and that the combustor is not of sufficient length.

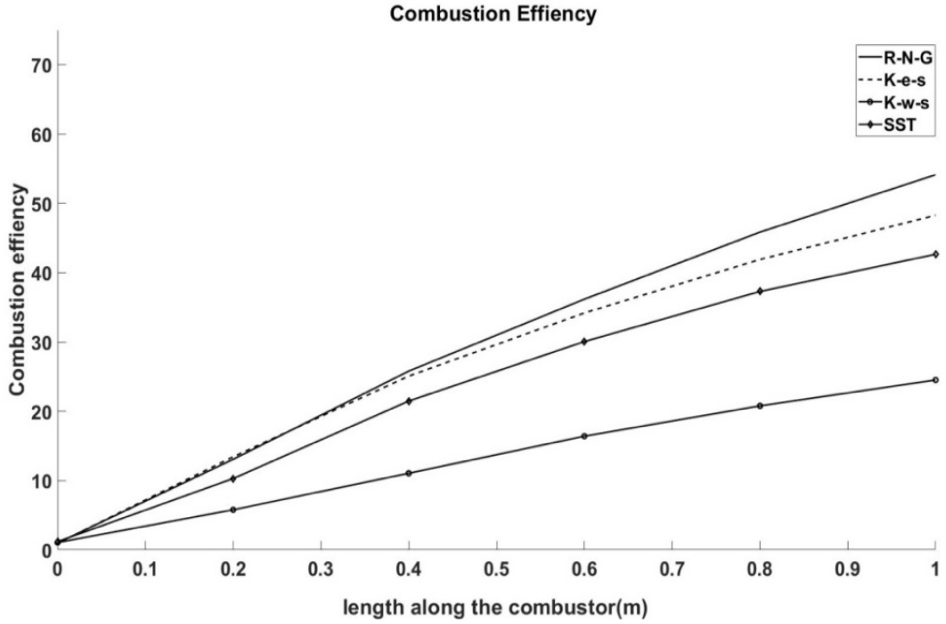

Figure 3-41 Combustion efficiency for various turbulence models along combustor (Condition-1) (ϕ_{gg} = 2.84)

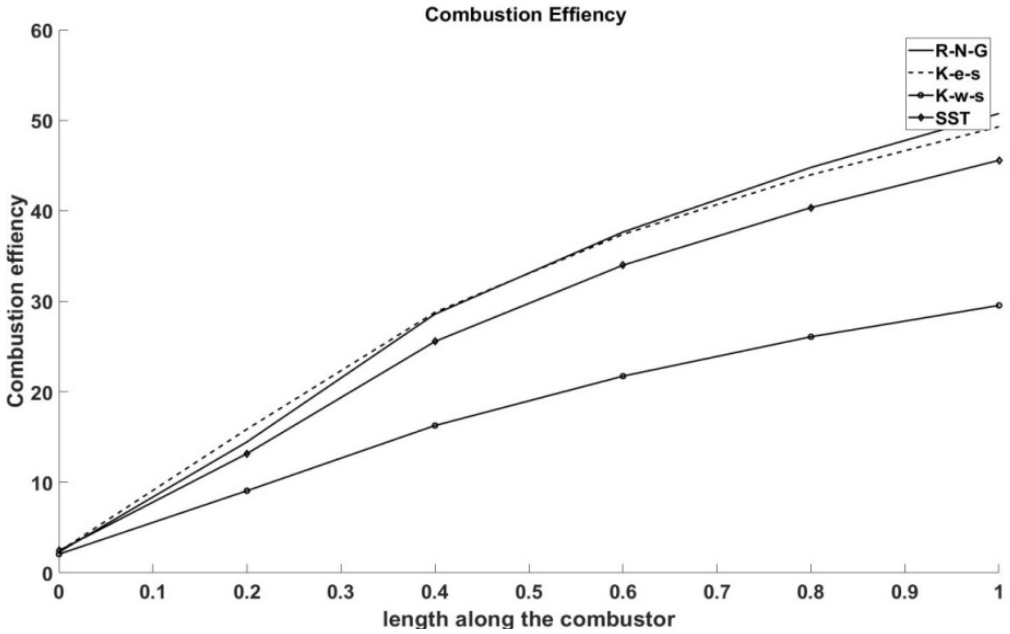

Figure 3-42 Combustion efficiency for various turbulence models along combustor (Condition-2) (ϕ_{gg} = 2.84)

d) Velocity profile:

Figure 3-43 and Figure 3-44 shows the velocity profile for both conditions 1 and 2. The velocity profile at the center axially is higher in all turbulence models except k-ω , which showed an inaccurate pressure distribution earlier.

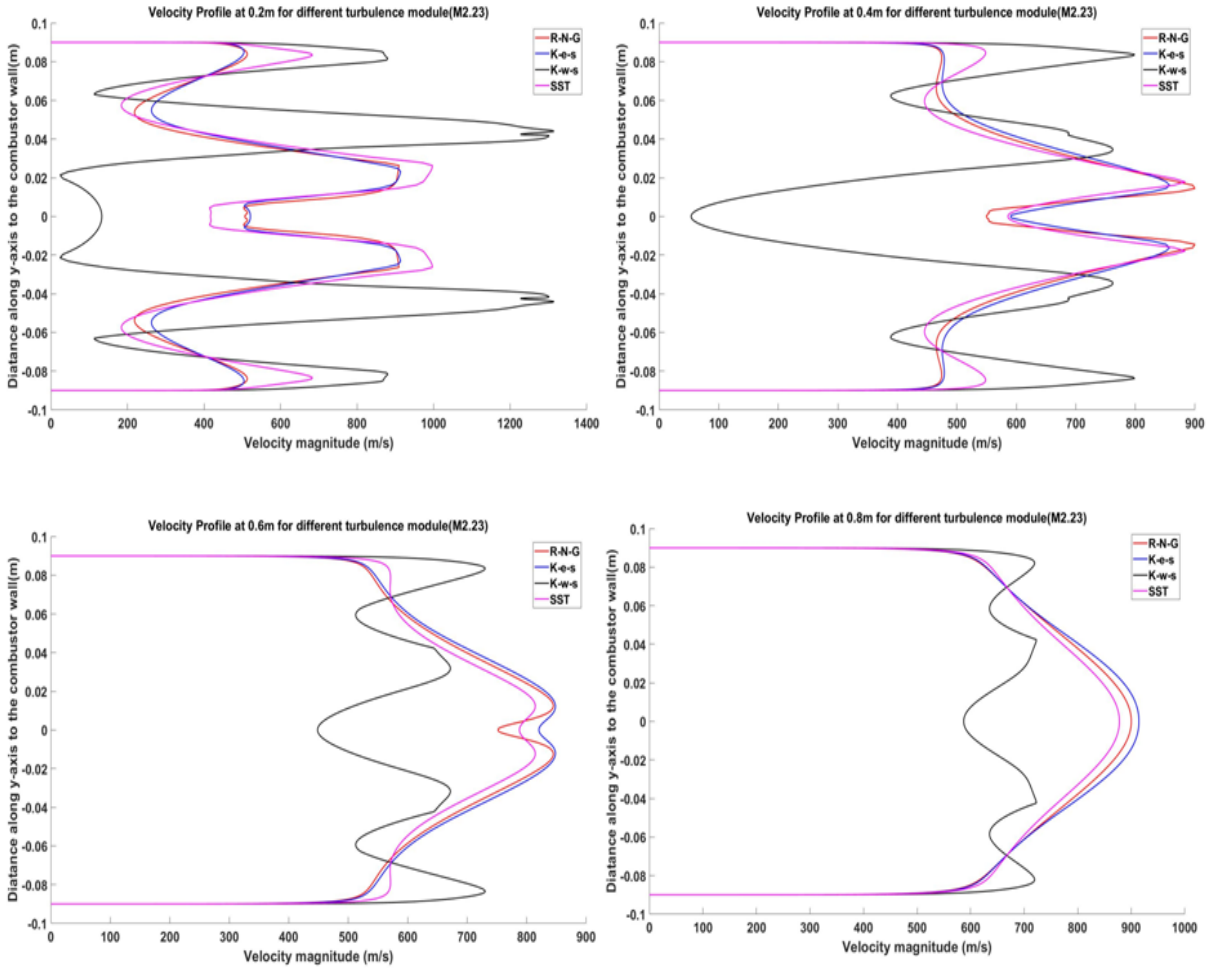

Figure 3-43 Velocity profiles with various turbulence models (Condition-1)

The flow at near the wall regions has a lower velocity than the centre flow, this is due to the supersonic nature of the flow at centre and lowered velocity towards the wall region due to normal shock trained formed in the isolator. Recirculation zone near the flame holder takes place, which causes the lower velocity in that region. Low velocity region formed at centre is due to shock train formed at exit of gas generator to adjust the pressure.

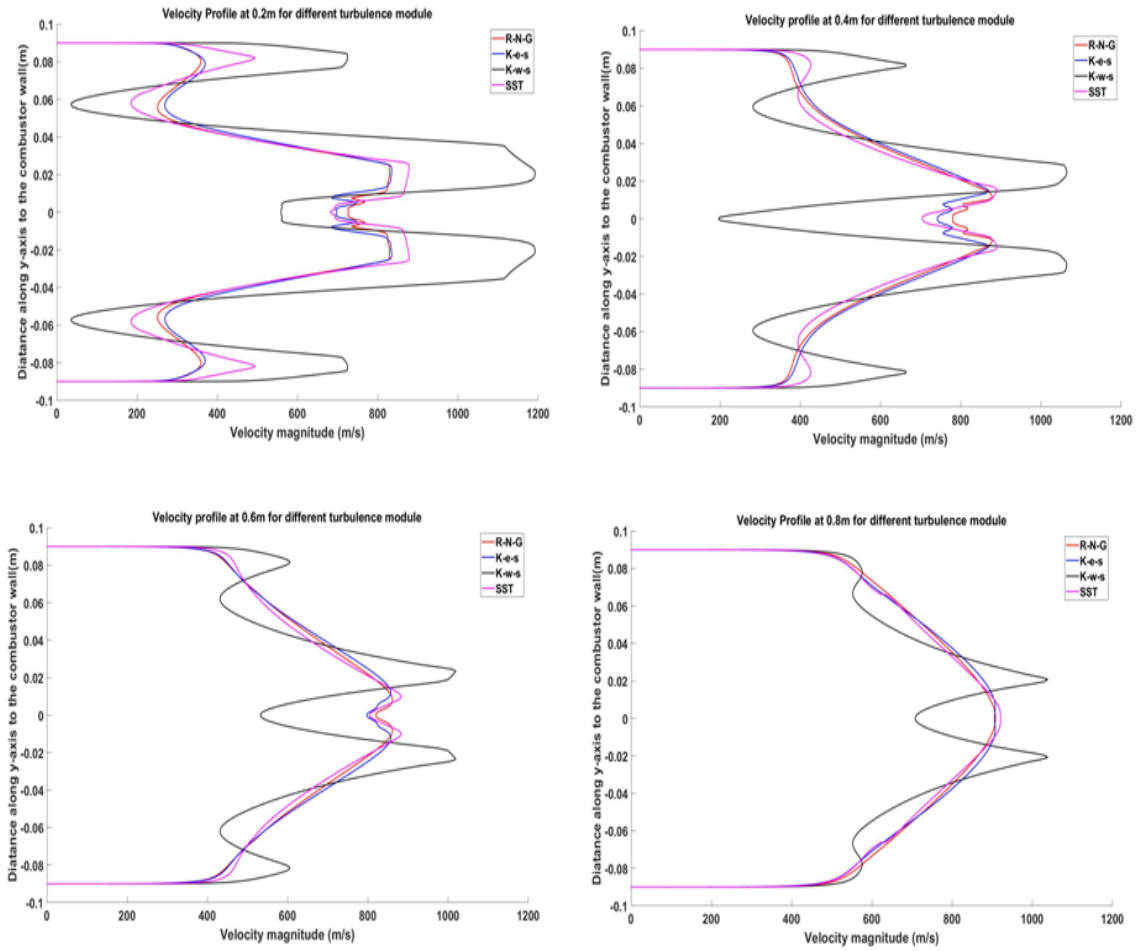

Figure 3-44 Velocity profiles with various turbulence models (Condition-2)

Turbulence study summary:

Four turbulence models RNG k-ε, kε(standard), kω(standard), SST- kω are studied and compared with experimental results to find best suitable one for supersonic flow inside a isolator-combustor. Wall static pressure along the combustor wall is compared with simulation data for all models with experimental results. Starting position of Pre-combustion shock train is not well captured, therefore large errors are observed in first 3 points but subsequently error reduces. (RNG) k-ε shows best match during pressure rise i.e capturing of shock train but beyond maximum pressure SST and k-ε shows better match. SST k-ω predicts average pressure with least error. k-ω standard could not predict phenomena properly. Combustion efficiency calculated based on concentration of CO_2 is also calculated and compared for each model. RNG predicts the highest combustion efficiency.

e) **Effect of Equivalence ratio on combustion and shock train**

The equivalence ratio (ϕ_{gg}) of gas generator is changed as in

Table 3-29. Figure 3-45shows the comparison of Wall static pressure for different equivalence ratio flows for Condition1 in

Table 3-29. Simulations results are in good match with experimental results. For low equivalence ratios (lean ϕ_{gg} <1) no pressure is developed. Pressure increases with increase in equivalence ratio which is well captured by simulations. Figure 3-46 shows effect on total temperature for different equivalence ratios for Condition 1. Figure 3-47 shows Mach contours for different equivalence ratio. As gas generator equivalence ratio ϕ_{gg} is increased, pressure in the supersonic combustor increases. To balance the increase in pressure shock train becomes strong and moves further upstream in the isolator. This phenomenon is well captured in the simulations. As compared to scramjet combustor where subsonic flow occurs near cavity, in DCR subsonic combustion occurs in front portion of combustor where maximum pressure rise takes place. Total temperature is indicative parameter of extent of combustion. As the Equivalence ratio is near one in gas generator, most of combustion takes place inside GG. The flow coming out of GG has product of complete combustion. As the equivalence ratio reaches near three in GG, Complete combustion cannot take place due to fuel rich condition and combustion products are cracked products of combustion.

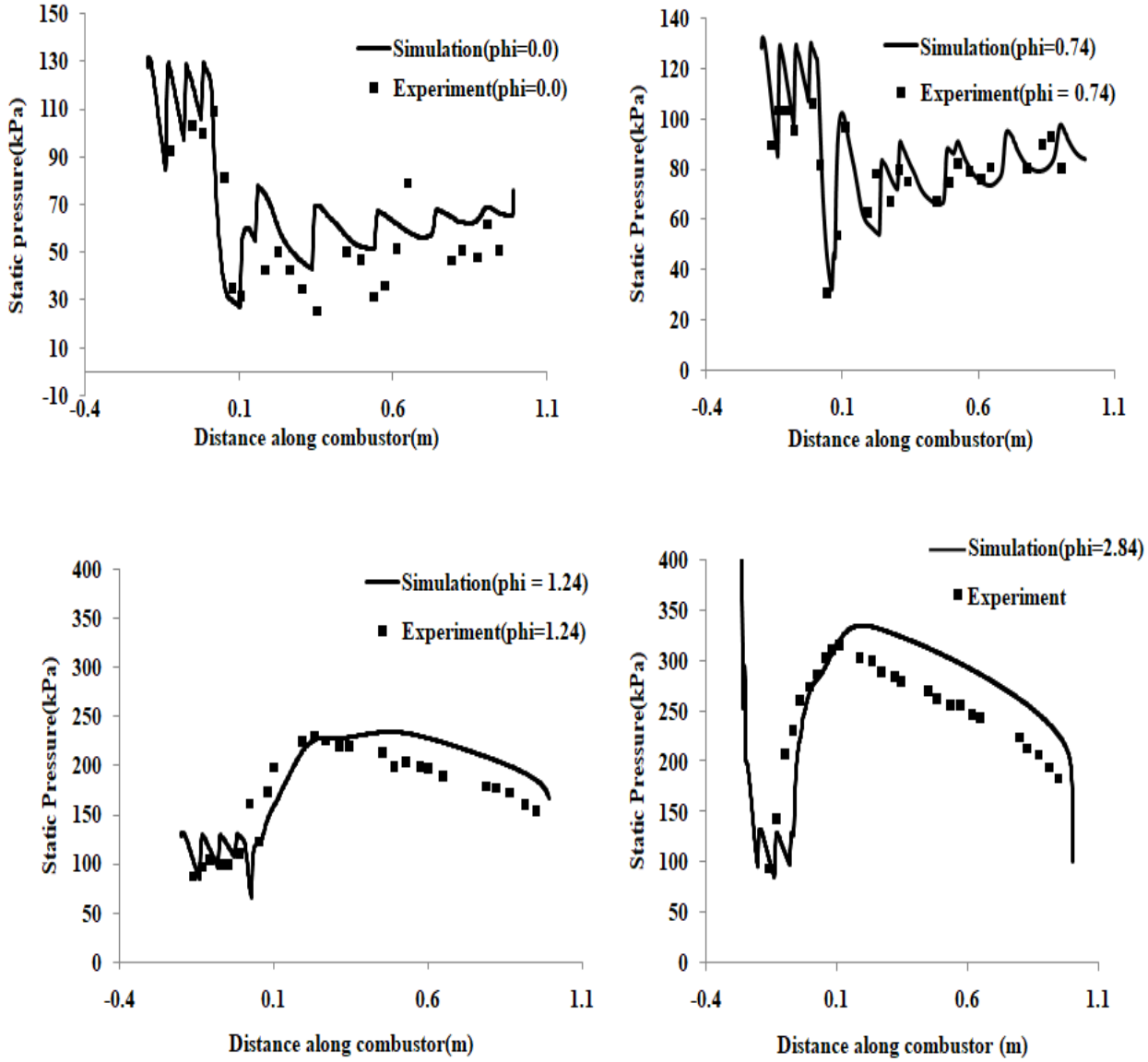

Figure 3-45 Wall static pressure along combustor length for Condition-1 with different equivalence ratios

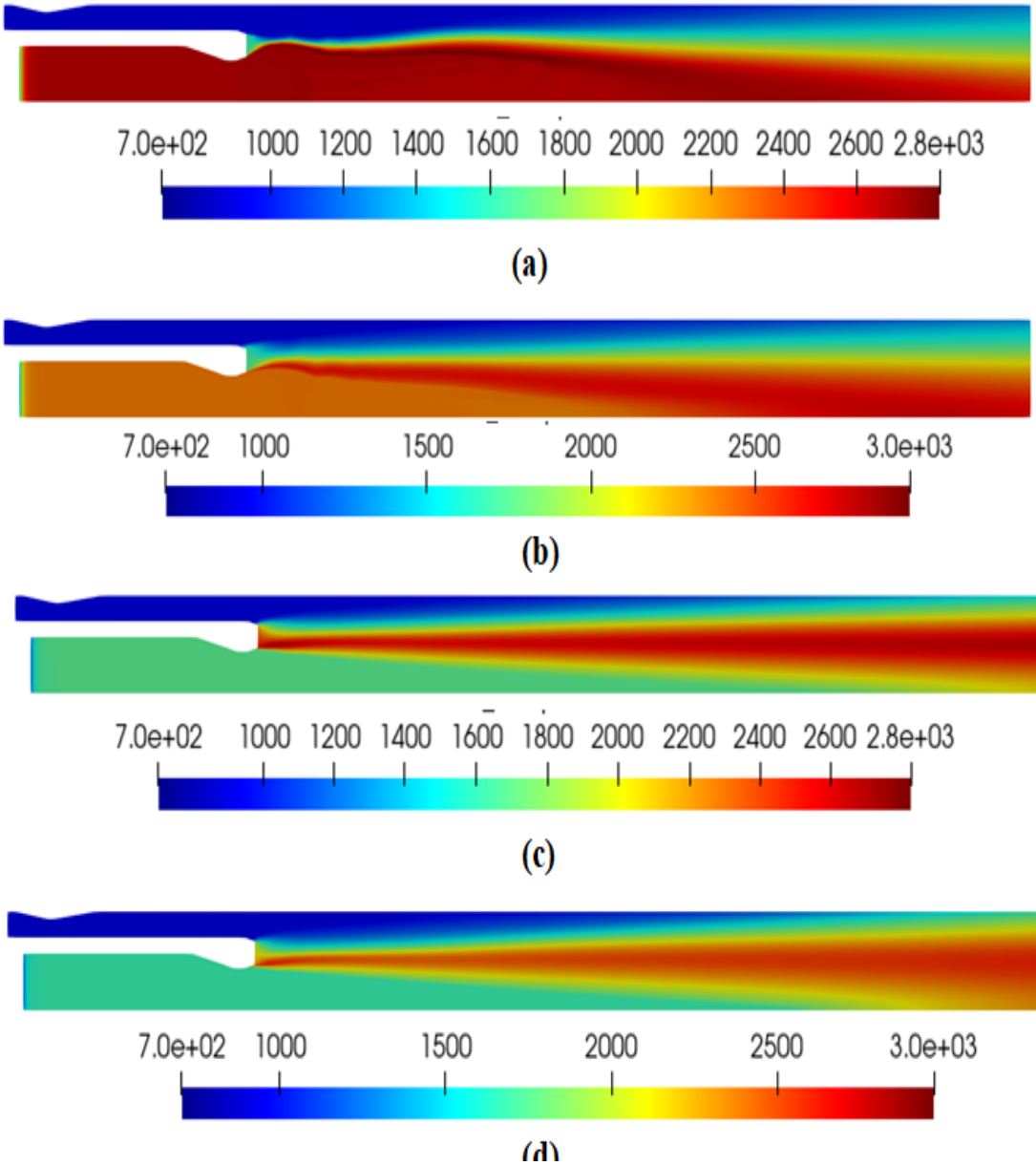

Figure 3-46 Total Temperature Contours for different equivalence ratio a) ϕ_{gg} =0.74, b)ϕ_{gg} =1.24, c)ϕ_{gg} = 2.84 ,d) ϕ_{gg} = 3.05

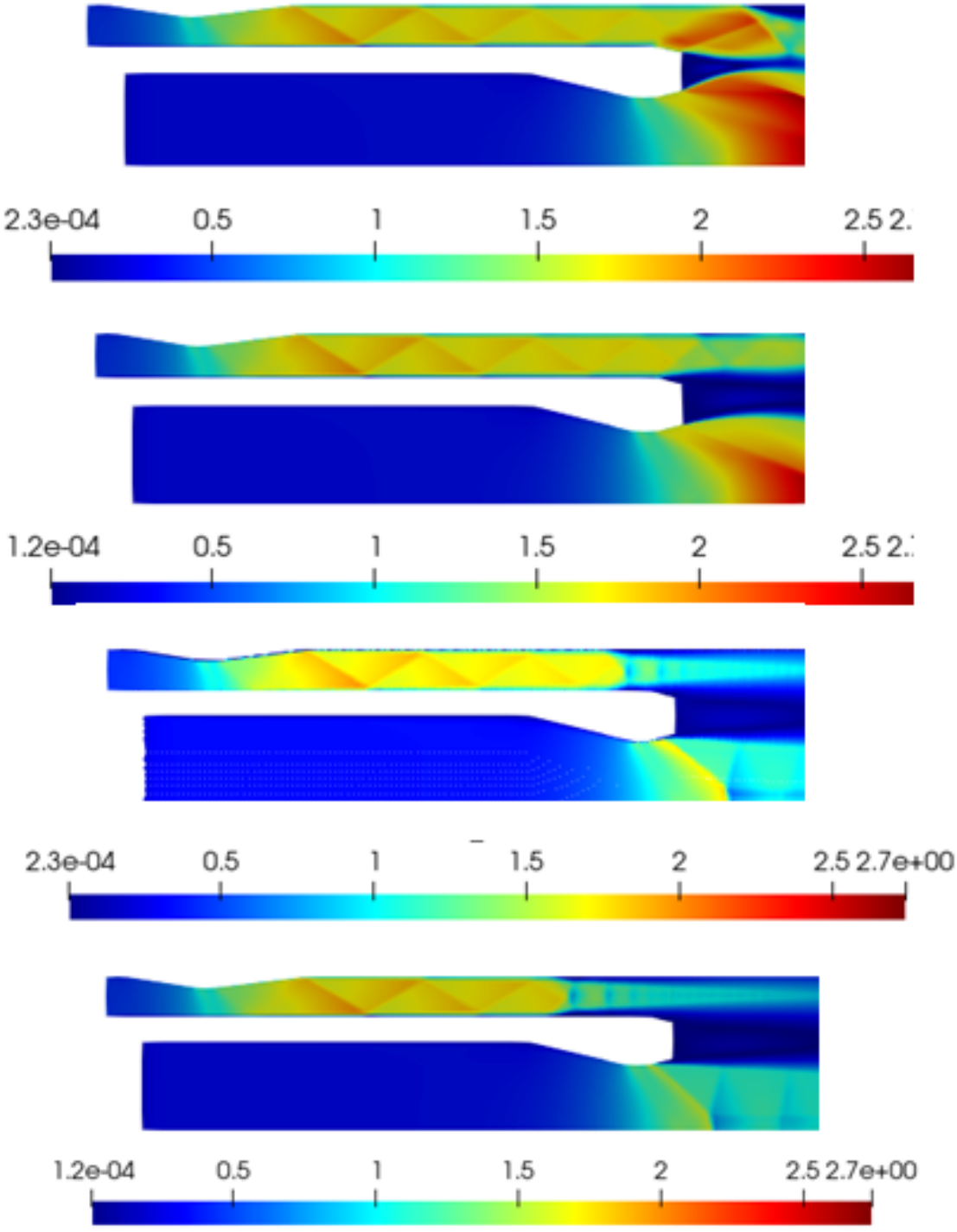

Figure 3-47 Mach Contours for different equivalence ratio a) ϕgg =0.74, b)ϕgg =1.24, c)ϕgg = 2.84, d) ϕgg = 3.0

3.4.3 Summary on Numerical simulation and validation of DCR Combustor

Numerical studies are carried out on the DCR combustor specifically addressing interactions of annular isolator with hydrocarbon fueled axisymmetric Scramjet/Ramjet combustor and the effectiveness of various turbulence models for this flow field analysis.

- CFD procedure is evolved and results are validated with literature based experiments. Geometry of model DCR is taken for simulations from literature. Favre Averaged equations were solved using Commercial code – ANSYS FLUENT. Premixed composition of air and Kerosene is inducted into dump combustor.
- Combustion modelling reaction rate is determined by chemical kinetic mechanism of Kerosene/Air. A reduced mechanism is applied. Reactive flow is modelled using 7 species and 4 step chemistry.
- Grid Independence study is done using Grid Convergence Index method. 3 grids were evaluated with ratio of 2 between each grid. For all simulations grid with 0.1 million grid points is selected.
- Simulations are carried out in two parts. In First part, numerical procedure is evolved which includes grid independence studies and various turbulence models evaluated for reactive and non-reactive cases. These simulations are carried out for conditions M4 and M5 flight conditions. In part two effect of gas generator equivalence ratio on isolator shock train location, pressure rise and combustion is studied.
- A Density based solver with 2^{nd} order spatially accurate ROE-FLUX difference splitting scheme applied to this found to be a good solver. Commercial solver Fluent 13 is used for carrying out simulations. Simulations were carried out with various turbulence models i.e k-ε (Standard), (RNG) kε, kω-Standard, k-ω SST and combustor wall pressures were validated with published experimental results. Various turbulence models are studied to find best suitable for flows with shock train and combustion in mixing shear layer. (RNG)k-ε showed best match followed by k-ε. k-ω SST also predicts shock train stating position similar to above mentioned models but maximum peak pressure is not predicted well. k-ω standard could not predict phenomena properly.
- Error in estimation of Starting Location of Shock train, Maximum Pressure, Average pressure in combustor is compared. (**RNG) k-ε is best model which could predict shock**

train location with an error of < 5% whereas k-ε (Standard) could predict with 10% error. Average Pressure and Maximum Pressure error is less with RNG.

- Further, effect on shock train position in Isolator with change in gas generator equivalence ratio is studied for free stream Mach number. = 4 and 5. Surface pressure is compared with Experimental results and found good match.
- Wall static pressure for various equivalence ratio conditions are predicted. Simulations results are in good match with experimental results. Pressure increasing with increase in equivalence ratio is well captured by simulations. As GG equivalence ratio is increased, pressure in the supersonic combustor increases. To balance the increase in pressure shock train becomes stronger and advance towards upstream in the isolator. This phenomenon is well captured in the simulation.
- Further effect of varying GG equivalence ratio is studied. Numerical simulation has good match with experiments. It is observed that operating GG equivalence ratio should be high so that cracked products mix in main combustor and further heat is released. It is observed in most patches flow is subsonic in main combustor. To keep the flow supersonic divergent angle to be given as this will avoid thermal choking.

3.4.4 Numerical study of DCR Combustor configuration

The initial design of the combustor is from the literature [38]. The design was then modified in accordance with the current requirements. The areas of the gas generator and supersonic intake were calculated for mass flow rate which is based on the thrust requirement of the missile at flight altitude and Mach number, the overall length of the combustor (which is constrained by overall dimensions of the missile) was fixed in all the cases. Several design iterations were simulated, geometries including different combustor divergent angles, isolator angle and flame holder thicknesses were tried before arriving at the final revisions. The dimensions of mixing throat, gas generator exit and isolator exit were varied to arrive at a design which produces an efficient mixing of isolator and gas generator streams, resulting in efficient combustion and subsequent pressure rise which in turn gives a higher thrust. The revisions were compared in terms of mixing of gas generator and isolator streams and combustion efficiency. The final 5 iterative cases are discussed in this chapter.

Solution methodology/Numerical simulation:

The CFD methodology validated in the previous chapter was followed for the simulations. Simulations were carried out in commercial CFD software ANSYS fluent. For closure of FANS, the two-equation turbulence model k-Ɛ RNG turbulence model which showed a good agreement with the experimental data was used. All simulations are axisymmetric. Second order implicit, Roe-FDS scheme was used. Solution steering was employed with the courant number set between 0.001 to 0.1.

For combustion reactions, Finite rate/Eddy dissipation model with 4 step and 7 species reaction was used to better predict the reactions due to both turbulent mixing of gas streams and the chemical kinetics was used. First simulation of non-reacting flow with species transport was run, until the flow is established, then with that flow data volumetric reactions were turned on to initiate combustion.

Grid:

Structured grid made in ICEM was used for all the simulations, the same procedure as in validation study was followed. The wall y+ is was below 30 for most part, the y+ along the wall is given is given in Figure 3-49**.** The mesh consisted of 12 blocks, hyperbolic mesh law was used in the nozzle region to better capture the geometry and bi-geometric mesh law was used elsewhere. The mesh is refined in the region immediately downstream of the flame holder where mixing layer of isolator flow and gas generator is present. Three meshes with increasing order of size were considered for grid independence study. The mesh sizes were in ratio of 1:2:4. The coarse, medium and fine mesh consisted of 0.35, 0.7 and 1.4 million nodes respectively. The mesh was refined globally for the subsequent increase in mesh sizes while the wall spacing was maintained the same in all the meshes. Wall static pressure is used as convergence criteria. Figure 3-50 shows the wall pressure distributions for coarse, medium and fine mesh. The GCI is between the medium and fine mesh is 3.09% which shows the solution is sufficiently independent of mesh size.

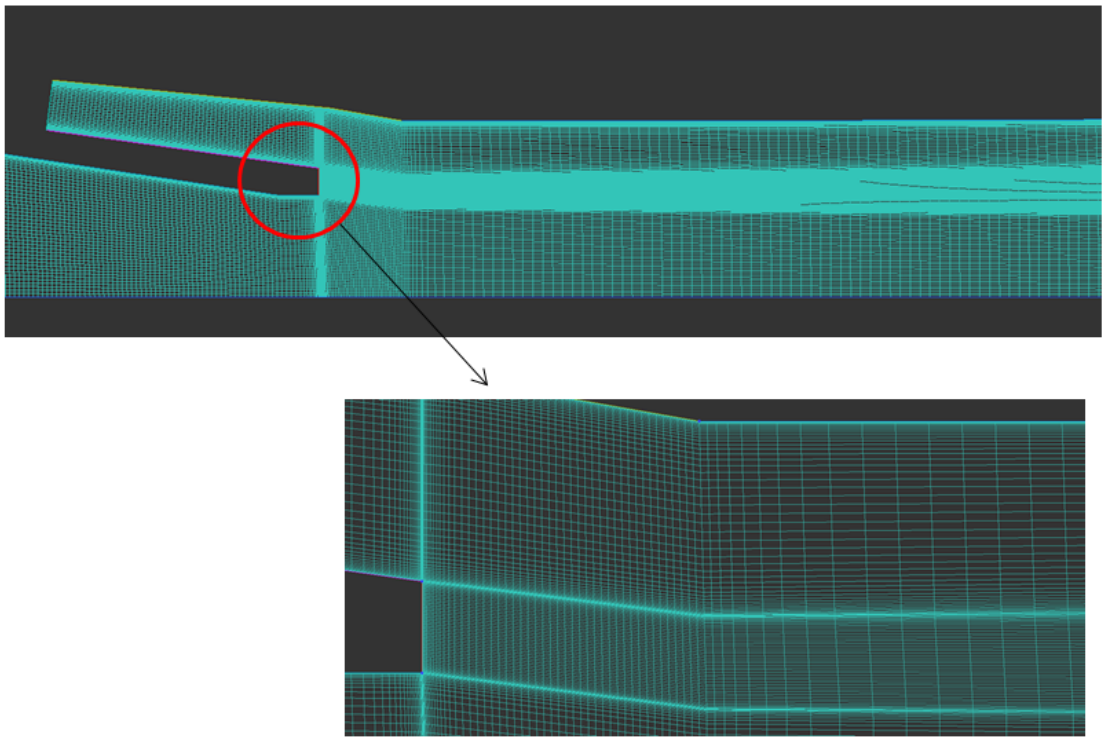

Figure 3-48 Grid structure: Close up view of grid near the mixing region

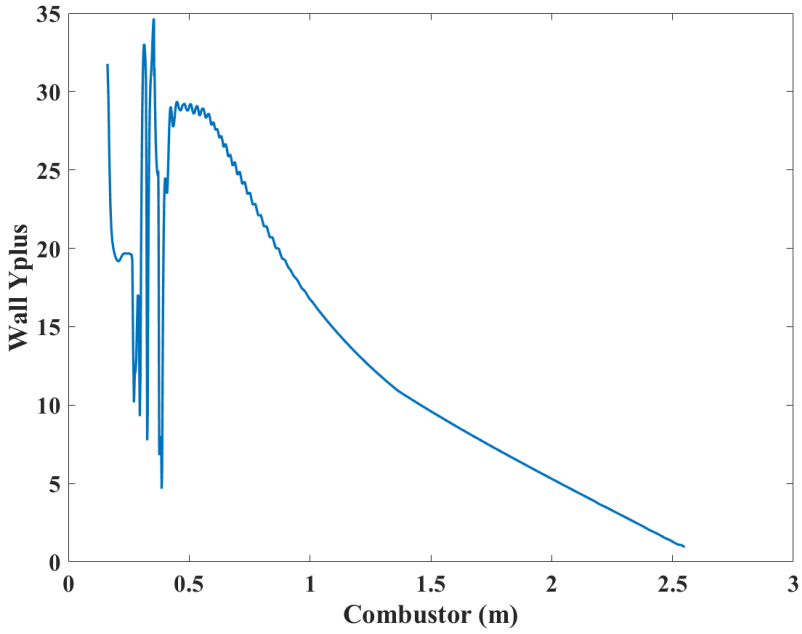

Figure 3-49 wall y+ along the combustor wall

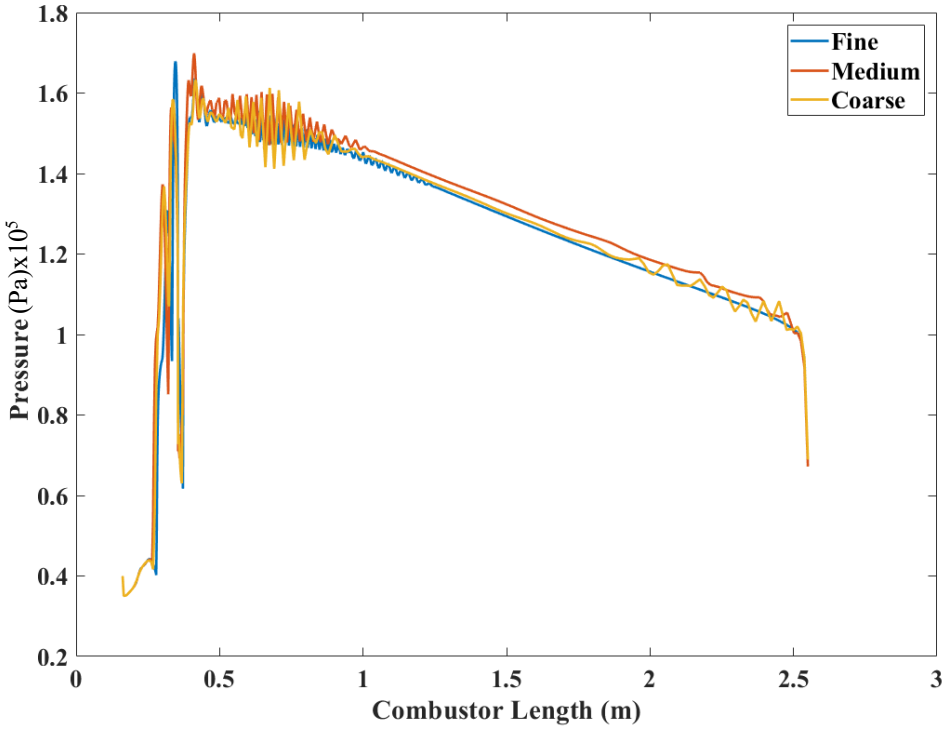

Figure 3-50 Grid convergence- Combustor wall pressure for coarse, medium and fine mesh

Geometry:

The flow domain consists of isolator, Gas generator, supersonic combustor and nozzle. The areas of gas generator and scram inlet are fixed based upon the required mass flow rate to produce mission specified thrust. Since the geometry of the combustor is cylindrical (axisymmetric), a 2D geometry with only half of the domain is constructed with an axis on the base. Only the aft part of the gas generator comprising of the convergent duct is considered, as the main focus here is the combustion in the main supersonic combustor. The nozzle is located at the end of the Main combustor at 2550mm from the start of the domain. The nozzle is 970 mm long, with an exit radius of 280mm and expansion ratio of 2.05. The dimension of the nozzle remained the same across all the cases, while the dimensions of the gas generator, isolator and the main combustor were varied to improve combustion performance.

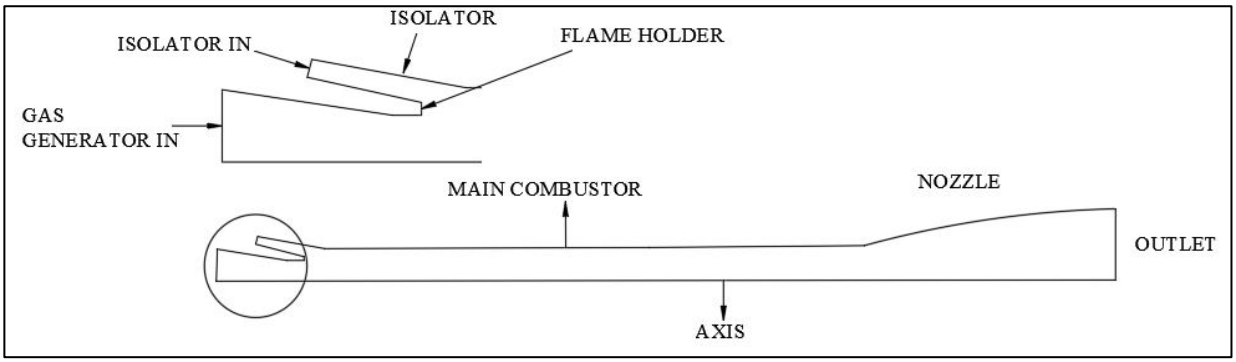

Figure 3-51 DCR Geometry for simulation

Boundary conditions:

Simulations were carried flight Mach number 6. Mass flow boundary condition was used for Gas generator and Scram inlet. The mass flow rate and the pressure were calculated based on the thrust requirements and the expected flight altitude at the Mach 6. Pressure outlet boundary condition was used for nozzle exit. Wall boundary condition with standard wall functions was used for all other boundaries. The boundary condition for Mach 6 is given in Table 3-32.

Table 3-32 Boundary conditions for Mesh convergence

Boundary	Boundary conditions
Scram inlet	**Mass flow** 1. $\dot{m}$ = 5.7 kg/s 2. P_{static} = 0.4 atm 3. T_o = 1503K
Species mass fractions	**Air inflow** O_2 - 0.23 N_2 - 0.77
GG Inlet	**Mass flow** Overall equivalence ratio(ϕ) – 0.9 1. $\dot{m}$ = 2.22kg/s (1.88 *air* + 0.34 *fuel*) 2. P_{static} = 1.5 atm 3. T_o = 1158K
Species mass fractions	Overall equivalence ratio(ϕ) – 0.9 **Cracked fuel -** *CEA* CO – 0.3099 H_2 – 0.0271
Nozzle outlet	**Pressure outlet –** *Exit conditions* 1. P_{static} = 0.01 atm 2. T_o = 300K
Walls	Standard wall functions (no slip conditions)

Parameters:
a) Velocity difference/Velocity ratio:

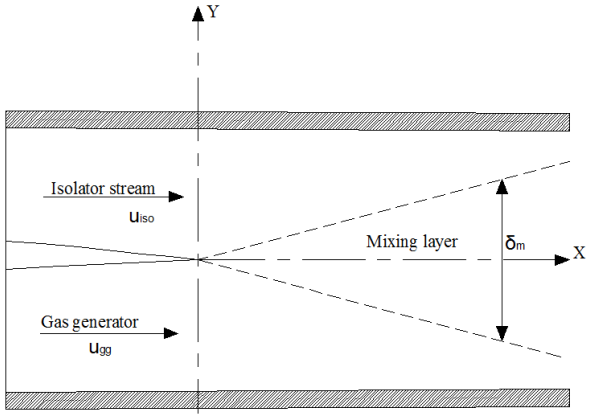

Figure 3-52 Mixing layer growth due to diffusion [3]

When the oxidizer rich stream from the isolator and the fuel rich stream from the gas generator arrive at the flame holder, a mixing layer is formed in the interface between these two streams, where combustion takes place. The combustion here is influenced by two phenomena, molecular diffusion (micro mixing) and shear, leading to laminar or turbulent mixing (macro mixing).

Diffusion of both the streams occurs at the interference layer between the fuel and oxidizer stream, it increases the width of the mixing layer and hence allowing more quantity of fuel and oxidizer to come in contact with each other. As the width the mixing layer grows, more quantity of fuel and oxidizer mix, resulting in increased combustion reactions. When the mixing layer width is equal to the width of the combustor, maximum mixing takes place, which results in higher combustion efficiency, this in turn results higher thrust.

The rate of diffusion is given by Fick's law [3], which states that the time rate of molecular transport of one stream to another is proportional to the interfacial layer area and the local concentration gradient.

When only molecular diffusion is considered i.e., No shear flow ($u_{iso} = u_{gg}$), the width of the mixing layer (δ_m) along the length of the combustor is given by [3]

$$\delta_m = 8\sqrt{\frac{D_F\, x}{u_c}} \qquad \text{..Eq(3.62)}$$

Where,

u_c - average of isolator and gas generator velocities $\frac{(u_{iso}+u_{gg})}{2}$

x - distance along the combustor

D_F – Molecular diffusivity

The above equation gives the width of the mixing layer with respect to the axial distance along the combustor, the macro mixing is said to be maximum when the width of the mixing layer is equal to the width of the combustor. The length of combustor x where the mixing layer width is equal to the width of the combustor (d) ,$x = L_m$ can be arrived from above equation,

$$L_m = \frac{u_c d^2}{64 D_F} \quad \text{..Eq(3.63)}$$

The above equation gives the length of the combustor required for molecular diffusion to complete. However, diffusion is a slow process and if the combustion in the main combustor is dependent only this phenomenon then a unrealistically long combustor would be require for the mixing layer to grow to large values such that efficient combustion occurs inside the combustor itself

When the velocities of both the streams are not equal then a shear layer is formed, when this velocity difference is sufficiently high turbulent flow occurs, which results in formation of vortices. These vortices elongated the interface layer between the two streams, according to Fick's law this increased interface area, accelerate diffusion process, thus accelerating the growth of the mixing layer and hence the rate of combustion process whilst keeping the required combustor length within a practical dimension.

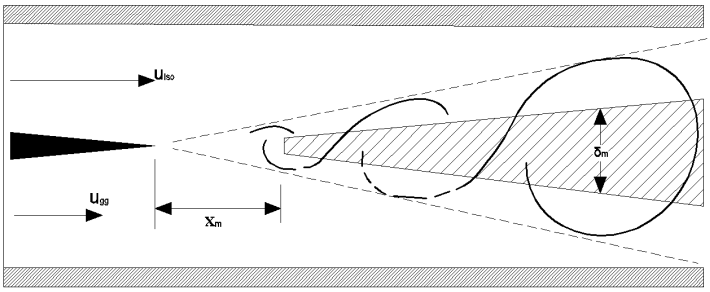

Figure 3-53 Turbulent mixing of gas generator and isolator streams showing micro mixed region (patched) and macro mixing region [3]

In case of turbulent mixing, the mixing of both the streams begins to take place downstream of the flame holder and increases along the length of the combustor. The point wherein significant amount of mixture of both the streams is first present is known as the mixing transition point (x_m). Which is given by [3]

$$x_m \cong \frac{20\vartheta u_c}{C_\delta(\Delta u)^2} \quad \text{..Eq(3.64)}$$

Where,

ϑ – molecular kinematic viscosity

Δu - velocity difference ($u_{iso} - u_{gg}$)

C_δ - Empirical constant

u_c – convective velocity

The above equation gives the relationship between where the mixing transistion point would occur and the velocities of isolator and gas generator streams. It can be seen that the downstream location of the mixing transistion point is directly proportional to the average velocity and inversely proportional to the velocity difference between the two streams ($u_{iso} - u_{gg}$). Hence, to have a lower mixing transistion point, the velocity difference between the gas-generator and isolator stream should be high.

c) Apex formation:

The increasing width of mixing layer creates distinct regions of flow where either Fuel is rich, oxidizer is rich or a mixing region. The increase in mixing region, inversely causes a decrease in oxidizer and fuel rich regions. In the central region of the combustor, the radius of fuel rich flow region reduces along the length of the combustor as turbulent mixing takes place, this decreasing radius of the fuel rich streams forms a cone shape, with an apex at its tip. This apex is an indication that the mixing region is at its maximum width and that the macro mixing of fuel rich gas-generator stream and the oxidizer rich isolator stream is at maximum. The total temperature of the gas increases due to combustion in the mixing region outside of the cone and apex. This apex formation can be seen in the total temperature contours at the end of a region of low total temperature in central region of the combustor along the axis. This apex formation can also been seen in the fuel mass fraction contours as the fuel mass fraction decreases the along the length of the combustor.

Apex does not indicate a complete mixing at a molecular level but only at a macro level, downstream of the apex further micro mixing (diffusion) of fuel and oxygen takes places which leads to better combustion. Micro mixing (diffusion) is a slower process. Hence apex formation has to take place at a minimum distance from the beginning of the combustor allowing for further micro mixing to take place within the combustor leading to complete combustion to take place within the combustor itself.

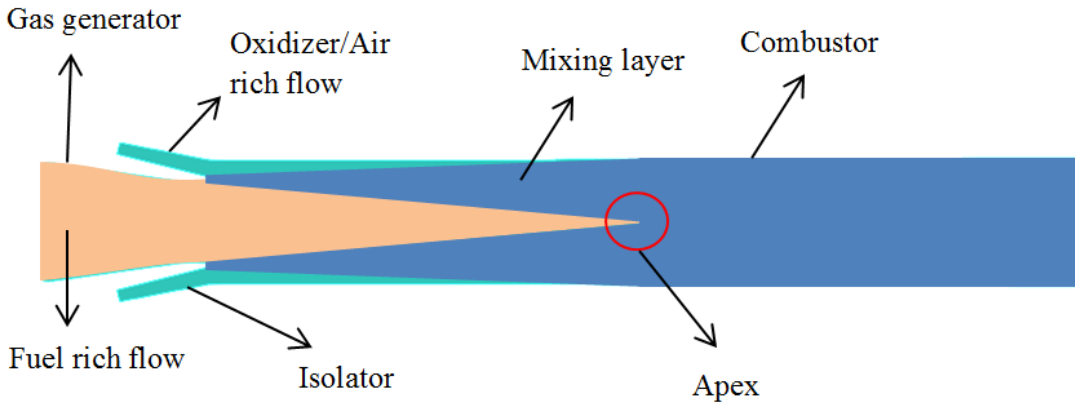

Figure 3-54 Apex formation due to macro-mixing of fuel-rich gas generator stream and oxidizer rich isolator stream.

d) Combustion efficiency:

The combustion efficiency gives the degree of combustion that has taken place in the combustor in comparison with ideal combustion reaction. The combustion efficiency is the ratio actual concentration of CO_2 at a position x in the combustor $(m_{CO_2})_x$ to the ideal CO_2 concentration $(m_{CO_2})_{ideal}$. The ideal concentration of CO_2 is arrived from analysis in NASA code for Chemical Equilibrium Analysis (CEA).

$$Combustion\ efficiency\ (\eta_c) = \frac{(m_{CO_2})_x}{(m_{CO_2})_{ideal}}$$

..Eq(3.65)

Geometrical variation:

The simulation domain consisted of the axis-symmetric isolator, supersonic combustor, gas generator, nozzle. Only the aft part of the gas generator was simulated, mixing and combustion inside the gas generator were not taken int account.

1. **Two isolator impingement angles were studied: Configuration–I with 7° and Configuration – II with 14°.**
2. **Two flight Mach numbers were simulated Mach 4 and Mach 6 with overall equivalence ratios of 0.6, 0.8, 1.0 and 1.2.**
3. **A parametric study of configuration – II by varying the area ratios**

The performance characteristics of combustor are analyzed. Followed by which a parametric study involving the 14° geometry was undertaken. Total of 5 cases of geometry with a fixed isolator angle of 14° were analyzed.

Table 3-33 Geometrical changes made in each revision (in mm)

Case	GG exit (R_{gg})	Iso exit (R_{iso})	Flame holder width (b_{fh})	SC entry (R_{ci})	Mixing throat (R_t)	A_{ci}/A_t	A_{gg}/A_{iso}	A_{si}/A_{iso}
1	80	44.33	19	143.33	127.53	1.26	3.25	0.515
2	80	44.33	19	143.33	130.9	1.19	3.25	0.515
3	80	36.15	15	131.15	120.73	1.18	4.89	0.484
4	85	36.15	10	131.15	124.14	1.11	5.52	0.484
5	85	35.2	10	130.2	130.2	1	5.83	0.484

Results are presented and discussed in the next chapter.

3.5 Full scale DCR Engine proto hardware testing

Full scale DCR propulsion system was realized in 1:1 scale as per the proposed design consisting of:

- vitiated air heater
- test bed nozzles to simulate the intake conditions
- truncated intake system
- fuel feed system
- fuel rich gas generator
- supersonic combustor
- necessary instrumentation for measurement of pressures, temperature and flow rates
- high sampling data acquisition system

Full scale test was conducted in a connected pipe mode test facility by simulating the entry conditions corresponding to flight altitude of 28km and freestream Mach number as M6.

DCR Test Objective:

Two test runs were conducted; the first test for cold flow (without combustion) followed by hot flow (with combustion). In the first case the characteristic of the test setup is verified. Followed by which the hot flow experiment with supersonic combustion was achieved. Fuel used: Jet-A

Case-I: Cold flow / without combustion

- Nozzle characterisation (static pressure).
- Ensure required entry condition at Gas Generator and Supersonic Combustor (pressures).

Case-II: Hot flow/with combustion

- Performance with Jet-A.
- Establish GG ignition and operation.
- GG chamber pressure < 2 bar.
- Achieve sustained combustion in Supersonic combustor
- Achieve pressure rise above 1 bar in supersonic combustor

3.5.1 DCR Test facility description and Test methodology

Existing Connect pipe mode Scramjet test facility is modified and used for DCR testing.

The details of the existing SCRAMJET test facility along with its feed systems is shown in Figure 3-55 and presented.

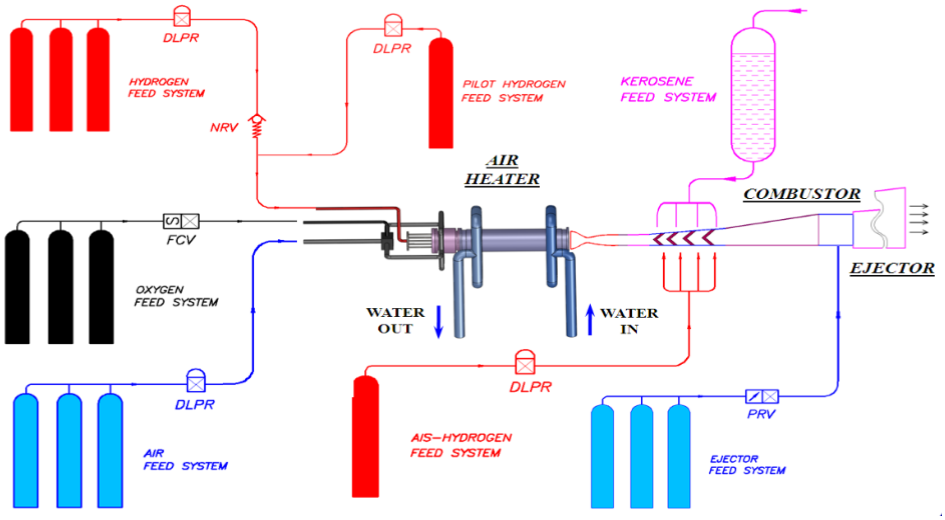

Figure 3-55 Block diagram of existing SCRAMJET combustor test facility at Laboratory

The facility consists of nine feed systems simultaneously working to generate required scramjet combustor test conditions. The feed system is automated; the test events and their duration are programmable. The features of test facility are:

Type of the test facility

Connect pipe mode test facility

Test facility specifications:

Mach number	: 2.0, 2.2, 2.35 and 2.7
Total temperature (max)	: 2100 K
Total pressure (max)	: 15 KscA
Max test duration	: 60 s
Combustor test duration	: 20 s

Simulates operating conditions at high altitude 31-32 Km

Vitiated air heater specifications

Air mass flow rate (max) : 12 Kg/s

Oxygen mass flow rate : 1.9 Kg/s

Hydrogen mass flow rate : 0.190 Kg/s

Ejector system

Air mass flow rate (max) : 40 Kg/s

Feed Systems

Scramjet Test facility has the following feed systems,that run simultaneously during test:

- Air feed system
- Oxygen feed system
- Hydrogen feed system
- Pilot hydrogen feed system
- Kerosene feed system
- N_2 purge for kerosene
- Ejector air storage
- Water feed pump for cooling of vitiated air heater

Instrumentation:

Pressure channels :120

Temp. channels :180

Flow rates :05

The vitiated air heater burns a mixture of air, hydrogen and oxygen (replenished) to produce the scramjet combustor inlet conditions of required temperature and oxygen molar concentration. 'Air + O_2' mixture is injected in two stages, namely stage-1 and stage-2, as shown. Stage-2 has been introduced recently to facilitate full scale testing and to improve uniformity of scramjet inlet temperature profile. Transition duct is used to convert the 'heater circular cross-section' to 'rectangular cross section' of nozzle and combustor. A converging diverging nozzle is used to generate the required Mach number flow.

Additional oxygen is injected into the air heater, to make up for loss in oxygen concentration due to hydrogen combustion. A 'pre-calculated oxygen mass flow rate' is added to increase oxygen mass fraction / mole fraction equal to that of atmospheric air.

3.5.1.1 Ground testing methodology:

a) Estimation of 'combustor entry vitiated flow conditions' in ground testing

The high temperature air to the combustor entry is simulated by online heating (by burning hydrogen and replenishing the oxygen deficit – known as vitiated gas), the composition of vitiated test gas is different from the flight. Due to the difference in composition, all flight conditions cannot be matched during the ground test. Hence, important parameters (listed in Table 3-34) are matched with flight conditions in ground test performance evaluation.

Table 3-34 Parameters to be matched between flight and ground testing

	Combustor entry flow parameter
1	Total sensible enthalpy (H_o)
2	Mach number (M)
3	Static pressure (P_{static})
4	Oxygen mass fraction (Y_{O2})

The performance of scramjet combustor depends on the amount of energy that can be added (upon the available energy at inlet) by combustion of scramjet fuel. Therefore, it is appropriate to simulate the 'flight total enthalpy' of the combustor inlet flow. During ground testing, matching the 'flight total enthalpy' at the combustor entry - will lead to lesser total and static temperatures than in flight. Lower static temperatures may lead to difficulties in auto-ignition. But, the achieved performance will be similar to flight testing.

Disadvantages of vitiated air heaters are– combustor entry air stream contamination by H_2O, NO_x and free radicals. These radicals in 'vitiated air' may promote ignition and yield false data in scramjet testing [57],[58]. Due to this limitation of 'vitiated air connect-pipe facility', fuel auto-ignition estimates may be inaccurate. In order to be on safer side (due to presence of free radicals), if the auto-ignition on ground is demonstrated at lower static temperatures than the corresponding flight condition, there is higher probability of ignition in flight. As mentioned above, if the combustor performance (in terms of auto-ignition and thrust) with 'inlet total

enthalpy' match case (~ 150 K lower combustor entry static temperature than flight), it will give enough confidence of achieving ignition in flight. It is reported in open literature that – the radical contaminations have the same effect on the scramjet behavior as a higher temperature of radical-free air [57]. In a way, this is the safety margin considering the uncertainties in connect-pipe vitiated air testing.

As all parameters cannot be simulated on ground in one test, it was decided to test the combustor with proof hardware for short duration with 'Enthalpy match case'. The total enthalpy is calculated by adding the enthalpies of the individual species as obtained from NASA CEC-71.

3.5.2 DCR Static Test setup hardware

The existing connect pipe mode test facility is modified to test DCR engine along with truncated intakes by using the Vitiated heater facility infrastructure and the storage reservoirs of air, oxygen, Nitrogen and Kerosene fuel. The following are redesigned to suit the DCR test requirements:

- Nozzles Design
- Heater Modifications
- Provision for Instrumentation
- Calibration of Sensors
- Kerosene Fuel Feed System Modification

The components of the DCR test set-up hardware are shown below

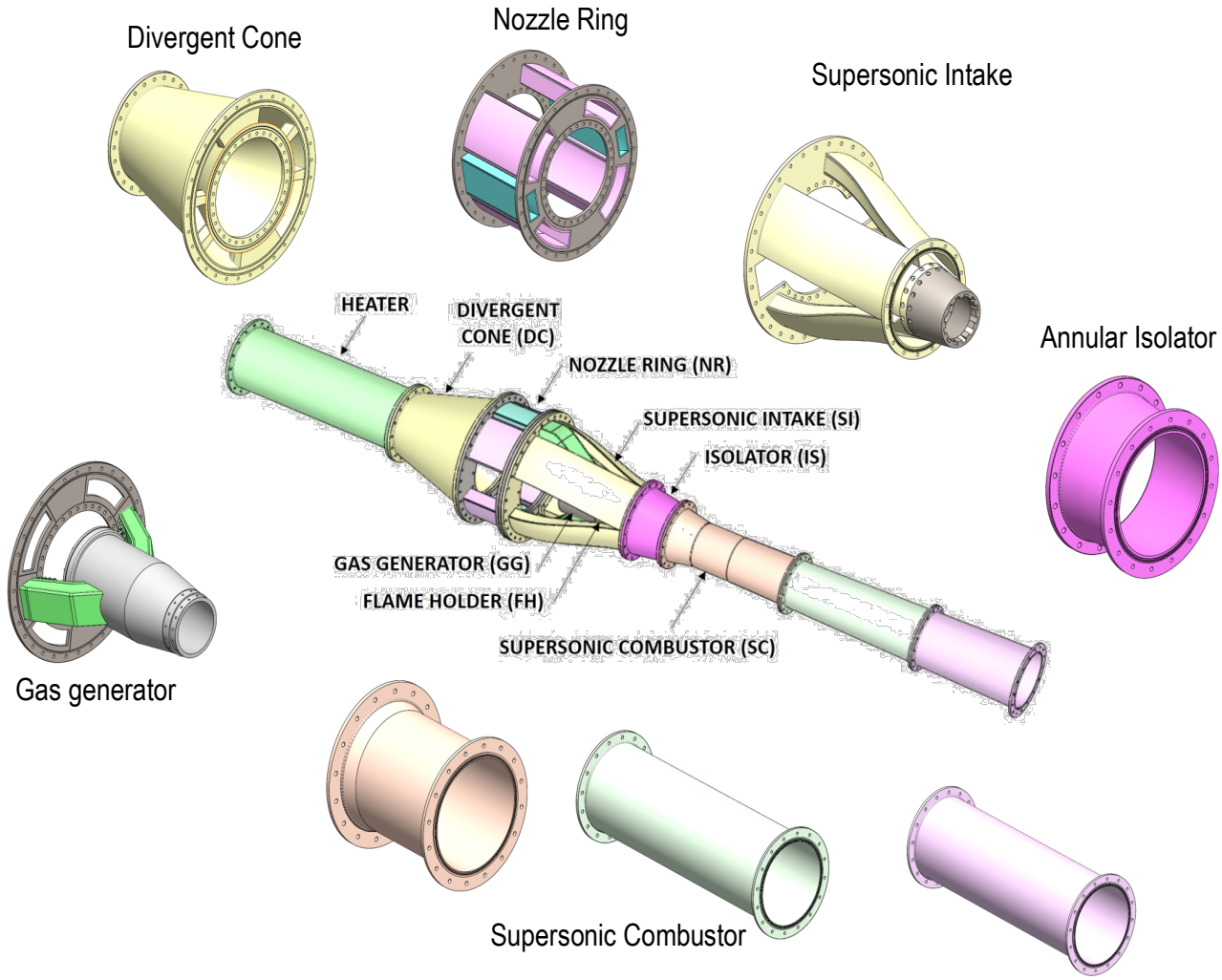

Figure 3-56 DCR Test set-up Hardware used for the static test

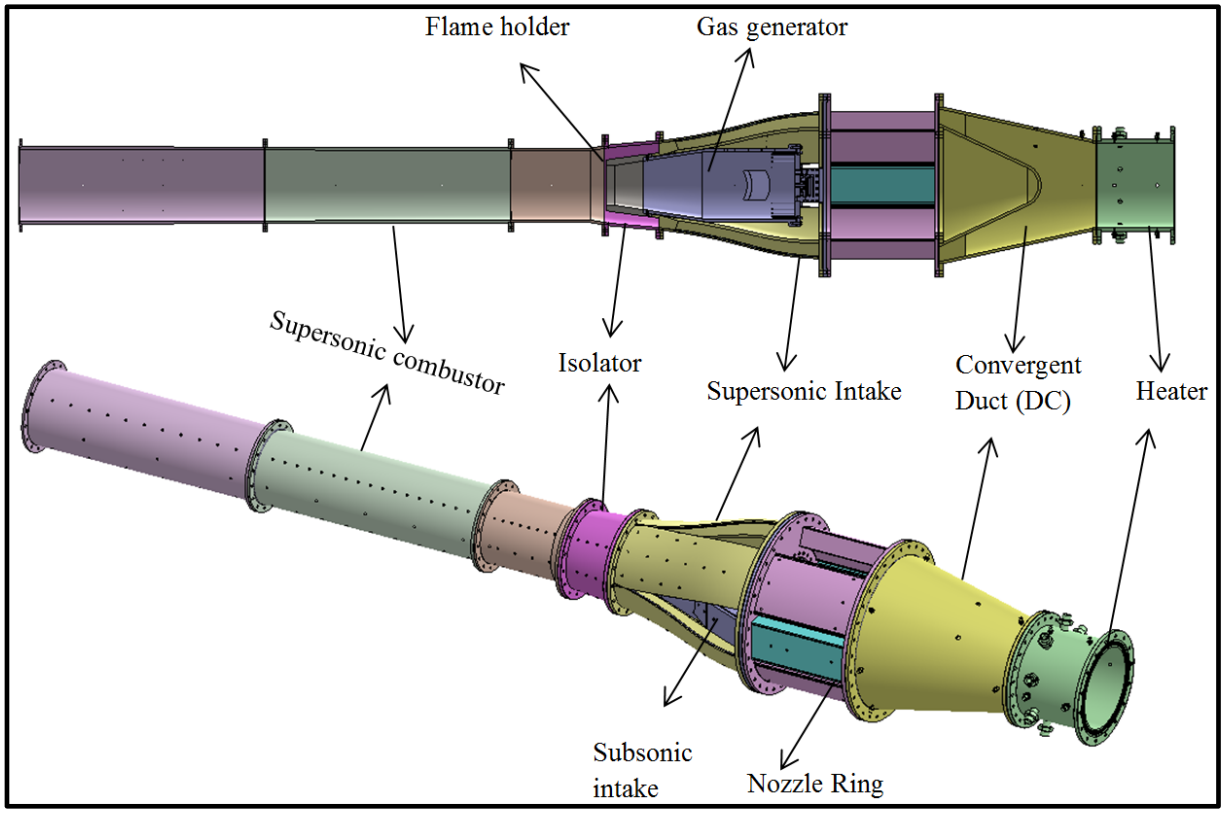

Figure 3-57 DCR test setup Cross-sectional view (top) and Isometric view (bottom)

3.5.2.1 Heater and Divergent cone assembly

The heater is a constant area duct of length 290 mm and diameter 330 mm. It is welded with flanges on either side. The heater uses hydrogen to heat the oncoming air, extra oxygen is supplied to the heater to compensate for oxygen reduction.

The divergent cone follows the constant area heater. The divergent cone consists of two cones one inner and outer. The half cone angle of the inner cone is 25°. The outer cone is attached to flanges on either side. Six fillers attach the inner cone to the outer cone. The six fillers divided the oncoming flow into six streams, diverting them into six ducts in the nozzle ring. Out of six fillers, two fillers are of width 133.94mm (S2) which are located axis-symmetrically opposite to each other, four remaining fillers are of width 26.16 mm (S1) located axis-symmetrically. The air split ratio between the supersonic inlet and subsonic inlet (Gas generator inlet) was at maintained at a ratio of 3:1.

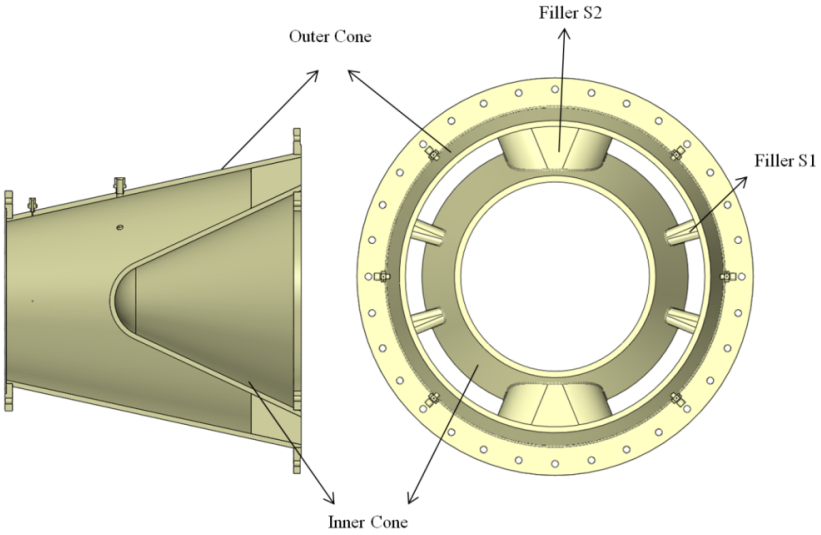

Figure 3-58 Divergent cone assembly

3.5.2.2 Nozzle ring:

The nozzle ring assembly consists of six ducts held together by two flanges in the forward section and in aft section. The flow is split into six ducts in the divergent cone and flows to the nozzle ring consisting of six ducts which consists of C-D nozzles for flow acceleration, four feeds the supersonic intake and two feeds gas generator inlet. The flow is accelerated to supersonic speeds through a convergent – divergent (CD) nozzle, with throat width of 7.9mm and an expansion ratio of 7.02. The supersonic flow directly enters the supersonic intake -isolator after the nozzle, whereas the flow Mach number is reduced before entering the Gas generator by another C-D nozzle (which acts as a diffuser) with an entry width of 55.5 mm, throat width of 34.5mm and an exit width of 45 mm

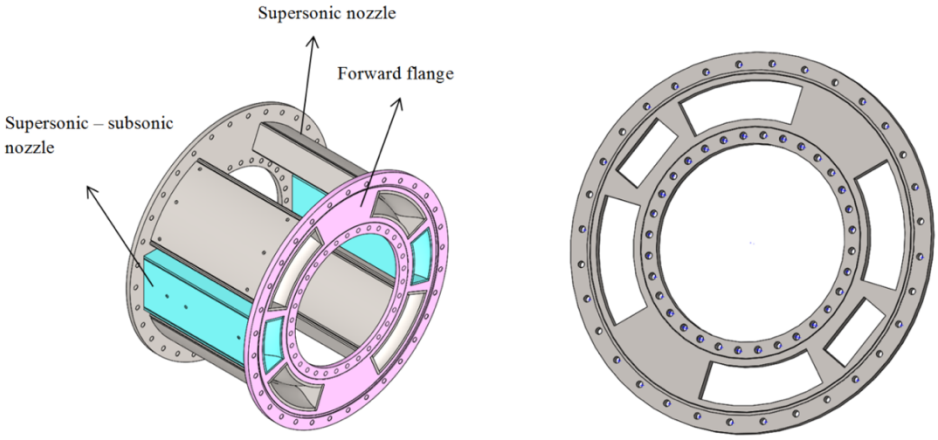

Figure 3-59 Nozzle ring assembly

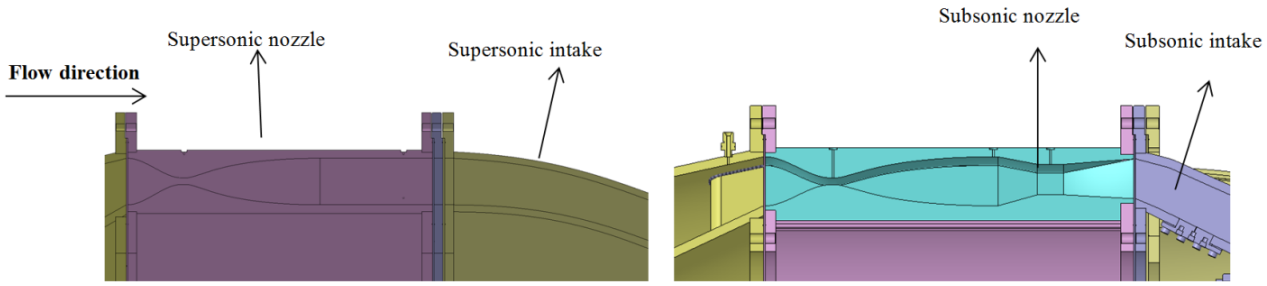

Figure 3-60 Supersonic Nozzle (Left) and Subsonic Nozzle (right)

3.5.2.3 Supersonic Intake Assembly:

A total of six intakes four of which are supersonic and two are subsonic intakes. Intakes are present downstream of nozzle rings. The supersonic intakes are connected to the Nozzle ring assembly through a flange. The supersonic intakes are of length 600.42mm. The inlet and exit areas are 11172.68 mm^2 and 8373.75 mm^2 respectively. It consists of top, bottom and two sides plates welded together give a single intake. At the exit the four intake ducts are joined together at a flange and connected to the isolator.

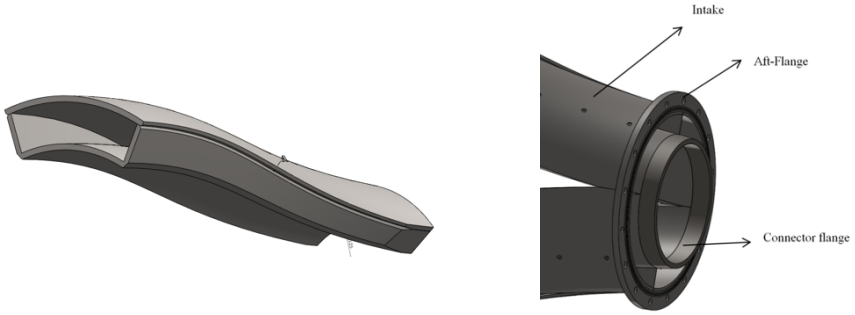

Figure 3-61 Supersonic Intake

3.5.2.4 Gas generator and subsonic intake assembly

a) Subsonic intake:

Subsonic intake is a part of the gas generator assembly, two subsonic intakes are present which connects to the nozzle ring assembly through a flange. The intake consists of four separate plates top, bottom and the two side plates, TIG welded together. The bottom plate consists of a rectangular cut of length 100mm and breadth 48mm to house the plate injector.

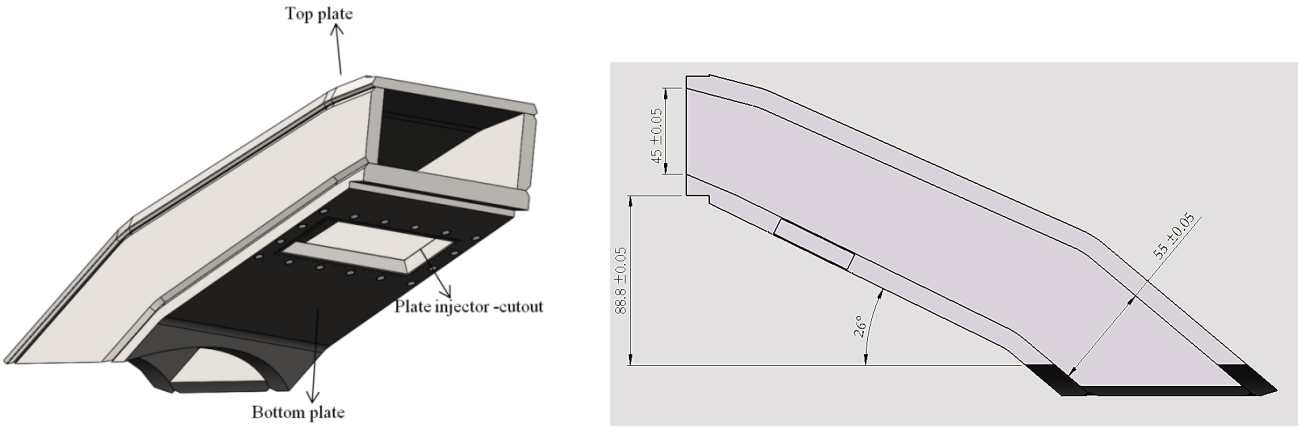

Figure 3-62 Subsonic intake assembly: Isometric view (Left); Side view (right)

b) Gas Generator (GG):

The gas generator is located on the longitudinal axis between the nozzle ring and the isolator assembly, surrounded by the four supersonic intakes. It consists of a combustion chamber, disc injector assembly with 18 injectors located along the circumference, 2 flat plate injectors for pilot flame and a flame holder at the end of the assembly. The air flow enters the gas generator downstream of the pipe injectors through two subsonic intakes located at 0^o and 180^o.The flame holder is located in between the isolator and gas generator flow streams with a width of 20mm at the end.

GG Injectors:

Two fuel injectors are present in the gas generator, a plate injector for pilot flame upstream of the gas generator in the subsonic intake, and the main disc injector in the combustion chamber. Two plate injectors are present in each of the subsonic intakes immediately downstream of the subsonic nozzle. It consists of an I-channel and a U- channel, with drilled holes in each of the channels for fuel injection. The bottom channels are enclosed by similarly shaped I and U strips which are welded to the plate assembly. An M12 adaptor is welded onto the strips for fuel supply. The fuel enters through the M12 adaptor and circulates through the channel and is injected through the holes in the plate. The disc injector consists of 18 pipe injectors, connected to the main head. The fuel supply is connected to the assembly through a pair of M12 adapters located on the disc head, the adapters are connected to the injector ring which distributes the fuel, through a Circular channel, which is enclosed by a injector ring to 18 pipe injectors located along the circumference. A silicon gasket is present between the injector head assembly and the gas generator.

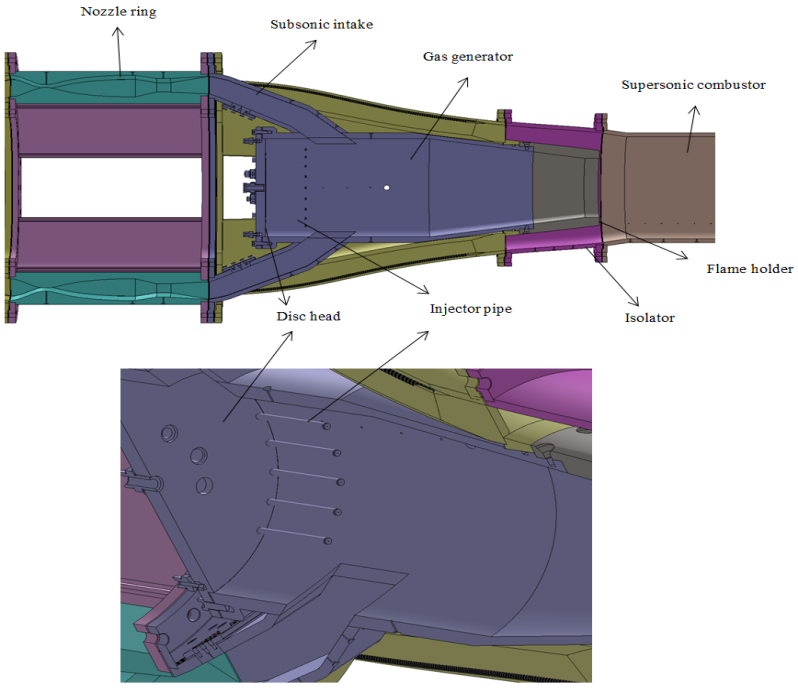

Figure 3-63 Gas generator assembly (Top); Close up view of injector section

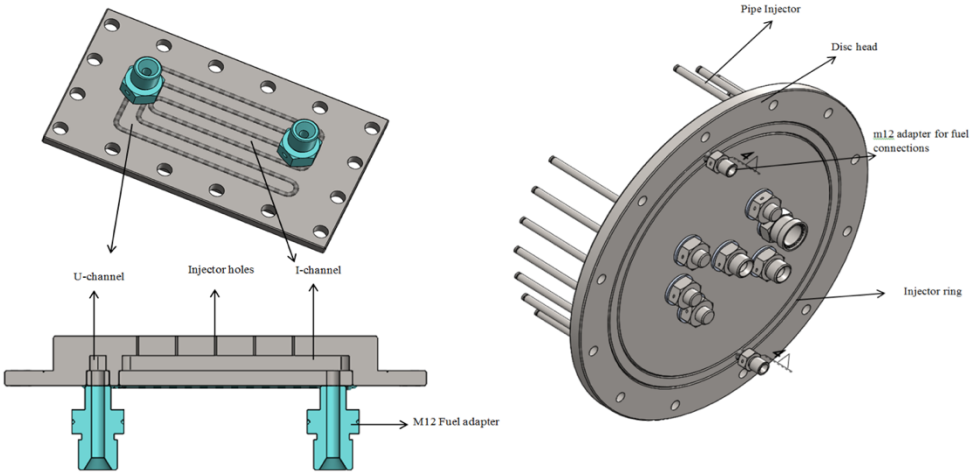

Figure 3-64 Flat plate injector (Left) ; Disc injector (Right)

c) **Isolator Assembly:**

The isolator consists of a convergent duct enclosed with flanges at the inlet and exit. The inlet connects with supersonic intake and the whole assembly encloses the aft part of the gas generator (flame holder). The gas generator's outer surface and the isolator's inner surface combine to form the isolator duct, with inlet and outlet width of 36.50mm and 45 mm respectively. The isolator duct is 200 mm long with an inlet and exit diameters of 159.81 mm and 139.32 mm respectively. At the beginning of the isolator the wall angle is parallel to the flow from the

supersonic intake, towards the end this angle increased to 14° gradually through a spline (constructed with 14° tangent) so as to provide better isolator angle.

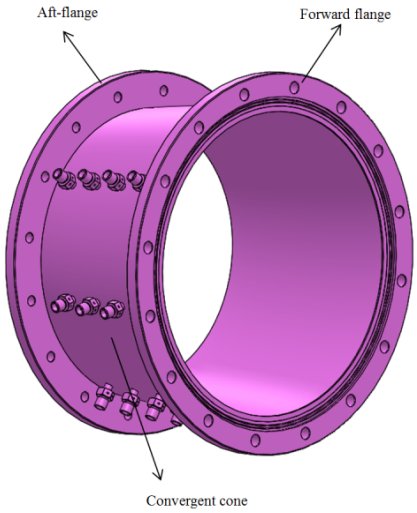

Figure 3-65 Isolator assembly (Isometric view)

d) Supersonic Combustor (SC)

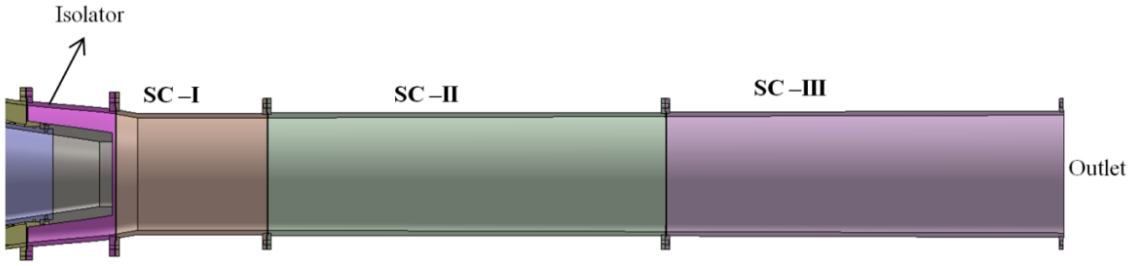

Figure 3-66 Supersonic combustor sections

The supersonic combustor (SC) is downstream of the isolator and gas generator. The supersonic intake ducts are all combined together at the intake exit, upstream of the isolator entry. The flow downstream from isolator is hence axis symmetric. The combustor is divided into three sections. Each of the combustor sections are welded to flanges at both of their ends. The combustor sections are connected by these flanges. The first section consists of a constant area duct (SC-I) with a diameter of 130mm and 352.83 mm long. Followed by two diverging sections (SC-II, SC-III) of 0.925m length each with end diameters of 133.25 and 136.5mm. No nozzle is incorporated during the test.

3.5.3 Instrumentation and flow measurements

Pressure transducers were placed along the walls of combustor, isolator and gas generator to record the pressure values. Five pressure transducers were placed on the divergent cone. In gas generator 9 pressure transducers were placed, 15 in the supersonic intake, 10 in the isolator, 15 in the scram combustor section I, 5 in the scram combustor section II and 11 in the scram combustor section III. Two temperature sensors were placed in divergent cone and in gas generator. Four flow meters for air, oxygen, hydrogen and fuel were also used to measure the mass flow rate.

3.5.3.1 Sensors description:

a) Pressure Transducers : Shown in the table

b) Temperature Sensors : as per the suitable range

c) Flow Sensors : Shown in the table

(Pressure and flow Sensor details are given in Annexure –1)

Data sampling rate was 2 kHz and bandwidth was 1 kHz.

Table 3-35 Instrumentation specifications and uncertainties

	Sensors	Type	Make	Uncertainty (± % of full scale)
1	Pressure sensor	Resistance type strain gauge sensors	Sensotech/ Honeywell	± 0.2524
2	Temperature sensor	B – type for 600K to 1800 K K – type for RT to 1200 K	Omega	± 1
3	Flow rate sensor	Turbine flow meters	Flow Technologies	± 0.5
4	Data acquisition system	---	National Instruments	± 0.07
5	Signal conditioning unit	---	---	± 0.01
6	Power supply unit	---	---	± 0.016

3.5.3.2 Sensor locations in the static test:

The pressure transducers were placed at fewer ports than the total number of ports available in the test article, based on the location of interest and number of transducers available.

Table 3-36 Sensors placement

Sub assembly	Pressure	Temperature	Flow
Divergent Cone	02	02	04
Nozzle Ring	12		Air
Gas Generator	8	02	Oxygen
Supersonic Intake	14		Hydrogen
Isolator	10		Fuel
Scram combustor 01	09		
Scram combustor 02	08		
Scram combustor 03	03		
TOTAL	**66**		

3.5.3.3 DCR Test set-up preparation:

Safety aspects at DCR Test facility:

- Non-sparking tools for hydrogen feed line
- Proper anchoring of the gas cylinders based on the inputs from safety group.
- Anti-static flooring for H_2 cylinders
- Hydrogen and oxygen storage are 40 meters away from each other.
- Emergency scenarios defined and explained to manpower at test facility.
- Manually operated emergency switches in all feed lines to be operated by test controller in case of emergency.
- Nitrogen purging of feed lines after the test
- Earthing of all feed lines, regularly monitored by safety group.
- Static charge dissipation system at the entry to the hydrogen storage area.

a) Test facility Acceptance testing:

- Hydraulic proof pressure test of feed system
- The total feed lines of DCR test facility have been hydrotested up to a minimum pressure of 1.5 times the operating pressure in the presence of Quality control representative and found to be satisfactory.
- Leak test

  The test setup is ensured for leak proofness before each static test. The feed lines are leak tested up to the operating pressure using air and nitrogen (for H_2 line only). The test article leak test is done at a pressure of 2.5 bar by integrating a flange at the exit of the combustor. During the test article leak test, the pressure data is recorded by Instrumentation group. The health of each sensor is analyzed and corrective actions are taken prior to the test.

b) Functional checks of automation system

- All electro-pneumatically operated ball valves are tested by giving the on-off command from the master computer panel. Each valve is operated 5 times after confirmation of the air filter regulator pressure by on-field personnel.
- The control valves are operated 2 times from minimum to maximum position and the physical opening is confirmed by on-field personnel.
- The flow meters response is seen by performing flow check prior to test.
- The spark plug operation is checked.
- The squib firing is conducted manually.
- Operation of emergency switches manually.
- Checking of 'STOP FIRING' commands.
- A simulation dry run is carried out in automatic mode by simulating the actual firing sequence, without pressurization of any system.
- The automation system is cleared for static test only after satisfactory performance of the above activities on the day of test.

c) Scrutiny of gases test certificates

The gaseous hydrogen, oxygen and nitrogen are procured from an outside agency. Test certificates for the quality of the gases are obtained for each lot.

d) Calibration of measuring instruments

The calibration of turbine flow meters is carried out. The pressure sensors are calibrated.

Test procedure:

Ground test was conducted for a flight Mach number of 6, two test cases were performed. In case-I a dry run of the setup was performed without any fuel addition, to ensure the entry conditions at the Gas generator and isolator entry are as expected and to estimate the heat loss. This was followed by the wet test of the setup in case-II, where fuel was added to the flow. An overall equivalence ratio of 0.9 was maintained with the gas generator equivalence ratio at 2.79.

Facility Operation Sequence:

Parameter/ Valve	On Time	Off Time	
Air	0	50	
Oxygen	3	20	
Pilot Hydrogen	5	17	
Heater Pyro	7	--	T0
Main Hydrogen	9	17	T0+2
Kerosene	12	17	T0+5
GG Pyro	13	--	T0+6

Heater Pyro is considered as T_0 or Zero time. Total DCR engine on time is ~ 6s. Though auto ignition is established in Gas generator, GG pyro has been placed to make sure the GG ignites.

Facility Heater and Nozzle: Hydrogen based vitiated heater was employed to achieve the desired combustor entry conditions. The heater conditions and the flow rates of the feed streams (Air, H2 and O2) was arrived by using the NASA CEA code to achieve the entry conditions.

NASA CEA input for enthalpy match:

O/F ratio: 60.4, Heater pressure: 11.3 bar (These values iteratively determined to match the desired total enthalpy, O2 mass fraction and nozzle exit pressure)

Results: Total Enthalpy: 1.56 MJ/kg, O2 (mass %): 23, Mass flow rate : 7.675kg/s

Theoretical Feed flow rates:

Table 3-37 Feed flow rates from NASA CEA

S.NO	Feed stream	Mass flow rate, kg/s
1	Air	6.2
2	Oxygen	1.35
3	Hydrogen	0.125
4	Total	7.675

Heater Nozzle:

The heater exit is connected to the truncated intake via. a set of nozzles designed to simulate the Mach number and flow rate at the truncated intake location.

Heat loss:

From the vitiated air heater to the combustor, the flow passes through a divergent cone, nozzle ring and truncated intake, the heat lost to these components will be substantial as the hardware is at room temperature. A total temperature loss of ~250K is estimated in these passage sections and the heater temperature is adjusted to ~1800 K.

Fuel feed system and injection:

The fuel used is Jet-A which is aviation kerosene. The fuel (407g/s, Engine Φ=0.9) is injected in the Gas Generator part of the engine at two locations. Swirl injectors are used for this injection. 35-40g/s of kerosene is injected at the head end of the GG. Remaining flow of 370 g/s is injected 250 mm from the head end of the Gas Generator. The fuel is supplied to the injectors using a pressure fed system. Nitrogen gas is used to pressurize the fuel tank to the required pressure from nitrogen cylinders at pressure above 90 bar using pressure regulator. The fuel flow rate is determined prior to the test using a mass flow meter and the feed line pressures are determined. During the actual test, the tank pressure and expected gas generator pressure difference is maintained to achieve the required flow rate.

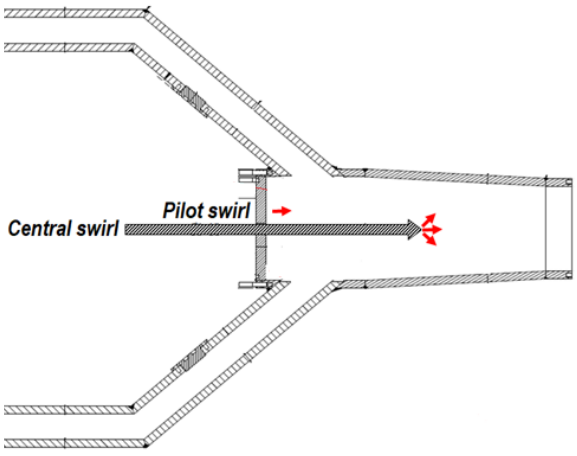

Figure 3-67 GG with Fuel Injection Configuration

Table 3-38 Non-Reacting and Reacting Test Conditions

	Test Condition	φ	Total fuel	Main swirl / Pilot	No. of tests
Case-I	M6 (Non-Reacting) T0 = 1558K	-	-	-	1
Case-II	M 6 (T0 = 1558K)	0.9	407 g/s	370 /35 g/s	1

The input conditions during the test are as tabulated below

Table 3-39 DCR Test Conditions at M6 Flight Mach number

Ground test condition simulating flight operation (M6 @ 28km) –1.56MJ/kg		
	GG entry	**Scramjet entry**
T0 (K)	1558	1558
Mass flow rate (kg/s)	1.88	5.72
Oxy mass fraction	0.23	0.23
Mach number.	1.23	2.43

Figure 3-68 DCR Engine mounted on test bed with instrumentation

Chapter 4

RESULTS AND DISCUSSION

Based on the investigations carried out in design, experimental and numerical studies; the findings of these studies are summarized in this section and presented as follows:

- Results of Gas generator characterization
    - **Experimental and 1-D model studies**
- Results on Numerical study on DCR Combustor geometry
    - **Two isolator impingement angles were studied: Configuration–I with 7° and Configuration – II with 14°.**
    - **Two flight Mach numbers were simulated Mach 4 and Mach 6 with overall equivalence ratios of 0.6, 0.8, 1.0 and 1.2.**
    - **A parametric study of configuration – II by varying the area ratios**

The performance characteristics of combustor are analyzed. Followed by which a parametric study involving the 14° geometry was undertaken. Total of 5 cases of geometry with a fixed isolator angle of 14° were analyzed.

- Results of Full scale DCR engine connect pipe mode tests
    - **Vitiated heater performance**
    - **DCR engine performance**

4.1 Experimental studies on Gas Generator:

Total 9 numbers of static tests were conducted in connect pipe mode and the test matrix followed is shown in Table 4-1. Even though few initial tests have failed due to some of the test bed problems, and injection issues; rest of the tests were conducted successfully with necessary improvements. Summary of test results of the gas generator experiments are as follows:

Table 4-1 Gas Generator Test matrix

S NO.	Configuration	Remarks
RUN 1	Fuel injection simultaneously (~ 700 g/s) 1. Intake injection (~ 220 g/s) 2. Film cooling injection(~120 g/s) 3. Central swirl injection(~360 g/s) 4. 100 DQ pyro for ignition initiation	No ignition
RUN2	Fuel injection simultaneously (~ 700 g/s) 1. Intake injection and Film cooling injection 2. Central swirl injection 3. 100 DQ pyro for ignition initiation 4. Heater ignition after 3 sec pyro firing	Ignition occurred. H_2 from the heater aided in ignition
RUN3	Staged fuel injection (~ 360 g/s) 1. Intake + Film cooling injection 2. 100 DQ pyro for ignition initiation 3. No – Central swirl injection	Ignition Occurred
RUN4	Staged fuel injection (~ 700 g/s) 1. Intake + Film cooling injection 2. 100 DQ pyro for ignition initiation 3. Central swirl injection	Ignition Occurred
RUN5and6	Staged fuel injection (~ 800 g/s) 1. Intake + Film cooling injection 2. 100 DQ pyro for ignition initiation 3. Central swirl injection	No ignition Intake eqv.ratio~1.2
RUN7	Staged fuel injection (~ 800 g/s) 1. Intake + Film cooling injection 2. 100 DQ pyro for ignition initiation 3. Central swirl injection	Ignition Intake equivalence .ratio ~ 0.85
RUN 8 and 9	Combined fuel injection (~ 800 g/s) 1. Intake + Film cooling inj. + Central swirl inj. 2. 100 DQ pyro for ignition initiation	Ignition

Total 9 runs were taken for the test. Sustained ignition was achieved for 700 g/s and 800 g/s fuel flow rates. Equivalence ratio required in the intake for sustained ignition was of the order 1 for 700 g/s flow rate and 0.8 – 0.9 for 800 g/s flow rate. There was no ignition for equivalence ratio of 1.2 for 800 g/s flow rate as it can be seen from test data for run 5 and 6. Data obtained from the **meaningful tests (Test runs 4, 7, 8, 9)** are plotted (Figure 4.1 to 4.18), analyzed and presented here. The achieved pressure, flow rates and temperatures are summarized in table 4.2 to 4.4.

4.1.1 RUN 4 Results

Test 4 Configuration:

- Staged fuel injection (~ 700 g/s)
- Intake + Film cooling injection
- 100 DQ pyro for ignition initiation
- Central swirl injection

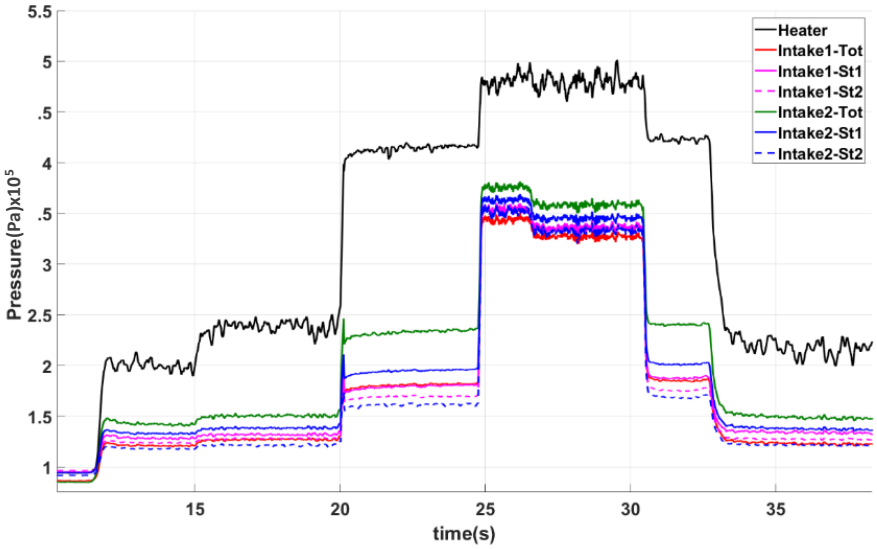

Figure 4-1 Gas generator pressures (Intake side) – Run4

As per the firing sequence, air flow is switched ON first. There is a pressure rise which is seen as the 1st step in the plot. Oxygen (O_2) is switched on after 4 seconds of air flow which leads to pressure rise to 2nd step. Hydrogen (H_2) flow is switched ON 3 seconds after O_2 flow is established. It leads to further rise in pressure and is seen as the 3rd step of pressure plot. Heater ignition is achieved using spark igniter. Vitiated air as per flight conditions is supplied to the gas generator.

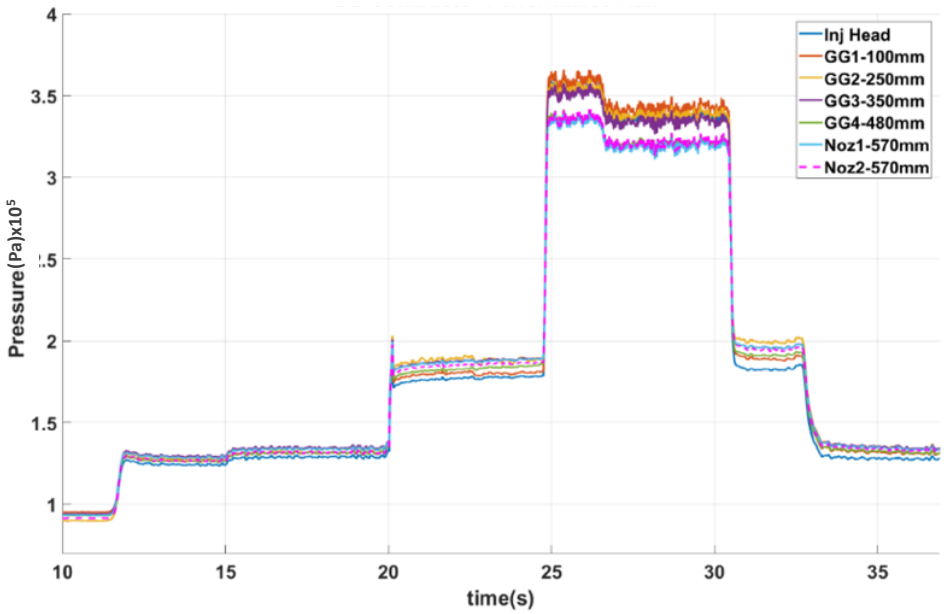

Figure 4-2 Gas generator pressures (Combustor side) – Run4

Once the intake arm fuel is switched on, GG combustion chamber pressure rises as shown in Figure 4-2. This indicates combustion has been achieved. After 2 seconds, central swirl injector is switched ON which leads slight dip in GG pressures. The sustained combustion is continued for another 4 seconds. Subsequently, H_2 supply to heater is switched off leading to cut off vitiated air to gas generator and combustion stops as indicated by drop in pressures.

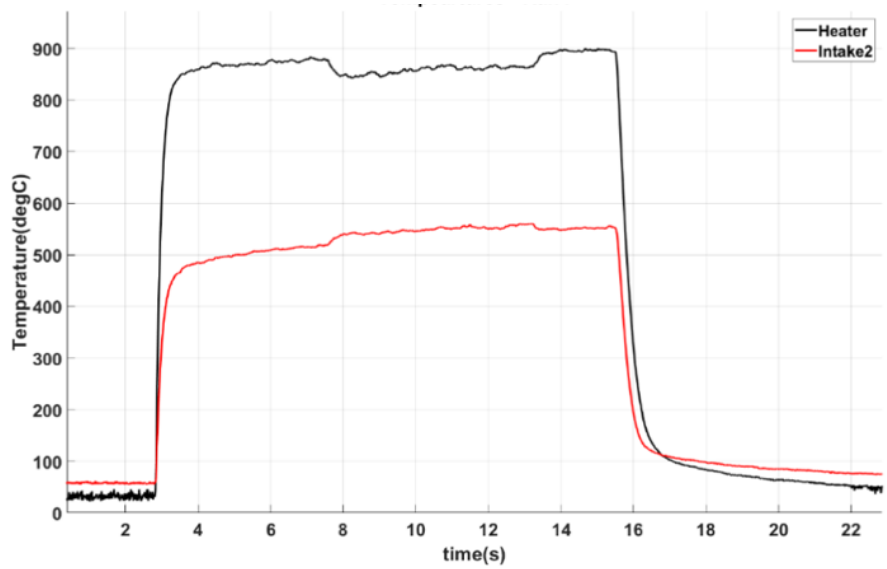

Figure 4-3 Heater and Intake entry gas temperature – Run4

Rise in temperature of vitiated air is shown in Figure 4-3. Heater temperature rise is of the order of 879°C and for intake exit vitiated air temperature requirement of 545° C.

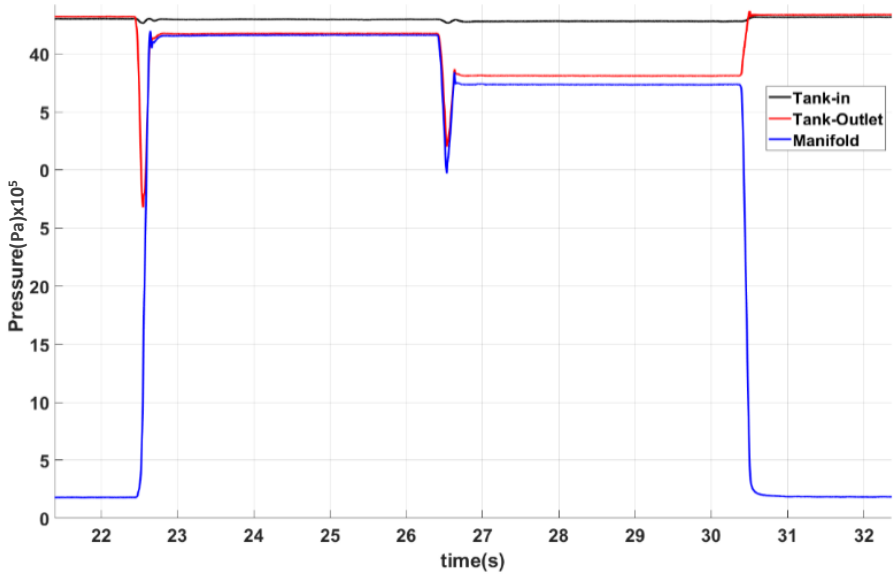

Figure 4-4 Jet-A feed system pressures – Run4

Figure 4-4 shows Jet-A fuel tank inlet, outlet and manifold pressures. Tank inlet pressure is constant throughout the test. There is a dip in pressure in tank outlet and manifold when central swirl flow is switched ON which is due to higher flow rate of Jet-A fuel.

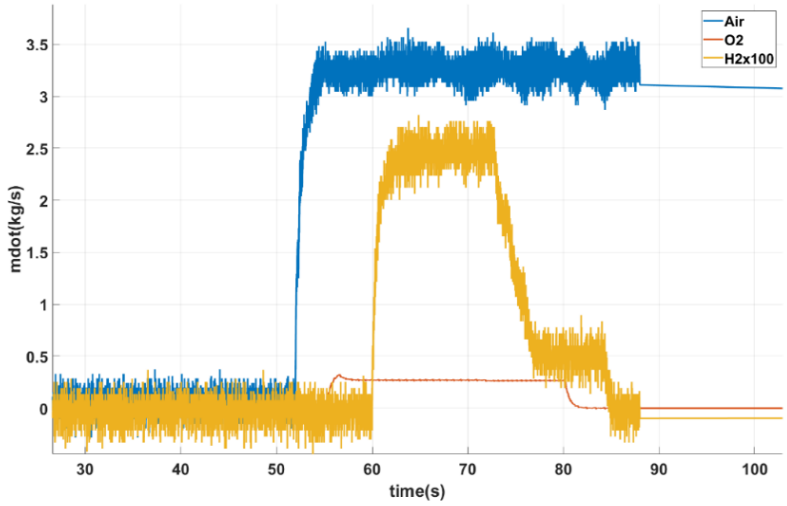

Figure 4-5 Heater air flow rates – Run4

Heater mass flow rates are shown in Figure 4-5. Heater mass flow rates dictate the performance of the entry conditions to the gas generator simulating the flight altitude conditions. Hydrogen fuel based vitiated air heater is used for the tests conducted. Air, hydrogen and oxygen are supplied as per the pre-calibrated requirements. Heater total flow rate achieved is 3.459 kg/s.

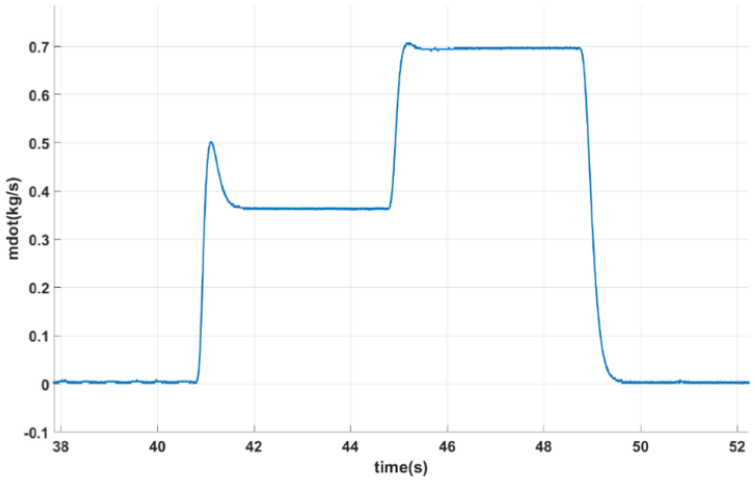

Figure 4-6 Jet-A mass flow rate – Run4

Part of the Jet-A fuel total flow is injected in the intakes and rest is injected through the central swirl injector. Fuel injected in intake arm and central swirl is 0.366 and 0.328 kg/s respectively and thus total flow of 0.694 kg/s is achieved as shown in Figure 4-6. The injectors are pre-calibrated with De-mineralized water to estimate their hydraulic resistance for the specified flow rates and upstream pressures. Equivalence ratio of 1.04 in intake arm and 2.91 for total flow are achieved in this run.

4.1.2 RUN 7 Results

Test 7 Configuration

- Staged fuel injection (~ 800 g/s)
- Intake + Film cooling injection
- 100 DQ pyro for ignition initiation
- Central swirl injection

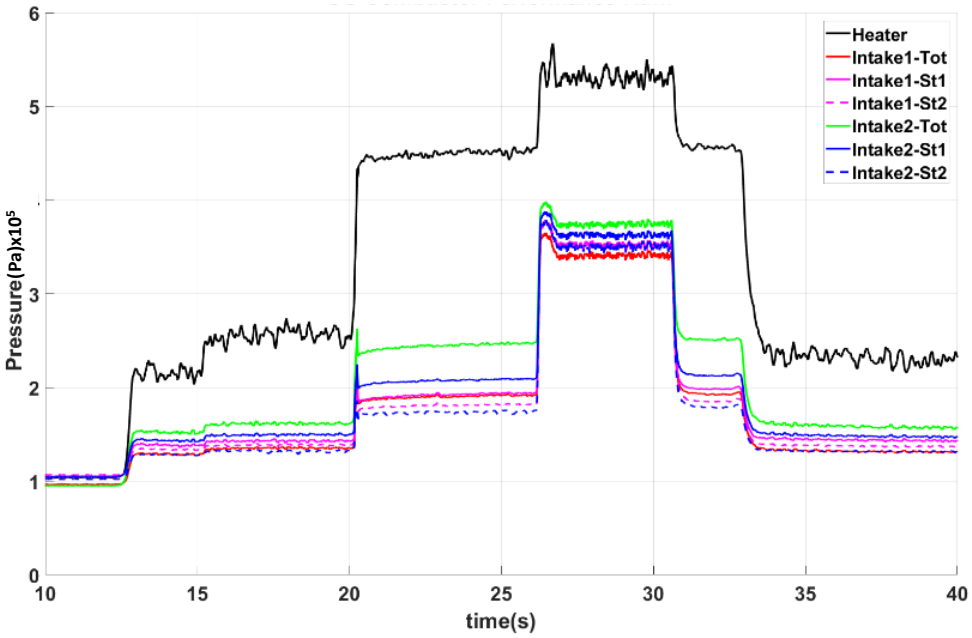

Figure 4-7 Gas generator pressures (Intake side) – Run7

As per the firing sequence, air flow is switched ON first. There is a pressure rise which is seen as the 1st step in the plot. Oxygen (O_2) is switched on after 8 seconds of air flow which leads to pressure rise to 2nd step. Hydrogen (H_2) flow is switched ON 6 seconds after O_2 flow is established. It leads to further rise in pressure and is seen as the 3rd step of pressure plot. Heater ignition is achieved using spark igniter. Vitiated air as per flight conditions is supplied to the gas generator.

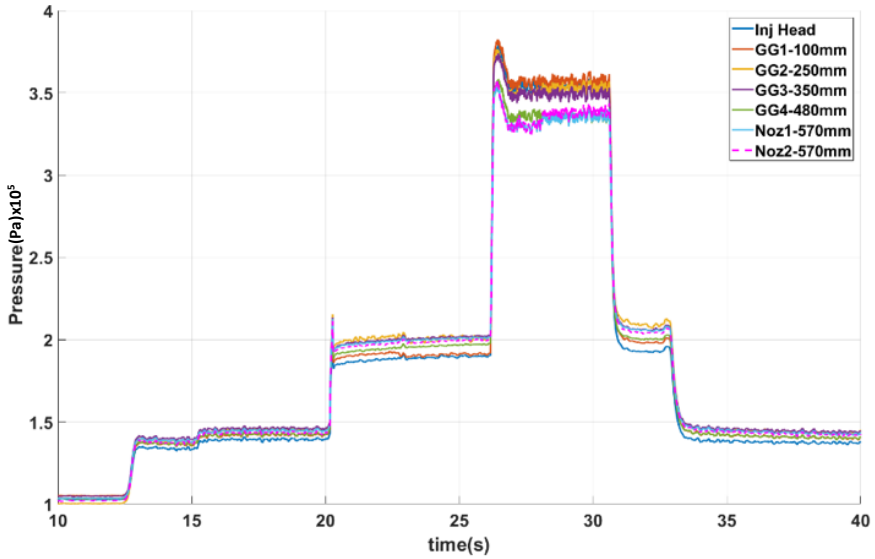

Figure 4-8 Gas generator pressures (Combustor side) – Run7

Once the intake arm fuel is switched on, GG combustion chamber pressure rises as shown in Figure 4-8. This indicates combustion has been achieved. After 2 seconds, central swirl injector is switched ON which leads slight dip in GG pressures. The sustained combustion is continued for another 4 seconds. Subsequently, H_2 supply to heater is switched off leading to cut off vitiated air to gas generator and combustion stops as indicated by drop in pressures.

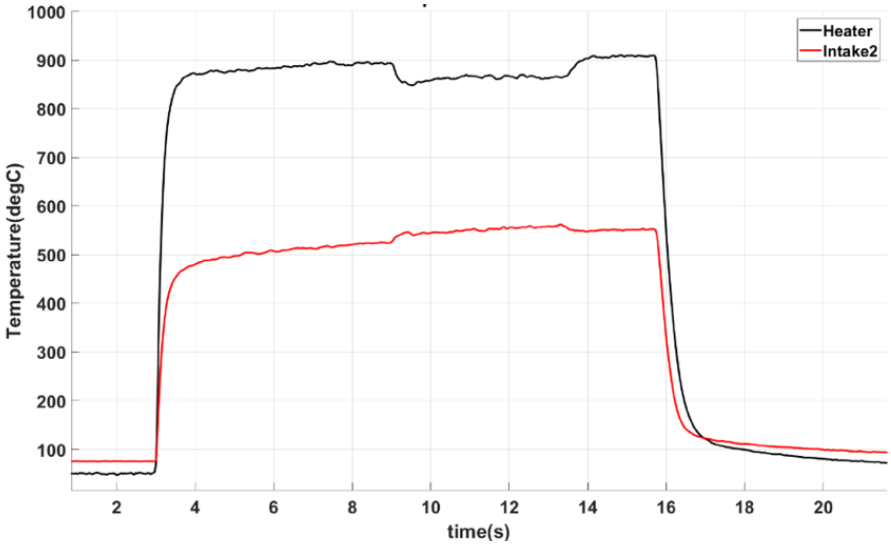

Figure 4-9 Heater and Intake entry gas temperature – Run7

Rise in temperature of vitiated air is shown in Figure 4-9. Heater temperature rise is of the order of 900°C and for intake exit vitiated air temperature requirement of 536° C.

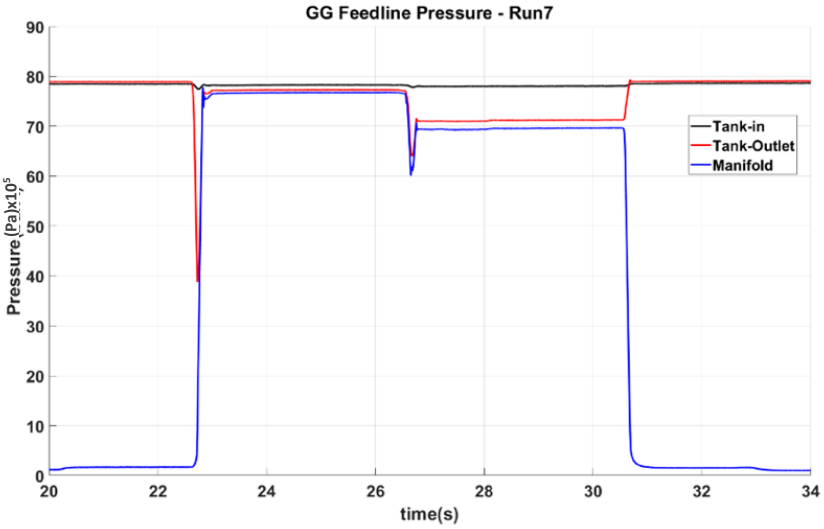

Figure 4-10 Jet-A feed system pressures – Run7

Figure 4-10 shows Jet-A fuel tank inlet, outlet and manifold pressures. Tank inlet pressure is constant throughout the test. There is a dip in pressure in tank outlet and manifold when central swirl flow is switched ON which is due to higher flow rate of Jet-A fuel.

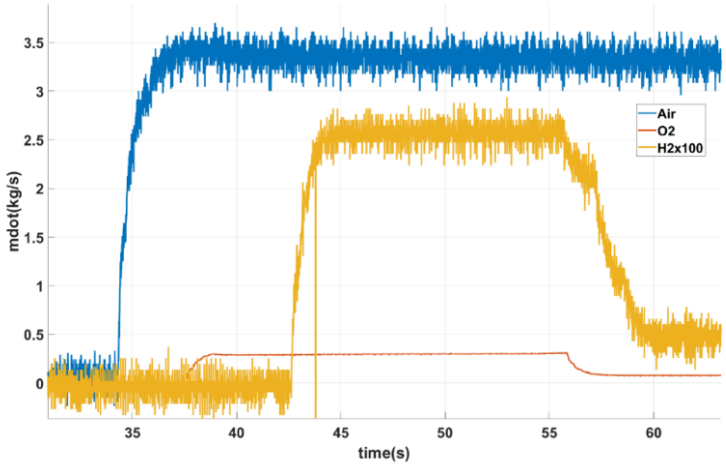

Figure 4-11 Heater air flow rates – Run7

Heater mass flow rates are shown in Figure 4-11. Heater mass flow rates dictate the performance of the entry conditions to the gas generator simulating the flight altitude conditions. Hydrogen fuel based vitiated air heater is used for the tests conducted. Air, hydrogen and oxygen are supplied as per the pre-calibrated requirements. Heater total flow rate achieved is 3.726 kg/s.

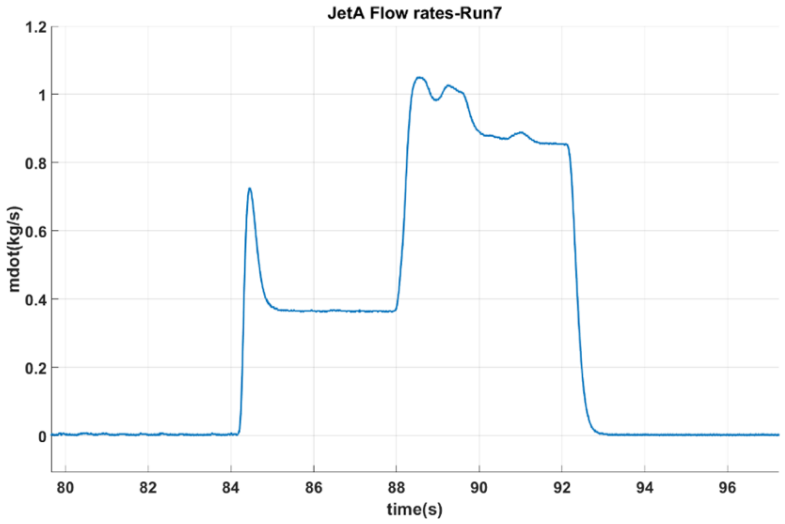

Figure 4-12 Jet- mass flow rate – Run7

Part of the Jet-A fuel total flow is injected in the intakes and rest is injected through the central swirl injector. Fuel injected in intake arm and central swirl is 0.366 and 0.534 kg/s respectively and thus total flow of 0.900 kg/s is achieved as shown in Figure 4-12. The injectors are pre-calibrated with De-mineralized water to estimate their hydraulic resistance for the specified flow rates and upstream pressures. Equivalence ratio of 0.8 in intake arm and 3.54 for total flow are achieved in this run.

4.1.3 RUN 8 and 9 Results

Test runs 8 and 9 are conducted for the same conditions to ensure the repeatability. The configuration for these runs is as follows:

- Combined fuel injection (~ 800 g/s)
- Injection of fuel in (Intake + Film cooling + Central swirl) is simultaneous.
- 100 DQ pyro for ignition initiation

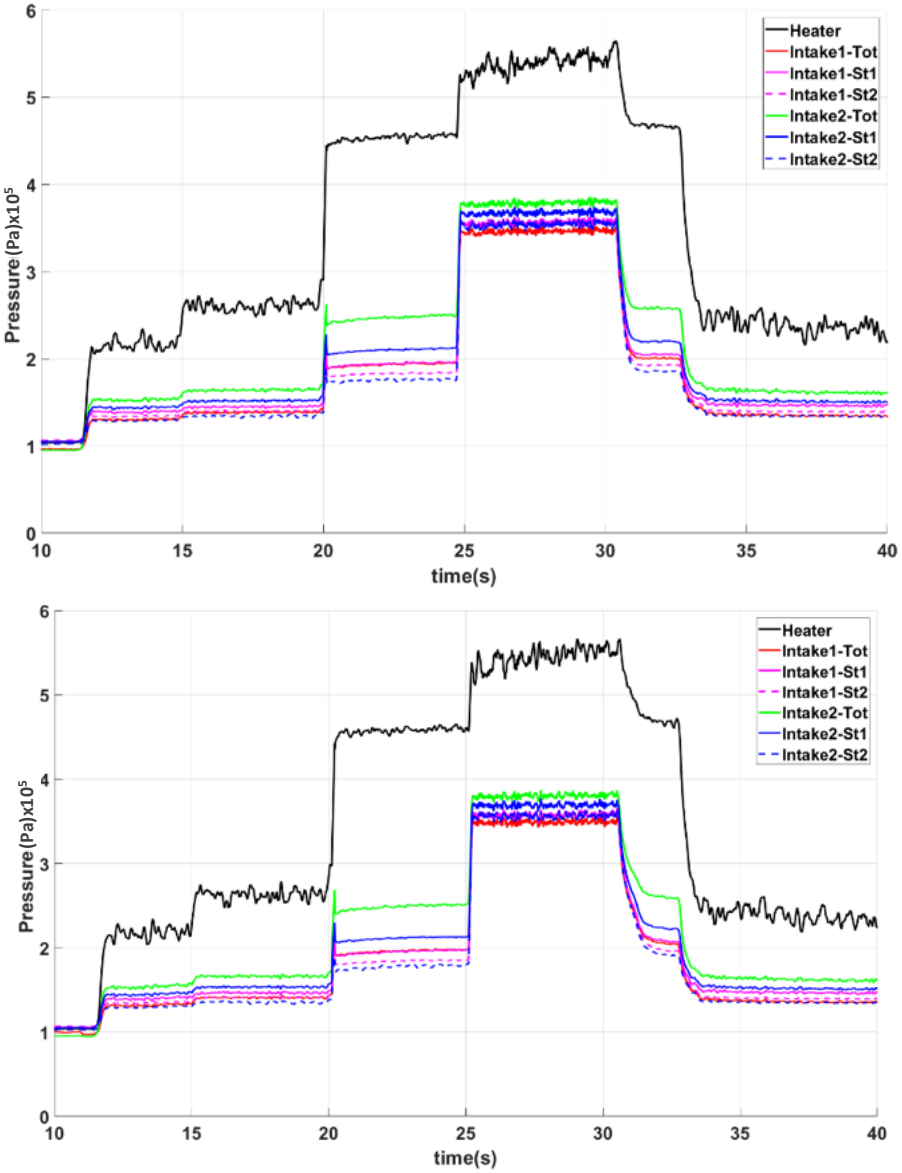

Figure 4-13 Gas generator pressures (Intake side) – Run 8 and Run 9

Both Runs 8 and 9 are initiated as per the same firing sequence and Intake side pressures are shown in Figure 4-13. As per the firing sequence, air flow is switched ON first. There is a pressure rise which is seen as the 1st step in the plot. Oxygen (O_2) is switched on after 8 seconds of air flow which leads to pressure rise to 2nd step. Hydrogen (H_2) flow is switched ON 6 seconds after O_2 flow is established. It leads to further rise in pressure and is seen as the 3rd step of pressure plot. Heater ignition is achieved using spark igniter. Vitiated air as per flight conditions is supplied to the gas generator.

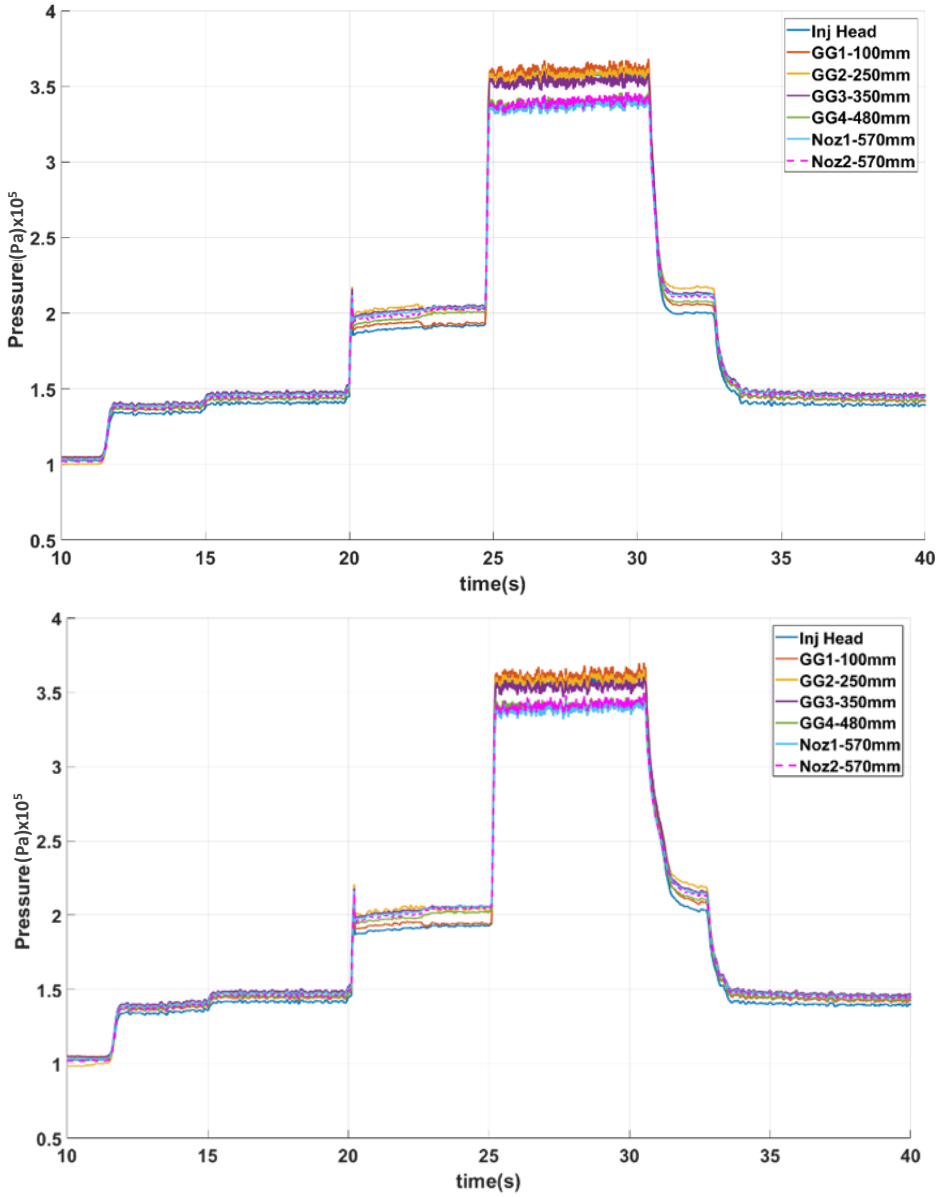

Figure 4-14 Gas generator pressures (Combustor side) – Run8 and Run 9

All fuel injection (~ 800 g/s) from 3 places (Intake + Film cooling injection + Central swirl injector) is made at a time.GG combustion chamber pressure rises as shown in Figure 4-14. This indicates combustion has been achieved. The sustained combustion is continued for another 6 seconds. Subsequently, H_2 supply to heater is switched off leading to cut off vitiated air to gas generator and combustion stops as indicated by drop in pressures.

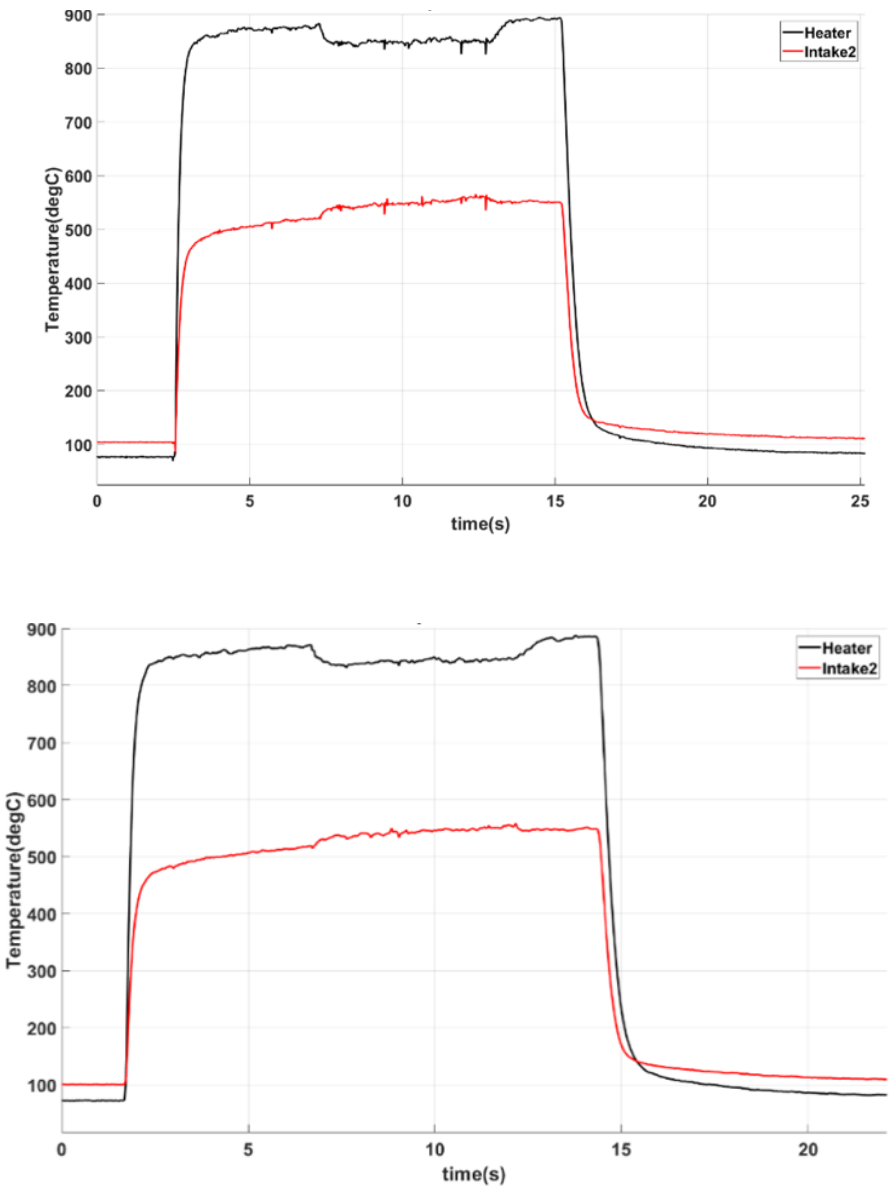

Figure 4-15 Heater and Intake entry gas temperature – Run8 and Run 9

Rise in temperature of vitiated air is shown in Figure 4-15. Heater temperature rise is of the order of 877°C and for intake exit vitiated air temperature requirement of 537° C. Performance in both the runs is almost same.

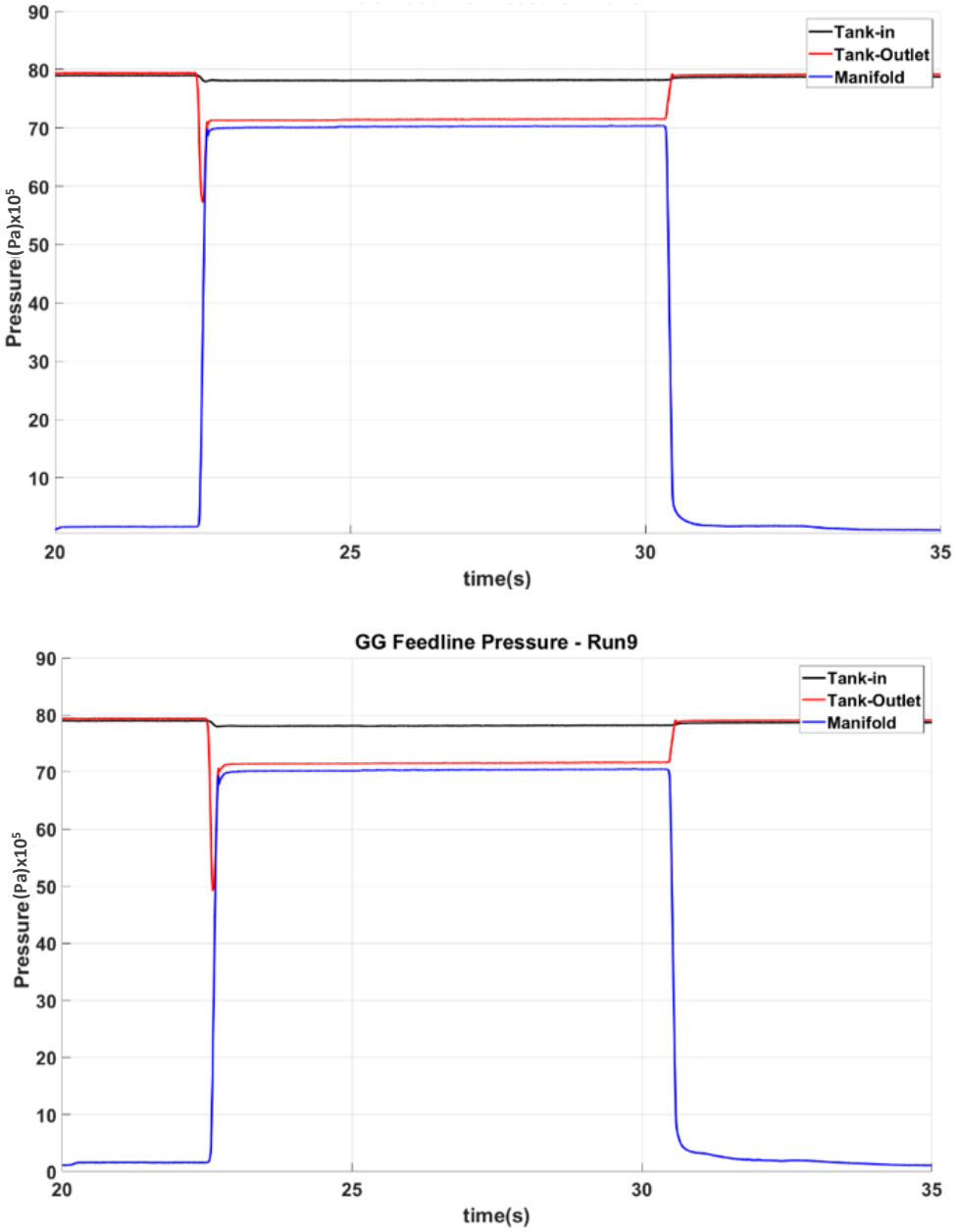

Figure 4-16 Jet-A feed system pressures – Run8 and Run 9

Figure 4-15 shows Jet-A fuel tank inlet, outlet and manifold pressures. Tank inlet pressure is constant throughout the test. As all the Jet-A fuel is injected at a time, the drop in the flow is constant throughout the test duration.

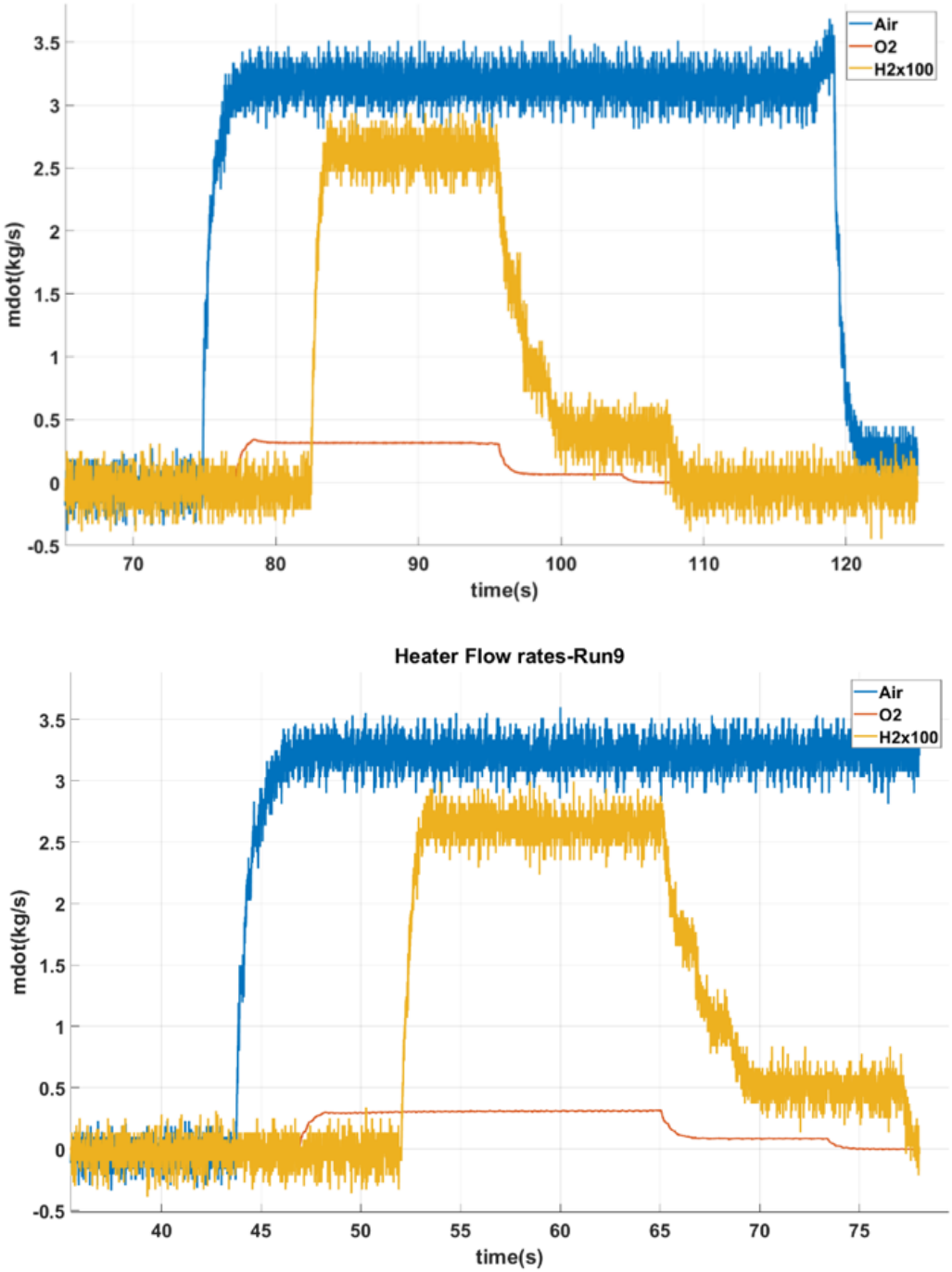

Figure 4-17 Heater air flow rates – Run8 and Run 9

Heater mass flow rates are shown in Figure 4-17. Heater mass flow rates dictate the performance of the entry conditions to the gas generator simulating the flight altitude conditions. Hydrogen fuel based vitiated air heater is used for the tests conducted. Air, hydrogen and oxygen are supplied as per the pre-calibrated requirements. Heater total flow rate achieved is 3.54 kg/s.

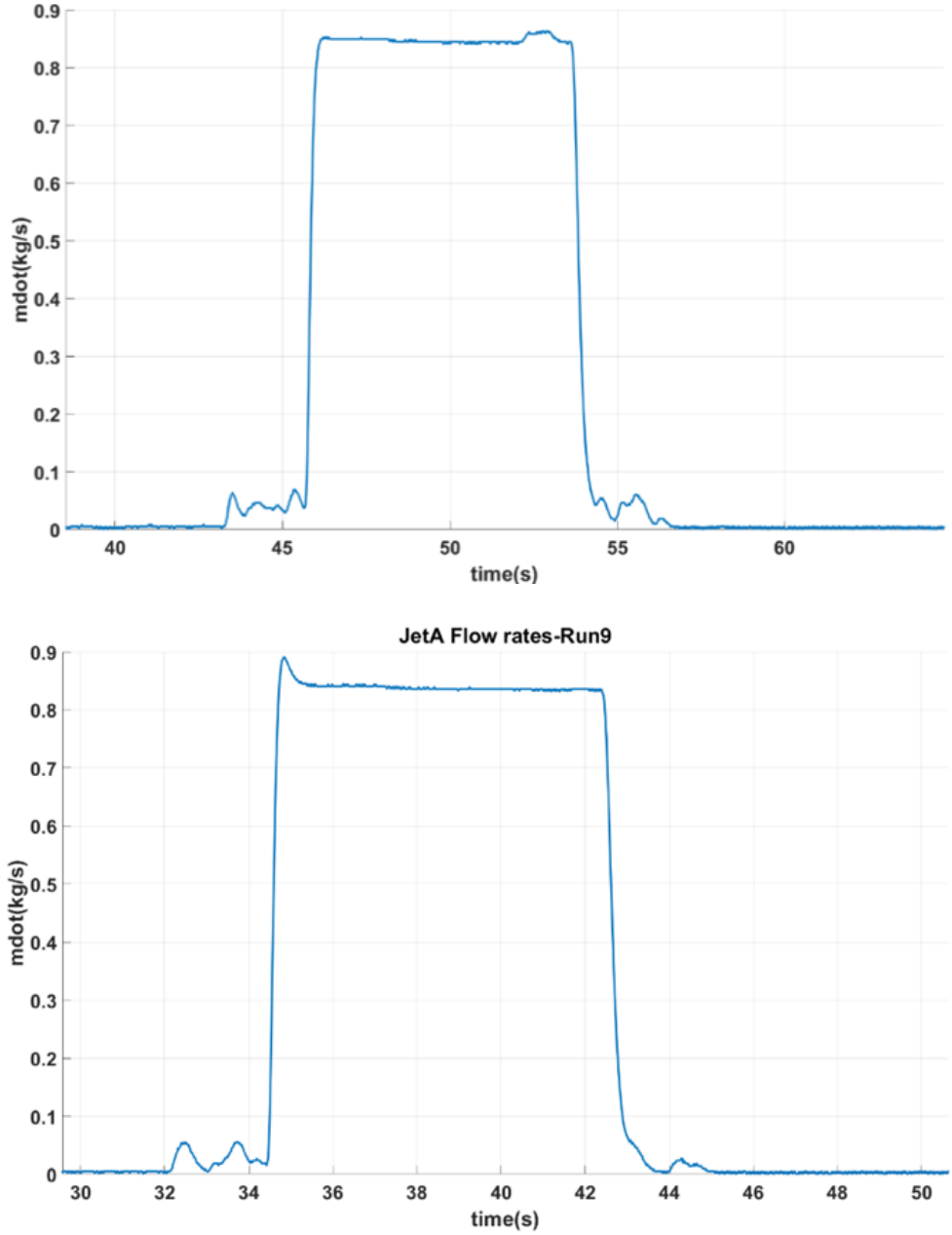

Figure 4-18 Jet-A mass flow rate – Run8 and Run 9

All fuel injection from 3 places (Intake + Film cooling inj. + Central swirl inj) is made at a time total flow of 0.845 and 0.836 kg/s is achieved in Runs 8 and 9 respectively as shown in Figure 4-18. The injectors are pre-calibrated with De-mineralized water to estimate their hydraulic resistance for the specified flow rates and upstream pressures. Equivalence ratio of 0.84 and 0.85 in intake arm and 3.54 and 3.45 for total flow are achieved in the respective runs.

Figure 4-19 Ground testing of gas generator

Yellow flame at combustor exit shows highly fuel rich burning of fuel and bluish flame in the plume shows its reaction with ambient air. Test data has been analyzed. Intake entry total and static pressures data are given in Table 4-2. Average flow Mach number at intake exit is less than 0.3 for reactive cases. Average pressure has been considered for flow Mach number estimation. Mach number is estimated assuming stagnation condition for flow. Average heater and intake entry temperature is given in Table 4-3. Heater average temperature is of the order of 1160 K and intake entry temperature is of the order of 810 K for reactive cases.

Heater mass flow rate and Jet-A flow rates are given for each run in Table 4-4. Average total mass flow rate is of the order of 3.5 kg/s except run7 where it was slightly higher. Total mass flow rate consists of Air, O_2 and H_2 and mass fraction of each component is of the order of 91.3,8 and 0.7 % respectively. Equivalence ratio for intake arm and its global value is also given in table 3.9. Equivalence ratio is calculated in the following ways:

$$\varphi = \frac{\left(\frac{O}{F}\right)_{stoich}}{\left(\frac{O}{F}\right)_{actual}}$$

..Eq(4.1)

Here, stoichiometric O/F ratio for Jet-A fuel and air is 14.66. For C* calculation, combustor achieved pressure from test data is used and combustor throat diameter is 134 mm. The achieved C* for all the runs is given in Table 4-5. For an equivalence ratio of 3.5, theoretical C* for chemical equilibrium is 1058.1 m/s and combustion efficiency achieved is of the order of 98% for this ratio.

C* is calculated in the following way:

$$C* = \frac{P_{static} \cdot A_t}{mdot}$$

…Eq(4.2)

Table 4-2 Intake arm pressures and Mach number

S No.	Entry Total Pr (bar)	Entry Static Pr(bar)	Exit Static Pr (bar)	M
RUN1	2.4	2.0	1.7	0.72
RUN2	2.4	2.0	1.7	0.72
RUN3	3.8	3.7	3.6	0.28
RUN4	3.6	3.4	3.3	0.35
RUN5	2.4	2.0	1.7	0.72
RUN6	2.4	2.0	1.7	0.72
RUN7	3.7	3.6	3.5	0.28
RUN8	3.7	3.6	3.5	0.28
RUN9	3.8	3.6	3.5	0.34

Table 4-3 Heater outlet and intake entry temperature

S No.	Heater Temperature (K)		Intake Entry Temperature(K)	
	Test	Average	Test	Average
RUN1	1133-1180	1156.5	757-824	790.5
RUN2	1095-1164	1129.5	760-787	773.5
RUN3	1143-1178	1160.5	758-819	773.5
RUN4	1128-1173	1150.5	750-833	791.5
RUN5	1136-1171	1153.5	773-838	805.5
RUN6	1140-1177	1158.5	773-833	803.0
RUN7	1166-1181	1173.5	798-821	809.5
RUN8	1156-1161	1158.5	798-827	812.5
RUN9	1144-1157	1150.5	791-820	805.5

Table 4-4 Achieved flow rates and equivalence ratio of fuel and air

S NO.	mdot-air (kg/s)	Fuel flow rates (kg/s)		Equivalence ratio, ø	
		Intake + FC	Total	Intake arm	Total
RUN1	3.489	0	0.713	---	3.00
RUN2	3.484	---	---	---	---
RUN3	3.476	0.361	---	1.03	---
RUN4	3.495	0.366	0.694	1.04	2.91
RUN5	3.515	0.416	0.813	1.20	3.40
RUN6	3.505	0.414	0.808	1.20	3.40
RUN7	3.726	0.366	0.900	0.80	3.54
RUN8	3.546	0.330	0.845	0.84	3.50
RUN9	3.536	0.330	0.836	0.85	3.46

Table 4-5 Achieved C* based on pressure data

S No.	Pressure (bar)	C* (m/s)
RUN1	1.9	605.5
RUN2	1.9	730.2
RUN3	---	---
RUN4	3.2	1022.9
RUN5	1.9	587.8
RUN6	1.9	589.9
RUN7	3.36	972.6
RUN8	3.4	1036.8
RUN9	3.4	1041.4

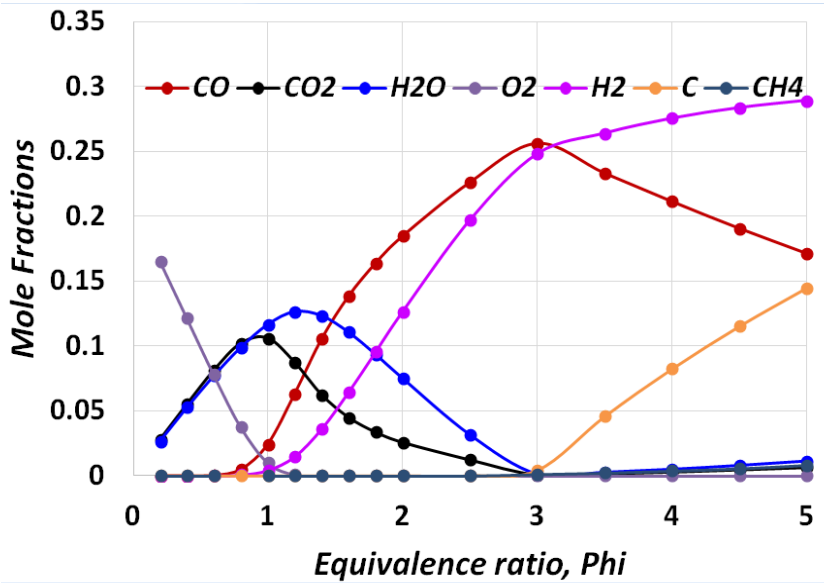

Figure 4-20 Combustion products as a function of equivalence ratio using NASA CEA

Combustion product species for equilibrium condition is plotted as a function of equivalence ratio using NASA CEA in Figure 4-20. For equivalence ratio of the order of 3.5, major species are CO, H2, and C. These are partially cracked fuel which will undergo secondary combustion in supersonic combustor.

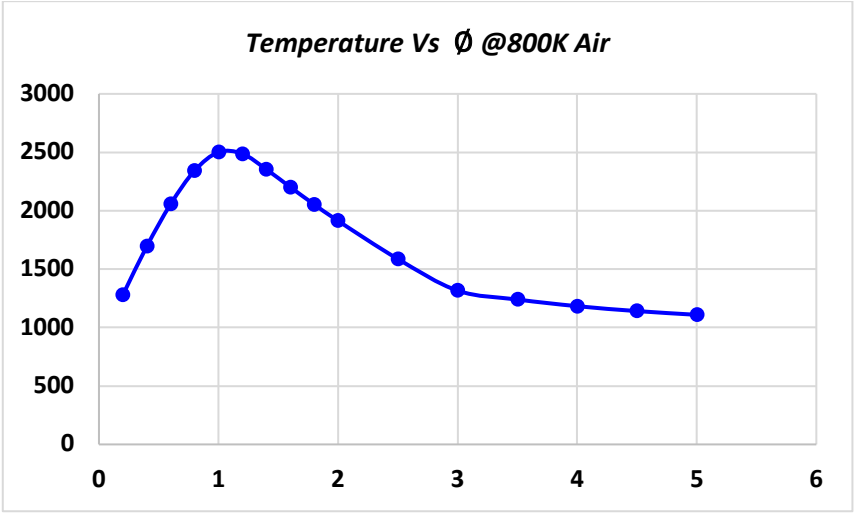

Figure 4-21 Adiabatic flame temperatures as a function of equivalence ratio using NASA CEA

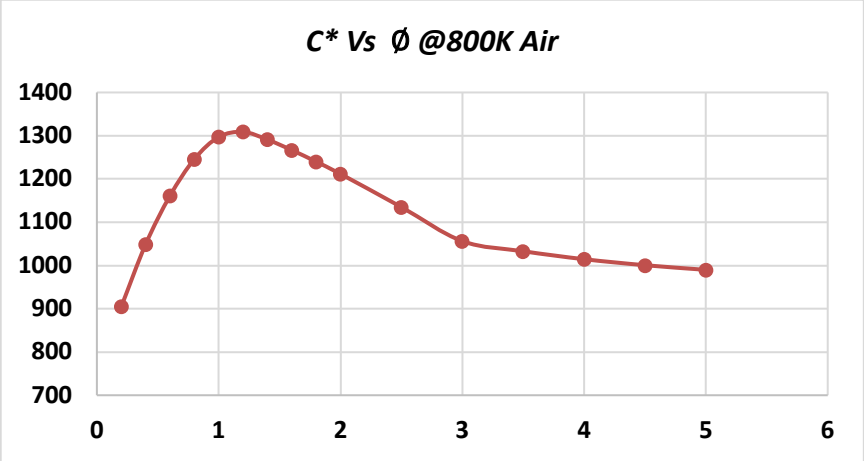

Figure 4-22 Theoretical C* as a function of equivalence ratio using NASA CEA

Adiabatic flame temperature and C* are shown in Figure 4-21 and Figure 4-22 for air entry temperature of 800K.

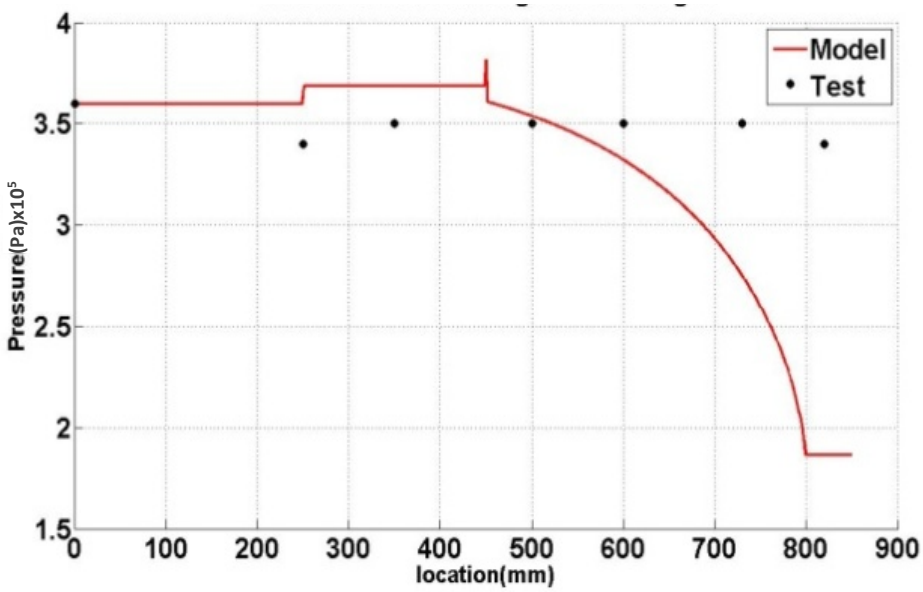

Figure 4-23 comparison of static pressure with test results

In the Figure 4-23 comparison of static pressure with test results is shown. There is a deviation in pressure between model and test when the duct starts converging. However, in the model ideal mixing and combustion has been assumed and properties are taken from NASA CEA. In the actual test, finite rate combustion is occurring and presence of other partially cracked products of Jet-A is also possible. The model gives the qualitative picture of process occurring in combustor.

4.1.4 Summary of experimental and design studies on gas generator

From the literature studies, design understanding and the experimental studies carried out; the following important aspects of fuel rich gas generator are found as critical observations:

- DCR with embedded gas generator mitigates ignition problems of supersonic combustion. This facilitates the ramjet and Scramjet operation in the same engine with wider Mach number operating regime.
- Design requirements of fuel rich gas generator are identified. Preliminary sizing of the gas generator is done keeping in view of the complete propulsion system performance and the intake performance limitations.
    a. Maximum back pressure that can be handled by subsonic intake is ~2.0. bar. This limits the maximum GG chamber pressure. Throat diameter has to be designed to achieve this. Effect of this variation on C* is important.
    b. Fuel injection sequence should be determined with this constraint in mind.
    c. Cracking of excess fuel leads to reduction of chamber C*. Design optimization to be carried out to get close to this value (~ 1050-1080). Chamber C* and GG throat diameter will determine Chamber pressure. Higher C* will call for a larger throat diameter to keep the chamber pressure under limit. This leads to the sizing the overall engine.
    d. Gases like CO, H_2, C_2H_4 etc., are highly reactive. Effort should be made to achieve cracking to produce more of these gases.

- Maximum fuel flow demand will be there for Mach number 4 condition rather than higher Mach numbers. Gas generator shall always be designed for this condition with high fuel rich equivalence ratio. Multistage injection scheme is found as an essential requirement. Partial injection of fuel in the intake arms helps in achieving benign ignition conditions for fuel rich mode combustor especially for M4 conditions. A good fuel flow controller will be essential for such applications.
- One-Dimensional model has been developed to predict the performance of Dump combustor/Gas generator with experimentally established correlations and reasonable assumptions from basic laws. Suitable injection scheme is designed to achieve proper

mixing of fuel and air and to maintain constant temperature. For model, ideal combustion/ mixing and intake arm equivalent cross-section area are taken for analysis.

- Governing equations are developed using conservation of mass, momentum and energy. Heat addition is assumed to be a point heat addition and chemical reactions between Fuel and air are calculated using NASA CEA with equilibrium combustion assumption. Chemical species obtained from step1 heat addition is used as oxidizer for step 2 fuel addition. The two main processes involved are Rayleigh flow and flow with area change.
- The performance and flow field parameters of a dump combustor are investigated through experiments and analytical model using MATLAB. The developed analytical model and extensive experimental data shows that sustained ignition is achieved for a particular equivalence ratio range of 2.9 to 3.5 and fuel flow rates of 700 to 830 g/s. The model is found useful for understanding the gas generator performance in a qualitative way.
- Full scale gas generator hardware was developed and series of tests were conducted to establish ignition (by using a pyro based igniter), sustained combustion if fuel rich gas generator at high equivalence ratio of 3.5.
- For a fuel rich equivalence ratio of 3.5, experimentally achieved C* is 1041.1 m/s

4.2 Numerical study on DCR Combustor geometry

4.2.1 Configuration -I

Isolator angle : 7 ° ; Equivalence ratio, $\phi_{overall}$ = 0.6, 0.8, 1.0 and 1.2 ; M_∞ : 6

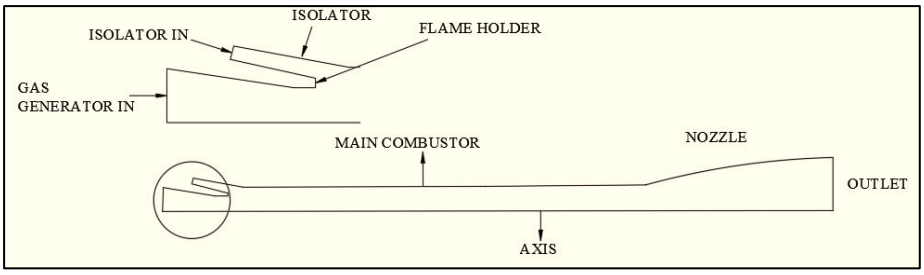

Figure 4-24 DCR Geometry for simulation

4.2.1.1 Mach -6 condition

Table 4-6 Boundary conditions for Mach 6

Boundary	**Boundary conditions**
Scram inlet	Mass flow $\dot{m}$ = 5.7 kg/s , P_{static} = 0.4 atm ,T_o = 1503K
GG Inlet	Mass flow *(for $\phi_{overall}$ = 0.6)* $\dot{m}$ = 2.15kg/s (1.88kg/s air + 0.27 fuel) and P_{static} = 1.5 atm

Reacting flow:

An equivalence ratio study was carried out to assess the performance of the combustor in terms of combustion efficiency, Combustor wall static pressure distribution, Total temperature contours, Mach contours, pre-combustion shock train (PCST). The equivalence ratio was varied by changing the mass flow rate of the fuel in the gas generator. The mass flow rate of air in the gas generator and the supersonic inlet was kept constant. The input fuel mass fractions were calculated using NASA code CEA. Table 4-7 gives the fuel mass flow rate and the mass fractions for different equivalence ratios.

Table 4-7 Fuel mass fractions

Overall ER ($\phi_{overall}$)	**Gas generator ER (ϕ_{gg})**	**CO mass fraction**	**H2 mass fraction**	**Mass flow rate fuel $\dot{m}_f$ (kg/s)**
0.6	2.55	0.283	0.0181	0.27
0.8	3.18	0.332	0.024	0.34
1	3.92	0.32	0.0229	0.42
1.2	4.76	0.294	0.0328	0.51

a) Combustion efficiency:

Figure 4-25 shows the combustion efficiency with respect to the equivalence ratio, Table 4-8 provides the ideal and actual mass fractions of CO2 at the combustor exit. The case with highest equivalence ratio has the lowest combustion efficiency. The combustion efficiency is seen to decrease with the increase in equivalence ratio. The highest combustion efficiency is observed in the case with the lowest equivalence ratio with $\phi = 0.6$ which has efficiency of = 56%.

Table 4-8 Combustion efficiency for Mach 6, Configuration -I

Overall ER ($\phi_{overall}$)	CO2 mass fraction (actual)	CO2 mass fraction (ideal)	Combustion efficiency (%)
0.6	0.0702	0.12410	56.8
0.8	0.068	0.15721	43.3
1	0.059	0.16614	35.5
1.2	0.0502	0.13986	35.9

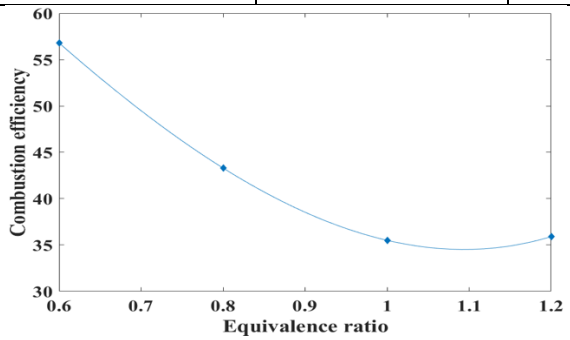

Figure 4-25 Combustion efficiency Vs. Equivalence ratio for Mach 6, Configuration -I

b) Combustor wall static pressure distribution:

Figure 4-27 shows the static pressure contours of different cases in the combustor. The pressure increases in the combustor immediately downstream of the isolator due to combustion is visible. The pressure in the combustor also increases with increase in equivalence ratio from $\phi = 0.6$ to $\phi=1.2$ as seen in the static wall pressure distribution Figure 4-26. The pressure at the beginning of the combustor is high while along the combustor the pressure reduces due to flow acceleration, the case with highest equivalence ratio has the highest pressure. As the equivalence ratio increases the fuel flow rate increases, which leads to higher heat addition to the flow. This leads to both higher pressure rise in the combustor and lower Mach number.

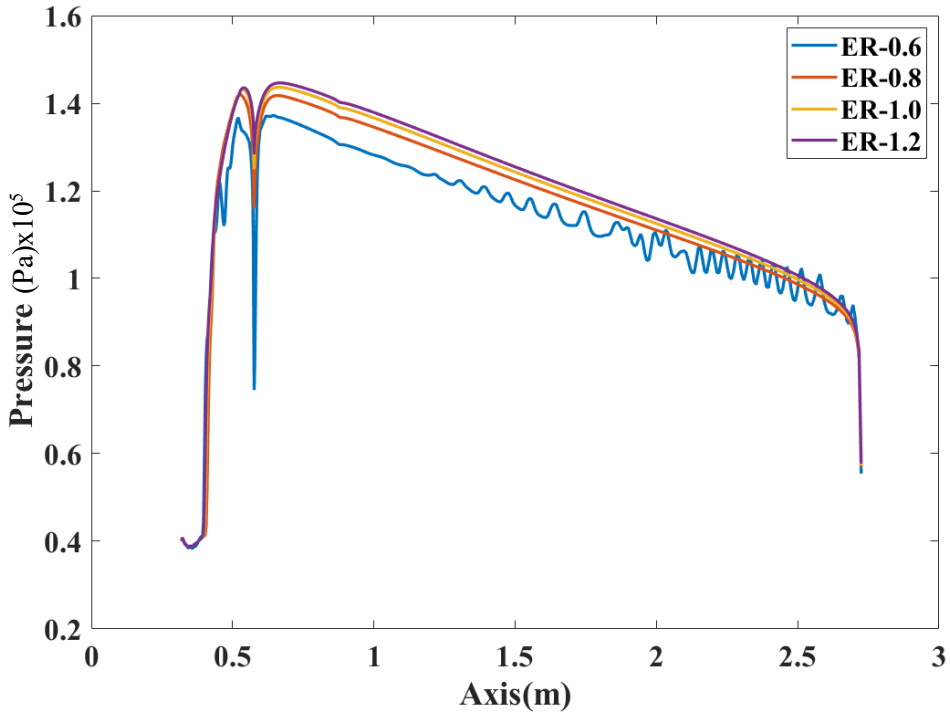

Figure 4-26 Wall static pressure distribution along the combustor

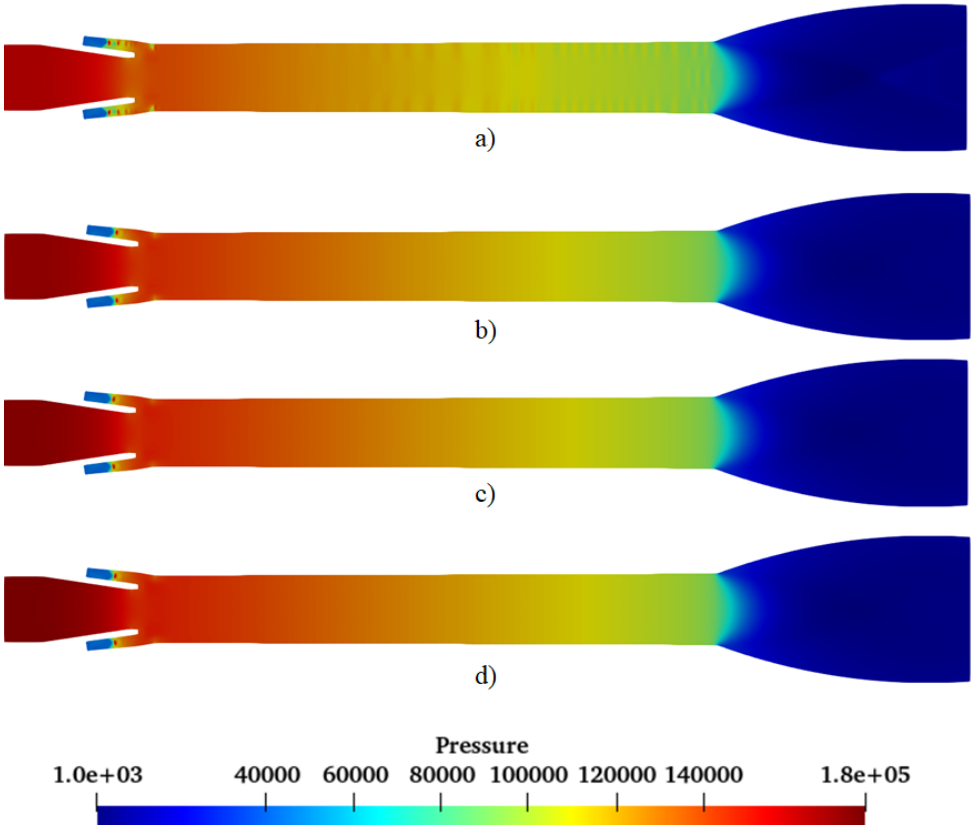

Figure 4-27 Static pressure contours for equivalence ratios a) 0.6 b) 0.8, c) 1.0 and d) 1.2

c) Total temperature contours:

Figure 4-28 shows the total temperature contours for different equivalence ratios, the total temperature is the indication of combustion. The regions of higher total temperatures indicate higher degree of combustion. It is also an indication of mixing of gas generator and the isolator flow streams. As higher degree of mixing leads to more efficient combustion to occur inside the combustor. Apex formation is not observed in any of the cases as a result of poor mixing between the isolator and gas generator streams leading to low combustion efficiency as observed earlier (Table 4-8).

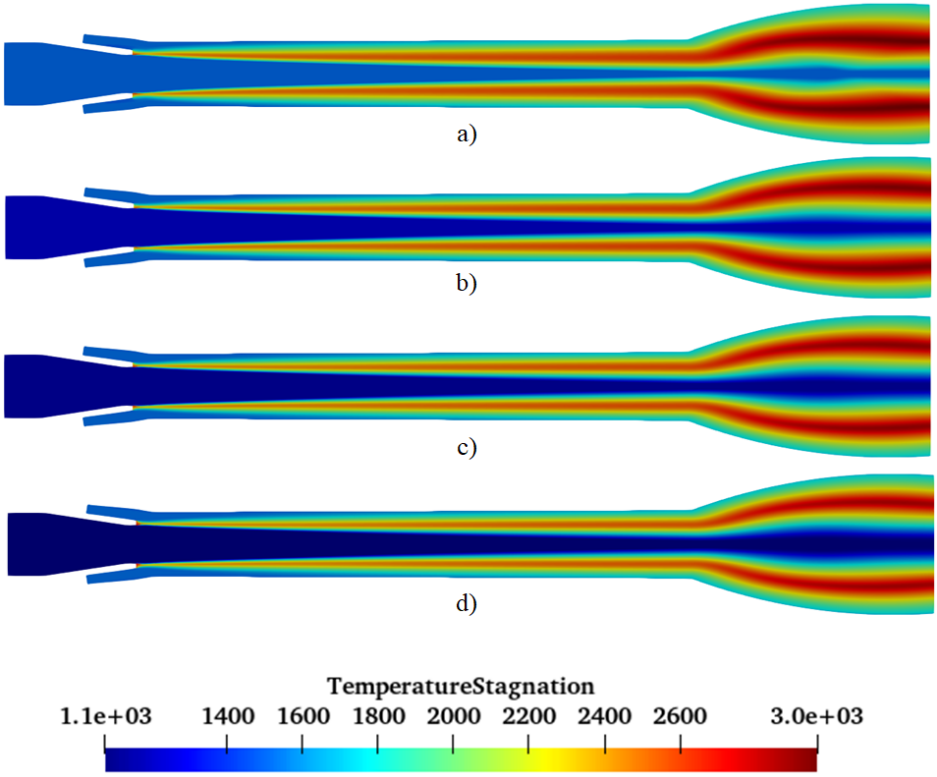

Figure 4-28 Total temperature contours for equivalence ratios a) 0.6 b) 0.8 c) 1.0 d) 1.2

d) Mach contours:

Figure 4-29 shows the Mach contours inside the combustor for regions with Mach number higher than 1, the formation of Pre-combustion shock train is visible in the isolator which also extends into the main combustor for $\emptyset = 0.6$. The flow in the gas generator is subsonic, while that of the isolator is supersonic. The flow velocity along the circumference of the combustor is higher than the core flow. The Mach number of the supersonic flow entering the combustion chamber from the isolator is reduced to subsonic speed as the temperature in the chamber is high due to heat addition as a result of the combustion. The head addition also results in the acceleration of the subsonic flow in the combustor which is accelerated to near sonic speeds at the end of the combustor. The heat addition increases with the increase in the equivalence ratio. This increased heat addition reduces the flow Mach number. Hence the region of near sonic Mach number reduces with the increase in the equivalence ratio.

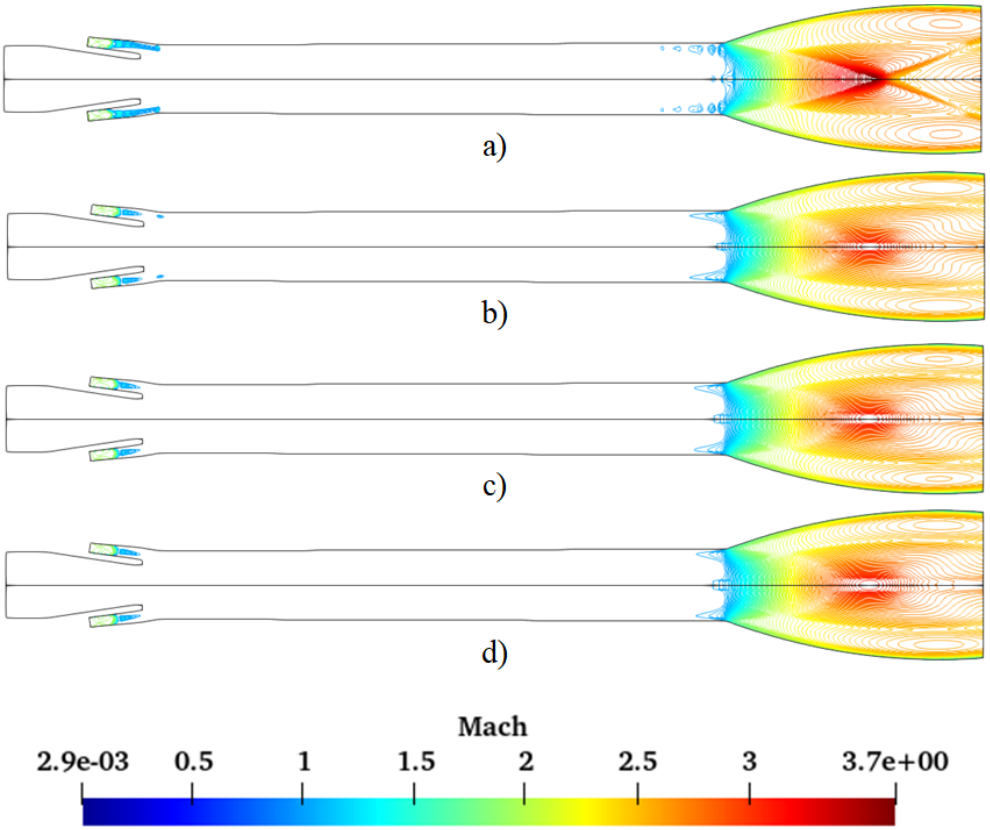

Figure 4-29 Mach(M>1) contours for equivalence ratios a) 0.6 b) 0.8, c) 1.0 and d) 1.2

e) Pre- combustion shock train (PCST):

The pre-combustion shock train is formation of an oblique shock train takes place at the end of the isolator region. This is formed due to the increased back pressure from the combustion chamber. The later this shock train is formed in the isolator the lower the chances of unstart of the inlet.

Table 4-9 gives the starting position of the pre-combustion shock train from the beginning of the isolator. The starting position for equivalence ratios of 0.8 and 1.0 are almost same. They are in accordance with the pressure distributions. The starting position of case with ER with 1.2 is at 0.089 lower than that of the previous two cases. The lowest starting point is observed in the case of equivalence ratio of 0.6.

Table 4-9 Starting position of PCST with equivalence ratio

Parameter (m)	**ϕ = 0.6**	**ϕ = 0.8**	**ϕ = 1.0**	**ϕ = 1.2**
Starting location	0.072	0.104	0.105	0.089

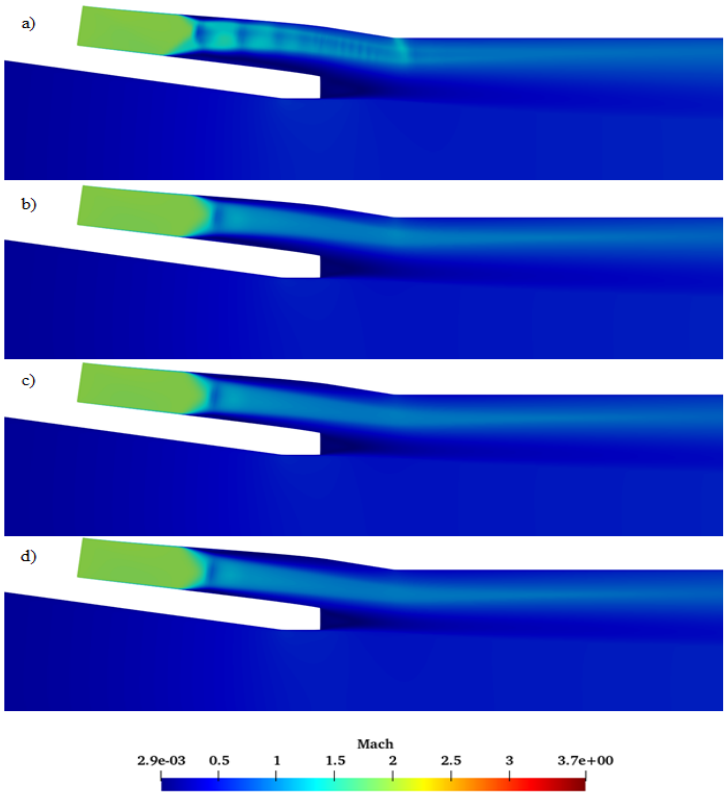

Figure 4-30 Mach contours showing PCST in isolator for equivalence ratios a) 0.6 b) 0.8, c) 1.0 d) 1.2

b)

4.2.1.2 Mach -4 condition:

Table 4-10 Boundary conditions for flight Mach 4

Boundary	Boundary conditions
Scram inlet	Mass flow $\dot{m}$ = 9.66 kg/s, P_{static} = 0.95 atm, T_o = 791K
GG Inlet	Mass flow $\dot{m}$ = 3.68 kg/s (3.25 air + 0.43 fuel) and P_{static} = 1.2 atm

Reacting flow

An equivalence ratio study was conducted for flight Mach number of 4. As in the previous case the mass flow rate of the gas generator and the isolator was kept constant while the fuel flow rate is varied. The table gives the fuel flow rate for different equivalence ratios. Table 4-10 gives the boundary conditions for Mach 4 simulation.

Table 4-11 Boundary conditions for flight Mach 4 condition

Overall ER ($\phi_{overall}$)	Gas generator ER (ϕ_{gg})	CO (msf)	H2 (msf)	Mass flow rate fuel $\dot{m}_f$ (kg/s)
0.6	2.55	0.257	0.014	0.43
0.8	3.18	0.332	0.024	0.58
1.0	3.92	0.32	0.0229	0.72
1.2	4.76	0.294	0.0328	0.87

a) Combustion efficiency:

The combustion efficiency is the ratio of ideal concentration of CO2 to the actual mass fraction of CO2 at a location. The combustion efficiency is low for all the cases. The highest combustion efficiency is observed in case with lowest equivalence ratio and decreases with increase in ϕ .

Table 4-12 Combustion efficiency for Mach 4, Configuration -I

Overall ER ($\phi_{overall}$)	CO2 mass fraction (actual)	CO2 mass fraction (ideal)	Combustion efficiency (%)
0.6	0.0474	0.1243	38.1
0.8	0.0404	0.1601	25
1.0	0.036	0.1734	20.7
1.2	0.0317	0.1428	22.1

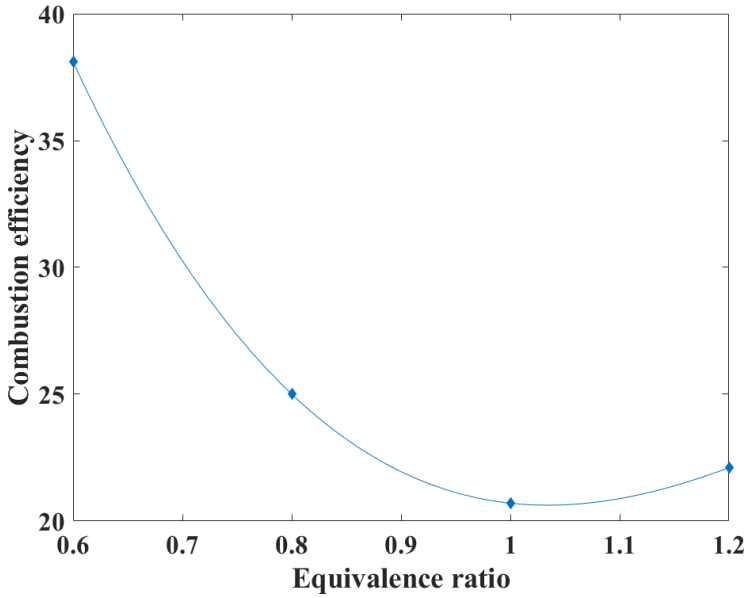

Figure 4-31 Equivalence ratio Vs. Combustion efficiency

b) Combustor wall static pressure distribution:

Figure 4-32 shows the wall static pressure distribution for equivalence ratios 0.6 to 1.2. The peak pressure in the combustor is lower than the isolator. The pressure in the combustor peaks immediately downstream of the flame holder but reduces along the length of combustor. As the flow is accelerated to sonic speeds at the end of the combustor pressure fluctuations are noticed in the wall pressure. The pressure distribution along the combustor increases with the increase in the equivalence ratio, except for equivalence ratio 0.6 where the pressure is lower than $\emptyset$ = 1.2 but higher than the other two cases. Figure 4-33 shows the static pressure contours which show no PCST and the pressure in the isolator higher than that of the combustor.

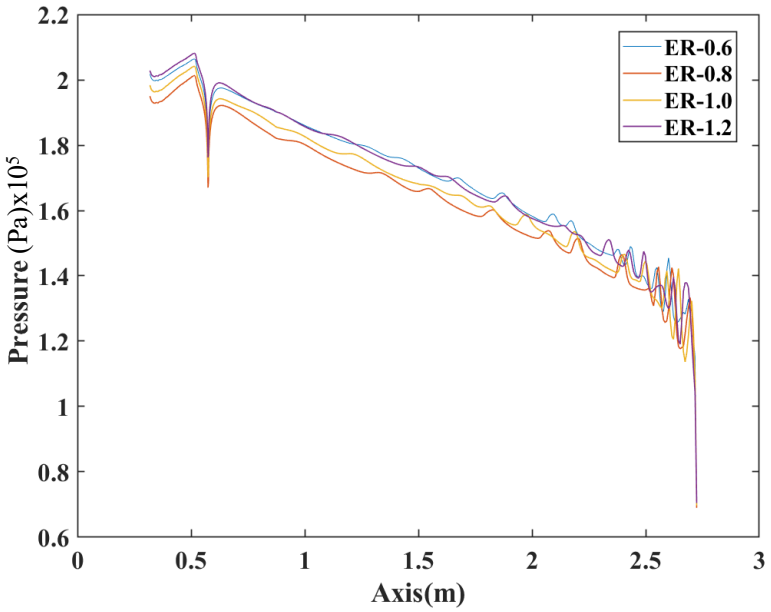

Figure 4-32 Wall static pressure distributions along the combustor

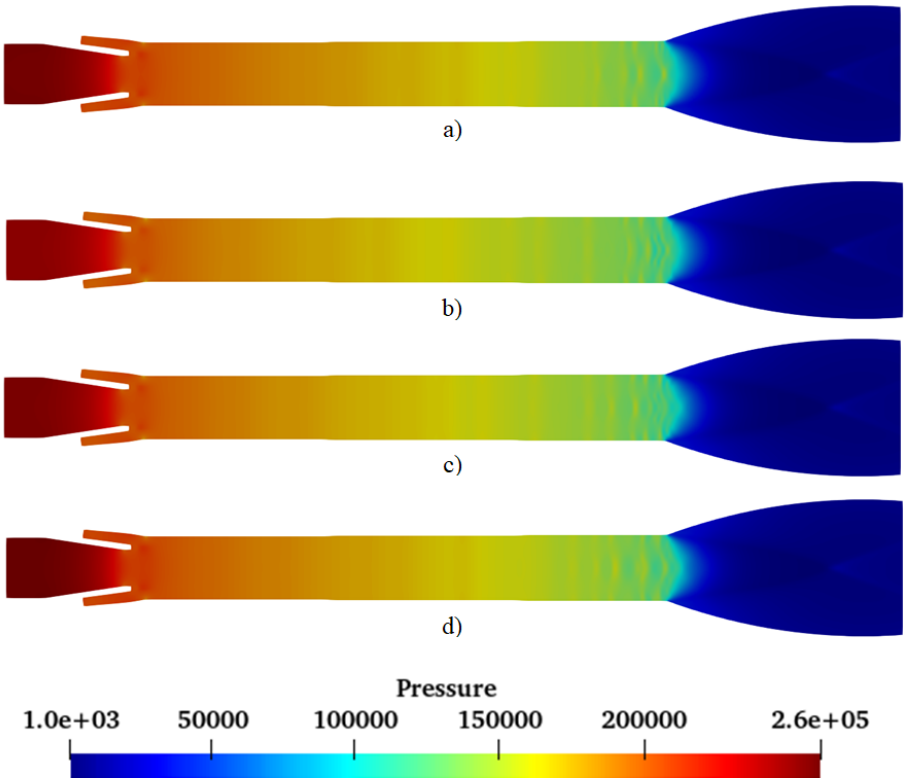

Figure 4-33 Static Pressure contours for equivalence ratios a) 0.6 b) 0.8, c) 1.0 and d) 1.2

c) Total temperature contours:

The total temperature contours are a representation of the combustion , the combustion leads to energy addition to the flow, which leads to a higher total temperature where combustion takes place. It is seen that the combustion takes place along the mixing layer. This mixing layer grows along the combustor. But the rate of growth is minimal and no apex formation takes place in the combustor, hence poor mixing lead to a lower combustion efficiency.

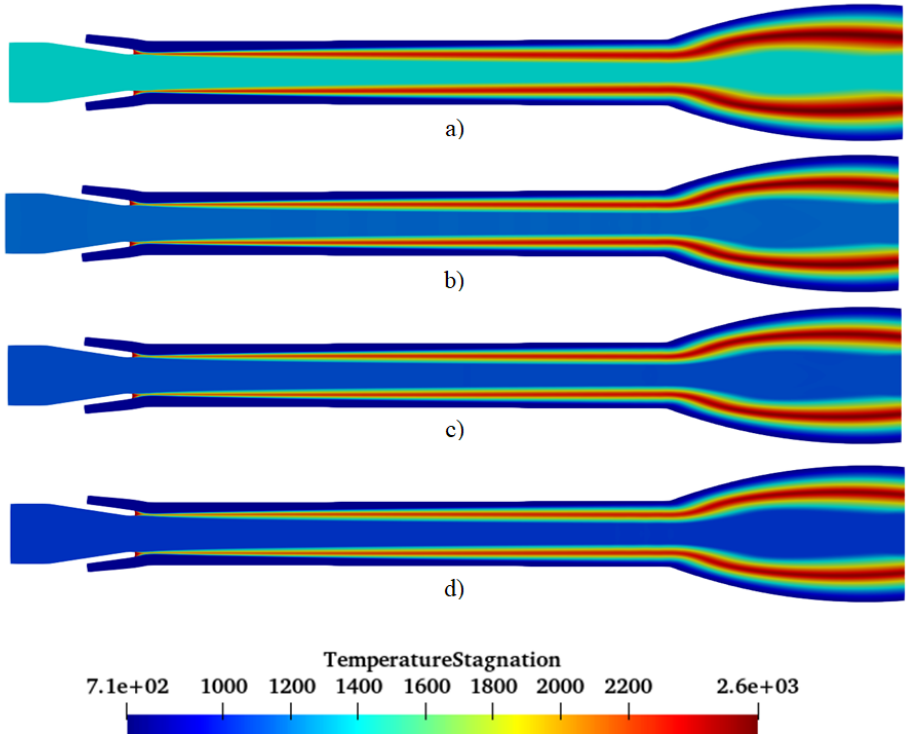

Figure 4-34 Total temperature contours for equivalence ratios a) 0.6 b) 0.8, c) 1.0 and d) 1.2

d) Mach contours:

Figure 4-35 shows the Mach contours inside the combustor, The flow entering the isolator is at a subsonic Mach number, hence no Pre-combustion shock train is visible in the isolator. Due to head addition in the combustor the flow is accelerated along the length of the combustor. This leads to the increase in Mach number along the combustor. This heat addition also results in decrease of Mach number in the combustor. This is observed in the Mach contours. The flow is subsonic when is enters the combustor and is accelerated. At the end of the combustor sonic Mach number is observed in all the cases.

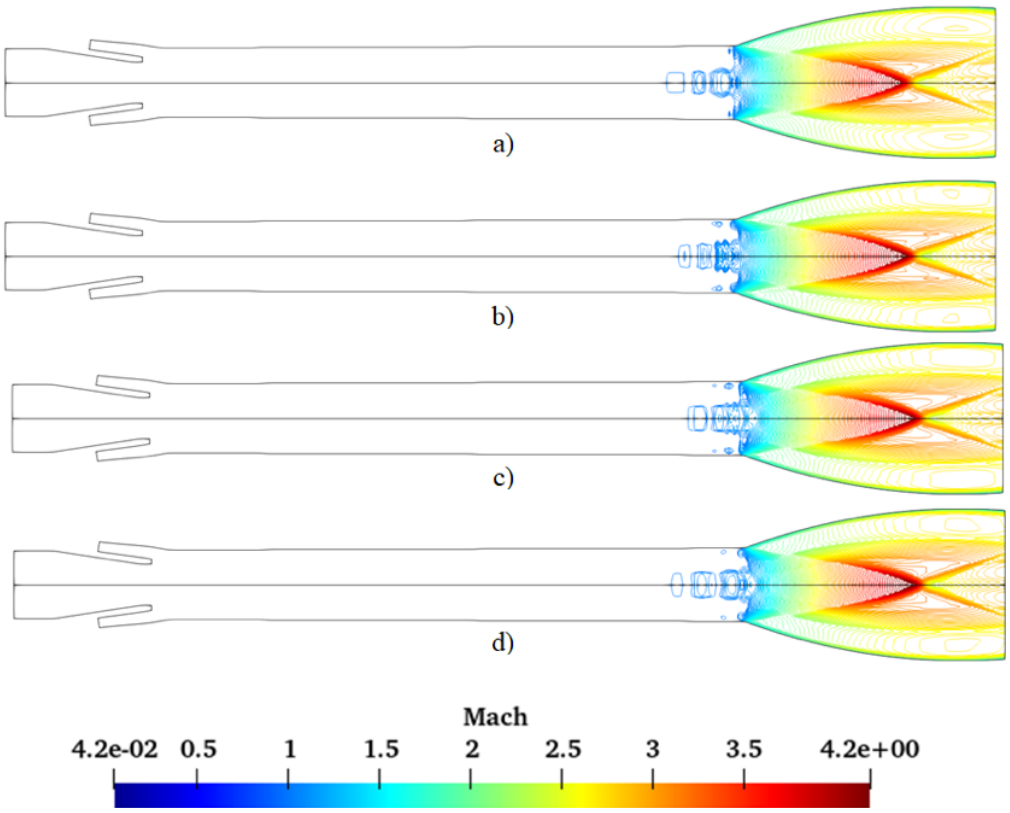

Figure 4-35 Mach (M>1) contours for equivalence ratios a) 0.6 b) 0.8, c) 1.0 and d) 1.2

4.2.2 Configuration –II

Simulation and study of geometry with 7° isolator angle revealed that the combustion efficiency is poor due to poor mixing of the isolator and gas generator flow streams. One of the methods to improve the mixing of two flow streams and to enhance mixing layer growth is to increase the relative flow impingement angle between the two flow streams. **Hence the isolator angle was increased from 7° to 14° which increases the impingement angle of the isolator flow. Thus, improving the mixing and hence the combustion.**

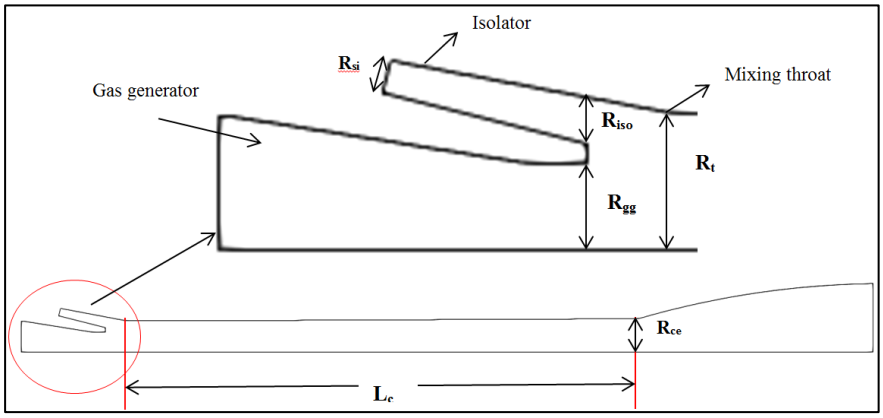

Figure 4-36 Locations of geometries indicated in Table 4-13and Table 4-14.

In Configuration –II combustor geometry with 14° isolator angle was investigated. Total of five cases were simulated. In each case the geometry of the combustor was varied to enhance mixing and improve combustion. The geometrical changes made in each case is in Table 4-13 and Table 4-14. Table 4-14 shows the radius of gas generator exit (R_{gg}), isolator exit (R_{iso}), Flame holder width, radius of the mixing throat (R_t) and the combustor entry radius (R_{ci}) for cases 1 to 5 with the corresponding area ratios. Table 4-6 shows the length of the supersonic combustor (L_c) from the mixing throat to the nozzle start for cases 1 to 5 with corresponding area ratio of Combustor length to radius of the combustor exit (L_c/ R_{ce}), while the exit radius was fixed at 136mm.

When the area ratios between the combustor inlet (A_{ci}) and the mixing throat (A_t), Gas generator exit (A_{gg}) and the isolator exit (A_{iso}) was calculated and compared with respect to proper mixing and combustion efficiency. A trend was observed in both the area ratios. The combustor inlet to mixing throat area ratio (A_{ci}/A_t) for the first case where the combustion efficiency was lowest and no apex was formed was 1.26 while in the last case where high combustion efficiency was observed and apex was formed upstream of the combustor was 1, A_{ci}/A_t showed a decreasing trend i.e., combustion improved with decrease in area ratio and was at maximum when = 1.

The gas generator exit to isolator exit area ratio (A_{gg}/A_{iso}) showed an increasing trend, the ratio was 3.25 in the first case which had the lowest combustion efficiency and increased with improvement in combustion. It reached a peak value of 5.83 in the final case with highest combustion efficiency. The combustor length from the mixing throat to the nozzle beginning steadily increases from case 1 to case 5 with increase in combustion efficiency. The inlet to isolator exit area ratio (A_{si}/A_{iso}) is highest in cases 1 and 2 at 0.515 in the last three cases it reduced to 0.484.

Table 4-13 Combustor length variation (in mm)

Case	Combustor Length (L_c)	L_c/ R_{ce}
1	2115.69	15.55
2	2133.67	15.6
3	2146.57	15.7
4	2164.06	15.9
5	2195.12	16.1

Table 4-14 Geometrical changes made in each revision (in mm)

Case	GG exit (R_{gg})	Iso exit (R_{iso})	Flame holder width (b_{fh})	SC entry (R_{ci})	Mixing throat (R_t)	A_{ci}/A_t	A_{gg}/A_{iso}	A_{si}/A_{iso}
1	80	44.33	19	143.33	127.53	1.26	3.25	0.515
2	80	44.33	19	143.33	130.9	1.19	3.25	0.515
3	80	36.15	15	131.15	120.73	1.18	4.89	0.484
4	85	36.15	10	131.15	124.14	1.11	5.52	0.484
5	85	35.2	10	130.2	130.2	1	5.83	0.484

Simulation:

Non- Reactive flow structure:

The simulation of non-reacting flow was done first, once the flow was established the reacting flow with combustion reactions was conducted. Figure 4-37 shows the Numerical Schlieren image imposed on the static pressure data. The Schlieren image was obtained using a gradient filter over the density flow field data from the simulation. The image gives a clearer view of the flow structure in the combustor. The enlarged image is that of the upstream region of the combustor at the isolator and gas generator exit.

In the isolator oblique shock train is observed, as the flow enters the combustor an expansion and an oblique shock wave is formed. As the flow from the isolator enters the combustor, the flow near the combustor wall is turned away from itself causing expansion fans

at the combustor entry; the flow downstream of this region has a lower pressure than the rest of the flow. In the lower wall region of the isolator near the flame holder the flow is turned towards itself by the shape of the mixing layer region. The mixing layer acts a boundary deflecting the flow. This leads to a higher pressure region due to formation of oblique shock.

This oblique shock wave meets the combustor wall at a location downstream where a reflected shock originates, which is reflected towards the central region of the flow. This reflected shock undergoes refraction as it goes through the mixing layer. At the axis this shock wave meets the corresponding reflected wave from the opposite combustor walls, the shock- shock interaction results in formation of a stronger normal shock and reflected shocks. These reflected shocks again goes through the cycle of further reflection, refraction and interaction, resulting in formation a normal shock train in the combustor. This shock train can be seen in the numerical Schlieren image (Figure 4-37). But due to the viscous interactions of the flow, boundary layer and reflections, this shock train weakens along the length of the combustor.

In the gas generator, the flow is subsonic and has highest pressure. As it flows through the convergent duct the flow is accelerated, at the constant duct, which is the throat of the gas generator, the flow reaches sonic speed and chokes. The shock waves that are formed at the throat wall propagate to the axis, where shock-shock interaction results in a stronger normal shock wave and a reflected shock wave. The pressure increases downstream of the normal shock. The reflected shock propagates downstream of the gas generator. In the downstream region the flow from the gas generator is surrounded by the mixing region. When the gas generator flow exits from the throat, it expands in the combustor due to the divergent shape of the mixing region.

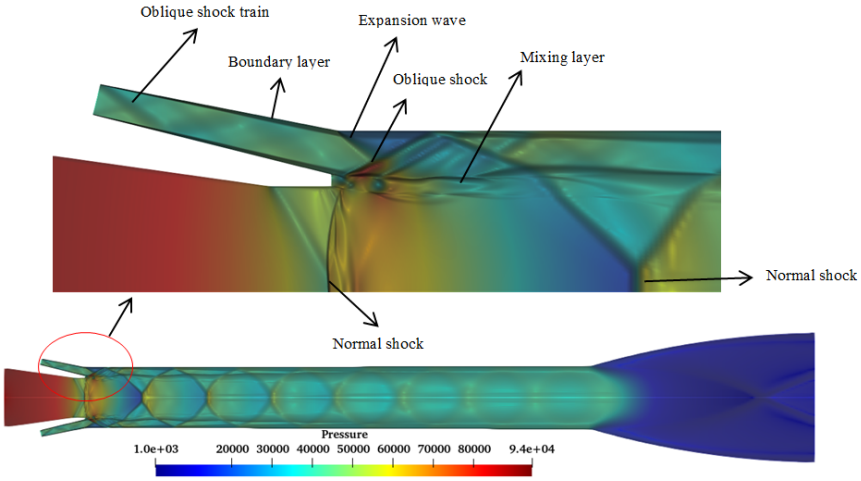

Figure 4-37 Numerical schlieren image of non-reacting flow (Case-5)

Reacting flow:

a) Apex formation:

The total temperature of the flow inside the combustor increases rapidly along the combustor due to combustion and the resultant heat addition. The combustion in the gas-generator is fuel-rich, hence complete combustion does not take place. Unreacted and partially reacted fuel is mixed with the oxidizer rich stream from the isolator leading to further combustion causing an increase in the total temperature.The total temperature is an indicator of progression of combustion. As the mixing region expands along the length of the combustor more quantity of gases react leading to further increase in the total temperature.

Figure 4-38 shows the total temperature contours of all 5 cases. The figures show distinct regions of flow , the regions where combustion has not taken place have a lower total temperature, Immediately down stream of the flame holder the total temperature starts to increase as the fuel and air mixing takes place. Along the length of the combustor this mixing region increases causing combustion reactions to take place leading to total temperature increase. The location where this mixing region meets the axis of the combustor, an apex is formed which encloses incompletely combusted relatively cold fuel rich gas, Another region of relatively cold gases is seen in the isolator where no fuel addition as occurred yet. In the boundary regions along the wall the total temperature remains low with relatively low combustion reactions.

The formation of apex takes place in cases 3 to 5, while no apex formation takes place in cases 1 and 2, indicating incomplete mixing betweent he isolator and gas generator flow stream. This incomplete mixing leads to lower combustion efficiency. The apex location is also seen to move downstream in the combustor. Indicating completion of macromixing earlier in the combustor, leading to higher combustion efficiency.

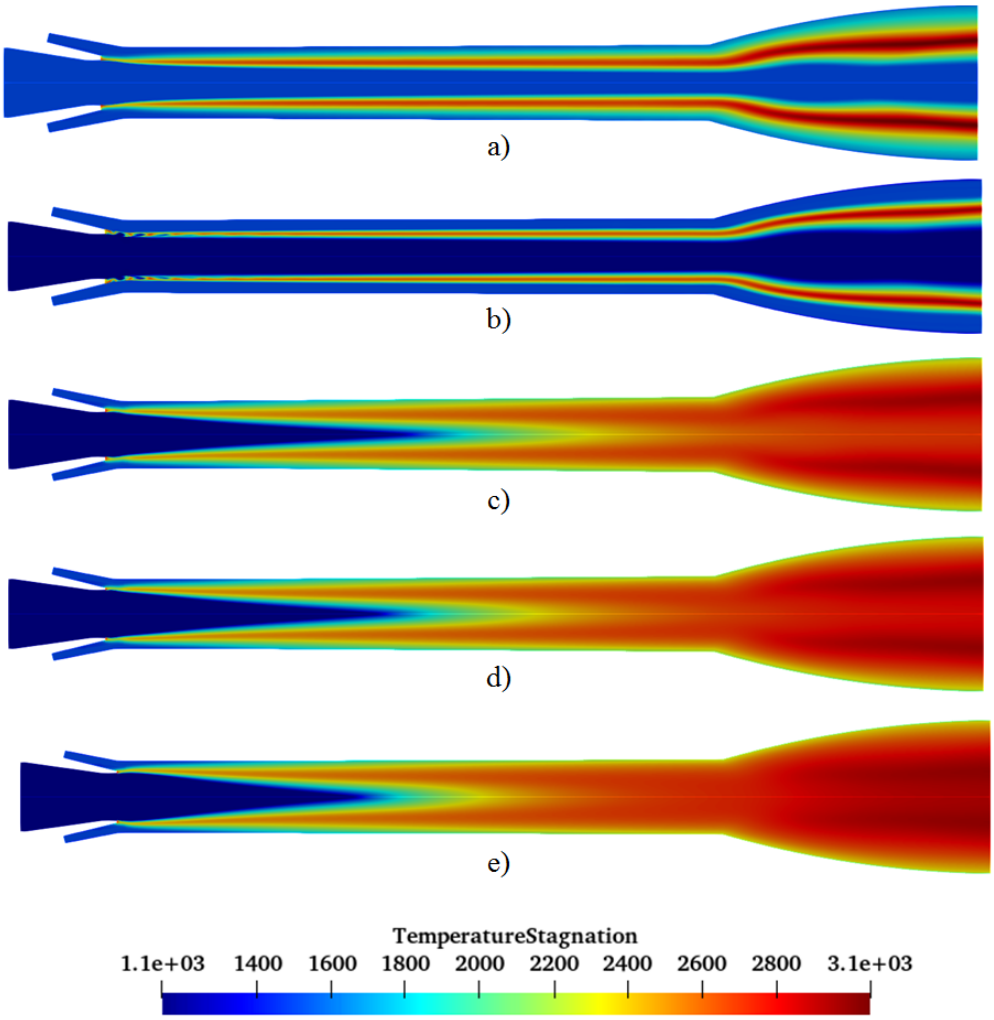

Figure 4-38 Total temperature contours for Mach 6 showing the apex: a)Case-1,b)Case-2, c)Case-3, d)Case-4, e)Case-5

b) Velocity profile:

The velocity profile was taken at four locations L1, L2, L3 and L4 in the supersonic combustor with an interval of $L_c/3$ between each of the locations, where Lc – length of the combustor from the mixing throat to the start of the nozzle(Figure 4-39). The first location (L1) is at the mixing throat followed by two intermediate locations (L2 and L3) of equal distance and the last location is at the end of the combustor/start of the nozzle (L4). Figure 4-40 shows the velocity profiles of all the cases. The velocity at the center is less due to the subsonic flow from the gas generator, the maximum velocity occurs in the location downstream of the isolator which is supersonic.Velocity magnitude falls to zero at the walls due to boundary layer formation. A low velocity region in between the gas generator and isolator streams, indicate a base region of recirculation in the vicinity of the flame holder.

At L1, the velociy profile shows a major difference between the flow downstream of the gas generator and the isolator, which receeds in the subsequent locations at points L2,L3 and L4. This shows transfer of momentum between the two streams resulting in reduction of velocity difference between the two streams. At the exit cases 3, 4 and 5 show velocity profile with almost same magnitude at the central and the pherperial regions of the flow. While in cases 1 and 2 a significant difference in velocity profile is seen in the same regions, indicating still the transfer of momentum between the both the streams is not complete, which also results in poor mixing and combustion as seen in the total temperature contours and in combustion efficiency.

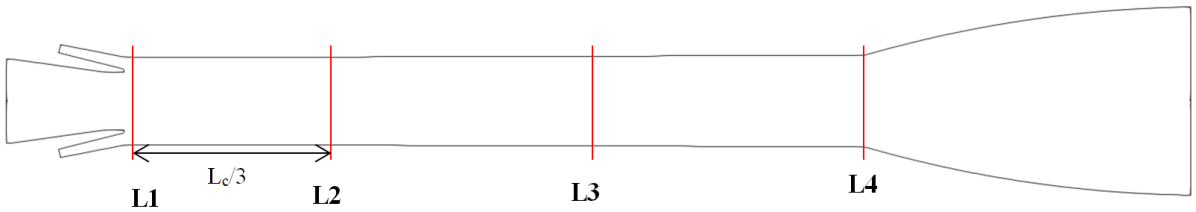

Figure 4-39 Locations of L1 to L4 point in the combustor

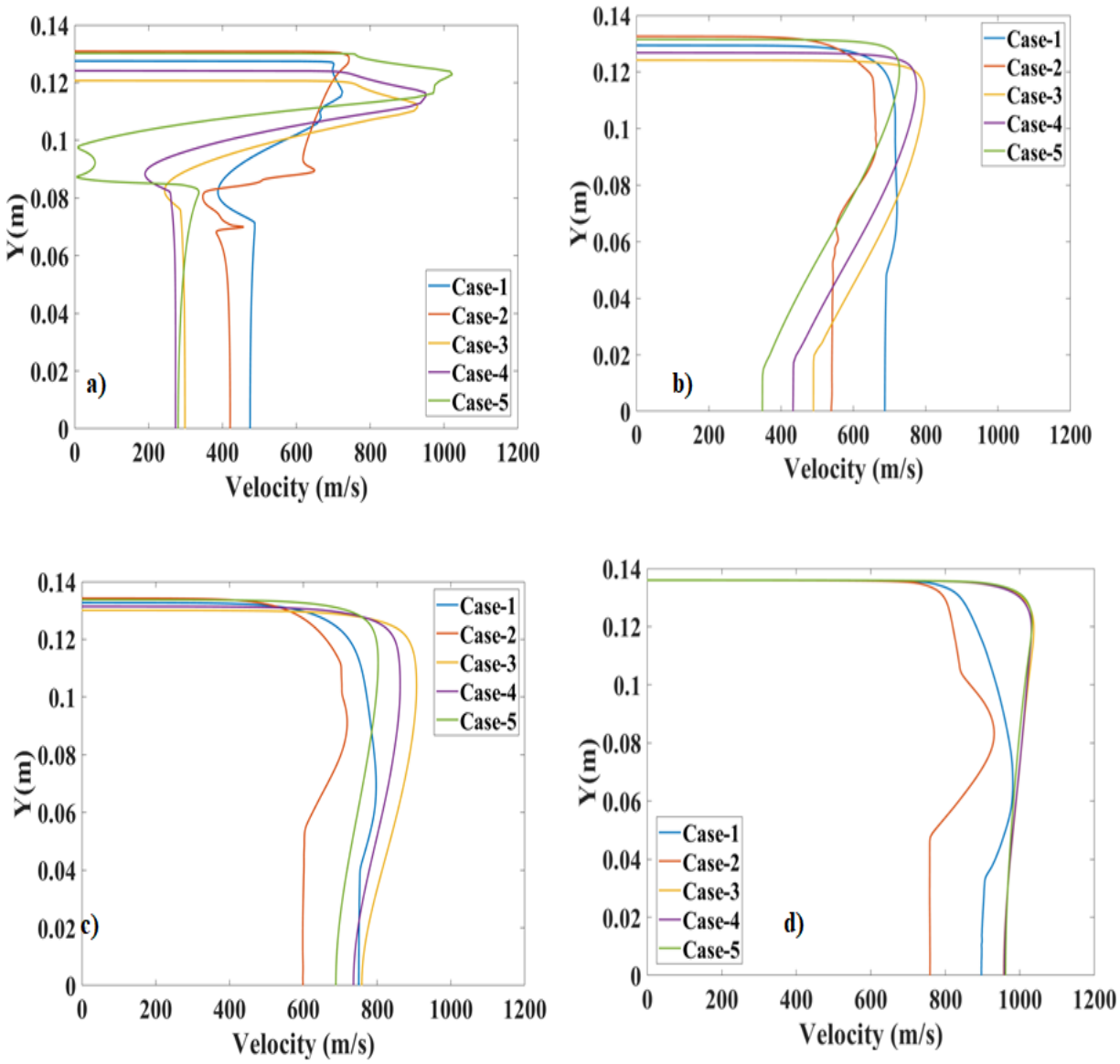

Figure 4-40 Velocity profiles along the radius at locations a) L1, b) L2,c) L3 , d) L4 in the supersonic combustor

Velocity ratio and difference:

Table 4-15 gives the maximum and mass averaged velcoities at the exit of isolator (u_{iso}) and gas generators (u_{gg}) , velocity difference between the isolator and gas generator exit (Δu) and velocity ratio of gas generator exit to isolator exit velocity (u_{gg}/u_{iso}).In all the cases the velocity in the isolator is higher than thay of the gas generator. The highest gas generator velocity is seen in Case -1 and reduces from Case 1 to 5. While the velcoity of isolator flow increases from Case-1 to Case5. The velcity ratio decreases from Case 1 to 5, while Δu increases the same direction. This trend is in accordance with equation 3.67 which shows a direct and inverse proportionalit between the mixing transistion point and the velocity ratio and difference. As observed previously the apex formation point movies upstream from cases 3 to 5, while the velcoity ratio decreases and Δu increases from case 3 to 5.

Table 4-15 Mass weighted average and maximum Velocity (m/s) Mach 6

Case	**Isolator exit(u_{iso})**		**GG exit(u_{gg})**		**Δu ($u_{iso} - u_{gg}$)**		**Velocity ratio (u_{gg}/u_{iso})**	
	Avg.	Max	Avg.	Max	Avg.	Max	Avg.	Max.
1	539.41	673.88	445.26	460.42	94.15	213.46	0.8255	0.6832
2	549.76	573.01	405.09	423.12	144.67	149.89	0.7368	0.7384
3	810.10	993.117	325.51	346.96	484.59	646.157	0.4018	0.3494
4	814.52	984.72	293.67	317.52	520.85	667.20	0.3605	0.3224
5	837.53	1015.13	304.78	335.65	532.75	679.48	0.364	0.3306

c) Combustion efficiency:

The combustion efficiency was the critical parameter that was compared between revisions to assess the degree of combustion. The geometrical parameters were changed with the objective of increasing the combustion efficiency. Mass weighted averaged mass fractions of CO_2 were taken at the exit of the combustor. The ideal values of mass fractions of CO_2 at each case are calculated assuming the overall equivalence ratio of 0.9 using NASA Chemical Equilibrium Analysis (CEA) code. Table.19 shows the combustion efficiency at the Combustor exit for cases 1 to 5. Case-5 shows the highest combustion efficiency of 70.5% followed by case 4 and 3 . Cases 1 and 2 show very low combustion efficiency. The lowest combustion efficiency is observed in Case -2 with an efficiency of 13%.

Table 4-16 Combustion efficiency at the nozzle exit for cases 1 to 5

Case	CO2 mass fraction (actual)	CO2 mass fraction (ideal)	Combustion efficiency (%)
1	0.049	0.1659	29.6
2	0.023	0.1659	13
3	0.109	0.1659	65.7
4	0.1128	0.1659	67.9
5	0.117	0.1659	70.5

d) Static pressure rise along the combustor:

The combustor static wall pressure distributions for Cases 1 to 5 are plotted in Figure 4-41 and Figure 4-42**.** Case-1 and Case-2 have lower static pressure distributions as compared to others. The lower pressure can be attributed to incomplete combustion in the supersonic combustor. The maximum wall pressure in both cases is below 1.4 atm. Case-2 has lowest pressure of all the cases followed by Case -1. In both the cases the pressure rise in the combustor is lower than that of the isolator.

In the next three Cases where the apex formation is inside the combustor, have a higher pressure rise than the first two. Case-3 has a higher peak pressure value immediately downstream of the flame holder but the pressure reduces along the combustor below Cases 4 and 5. The next highest peak pressure is observed in Case 4. While Case - 5 has the highest pressure distribution along the combustor.

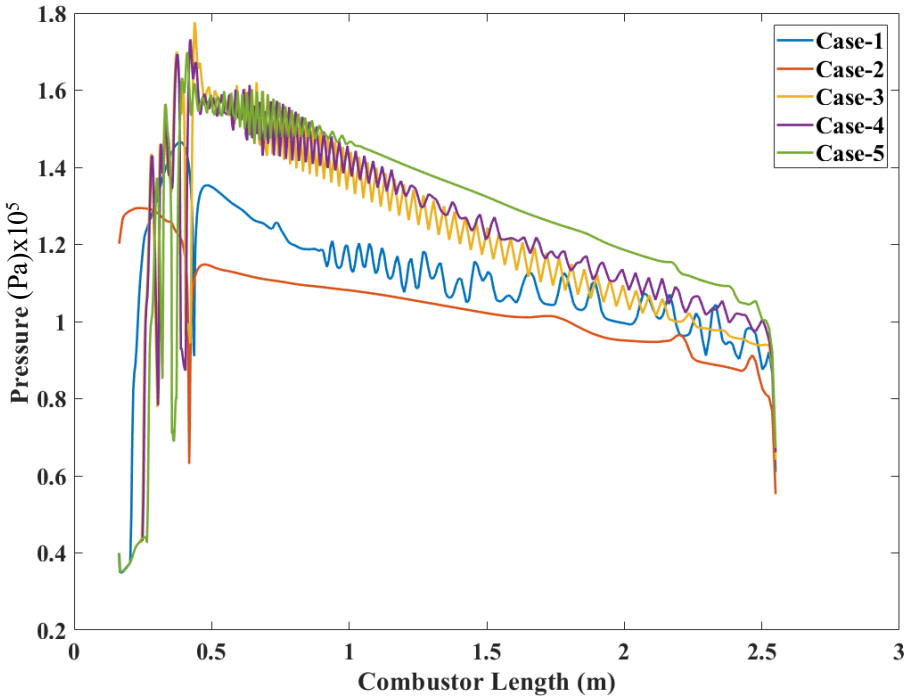

Figure 4-41 Combustor wall static pressures for cases 1 to 5, Mach 6

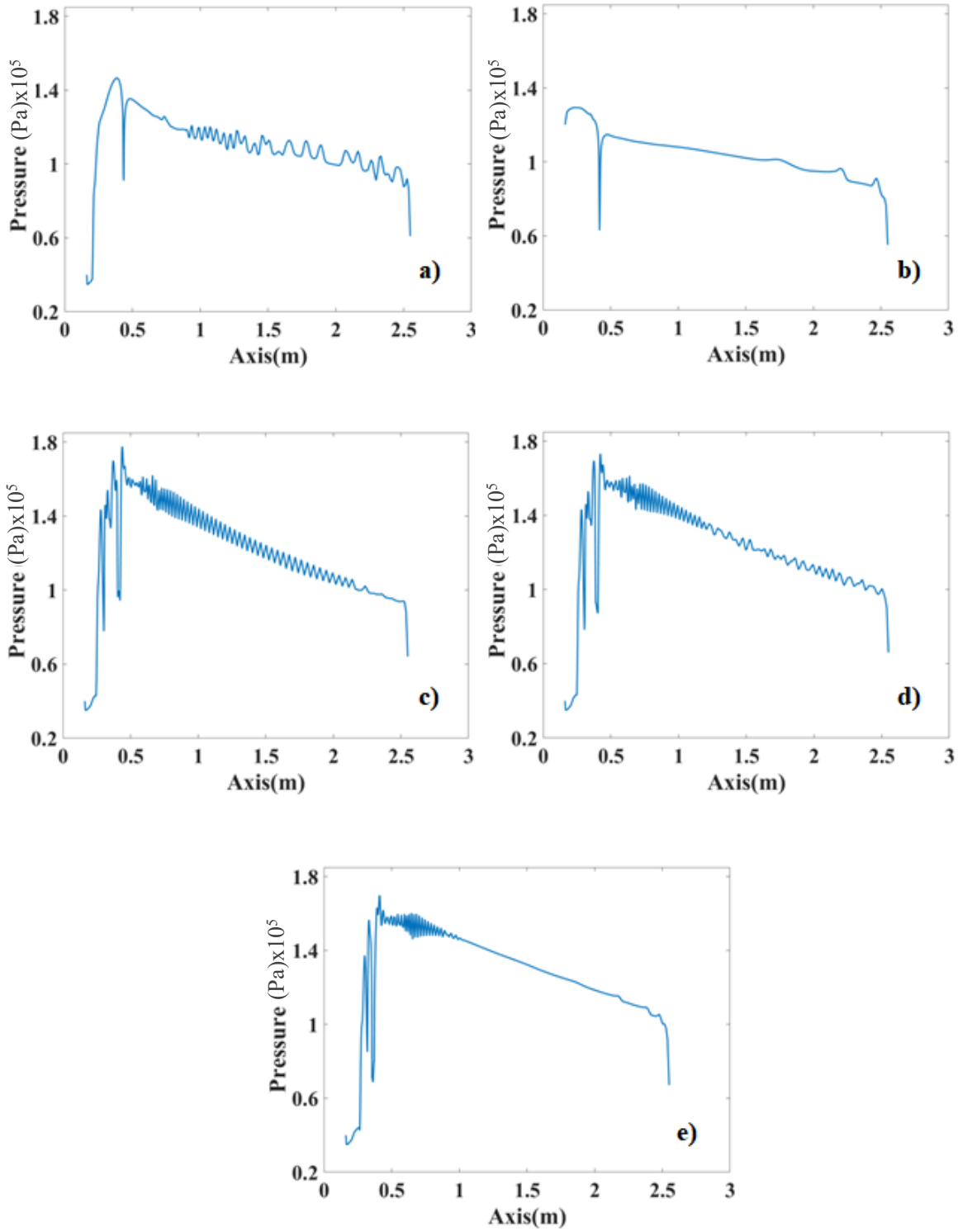

Figure 4-42 (clockwise from top left) Combustor wall static distributions along the length of the combustor a) Case-1 b) Case-2 c) Case-3 d) Case-4 e) Case-5

Wall pressure fluctuations are observed along the length of the combustor. Figure 4-43 shows the flow structure in the combustor for Case-3. Showing the pressure fluctuations in the isolator and combustor due to shock waves. These fluctuations are more crowded in the beginning portion of the combustor in Case-5. While the fluctuations are seen along the length of the combustor for Cases 3 and Case 4. The fluctuations at the beginning can be attributed to the pre-combustion shock train that is formed in the isolator, extending partially into the combustor.

Figure 4-44 shows the Mach contours for Cases 1 to 5. The gas generator flow is subsonic in all the cases. For Case 2 the flow entering the isolator is subsonic and consequently the flow throughout the combustor the flow is subsonic initially, but the flow is accelerated to near sonic speeds in the periphery region at a downstream location of the combustor. For Case -1 the flow entering the isolator is supersonic but is decelerated to subsonic speeds in the isolator itself. For Cases 3 to 5 the flow entering the combustor is supersonic but the flow Mach number reduces along the combustor due to heat addition, but at a downstream location the acceleration of the flow increases the Mach number. The core flow remains subsonic until the end of the combustor in all the cases. For Case -3 the flow remains supersonic throughout the peripheral region of the combustor, this is also reflected in the pressure fluctuations observed in the wall static graphs.

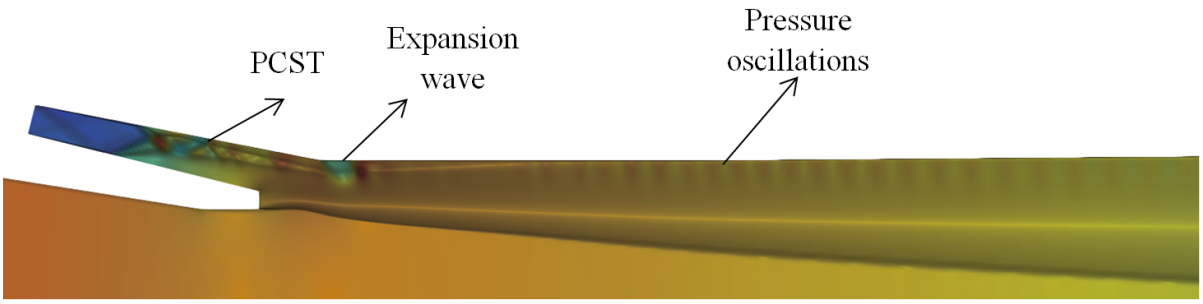

Figure 4-43 Numerical Schlieren image superimposed on static pressure contour showing pressure oscillations inside the combustor for Case -3

The supersonic region reduces from case 3 to 5. There is a considerable region of subsonic flow near the wall in Case -5 which is region of no fluctuations in the wall static pressure graph.

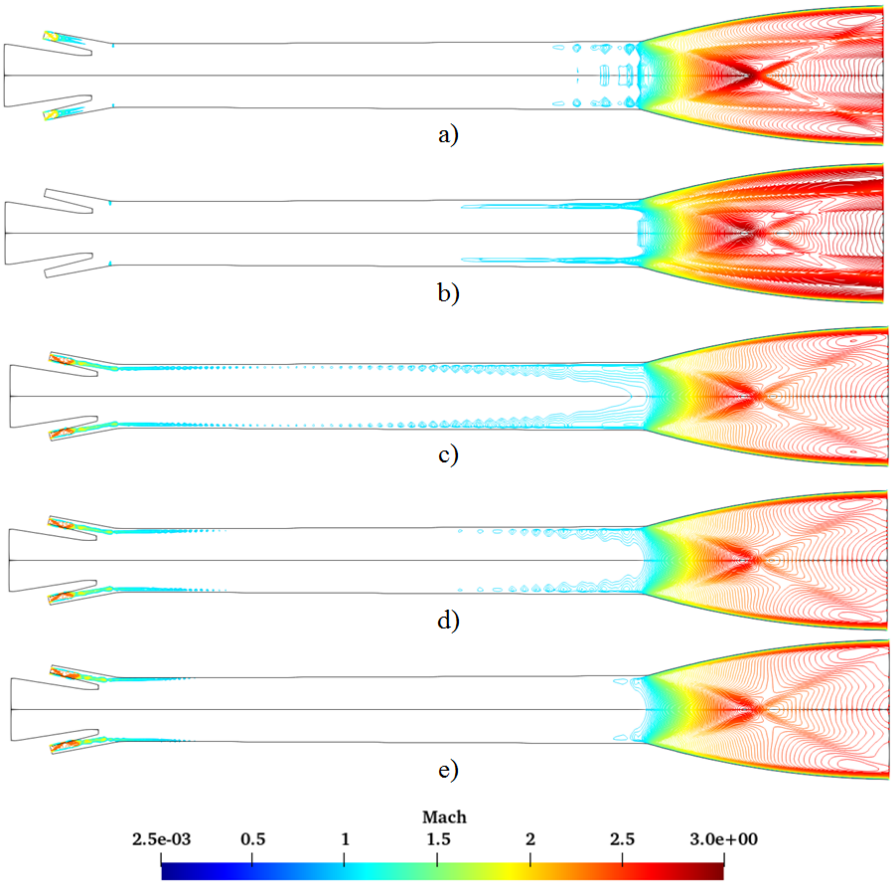

Figure 4-44 Mach contours (M>1) in the combustor; from *top to bottom*: a) Case-1, b) Case-2, c) Case-3, d) Case-4 and e) Case-5

e) Pre-combustion shock train:

Precombustion shock train (PCST) occurs upstream of the supersonic combustor in the isolator, partially extending into the combustor. Due to combustion the pressure and temperature rises in the combustor. The PCST is formed to compensate for this rise in pressure, it also isolates the inlet from high back pressure from the combustor.The static pressure in the combustor is higher than that of the pressure from the inlet, hence the supersonic flow has to go through compression to adjust to the combustor pressure. For this compression to occur oblique shock waves are formed. Oblique shocks orginate from the upper and the lower surface of the isolator.The shocks result in a higher pressure gradient which causes the boundary layer to separate immediately after the shock. The two oblique shocks interact at the core of the shock train and propagates downstream to meet the separated boundary layer where the shocks are reflected back as expansion fans. The pressure immediately downstream of the shock increases, the shock interaction produces a region of highest pressure in the central region, followed by a

lower pressure region due to expansion fans, after this the shape of the boundary layer causes the flow to accelerated further creating another series of oblique shock which goes through another series of interaction and reflection forming a shock train. The formation of shock train can be seen in the numerical schlieren image (Figure 4-45).

The shocktrain location depends upon the pressure in the combustor.As the back pressure from the combustor increases it pushes the shock train forward in the isolator, when a certain higher back pressure value (critical pressure) is reached in the combustor, backflow to the inlet occurs resulting in inlet unstart.It is important to have a sufficient isolator length such that the PCST have sufficient degree of movement. If the PCST is located at an upstream location in the isolator in the design Mach number, any deviation from design operating conditions may lead to inlet unstart, this gives a lesser margin of error for engine operation.

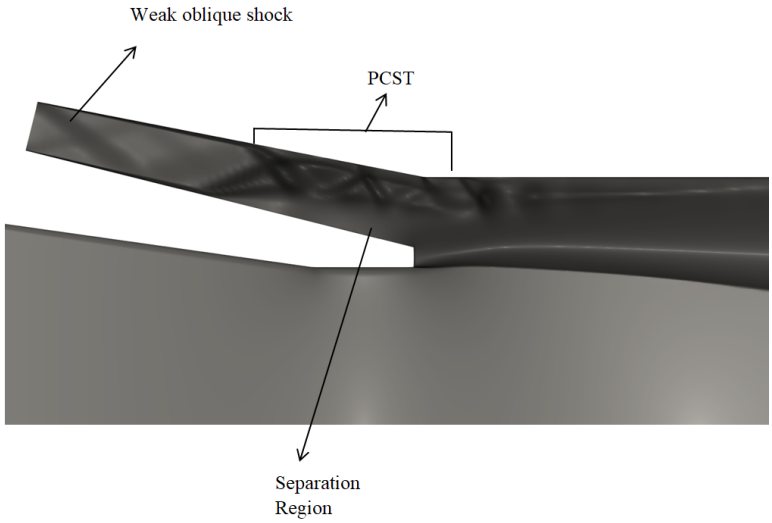

Figure 4-45 Numerical Schlieren showing the Pre-combustion shock train (Case-5)

Table 4-17 gives the starting position of the shock train from the inlet , shock train length, shock train length in the isolator (So), shock train length inside the combustor (Sd). Figure 4-46 shows the PCST in the Mach contours in isolator region. In case -1 PCST is located at upstream location of the isolator at 0.042m from the inlet. In case -2 no PCST is formed.In all other cases it is located at an downstream location in the combustor.From case 3 to 5 the starting location progressively moves downstream . The length of the shock train reduces from cases 3 to 5, with case-5 having the second lowest shock train length at 0.167m and Case -1 with the lowest shock train length. In case -1 the whole of shock train is located within the isolator, whereas in all other cases the majority of the shock train is in the combustor.

Table 4-17 Shock train starting location and length

Parameter (m)	Case-1	Case-2	Case-3	Case-4	Case-5
Starting location	0.042	-	0.07	0.074	0.089
Length (St)	0.073	-	0.21	0.19	0.167
Length in combustor (Sd)	0	-	0.085	0.069	0.061
Length in isolator (So)	0.073	-	0.125	0.121	0.106

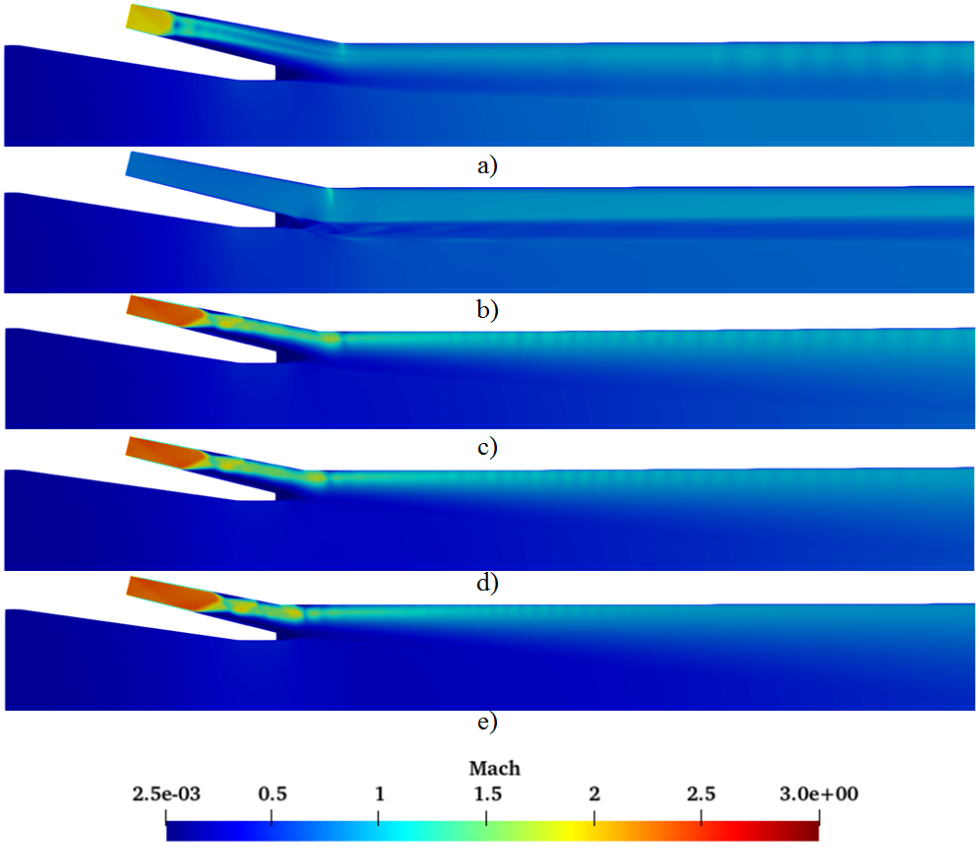

Figure 4-46 Mach contours in the isolator regions showing PCST at Mach 6; from *top to bottom*: a) Case-1, b) Case-2,c) Case-3, d) Case-4 and e) Case-5

4.2.3 Effect of Equivalence ratio on DCR (Case -5 geometry):

Case–5 geometry has offered the highest combustion efficiency of the five geometries studied. Further an equivalence ratio study was undertaken for the same case and boundary conditions but with different fuel flow rate to vary the equivalence ratio. Table 4-18 gives the fuel mass fraction and flow rate for various equivalence ratios and accordingly the gas generator mass flow was also varied.

Table 4-18 Fuel mass fractions

Overall ER ($\phi_{overall}$)	Gas generator ER (ϕ_{gg})	CO (mole fraction)	H2 (mole fraction)	Mass flow rate fuel $\dot{m}_f$ (kg/s)
0.6	2.55	0.283	0.0181	0.27
0.8	3.18	0.327	0.0242	0.34
1.0	3.92	0.3030	0.0280	0.42
1.2	4.76	0.269	0.0314	0.51

a) Combustion efficiency:

Combustion efficiency is the ratio of actual CO2 mass fraction to the ideal CO2 mass fraction. The actual CO2 mass fractions are the mass averaged CO2 mass fraction in the outlet plane of the engine. The ideal values are calculated from NASA chemical equilibrium code CEA. Table 4-19 gives the actual and ideal CO2 mass fractions at the outlet with the corresponding combustion efficiency. Figure 4-47 shows the trend of combustion efficiency with respect to the equivalence ratio. As the equivalence ratio reduces the combustion efficiency improves, the case with low equivalence ratio ϕ – 0.6 has η_c= 85.89% , which is the highest. The efficiency decreases with the increase in the equivalence ratio until 1.0 with η_c= 69.8% and then again increases to η_c= 72.6% when ϕ – 1.2.

Table 4-19 Combustion efficiency

Overall ER ($\phi_{overall}$)	CO2 mass fraction (actual)	CO2 mass fraction (ideal)	Combustion efficiency (%)
0.6	0.1066	0.12410	85.89
0.8	0.119	0.15721	75.7
1.0	0.116	0.16614	69.8
1.2	0.101	0.13986	72.6

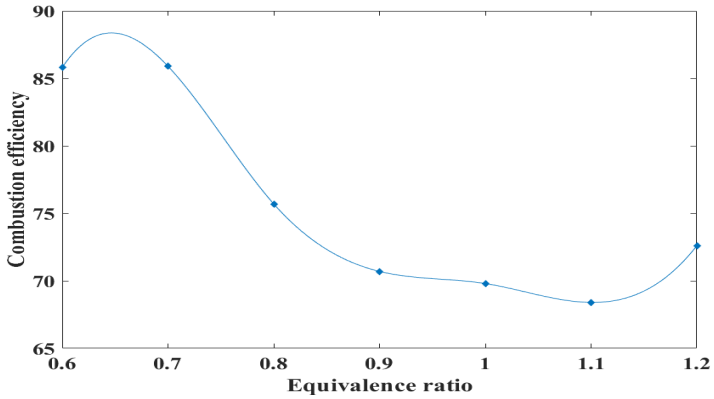

Figure 4-47 Equivalence ratio Vs. Combustion efficiency

b) **Wall static pressure:**

Figure 4-48 shows the wall static pressure distribution for combustor wall. The pressure distribution increases with the increase in equivalence ratio. The pressure at the beginning of the combustor, immediately downstream of the flame holder is high, while the pressure reduces towards the end of the combustor. The case with the lowest equivalence ratio of 0.6 has the lowest pressure distribution. The highest pressure distribution is observed in the case with highest equivalence ratio of 1.2, the peak pressure is about 1.74 atm. The cases with equivalence ratios of 0.8 and 1.0 show almost identical pressure distribution but with ϕ – 1.0 having a minimally higher pressure distribution than ϕ – 0.8.

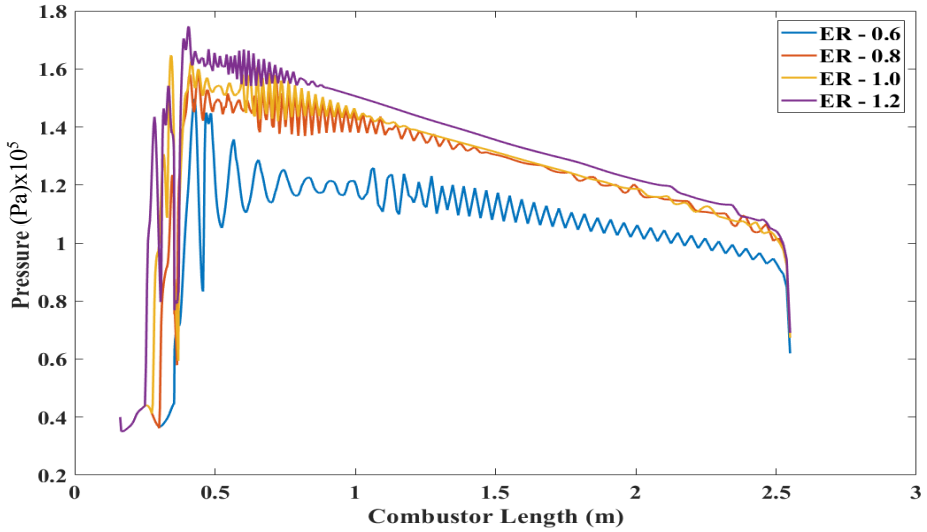

Figure 4-48 Static wall pressure distributions for cases with equivalence ratios 0.6 to 1.2 and comparison with experimental data

c) **Flow field:**

Figure 4-49 shows the Mach contours inside the combustor. The flow in the gas generator is subsonic, while that of the isolator is supersonic. The flow velocity along the circumference of the combustor is higher than the core flow. A trend between the equivalence ratio and the region of supersonic flow in the combustor can be observed. As the equivalence ratio increases, the heat addition and the subsequent pressure rise increases which decreases the Mach number. Hence as the equivalence ratio increases the region of supersonic flow decreases from (a) to (b) in Figure 4-49.

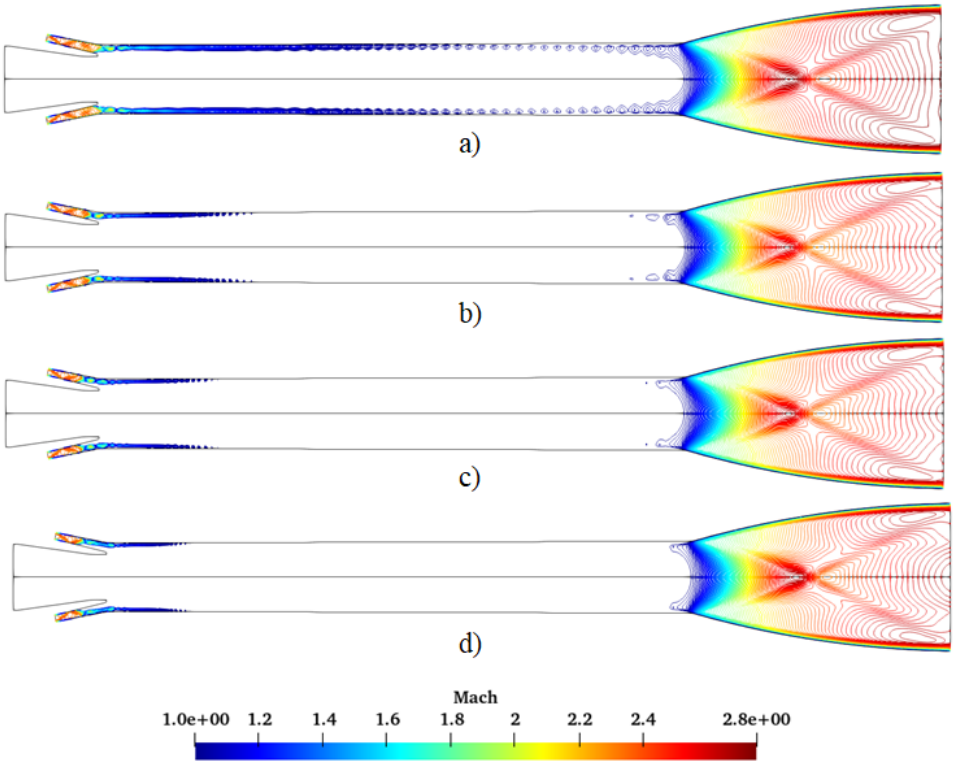

Figure 4-49 Mach (M>1) contours for equivalence ratios a) 0.6 b) 0.8 c) 1.0 and d) 1.2

Figure 4-50 shows the static pressure contours of different cases in the combustor. The pressure increases in the combustor immediately downstream of the isolator due to combustion is visible. The pressure in the combustor also increases with increase in equivalence ratio from $\phi = 0.6$ to $\phi = 1.2$ as seen in the static wall pressure distribution (Figure 4-48). The pressure at the beginning of the combustor is high while along the combustor the pressure reduces due to flow acceleration, the case with highest equivalence ratio has the highest pressure. As the equivalence ratio increases the fuel flow rate increases, which leads to higher heat addition to the flow. This leads to both higher pressure rise in the combustor and lower Mach number. The shock train in the isolator caused due to pressure increase is also seen moving forward with increase in pressure due to increase of equivalence ratio.

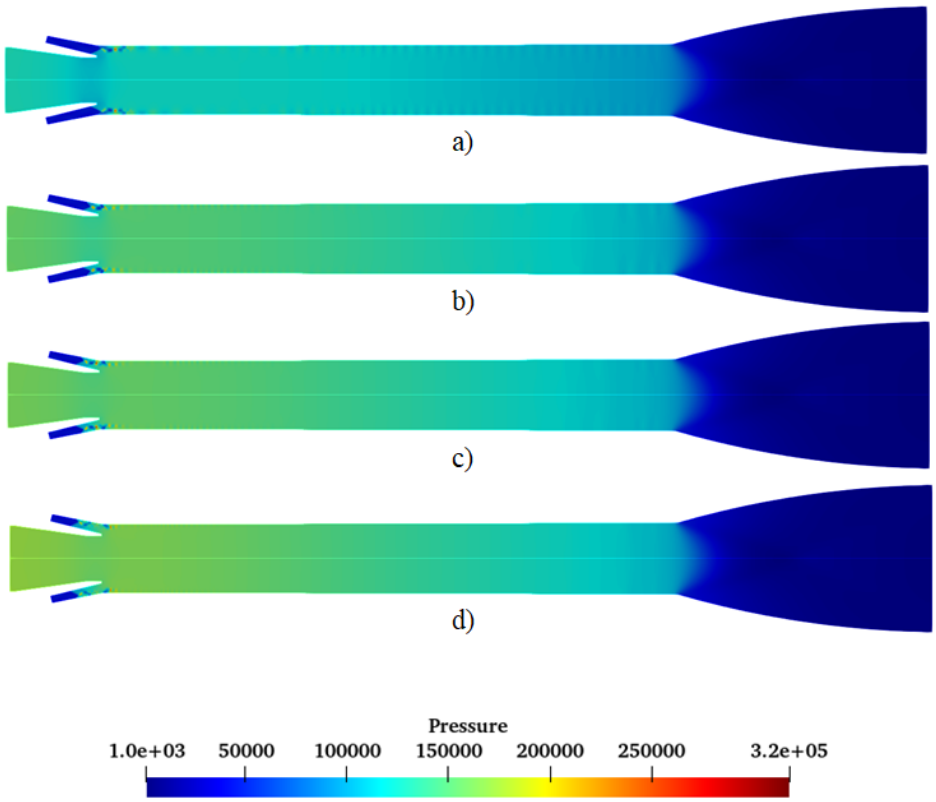

Figure 4-50 Static Pressure contours for equivalence ratios a) 0.6 b) 0.8 c) 1.0 and d) 1.2

Figure 4-51 shows the total temperature contours for different equivalence ratios, the total temperature is the indication of combustion. The regions of higher total temperatures indicate higher degree of combustion. It is also an indication of mixing of gas generator and the isolator flow streams. As higher degree of mixing leads to more efficient combustion to occur inside the combustor. The apex formation due to higher degree of flow missing is observed in all the four equivalence ratios. As the equivalence ratio increases the apex formation point moves further downstream of the combustor indicating better mixing takes place with the decrease in equivalence ratio.

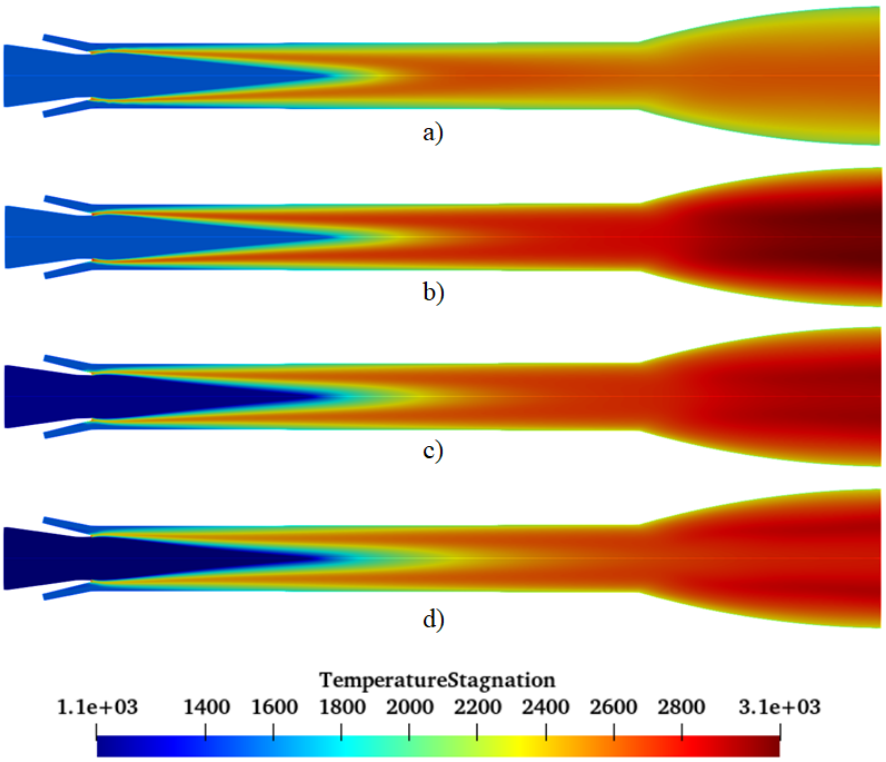

Figure 4-51 Total temperature contours showing apex formation for equivalence ratios a) 0.6 b) 0.8 c) 1.0 and d) 1.2

d) Pre-Combustion shock train:

Pre-combustion shock train is formed in the isolator and extends partially into the combustor. The combustion reactions in the combustor increases the pressure significantly, this gives rise to shock train which increases the static pressure of oncoming flow to the pressure in the combustor, these shock trains are known as pre-combustion shock train. The length and the position of the shock train inside the isolators are important. As the combustor pressure increases, the shock train starting point moves further upstream of the isolators, beyond a critical pressure this leads to unstart of the inlet. Hence the further downstream the starting position of the shock trains in the isolator, the higher the margin of safety.

Figure 4-52 show the PCST in the isolator, extending into the combustor. Table 4-20 gives the starting position and the length of the shock train. As the equivalence ratio increases, the back pressure from the combustor increases leading to formation of shock train further upstream location. The lowest starting position is observed in case with the highest equivalence ratio of 1.2 and the highest starting point is observed in case with lowest equivalence ratio. The length of the shock train also increases with increase in the equivalence ratio.

Table 4-20 Length and starting position of PCST

Parameter (m)	ϕ = 0.6	ϕ = 0.8	ϕ = 1.0	ϕ = 1.2
St	0.140	0.148	0.155	0.176
So	0.024	0.059	0.091	0.121
Sd	0.116	0.089	0.064	0.055
Starting location	0.171	0.136	0.104	0.074

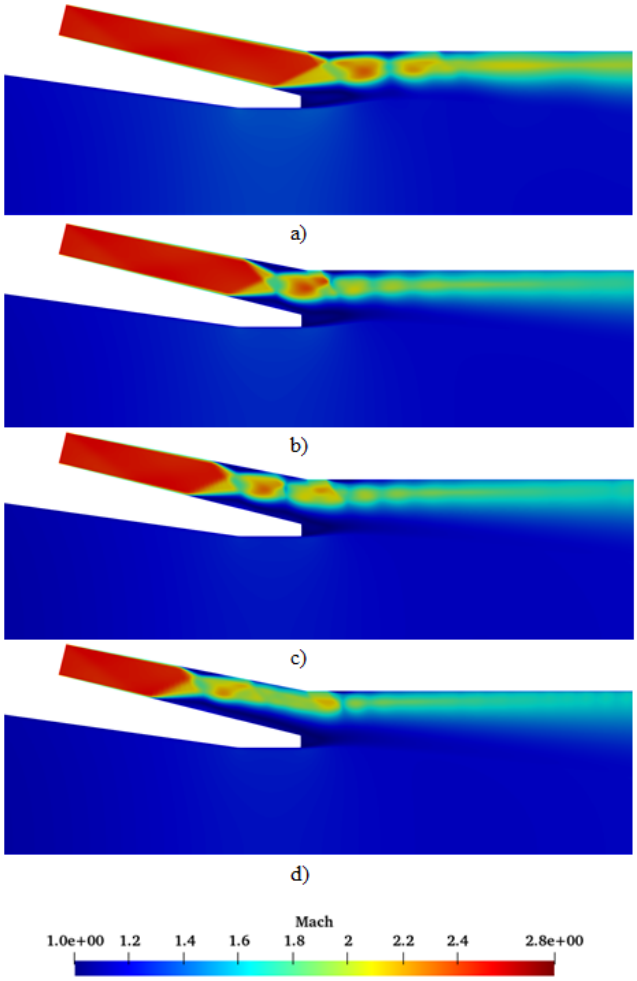

Figure 4-52 Mach contours near the isolator region showing PCST for equivalence ratios a) 0.6 b) 0.8 c) 1.0 and d) 1.2

4.2.3.1 Mach -4 condition

a) Combustion efficiency:

Table 4-21 gives the actual and ideal CO2 mass fractions at the outlet with the corresponding combustion efficiency. Figure 4-53 shows the trend of combustion efficiency with respect to the equivalence ratio.

Table 4-21 Combustion efficiency

Equivalence ratio(ϕ)	$CO_{2(actual)}$	$CO_{2(ideal)}$	Combustion efficiency(η_c)
0.6	0.0401	0.1243	32.2
0.8	0.0411	0.1601	25.6
1.0	0.0352	0.1734	20.2
1.2	0.029	0.1428	20.3

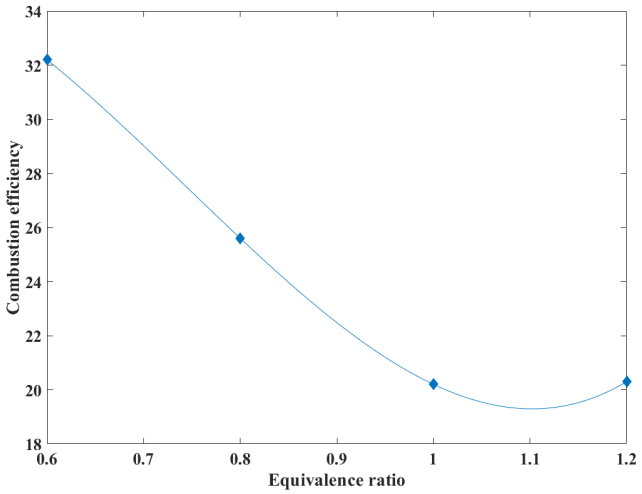

Figure 4-53 Equivalence ratio Vs. Combustion efficiency

b) <u>Wall static pressure:</u>

The wall static pressure distribution is given by Figure 4-54. As the equivalence ratio increases the pressure increases due to increased heat addition as more fuel is added. The case with the lowest equivalence ratio of ∅ =0.6 has the lowest peak and the lowest overall pressure. Cases with equivalence ratios 0.8 to 1.2 have almost same peak pressure. The pressure is high initially immediately after the gas generator exit but reduces along the combustor. Pressure fluctuations are noticed along the length of the combustor for ∅ = 0.6 while as the equivalence ratio increases the fluctuations reduce.

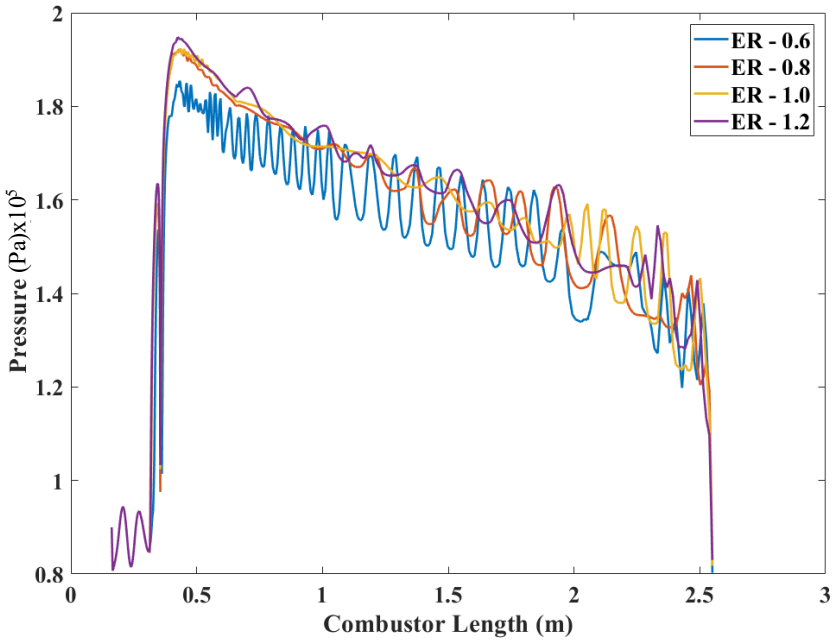

Figure 4-54 Static wall pressure distributions for cases with equivalence ratios 0.6 to 1.2 and comparison with experimental data

c) **Flow field:**

The flow in the combustor is purely subsonic, the air stream from the isolator passes through a normal shock train which makes the flow subsonic before entering into the main combustor. Followed by which subsonic mixing of isolator and gas generator flows take place leading to combustion. The flow is subsonic as it flows through the main combustor. Due to heat addition in the combustor the flow is accelerated through the combustion chamber. This leads to sonic Mach numbers at the exit of the combustor. Also with increase in the equivalence ratio the increase in heat addition leads to lower Mach number in the combustor, which is visible in the Mach contours, from (a) to (b) as the equivalence ratio increases the region of higher Mach number decreases in the combustor.

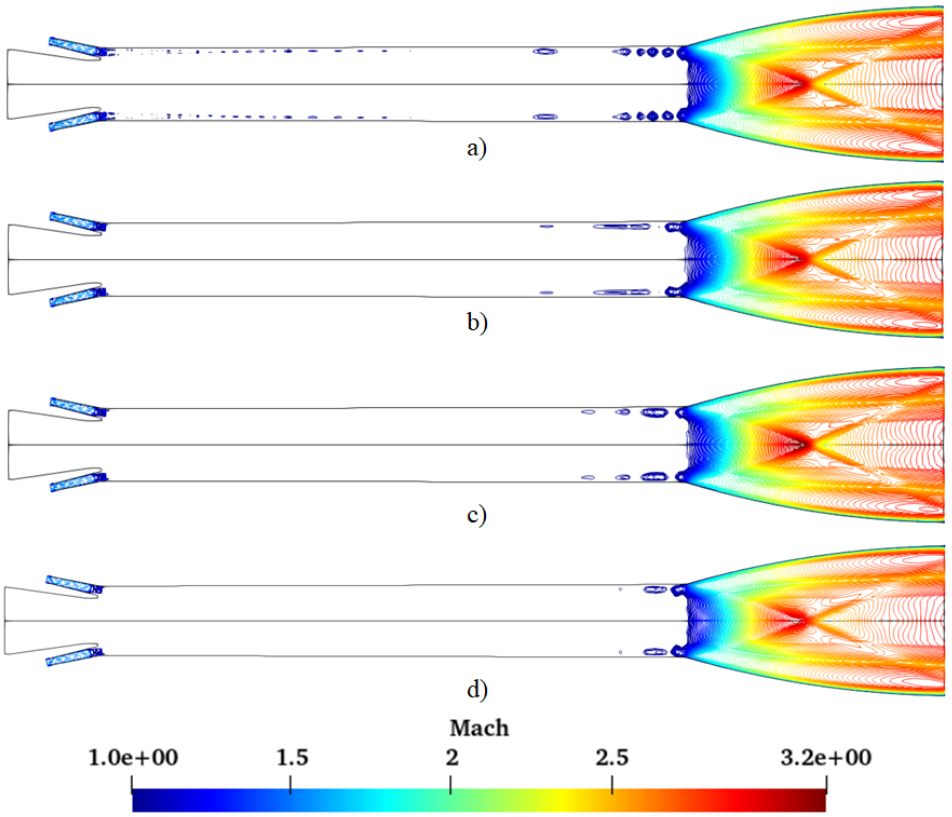

Figure 4-55 Mach (M>1) contours for equivalence ratios a) 0.6 b) 0.8 c) 1.0 and d) 1.2

Figure 4-56 shows the static pressure distribution in the combustor, the pressure rise due to the normal shock in the isolator is also visible. The shock wave is located in a downstream location when ER = 0.6. The pressure is high in the combustor and reduces along the combustor. The aft part of the combustor pressure fluctuations is visible, just before the flow becomes sonic. As the equivalence ratio increases the heat addition in the combustor increases leading to a higher static pressure inside the combustor. This can be noticed in the contours, from (a) to (b) as the equivalence ratio increases, the pressure increase is also higher.

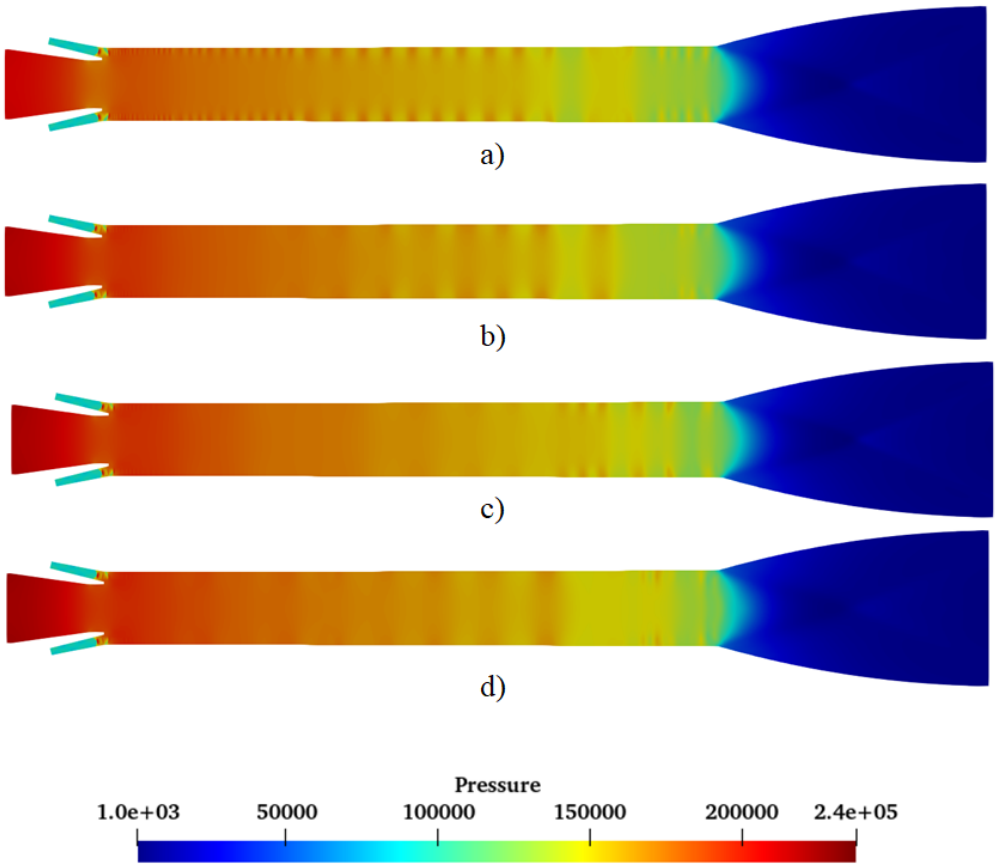

Figure 4-56 Static Pressure contours for equivalence ratios a) 0.6 b) 0.8 c) 1.0 and d) 1.2

Figure 4-57 shows the total temperature contours which are indicators of combustion taking place. No apex formation has taken place in the 4 equivalence ratios under study. The growth of the mixing layer along the length of the combustor is apparent from the increasing region of high temperature along the combustor, which is visible in the contours, however merging of mixing layer inside the combustor does not take place , hence no apex is formed. Which indicates poor mixing of fuel rich gas generator and oxidizer rich isolator flow streams.

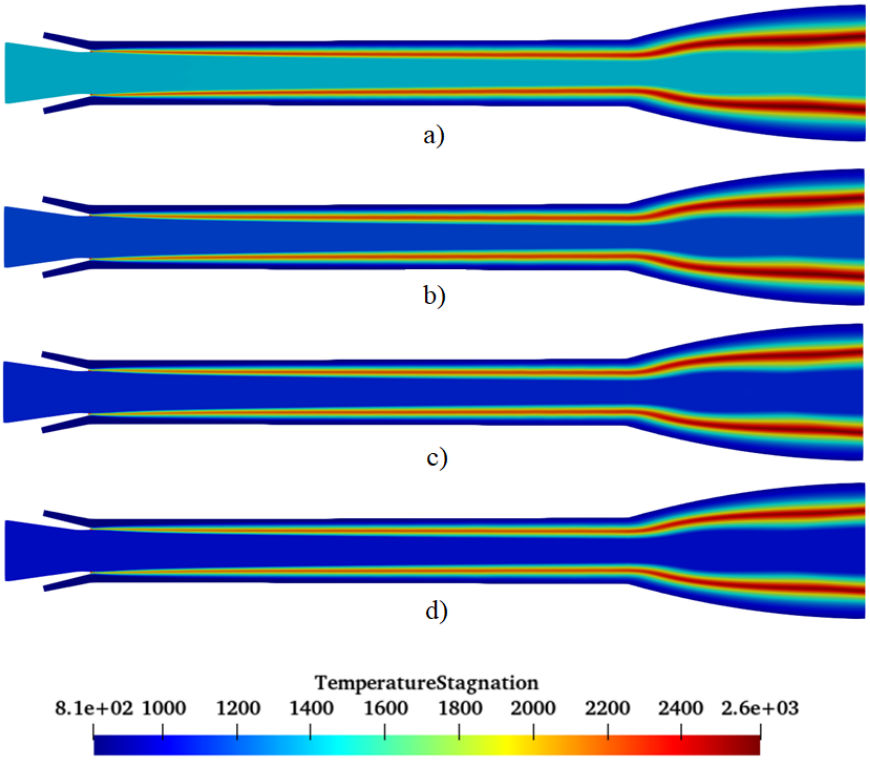

Figure 4-57 Total temperature contours showing apex formation for equivalence ratios a) 0.6 b) 0.8 c) 1.0 and d) 1.2

d) Pre-Combustion shock:

The pre-combustion shock train that is usually observed in high-speed air breathing engines are of oblique shock train. In this case due to low Mach number at the isolator entry, a normal shock is formed towards the end of the isolator. Subsequently a normal shock train is formed near the end of the isolator. The starting position of the shock depends upon the back pressure from the combustion chamber. Table 4-22 shows the starting position of the shock in cases of different equivalence ratios.

Table 4-22 Starting position of PCST

Parameter (m)	**ϕ = 0.6**	**ϕ = 0.8**	**ϕ = 1.0**	**ϕ = 1.2**
St	0.057	0.057	0.057	0.057
So	0.033	0.041	0.041	0.043
Sd	0.024	0.016	0.016	0.014
Starting location	0.162	0.154	0.154	0.152

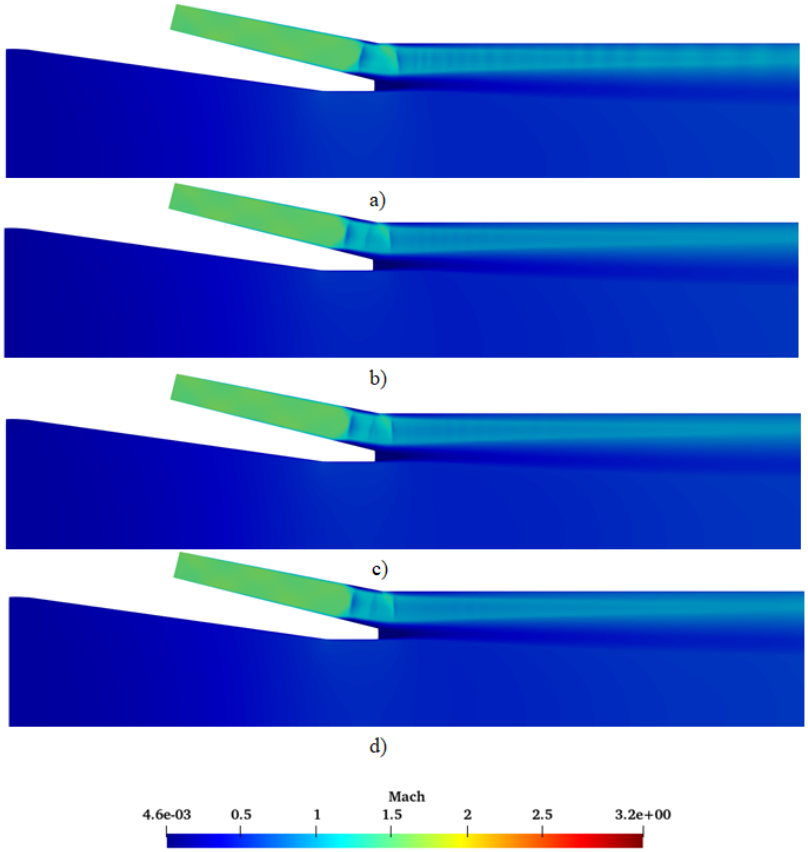

Figure 4-58 Mach contours near the isolator region showing PCST for equivalence ratios a) 0.6 b) 0.8 c) 1.0 and d) 1.2

e) Combustor divergence angle:

As noticed in the Mach contours in the equivalence ratio study of the Case -5 geometry. The flow in the combustor was mainly subsonic in the core region of the combustor. This low Mach number in the combustor is caused due to the heat addition, which lowers the Mach number of the flow. To increase the Mach number in the combustor further and to achieve supersonic combustion, the divergence angle of the combustor was increased from 0.17° to 0.5°. The increased expansion caused by the higher divergence angle leads to higher flow acceleration along the combustor increasing the flow Mach number. All other geometric parameters remain same except for the combustor divergence angle which is increased to 0.5°. The combustor consists of a constant area duct upto 300mm after the mixing throat, downstream of which the diverging section of the combustor is located.

Combustion efficiency:

Table 4-23 gives the combustion efficiency. The combustion efficiency is the lowest for $\phi = 0.6$ it increases to 75% with $\phi = 0.8$ and then reduces with further increase in the equivalence ratio. When compared with the combustion efficiency with the original geometry of Case-5 the combustion efficiency is lower. This can be attributed to the increased combustor divergence angle. As the combustor divergence angle is increased the flow undergoes expansion and is thus accelerated. This leads to low residence time for the flow inside the combustor to mix, leading to lower combustor efficiency than the original case. In addition to that the expansion also diverts the flow towards the periphery of the combustor leading to reduced mixing. Thus a lower combustion efficiency.

Table 4-23 Combustion efficiency

Overall ER ($\phi_{overall}$)	**CO2 mass fraction (actual)**	**CO2 mass fraction (ideal)**	**Combustion efficiency (%)**
0.6	0.0479	0.1241	38.5
0.8	0.119	0.1572	75
1.2	0.100	0.1398	71

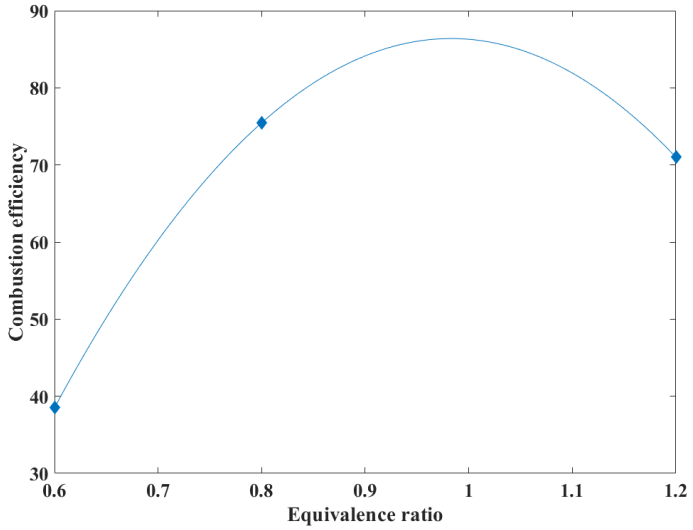

Figure 4-59 Equivalence ratio Vs. Combustion efficiency

Wall Static pressure:

Figure 4-61 gives the static pressure contours and Figure 4-60 shows the static pressure distribution along the combustor. It can be seen that the pressure in the 0.6 is lowest and the wall pressure increases with increase in the equivalence ratio. The lower pressure in the ϕ =0.6 is caused due to the poor combustion and lower heat release compared to other two equivalence ratios. Hence the flow is mainly supersonic in this case and the pressure stays low along the combustor. Formation of shock trains in the combustor is also visible in the ϕ = 0.6 case. The flow structure is similar to the non- reacting flow discussed earlier. The wall pressure is also lowest in case with the lowest equivalence ratio and increases with equivalence ratio. The highest-pressure distribution is seen in the case with ϕ = 1.2.

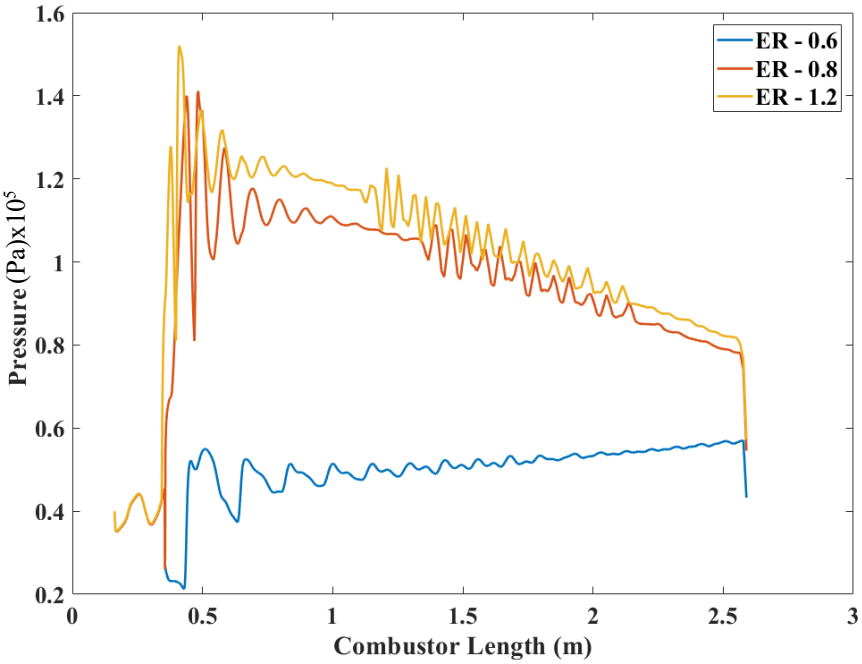

Figure 4-60 Wall static pressure distribution along the length of the combustor.

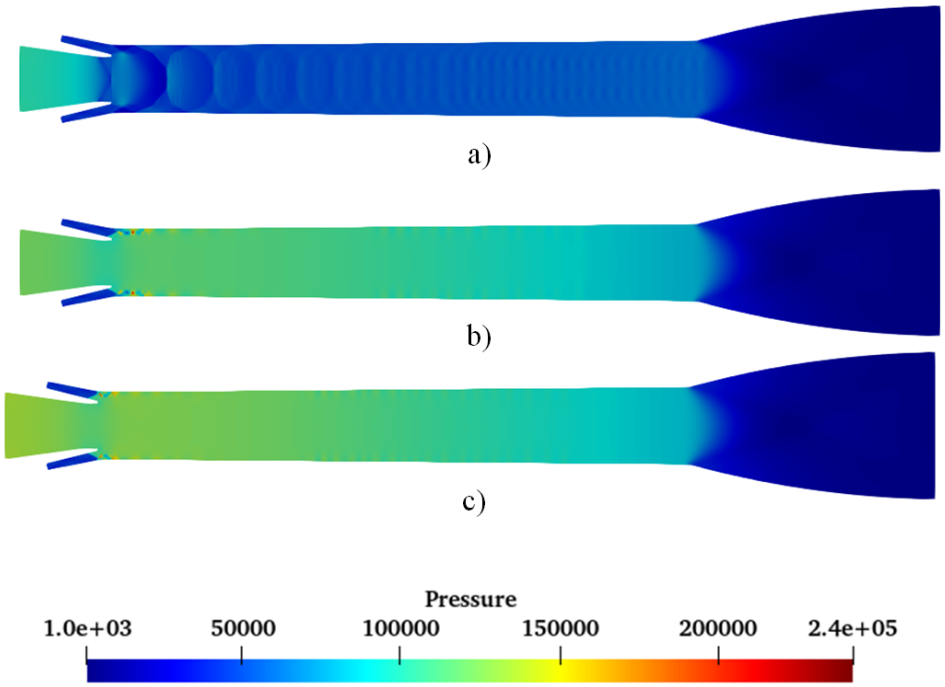

Figure 4-61 Static pressure contour for equivalence ratios a) 0.6 b) 0.8 and c) 1.2

Mach contours:

Figure 4-62 shows the Mach contours. The flow field in the combustor is largely supersonic when the equivalence ratio is 0.6 as the equivalence increases the increased heat addition leads to lower supersonic region largely restricted to periphery region of the combustor along the wall. When the equivalence ratio is 0.6 the supersonic flow in the combustor results in a shock train which gradually weakens along the combustor. The flow in the other two cases where significantly increased combustion was achieved have a lesser extent of supersonic flow region. However, the supersonic region is much higher than in Case-5 with a lower divergence angle.

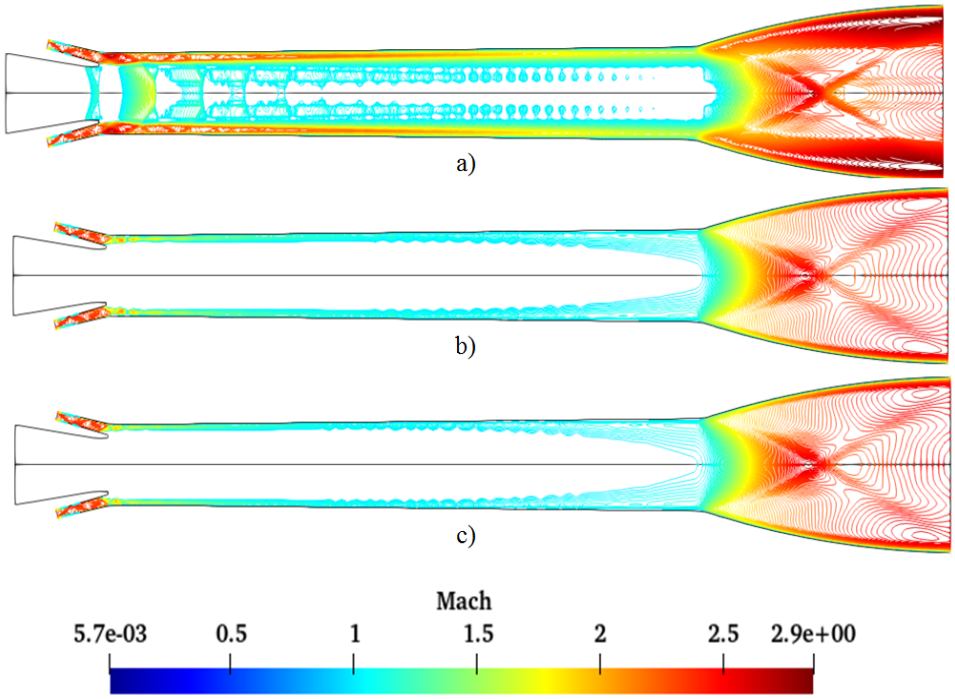

Figure 4-62 Mach contour for equivalence ratios a) 0.6 b) 0.8 and c) 1.2

Total temperature:

Figure 4-63 shows the Total temperature contours. The apex formation has not taken place in the case where the equivalence ratio was 0.6 and the combustion efficiency of this case was also observed to be lower. The reduced combustion efficiency and the mixing can be attributed to the supersonic flow in the combustor which led to shorter combustion residence time for the fuel. Hence not providing enough time for proper mixing to take place inside the combustor. In the other two equivalence ratios apex formation is visible indicating good mixing had taken place in the combustor leading to higher combustion efficiency.

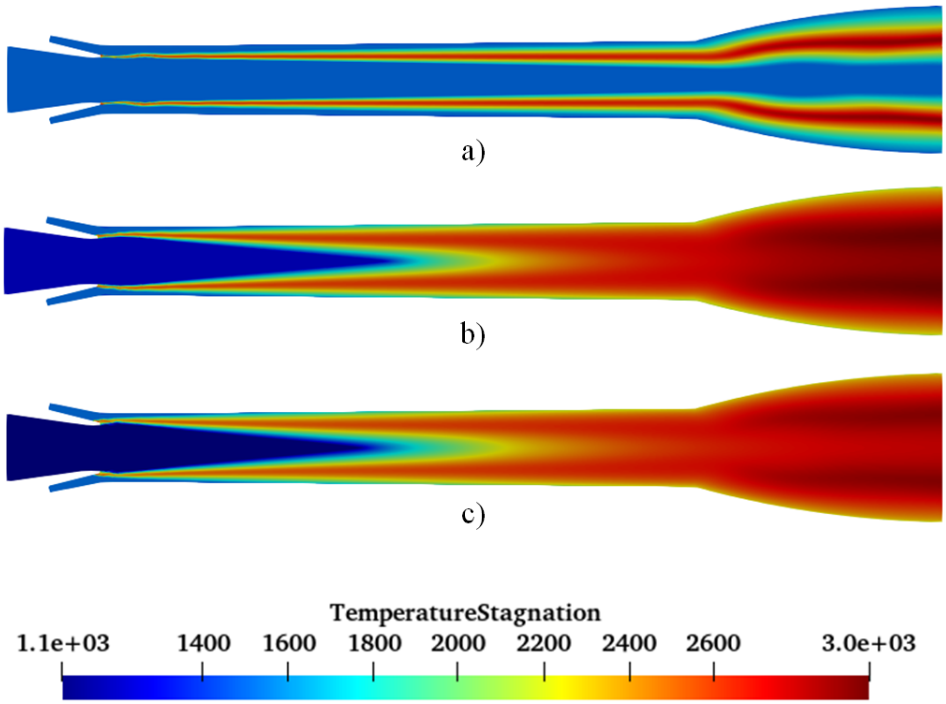

Figure 4-63 Total temperature contour for equivalence ratios a) 0.6 b) 0.8 and c) 1.2

Pre-combustion shock Train(PCST):

The pre-combustion shock train formation is visible in all the cases. In case of $\phi = 0.6$, the whole of the PCST is in the combustor. The length of the shock train reduces with the increase in the equivalence ratio. As the equivalence ratio increases the staring position of the shock train moves upstream of the isolator due to increase in back pressure from the combustor.

Table 4-24 PCST parameters

Parameter (m)	**$\phi = 0.6$**	**$\phi = 0.8$**	**$\phi = 1.2$**
St	0.340	0.145	0.105
Length in isolator	0	0.017	0.038
Length in Combustor	0.34	0.128	0.067
Starting location	0.195	0.178	0.157

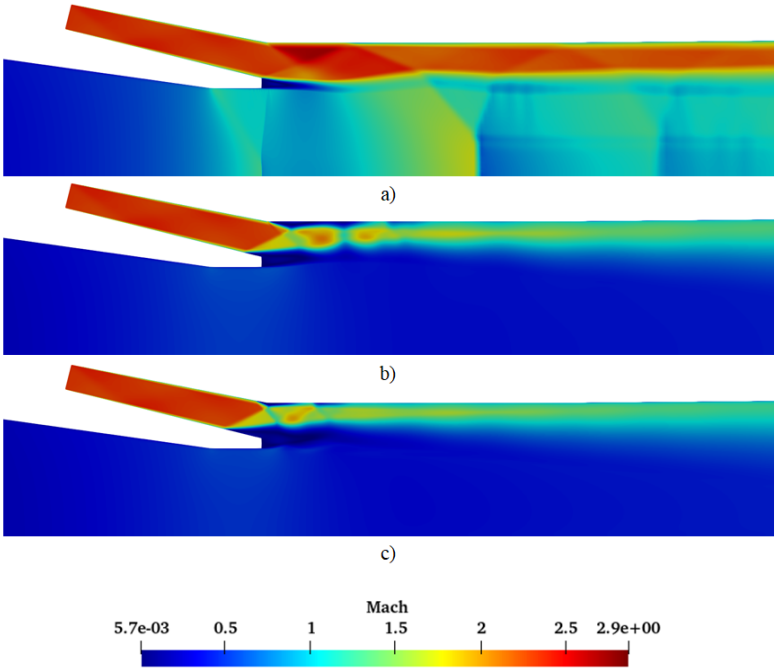

Figure 4-64 Mach contour showing PCST in the isolator, for equivalence ratios a) 0.6 b) 0.8 and c) 1.2

4.2.4 Summary on Numerical Study of DCR combustor

- Numerical simulation of different combustor geometries was carried out to arrive at the optimum geometry. Variations include isolator angle, area ratios and divergence angle of the combustor. Different parameters such as velocity difference, apex formation and combustion efficiency were monitored to assess the degree of combustion and flow mixing in the combustor.

- The geometry with 14° isolator impingement angle showed better performance than one with 7°. A parametric study was also conducted with the 14° geometry. The area ratios of combustor inlet to mixing throat (A_{ci}/A_t) and gas generator to the isolator (A_{gg}/A_{iso}), showed a trend with the apex formation and combustion efficiency. As the ratio A_{ci}/A_t decreased the apex formation and the combustion efficiency improved, with the maximum efficiency observed when $A_{ci}/A_t = 1$ in case 5. As the ratio A_{gg}/A_{iso} increased, the combustion efficiency and the apex formation improved, with the maximum combustion efficiency observed in case -5 at $A_{gg}/A_{iso} = 5.83$.

- Case – 5 showed the highest combustion efficiency at η_c = 70.5%. An equivalence ratio study was undertaken for flight Mach numbers of 4 and 6. The flow Mach number observed during all the cases were predominantly subsonic in the main combustor. Hence the divergence angle of the combustor was increased to achieve supersonic combustion. The increase in the divergence angle was promising in that it increased the region of supersonic Mach number inside the combustor. However, the subsonic regions were still predominant. Further studies involving geometric variations of the divergence angle of the combustor has to be performed to get a better combustor geometry with good combustion efficiency and pressure.

4.3 Full scale DCR engine test results

Full scale DCR engine was tested in connect-pipe mode by simulating the M6 and 28km altitude flight conditions on ground by using a hydrogen based vitiated air heater. The details of test methodology, instrumentation and hardware are presented in previous section. Experimental test conditions are as given below :

Reacting Test Conditions:

Test Condition	φ	Total fuel	Main swirl / Pilot	No. of tests
M 6 (T0 = 1558K)	0.9	405 g/s	370 /35 g/s	1

DCR Test Conditions at M6 Flight Mach number:

Ground test condition simulating flight operation (M6 @ 28km) –1.56MJ/kg		
	GG entry	**Scramjet entry**
T0 (K)	1558	1558
Mass flow rate (kg/s)	1.88	5.72
Oxy mass fraction	0.23	0.23
Mach number.	1.23	2.43

4.3.1 Test Results

4.3.1.1 Feed system injection pressure

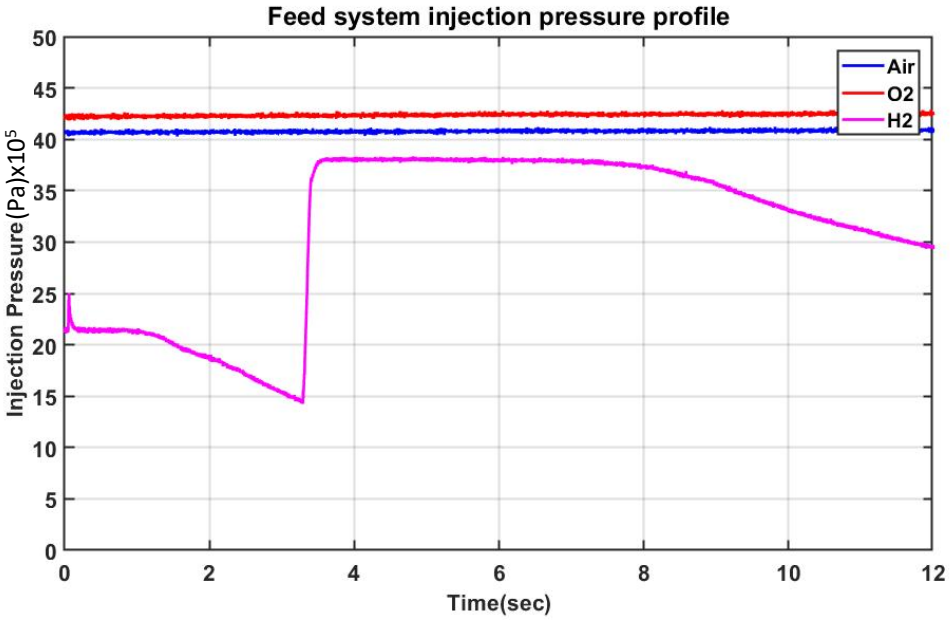

Figure 4-65 Feed system injection upstream pressure

4.3.1.2 Feed system flow rates:

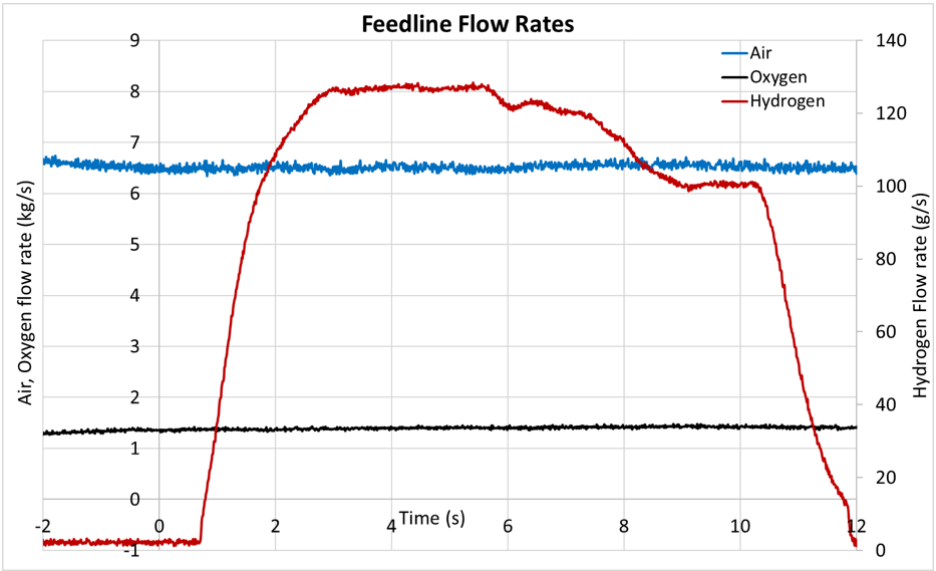

Figure 4-66 Feed system flow rates

4.3.1.3 Heater total temperature:

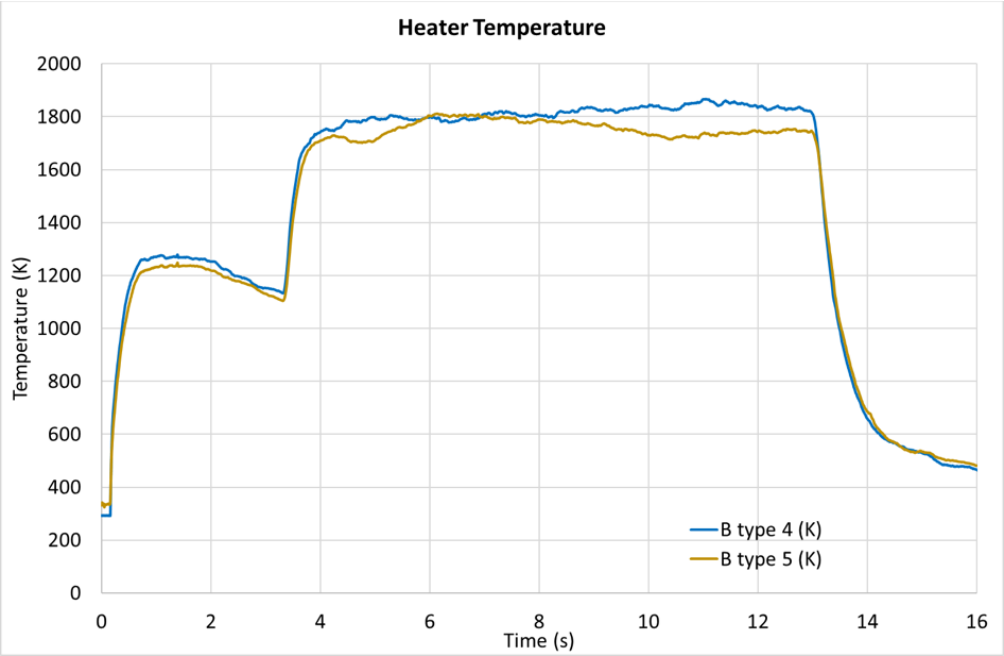

Figure 4-67 Heater total temperature

4.3.1.4 Heater pressure

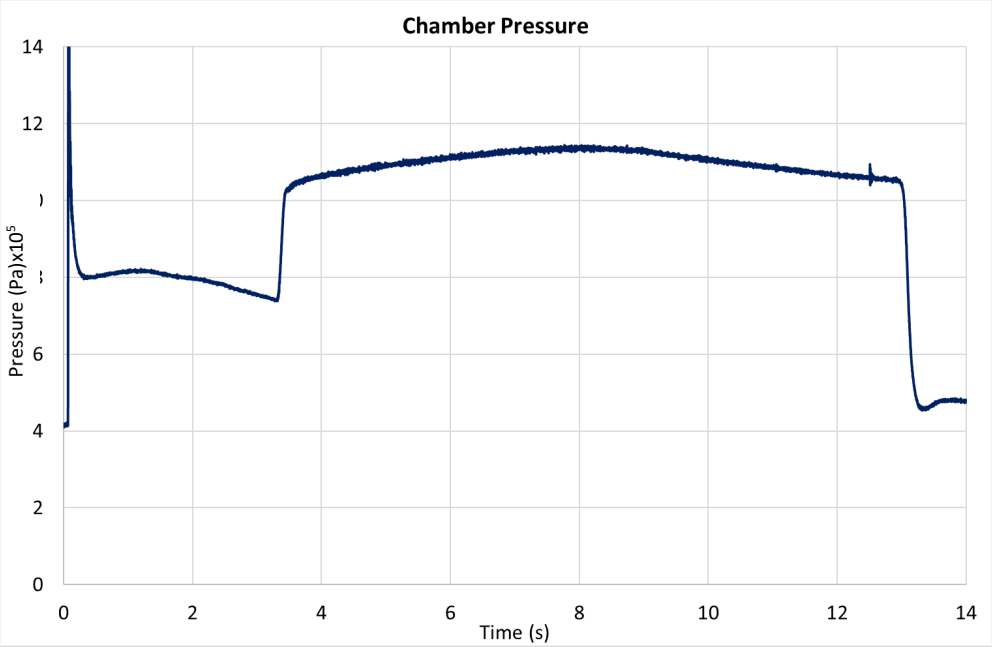

Figure 4-68 Heater pressure

4.3.1.5 Engine pressures:

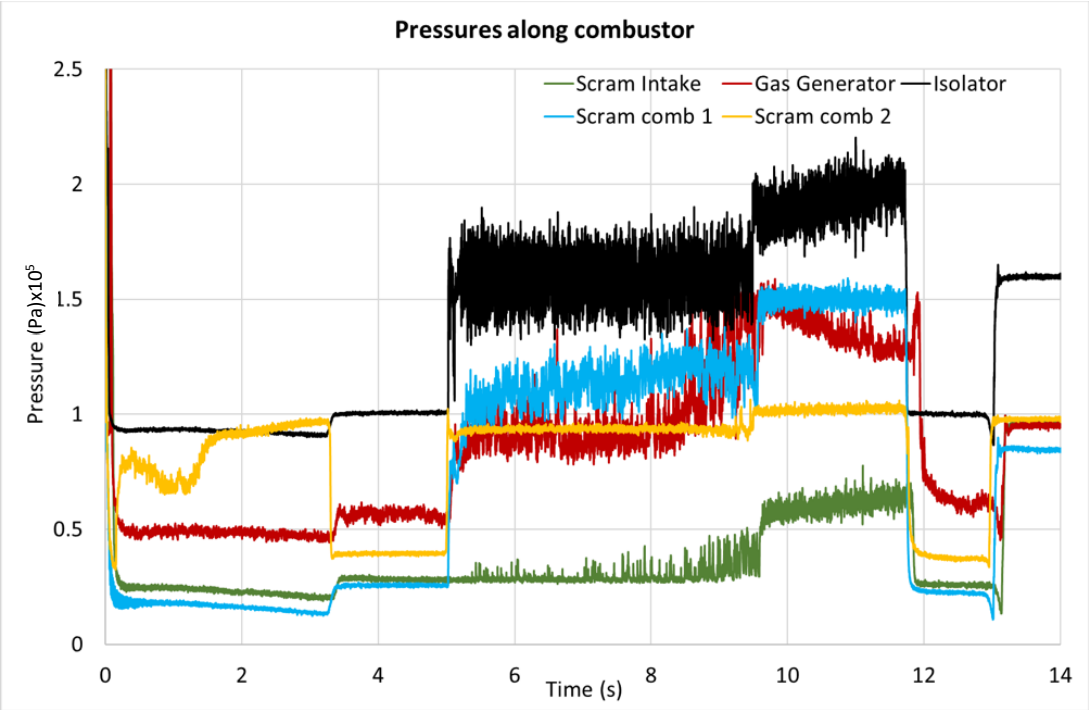

Figure 4-69 Nozzle pressure

4.3.1.6 Pressure plot along the length of the combustor

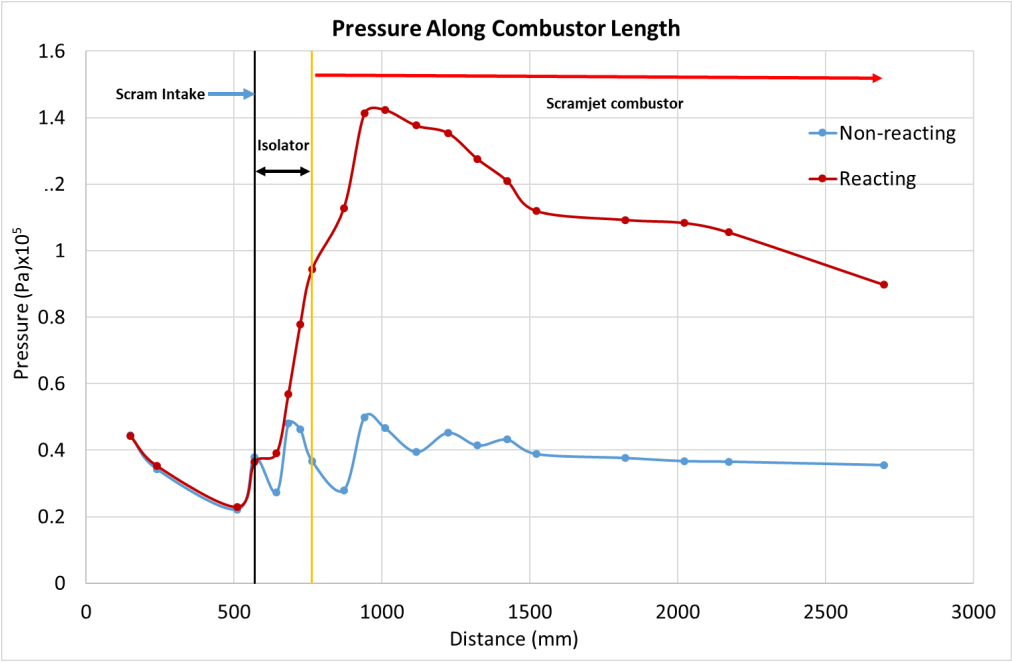

Figure 4-70 Pressure along length of combustor

4.3.1.7 Fuel feed pressure

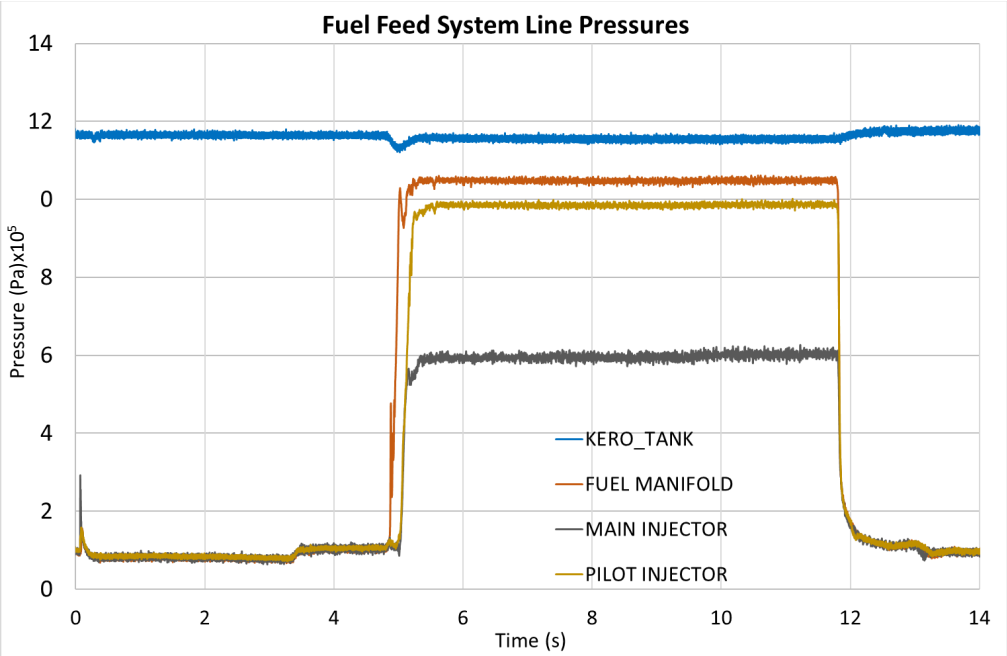

Figure 4-71 Kerosene feed system injection pressure

4.3.1.8 *Comparison with aimed/Predicted values*

Table 4-25 Comparison with aimed/Predicted values

Parameter	Aimed, CEA	Experiment (measured)	CEA_Exp	Remarks
Mass flow of air (kg/s)	6.2	6.5		Experimental flow rates were higher by 4%
Mass flow of O2 (kg/s)	1.35	1.4		
Mass flow of H2 (kg/s)	0.125	0.127		
Total mass flow (kg/s)	7.675	8.027		
Heater To	1787 K	~1800 K	1755 K	
Heater Po (Pa)	$10.5x10^5$	11.2	11.2	
Composition (mass fractions)	H2O- 0.145 O2- 0.231 Balance N2	-	H2O- 0.141 O2- 0.234 Balance N2	
Fuel flow rate (g/s)	407 (ϕ=0.92 considering only H2O, O2 and N2 species)	400 – 410	(ϕ=0.885)	Effective equivalence ratio for engine changed from 0.92 to 0.885
Fuel Injection Pressure (Pa) ($x10^5$)	12	11.5 – 12	-	

4.3.1.9 Thrust produced

The thrust produced in the ground combustor is estimated by the pressures generated in the combustor. Drag due to intake is not considered in this estimate. Net T-D value will be generated from CFD after matching ground test data.

S No	Location/ Component	Calculation	Thrust (N)
1	Gas Generator	GG Pr. x Throat Area	2120
2	Flame Holder	Isolator Pressure x Flame holder area	1708
3	Scramjet Combustor	Integral of Pressure x Area	733
Total Thrust			4561

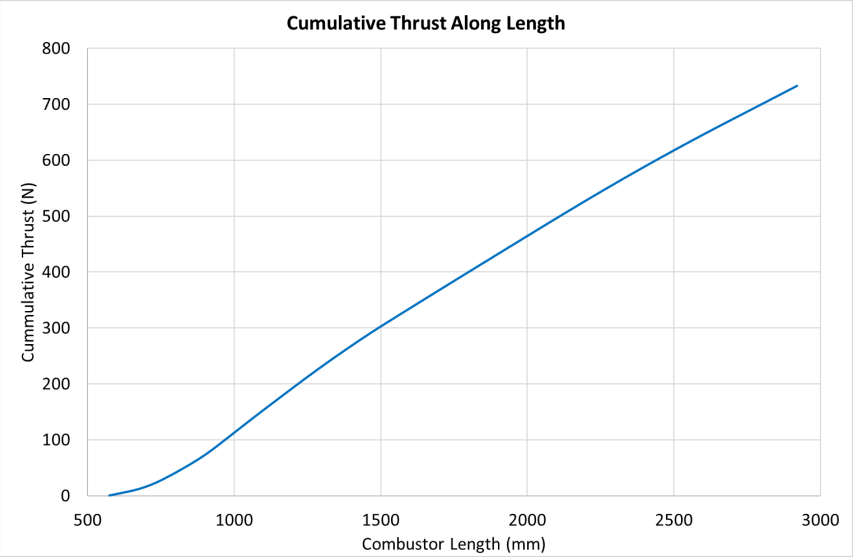

Figure 4-72 Cumulative thrust (P.dA) from Isolator entry till combustor exit.

4.3.1.10 Gas generator

The C*/efficiency of Gas generator could not be estimated from the DCR test as there was no provision to measure the GG total temperatures. Only the pressure could be estimated which was around 1.2 bar (1 bar to 1.5 bar increasing trend).

4.3.1.11 Test Observations and Inferences

- The operation of heater was satisfactory. Ignition was achieved in vitiated air heater and the non-reacting conditions were established.
- Upon injection of fuel into the Gas Generator, ignition was observed and sustained combustion was achieved in the supersonic combustor.

- The flow rate of air and oxygen were higher during test by 4% which reduced the effective fuel equivalence ratio of the engine. (0.92 to 0.885)
- The kerosene fuel flow rate was within the expected range.
- The pressure rise seen in the Scramjet combustor has a close match with the CFD simulation data. Comparison between the CFD simulations performed in the last chapter for the Case-5 geometry and the experimental pressure data obtained. The prediction by CFD is matching in the initial region in the isolator. While along the combustor, the CFD over predicts the pressure rise. This indicates a 3-dimensional flow inside the combustor in the experimental flow.

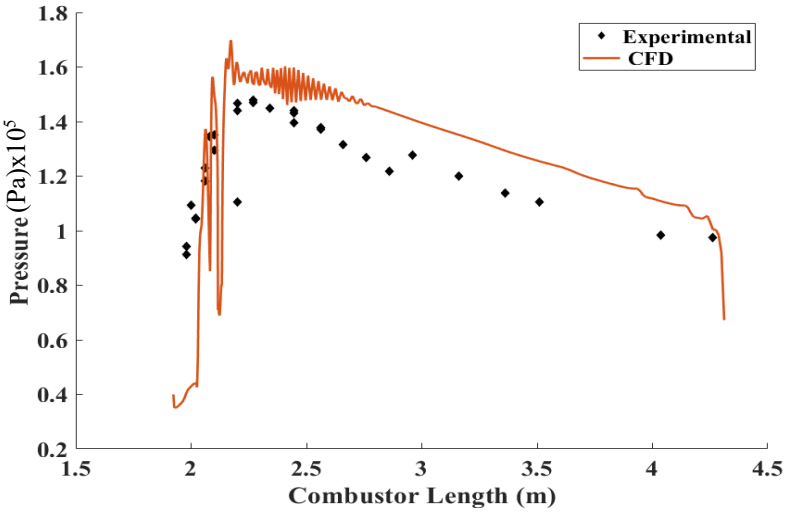

- The flow rate of hydrogen into the heater was not steady throughout the test. After 9 seconds, the flow of hydrogen kept falling, which had resulted in pressure variations in the chamber, nozzle section and the combustor. Hence the data beyond 9 seconds was not considered for any performance predictions.
- Thrust from the combustor is estimated at 4561 N.

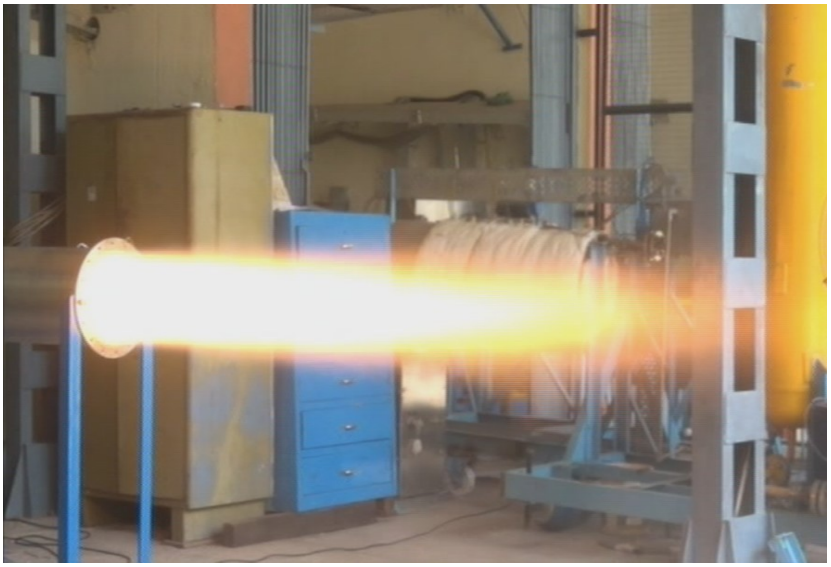

Figure 4-73 DCR Engine Proof Hardware Connect Pipe Mode Test

4.3.2 Summary on Full scale DCR combustor test

- Jet-A fueled full scale DCR engine was tested successfully in connect-pipe mode by simulating the M6 and 28km altitude flight conditions on ground by using a hydrogen based vitiated air heater.
- The facility was modified to conduct a test of DCR engine by suitably identifying the vitiated heater, intake requirements. Fuel injection scheme was designed for fuel rich combustion, to raise the air temperature, Cooling the GG walls and the rest of the fuel for cracking/decomposition.
- The test was conducted with truncated air intake specially designed for ground test, extensive instrumentation along the length of the combustor components.
- Wall static pressure rise along the length of the combustor indicates that the ignition, sustained combustion were achieved.

Chapter 5

CONCLUSIONS

Experimental and numerical studies on hydrocarbon fueled Dual Combustion Ramjet (DCR) are carried out. The studies are aimed towards development of a DCR propulsion system useful for a tactical hypersonic weapon system which can operate in a wider band of Mach number (M4 to M6) regime. A dual-mode ramjet scramjet propulsion system combines the advantages of a ramjet and a scramjet. This hybrid scramjet engine incorporates the best features of the ramjet and scramjet to achieve high-combustion efficiency and performance.

The studies include literature survey, evolving design methodology and identifying the constraints, experimental characterization of fuel rich gas generator, numerical studies on combustor-isolator interactions, design of combustor geometry parameters and full-scale DCR engine realization and testing in a modified connect pipe mode test facility with truncated intake system for the simulated flight conditions of Mach number 6.

The conclusions drawn from the design, numerical and experimental studies are :

- The design requirements of a full-scale liquid hydrocarbon fueled Dual combustion Ramjet propulsion system that can be used for wider range Mach number regime (between M4 and M6) for high speed vehicles are clearly brought out. It is found that the propulsion system design methodology is highly configuration dependent; all sub-systems namely Intake system, gas generator, isolator, supersonic combustor and nozzle are to be designed in integrated manner considering the influence of one with another for the varying Mach numbers.
- A fuel rich gas generator is designed with jet-A fuel with high equivalence ratio between 2.9 to 3.5 and with a C* of 1050 m/s. An innovative fuel injection scheme is designed with multi point injection in intake, gas generator head end to ensure the high flow rate of fuel distribution in the system.
- From DCR and its intake system studies, it was found that gas generator chamber pressure is limited by its intake capability to avoid unstart problems and must be chosen very accurately. For the present configuration, that combustion chamber pressure design limit upto 2.5 bar is allowed.
- Full scale gas generator hardware is realized and experimentally characterized in multiple tests for reliable ignition, fuel rich combustion in connect pipe mode facility by simulating the inlet conditions with hydrogen vitiated heater. For fuel rich gas generator, ignition was reliably proven between total temperature 880K and 1700K for different freestream Mach number conditions.
- One dimensional code with NASA CEA interface is developed for performance prediction of the gas generator and is found as very useful tool for design of fuel rich gas generator. Comparison of experimental data and 1-D predictions is found satisfactory.
- CFD procedure is evolved for design of full scale axi-symmetric DCR combustor and its annular isolator performance studies.
- Numerical simulations were carried out on DCR combustor flow field with various turbulence models namely k-ε (Standard), (RNG) k-ε, k-ω Standard, k-ω SST and combustor wall pressures were validated with published experimental results.

- Turbulence model RNG k-ε showed best match followed by k-ε. SST. k-ω also predicts shock train stating position similar to other two models but maximum peak pressure is not predicted well. k-ω standard could not predict phenomena properly.
- Starting location of shock train, maximum pressure, average pressure in DCR combustor are predicted using validated CFD methodology. Effect of equivalence ratio on the shock train position, wall static pressures is well captured for varying free stream Mach numbers M4 and M5 conditions. Higher global equivalence ratios (0.85 to 1.0) yield better performance but lower values below 0.7 and higher values above 1.2 lead to poor mixing and low combustion efficiency.
- Error in estimation of starting location of shock train, maximum pressure, average pressure in combustor is compared. (RNG) k-ε is best model which could predict shock train location with an error of < 5%.
- Numerical simulations of different combustor geometries were carried by varying isolator angle, area ratios and divergence angle of the combustor. The geometry with 14° isolator impingement angle showed better performance than one with 7° with the highest combustion efficiency at η_c = 70.5%. The increase in the divergence angle was promising in that it increased the region of supersonic Mach number inside the combustor. However, the subsonic regions were still predominant.
- Jet-A fueled full scale DCR engine was tested in connect-pipe mode by simulating the free stream Mach number M6 and 28km altitude flight conditions on ground by using a hydrogen based vitiated air heater and a truncated intake system with extensive instrumentation along the length of the combustor components.
- The static test was successfully conducted for 9 seconds in the full scale DCR propulsion system with a global equivalence ratio of 0.9 with a proof of Wall static pressure rise along the length of the combustor indicating the ignition, sustained high speed combustion in DCR engine.
- Full scale liquid fueled DCR propulsion system is experimentally proven for the first time in India on ground successfully demonstrating high speed combustion and found as promising technology for futuristic high speed propulsion systems.

Chapter 6

SCOPE FOR FUTURE WORK

The present study is mainly experimental and numerical study on hydrocarbon fueled DCR combustor, that can be used for high-speed applications. It is emphasized on the techniques to achieve combustion of hydrocarbon fueled Gas generator used as an embedded combustor of a dual ramjet combustor. The flow field of the axisymmetric DCR, its isolator is studied to understand the interactions of the intake, isolator and combustor. The influence of equivalence ratio, geometrical parameters are studied to some extent. Simulations were done at discrete flight conditions (M4, M6) and the DCR performance was studied by focusing on few critical parameters such as wall pressures, Mach number contours, temperature contours and velocity contours.

However, more research is required to declare that these designs are fit for reliable propulsion systems. Some of such points mentioned below:

- In the 1-D model of fuel rich gas generator, ideal combustion and mixing is assumed in the model. This can be improved by incorporating reduced order finite rate chemistry model to reduce the deviation between test results and model data. Also, the stages of liquid droplets breakup, evaporation and mixing with oxidant in heated flow can be studied in detail. Suitable ignition models can be developed.
- By introducing a gas analyzer to the current experimental set-up, CO_2 and CO can be measured and based on which combustion efficiency can be estimated better. Test set-up can be upgraded with heated kerosene facility to evaluate the combustor performance by simulating the fuel injection conditions similar to long range cruise flight conditions.
- Numerical studies and Connect pipe mode tests on “Ramjet to Scramjet Transition” from M4 to M6 are of very much interesting and less addressed for DCR configuration.
- Effect of flight angle of attack on the intake performance and its influence on the combustor also to be studied.

ANNEXURE-1: Details of Pressure Sensors and Flow Sensors

Detailed Specifications of Pressure Sensors:

PERFORMANCE SPECIFICATIONS

Characteristic	Measure
Accuracy[1]	±0.10 % full scale
Linearity	±0.10 % full scale
Hysteresis	±0.05 % full scale
Media	All gases/liquids compatible with wetted parts
Resolution	Infinite
Calibration	5-point calibration: 0 %, 50 %, and 100 % of full scale

ENVIRONMENTAL SPECIFICATIONS

Characteristic	Measure
Temperature compensated	15 °C to 71 °C [60 °F to 160 °F]
Temperature effect, zero	0.0025 % full scale/°F
Temperature effect, span	0.0025 % reading/°F
Sealing	Hermetically sealed IP68/NEMA 6P

ELECTRICAL SPECIFICATIONS

Characteristic	Measure
Strain gage type	Bonded foil
Insulation resistance	5000 mOhm @ 50 Vdc
Bridge resistance	350 ohm
Shunt calibration data	Included
Electrical termination (std)	PTIH-10-6P or equiv. (hermetic stainless)
Mating connector (not incl)	PT06A-10-6S or equiv. (AA111)

MECHANICAL SPECIFICATIONS

Characteristic	Measure
Wetted parts material	number here
< 2000 psig/a	17-4 PH stainless steel
> 2000 psig/a	15-5 PH stainless steel
Weight	10 oz
Case material	304 stainless steel
Marking	Permanent metal name plate MIL-STD130F 4.3; Individual sequential serial number per sensor; Country of origin and date of manufacture

Model TJE

OPTION CODES

Range Code	**Many range/option combinations are available in our quick-ship and fast-track manufacture programs. Please see http://sensing.honeywell.com/TMsensor-ship for updated listings.**		
Pressure ranges	1, 2, 5, 10, 15, 25, 50, 75, 100, 150, 200 300, 750, 1500, 2000, 15000, 20000, 30000, 50000, 60000 psig/a 500, 1000, 3000, 5000, 7500, 10000 psia 500, 1000, 3000, 5000, 7500, 10000 psig		
Temperature compensation	1a. 60 °F to 160 °F 1b. 30 °F to 130 °F 1c. 0 °F to 185 °F 1d. -20 °F to 130 °F 1e. -20 °F to 200 °F	1f. 70 °F to 250 °F [11] 1g. 70 °F to 325 °F [11] 1h. 70 °F to 400 °F [11] 1i. -65 °F to 250 °F [11]	
Internal amplifiers [10]	2a. 0 Vdc to 5 Vdc (four wire) output[15] 2c. 0-5 Vdc output[15] 2j. 4 mA to 20 mA (three wire) output 2k. 4 mA to 20 mA (two wire) output[6, 17]	2n. 4 mA to 20 mA (two wire) intrinsically safe[A, 17] 2t. 0 Vdc to 10 Vdc output 2u. Unamp., mV/V output	
Internal amplifier enhancements	3a. Input/output isolation[15] 3d. Remote buffered shunt calibration		
Pressure ports[9]	5a. 1/4-18 NPT female (3000 psig to 10000 psig) 5b. 1/4-18 NPT male (15 psig/a to 10000 psig/a) 5c. 7/16-20 UNF female (per MS33649-4)	5d. 7/16-20 UNF male 5g. G 1/4 male	
Electrical termination	6a. Bendix PTIH-10-6P (or equiv), 6 pin (max 250 °F) 6b. MS type connector to mate with MS3106-14S 6S (max 160 °F)[13] 6e. Integral cable: Teflon (0 °F to 180 °F) 6f. Integral cable: PVC (-20 °F to 160 °F)	6g. Integral cable: Neoprene (0 °F to 180 °F) 6h. Integral cable: Silicone (-65 °F to 300 °F) 6i. Integral underwater cable (max 180 °F) 6j. 1/2-14 conduit fitting with 5 ft of 4 conductor PVC cable	6m. DIN 43650 6q. Molded integral cable: Polyurethane (max 180 °F) 6t. Integral cable with Heyco spring strain relief (5 ft)
Shunt calibration	8a. Precision internal resistor[11]		
Special calibration[9]	9a. 10 point (5 up/5 down) 20 % increments @ 70 °F (gage) 9b. 20 point (10 up/10 down) 10 % increments @ 70 °F (gage)		
Wetted diaphragm[9]	10a. 316 stainless steel[9] 10b. Crucible A-286	10c. Hastelloy-C 10d. Monel K-500	
Bridge resistance[9]	12a. 1000 ohm (foil) (max 400 °F) 12b. 5000 ohm (foil) (max 400 °F)		
Zero and span adjustment	14a. No access to pots 14b. Top access to pots		
Shock and vibration	44a. Shock and vibration resistance		
Interfaces	53e. Signature calibration[11] 53t. TEDS IEEE1451.4 module[16]		

Data sheet of Pressure Sensor
(Ref : Honeywell Catalogue)

Features

- Linearity < 0.10% with linearizing electronics
- High turn-down capability, up to 100:1.
- Excellent repeatability, less than +/- 0.05%.
- Typical response time 3-4mS
- Extensive primary standard NIST traceable calibration capability, offering a wide range of fluids, viscosities and flow rates. Accuracy less than +/-0.05% typical
- Standard materials of construction are 316 SS housing and 430F SS rotor. Additional materials available.
- Robust, compact design capable of compliance to severe shock and vibration requirements.
- Standard pressure capabilities up to 349 BarG.
- Extreme operating pressures available in custom packages.
- High shock designs available for applications with large hydraulic water hammer effects.
- Custom designs to meet the specific application are routine, not the exception.

Specifications

Calibration accuracy	±0.05% of reading, traceable to NIST
Repeatability	±0.05% of reading
Linearity	±0.10% with linearizing electronics
Response time	3-4mS typical
Housing material	316 stainless steel, standard
Rotor material	430F stainless steel, standard
Temperature range	-268 to 399°C, dependent on bearing and pick-off
Operating pressure	Up to 2,068 BarG, dependent on fitting
Ball bearing material	440C stainless steel or equivalent, Ceramic
Journal bearing material	Ceramic, tungsten carbide, graphite
Pick-off's	Modulated carrier and magnetic
Straight Run	10D upstream and 5D downstream minimum
Recommended filtration	Ball bearings: 10 to 100 microns (less filtration with larger sizes) Journal bearings: 75 to 100 microns

FLOW TECHNOLOGY™

FT Series

Data sheet of Flow Sensor for liquid fuel
(Ref : Flow technology Catalogue)

Features

- High turn-down capability.
- Excellent repeatability, less than +/- 0.1% typical
- Linearity < 0.10% with linearizing electronics, typical with 20 pt calibration.
- Extensive primary standard NIST traceable calibration capability, offering a wide range of flow rates and pressure. Accuracy less than +/-0.30 to +/-0.50%, dependent on calibrator.
- Standard materials of construction are 316 SS housing and 430F SS rotor.
- Robust, compact design capably of compliance to severe shock and vibration requirements.
- Standard pressure capabilities up to 349 BarG.
- Custom designs to meet the specific application are routine, not the exception.

Specifications

Calibration accuracy	±0.30% of reading, traceable to NIST
Repeatability	±0.10% of reading, typical
Linearity	±0.10% with linearizing electronics typical with 20 pt calibration
Housing material	316 stainless steel, standard
Rotor material	430F stainless steel, standard
Temperature range	-268 to 149°C
Operating pressure	Up to 2,068 BarG, dependent on fitting
Ball bearing material	440C stainless steel or equivalent
Pick-off's	Modulated carrier and magnetic
Straight Run	10D upstream and 5D downstream minimum
Recommended filtration	Ball bearings: 10 to 100 microns (less filtration with larger sizes)

FTI FLOW TECHNOLOGY™

nqa. ISO 9001 Registered · ANAB ACCREDITED · nqa. AS9100 Registered

FT Series

Data sheet of Flow Sensor for gases
(Ref : Flow technology Catalogue)

References

[1] Dean Andreadis. Scramjet engines enabling the seamless integration of air and space Operations. Pratt and Whitney Space propulsion, Hypersonics, West Palm Beach, Florida

[2] Ronald S Fry. A century of Ramjet propulsion technology evolution. Journal of Propulsion and Power, Vol. 20, No 1, January-February 2004

[3] William H. Heiser, David T. Pratt, Hypersonic Air breathing Propulsion. AIAA Education Series, 1994

[4] Sean M Torrez, et al. A scramjet engine model including effects of pre-combustion shocks and dissociation. AIAA 2008-4619,44th AIAA/ASME/SAE/ASEE Joint propulsion conference and Exhibit, 21-23 July 2008

[5] Ronald S. Fry, The Johns Hopkins University, Columbia, Maryland. The U.S. Navy's Contribution to Airbreathing Missile Propulsion Technology. AIAA 2011-6942

[6] David M. Van Wie, Stephen M. D'Alessio, Michael E.White. Hypersonic Airbreathing Propulsion. Johns Hopkins APL Technical Digest, Volume 26, number 4 (2005)

[7] Billig F.S, Waltrup P.J and Stockbridge R.D. Integral-Rocket Dual-Combustion Ramjets: A New Propulsion Concept. J. Spacecraft and Rockets, 1980, Vol. 17, No. 5, P. 416−424

[8] Paul J. Waltrup, Applied Physics Laboratory, Johns Hopkins University. Liquid-Fueled Supersonic Combustion Ramjets: A Research Perspective. VOL. 3, NO. 6, NOV.-DEC. 1987 J. PROPULSION 515

[9] Paul J. Waltrup, The Johns Hopkins University Applied Physics Laboratory, Maryland, U.S.A. The Dual Combustor Ramjet: A versatile propulsion system for hypersonic tactical missile applications.

[10] Moerel J.L.P.A, Halswizk W.H.C. System Analysis of High Speed, Long Range Weapon Systems. AIAA Atmospheric Flight Mechanics Conference and Exhibit, 15 - 18 August 2005, San Francisco, California, AIAA 2005-5819

[11] Michael E. White and Walter R. Price. Affordable Hypersonic Missiles for Long-Range Precision Strike. Johns Hopkins APL Technical Digest, Volume 20, Number 3 (1999)

[12] Jong-Ryul Byun, Joong-Ki Ahn, Hyun-Gull Yoon, Jin-Shik Lim. A Preliminary Performance Analysis of a Dual Combustion Ramjet Engine. January 2011, Journal of the Korean Society of Propulsion Engineers15 (5)

[13] Jims John Wessley G, Shilpa Pradeep. Parametric Analysis of a Dual Combustion Ramjet Engine. International Journal of Recent Technology and Engineering (IJRTE) ISSN:2277-3878, Volume-7, Issue-6S4, April 2019 pp13-135

[14] Wadwankar N, G Kandasamy, N Ananthkrishnan, VS Renganathan, Ik-Soo Park and Ki-Young Hwang. Dual combustor ramjet engine dynamics modeling and simulation for design analysis. Proc IMechE Part G: J Aerospace Engineering 0(0) 1–16, IMechE 2018; DOI: 10.1177/0954410017749867 journals.sagepub.com/home/pig

[15] Schetz J.A, Billig F.S and Favin S. Analysis of Mixing and Combustion in a Scramjet Combustor with a Co-Axial Fuel Jet. AIAA-80-1256, AIAA/SAE/ASME 16th Joint Propulsion Conference, June 30-July 2, 1980/Hartford, Connecticut

[16] Betelin V.B, Smirnov N.N, Nikitin V.F, Dushin V.R, Khusnirenko A.G, Nerchenko V.A. Evaporation and ignition of droplets in combustion chambers modeling and Simulation. Acta Astronautica , vol. 70 (2012) 23-35.

[17] Smirnov N.N, Betelin V.B, Khusnirenko A.G, Nikitin V.F, Dushin V.R, Nerchenko V.A. Ignition of fuel sprays by shock wave mathematical modeling and numerical Simulation. Acta Astronautica, vol. 87 (2013) 14-29.

[18] Nickolay N. Smirnov, Valeriy F. Nikitin, Vladislav R. Dushin, Yuri G. Filippov, Valentina A. Nerchenko, Javad Khadem. Combustion onset in non-uniform dispersed Mixtures. Acta Astronautica, vol. 115 (2015) 94-101.

[19] Stull F.D, Craig R.R, Streby G.D. Investigation of a dual inlet side dump combustor using liquid fuel injection. J. Propuls. Power, vol. 1.1, pp. 83-88, 1985.

[20] Vanka S.P, Craig R.R, Stull F.D. Mixing, chemical reaction and flow field development in ducted rockets. AIAA-85-1271, 1985.

[21] Brophy C.M, Hawk C.W. Flow visualization of four-inlet ducted rocket engine Configurations. Journal of Flow Visualization and Image Processing, vol. 3.1, 1996.

[22] Mcbride, Gordon. Computer program for calculation of complex chemical equilibrium compositions and application. NASA reference publication, 1996.

[23] Ascher H. Shapiro, The dynamics and thermodynamics of compressible fluid flow, vol 1, 1953. The Ronald Press Company, New York.

[24] Maurice J. Zucrow, Joe D. Hoffman, Gas Dynamics, vol 1, 1976, Publisher Wiley (1st edition), ISBN-10: 04719844X

[25] Philip G. Hill, Carl R. Peterson. Mechanics and Thermodynamics of Propulsion. 2nd edition, 1992.Publisher Pearson, ISBN-10: 0201146592

[26] Veronika Tyurenkova, Nickolay Smirnov, Mariya Smirnova.Mathematical modeling of burning surface in parallel flow of oxidant. MATEC Web of Conferences, 209, 00007 (2018).

[27] Tyurenkova V.V, Smirnova M.N. Material combustion in oxidant flows: Self-similar Solutions. Acta Astronautica, vol. 120 (2016) 129-137.

[28] Avanish Kumar, V. Venkateswarlu, P. Satyaprasad, M. Raghavendra Rao. Development of film cooled thruster for rocket application. ASME 2019 Gas Turbine India Conference, 2019-2320, Indian Institute of Technology Madras, Chennai, India

[29] Jeong-Yeol CHOI, Vigor YANG. High Resolution Numerical Study on the Supersonic Turbulent Flame Structures and Dynamics in Dual Combustion Ramjet. Propulsion and Energy Forum July 28-30, 2014, Cleveland, OH, 50th AIAA/ASME/SAE/ASEE Joint Propulsion Conference

[30] Liwei Zhang, Hong-Gye Sung, Vigor Yang. Flow and Flame Dynamics in a Hydrocarbon fueled Dual Combustion Ramjet Engine. AIAA SciTech Forum 6-10 January 2020, Orlando, FL AIAA Scitech 2020 Forum, 10.2514/6.2020-0648)

[31] Colket, M. B., III, and Spadaccini, L. J. Scramjet Fuels Autoignition Study. Journal of Propulsion and Power,Vol. 17, No. 2, 2001, pp. 315–323. doi:10.2514/2.5744

[32] Puri, P., Ma, F.-H., Choi, J.-Y., and Yang,V. Ignition Characteristics of Cracked JP-7 Fuel. Combustion and Flame, Vol.142, No.4, 2005, pp.454–457. doi:10.1016/j.combustflame. 2005.06.001

[33] Schetz J.A, Billig F.S and Favin J S. Flow field Analysis of a Scramjet Combustor with a Coaxial Fuel Jet. Journal Article1982, AIAA Journal, 1268-1274

[34] Liwei Zhang, JeongYeol Choi, Vigor Yang. Supersonic Combustion and Flame Stabilization of Coflow Ethylene and Air with Splitter Plate. Journal of Propulsion and Power, Vol. 31, No. 5, Sept oct 2015

[35] Jianguo Tan, Jiping Wu and Zhenguo Wang. Experimental and numerical investigations on flow fields and performance of dual combustion ramjet. Proc IMechE Part G: J Aerospace Engineering 2014, Vol. 228(6) 920–929)

[36] Situ M, Sun Y.Y, Zhang S.D, and Wang C. Investigation of Supersonic Combustion of Hydrocarbon Fuel-Rich Hot Gas in Scramjet Combustor. AIAA - 99 – 2245, 35th AIAA/ASME/SAE/ASEE Joint Propulsion Conference and Exhibit 20-24 June 1999 Los Angeles, California

[37] Jianguo Tan, Yi Wang. Freejet Experimental Investigation on Performance of Dual-Combustion Ramjet. National University of Defense Technology, 410073 Changsha, People's Republic of China, DOI: 10.2514/1B35263

[38] Jong-Ryul Byun, Chul Park, and Oh Joon Kwon, Joongki Ahn, Experimental Study of Combustor–Isolator Interactions in a Dual-Combustion Ramjet. Journal of Propulsion and Power, DOI: 10.2514/1. B35391

[39] Chenlin Zhang, Juntao Chang, MengMeng Liu, Shuo Feng, Wen Shi, Wen Bao. Effect of heat release on movement characteristics of shock train in an isolator. Acta Astronautica, Volume 133,2017,Pages 185-194,ISSN 0094-5765,

[40] Wei Huang, Zhen-guo Wang, Mohamed Pourkashanian, Lin Ma, Derek B. Ingham, Shi-bin Luo, Jing Lei, Jun Liu. Numerical investigation on the shock wave transition in a three-dimensional scramjet isolator. Acta Astronautica, Volume 68, Issues 11–12,2011, Pages 1669-1675, ISSN 0094-5765

[41] Fei Xing, Can Ruan, Yue Huang, Xiaoyuan Fang, Yufeng Yao. Numerical investigation on shock train control and applications in a scramjet engine. Aerospace Science and Technology, Volume 60,2017, Pages 162-171, ISSN 1270-9638,

[42] Yubao He, Hongyan Huang, Daren Yu. Investigation of boundary-layer ejecting for resistance to back pressure in an isolator. Aerospace Science and Technology, Volume 56,2016, Pages 1-13, ISSN 1270-9638,

[43] Stockbridge, R.D. Experimental Investigation of Shock Wave/Boundary-Layer Interactions in an Annular Duct. Journal of Propulsion and Power, Vol. 5, No. 3, 1989, pp. 346–352.doi:10.2514/3.23159

[44] Wenxin Hou, Juntao Chang, ZongqiXie, Youyin Wang, Linke Wu, Wen Bao. Behavior and flow mechanism of shock train self-excited oscillation influenced by background waves. Acta Astronautica, Volume 166, 2020, Pages 29-40, ISSN 0094-5765, https://doi.org/10.1016/j.actaastro.2019.09.032.

[45] Wen Shi, Juntao Chang, Junlong Zhang, Jicheng Ma, Ziao Wang, Wen Bao. Numerical investigation on the forced oscillation of shock train in hypersonic inlet with translating cowl. Aerospace Science and Technology, Volume 87, 2019, Pages 311-322, ISSN 1270-9638, https://doi.org/10.1016/j.ast.2019.02.022.

[46] Wen Shi, Juntao Chang, JiCheng Ma, Youyin Wang, Lin Gao, Wen Bao. Path dependence characteristic of shock train in a 2D hypersonic inlet with variable background waves. Aerospace Science and Technology, Volume 86, 2019, Pages 650-658, ISSN 1270-9638, https://doi.org/10.1016/j.ast.2019.02.001.

[47] Waltrup, P. J., and Bilig, F. S. Precombustion Shock Structure in Scramjet Engines. AIAA Paper 1972-1181, 1972.

[48] Waltrup, P. J., and Billig, F. S. Structure of Shock Waves in Cylindrical Ducts. AIAA Journal, Vol. 11, No. 10, 1973, pp. 1404–1408. doi:10.2514/3.50600

[49] Waltrup, P. J., and Bilig, F. S. Prediction of Precombustion Wall Pressure Distributions in Scramjet Engines. Journal of Spacecraft and Rockets, Vol. 10, No. 9, 1973, pp.620–622.doi: 10.2514/3.27782

[50] Michael K. Smart. How much compression should a scramjet inlet do. AIAA Journal, vol. 50, No.3, March 2012.

[51] Launder B.E and Spalding D.B. Lectures in Mathematical Models of Turbulence. Academic Press, London, England. 1972.

[52] Orszag S.A, Yakhot, W.V, Flannery S, Boysan F,Choudhury D, Maruzewski J, and Patel B. Renormalization Group Modeling and Turbulence Simulations. In International Conference on Near-Wall Turbulent Flows, Tempe, Arizona. 1993.

[53] Wilcox D.C. Turbulence Modeling for CFD. DCW Industries, Inc. La Canada, California. 1998.

[54] Menter F.R. Two-equation eddy-viscosity turbulence models for engineering applications. AIAAJ.32(1994)1598–1605.

[55] Luo S, Huang W, Qin H. Investigation of turbulent models for the flow field from a typical strut-based scramjet combustor. In Proceedings of ASME Turbo Expo, Vancouver, Canada, 6–9 June 2011, paper no. GT-2011-45078, pp. 25–31. New York: ASME.

[56] Roache P.J, Error base for CFD, AIAA Paper No: 2003-0408, 2003

[57] Gruenig, F. Mayinger. Supersonic Combustion of kerosene/H_2 -mixtures in a model scramjet combustor. Combustion Science and Technology,1999. Vol. 146 pp 1-22

[58] Tohru Mitani. Ignition Problems in Scramjet testing. Combustion and Flame, 101:347-359,1995

[59] Pellet G.L, Bruno C, and Chintz W. Review of air vitiation effects on scramjet ignition and flame holding combustion process. AIAA 2002-3880, 38thAIAA/ASME/SAE/ASEE Joint Propulsion Conference and Exhibit, 7-10 July 2002, Indianapolis, Indiana.

[60] Curran, E. T. Scramjet Engines: The First Forty Years. Journal of Propulsion and Power, Vol. 17, No. 6, 2001, pp. 1138–1148. doi:10.2514/2.5875

[61] Ruifeng Cao, Yue Lu, Daren Yu, Juntao Chang. Study on influencing factors of combustion mode transition boundary for a scramjet engine based on one-dimensional model. Aerospace Science and Technology, Volume 96, 2020, 105590, ISSN 1270-9638, https://doi.org/10.1016/j.ast.2019.105590.

[62] Colket, M. B., III, and Spadaccini, L. J. Scramjet Fuels Autoignition Study. Journal of Propulsion and Power, Vol. 17, No. 2, 2001, pp. 315–323. doi:10.2514/2.5744

[63] Puri, P., Ma, F.H., Choi, J.-Y., and Yang,V. Ignition Characteristics of Cracked JP-7 Fuel. Combustion and Flame, Vol.142, No.4, 2005, pp.454–457.doi: 10.1016/j.combustflame. 2005.06.001

[64] ANSYS Fluent User's Guide, ANSYS 16, July 2015, ANSYS Inc

[65] ANSYS ICEM CFD User's Manual, ANSYS ICEM CFD 15.0, Nov 2013, ANSYS Inc

[66] Guide for verification and validation of computational fluid dynamics simulation, G-077-1998, AIAA, Reston, VA,1998

[67] Mitsuno.M, Kuwahara T, Nakagawa I. Measuring method of Ramjet test Facility. AIAA 95-0235, 33rd Aerospace Sciences, Meeting and Exhibit, January1995, Reno, NV

[68] AGARD Advisory Group Report, AGARD-AR 323. Experimental and Analytical methods for determination of Connected-pipe Ramjet and ducted Rocket integral Performance. NATO, July 1994

[69] John A. Blevins, Hugh W. Coleman. An Assessment of Connected-pipe Ramjet Testing. AIAA 95-3074, 31st AIAA/ASME/SAE/ASEE Joint Propulsion Conference and Exhibit, July 1995, San Diego, CA

List of Publications

International Journals:

S.No	Title of the paper	Name of the Journal and Publisher	Status
1	Experimental validation of liquid hydrocarbon based fuel rich gas generator for highspeed propulsion systems	International Journal on **"Acta Astronautica"** (Ref: Acta Astronautica 174 (2020)180–188, https://doi.org/10.1016/j.actaastro.2020.05.009). Publisher : ELSEVIER	**Published**
2	Numerical studies and validation of combustor and annular isolator interactions of hydrocarbon based axisymmetric dual combustion ramjet	International Journal on **"Aerospace Science and Technology"** (Ref: Aerospace Science and Technology 106 (2020) 106185 https://doi.org/10.1016/j.ast.2020.106185) Publisher : ELSEVIER	**Published**
3	Review on analytical and experimental treatment of hydrocarbon based dual combustion ramjet technology	International Journal of Propulsion and Power, AIAA	**Under Review**

Acta Astronautica 174 (2020) 180–188

Contents lists available at ScienceDirect

Acta Astronautica

journal homepage: www.elsevier.com/locate/actaastro

Experimental validation of liquid hydrocarbon based fuel rich gas generator for high speed propulsion systems

M. Raghavendra Rao[a], G. Amba Prasad Rao[b], Avanish Kumar[a,*]

[a] Directorate of Liquid Propulsion, Defence Research & Development Laboratory (DRDL), Hyderabad, India
[b] Department of Mechanical Engineering, National Institute of Technology, Warangal, India

ARTICLE INFO

Keywords:
Dump combustor
DCR
Hypersonic
Gas generator
Subsonic combustion

ABSTRACT

For long duration hypersonic flight vehicles, research on high speed air-breathing propulsion systems has been progressing across the world for the past few decades. Ramjets/Scramjets fueled with hydrogen/liquid hydrocarbon fuels are the propulsion systems considered for different regimes of flight envelope. Dual Combustion Ramjet (DCR) engine is a prospective candidate for one of such kind of applications, where the engine is expected to work for a wider range of flight Mach number regime. It has a fuel rich subsonic dump combustor and a supersonic combustor, which work in tandem. In the present work, extensive experimental and analytical work has been carried out to develop a fuel rich gas generator often called as dump combustor suitable for operation from 20 to 28 km altitude and in the range of 4–6 flight Mach number. Connect pipe mode testing has been carried out by varying the throat area of dump combustor for Mach 4 conditions. Tests have been carried out with Jet-A fuel at different equivalence ratio and with fuel injection in different combination and stages. Fuel injection scheme used here is of shower head type in intake arm and a single simplex swirler with film cooling holes in the dump combustor. Study has been also carried out by varying the location of swirler along the combustor length. Combustor air entry conditions are simulated using H_2–O_2 based air heater and a test bed nozzle. An exhaustive amount of tests have been carried out to establish condition suitable for consistent ignition & sustained combustion in this highly fuel rich condition. A One dimensional (1D) mathematical model with NASA CEA interface has been developed to predict & compare the test performance. Sustained ignition is achieved for fuel flow rate of 0.8 kg/s and at an equivalence ratio of 0.8–0.9.

1. Introduction

High speed air-breathing propulsion systems are currently prospective candidate for flight vehicles operating in hypersonic regime. They can be operated over a wide range of flight Mach numbers by using multiple integrated propulsion systems. Dual combustion ramjet is a possible viable option for Liquid hydrocarbon fueled based vehicle operating up to 7 Mach number. This concept has been proposed first by Billig-Waltrup-Stocbridge [1] for volume limited hypersonic missiles. A review of past & current research in liquid fueled supersonic combustors has also been provided by Waltrup [2,3] who also emphasized the need of DCR and the role it would play in future. A vast review of emergence of different kind of scramjet engine technologies in different countries have been given by Curran [4] and Fry [5] and they also emphasized DCR's role as a promising and realistic candidate in enabling long duration hypersonic flights. It can be used in cruising mode alone or for both boost & cruising. Tan et al. [6] have carried out extensive experimental work in direct connected mode to evaluate DCR performance in flight Mach number range of 4–6. DCR operated in two combustion modes i.e. purely subsonic mode in Mach 4 condition and central subsonic & peripheral supersonic mode in Mach 6 condition. Tan & Wang [7] further carried out freejet experimental investigation on a full-size DCR focusing on thrust & specific impulse. They proposed a modified DCR with cavity and systematically investigated the effect of equivalence ratio, angle of attack and flight Mach number on its performance.

DCR has a fuel-rich subsonic dump combustor where complete fuel is partially cracked into smaller molecular species by mixing with air from subsonic intake and this partially cracked fuel subsequently mixes and burns efficiently with the peripheral air from supersonic intake in main combustor. Such a dual propulsion system employs the best features of both ramjet & scramjet in order to achieve stable combustion, higher performance at low Mach numbers and more convenient cooling of the wall. The schematic of dual combustion ramjet propulsion system

* Corresponding author.
E-mail address: avanish.nitw@gmail.com (A. Kumar).

https://doi.org/10.1016/j.actaastro.2020.05.009
Received 21 April 2020; Received in revised form 1 May 2020; Accepted 5 May 2020
Available online 11 May 2020

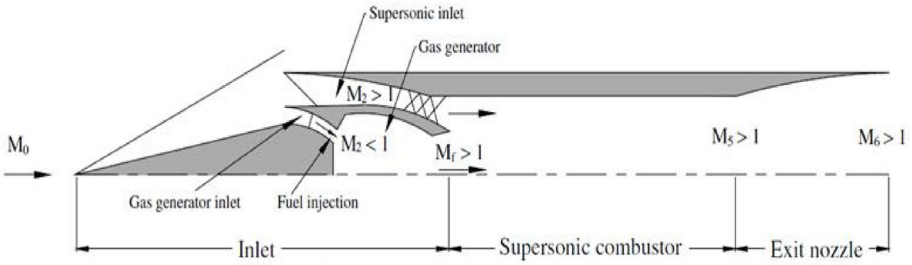

Fig. 1. Dual combustion ramjet engine schematic [8].

is shown in Fig. 1. The major components are supersonic & subsonic intake, fuel rich gas generator/dump combustor, supersonic combustor and exit nozzle. Typically one-fourth of total captured air is diffused through a subsonic inlet to dump combustor. The fuel rich exhaust gases enter the supersonic combustor where it undergoes secondary combustion in supersonic flow. The dump combustor aids in easier ignition & more stable combustion, higher performance at low Mach number. It helps in achieving a wider range of operating flight Mach number (typically 3.5–7) with hydrocarbon based fuel system. The upper limit is due to energy consumption by dissociating and ionizing species at elevated temperature, which cannot be compensated for by additional fuel as in the case of a diatomic gas such as hydrogen.

In gas generator, liquid fuel injection into heated air stream, mixture formation, ignition and combustion need adequate modeling of evaporation. Combustion of mostly widespread hydrocarbon fuels takes place in a gas-phase regime. Thus, evaporation of fuel from the surface of droplets is one of the limiting factors for non-uniform reacting mixtures. Betelin and Smirnov et al. [9,10] have carried out modeling and simulation on evaporation and ignition of droplets in heated atmosphere of combustion chambers. They have done extensive investigation of process of non-equilibrium evaporation of small droplets with streaming flows. The lifetime for single evaporating droplet could be several times longer under non-equilibrium conditions as compared with equilibrium ones. They distinguished two scenarios for droplet heating and evaporation in a heated air flow i.e. small droplets undergo successively heating, then cooling due to heat losses for evaporation, and then rapid heating till the end of their lifetime while larger droplets could directly be heated up to a critical temperature and then evaporate rapidly. Thus, atomization affects droplet lifetime. They also concluded that fuel spray injection & self ignition in a heated air flow has three characteristic stages. At the first stage of jet injection, droplets evaporate rapidly thus cooling the gas at injection point, the liquid jet is very short and changes for a vapor jet. At second stage liquid jet is becoming longer, because evaporation rate decreases due to decrease of temperature. But combustion of fuel vapor begins which brings to increase of heat flux to droplets and accelerates evaporation. The length of the liquid jet decreases again and remains constant slightly oscillating.

N. N. Smirnov et al. [11] have also done theoretical investigations of combustion and detonation initiation in heterogeneous polydispersed mixtures using deterministic methods of continuous mechanics of multiphase flows to determine the mean values of parameters of the gaseous phase and stochastic methods to describe the evolution of polydispersed particles in it and fluctuations of parameters. They have carried out numerical investigations of detonation initiation in dispersed hydrocarbon fuel–air mixtures after mild ignition via DDT and by shock waves of different intensities were performed in tubes of cylindrical geometry.

Several geometrical and flow parameters could influence the efficiency and the thrust produced by the ducted rocket. These include the dome height, angle of side arms, and location of the fuel injector, fuel-air ratio, combustor pressure and dimension.

Stull & Craig [12] investigated dual inlet side dump combustor using liquid fuel injection. The combustion performance at different dome height (varying from 0″ to 4”), inlet angles (30°, 45°and 60°) and inlet air temperature were studied. They also investigated the effect of pressure oscillations in combustor on its performance.

Vanka et al. [13,14] studied and made calculations to examine the effect of mixing, chemical reaction and flow field development in reacting flow. They observed that with increase of dome length, the combustion efficiency increases. Also, steeping the inlet arm increases the mixing. The location of the fuel injector also affects the combustion efficiency. The eccentrically placed fuel injector system gave better results than the one with concentric fuel injector.

Brophy & Hawk [15] conducted experiments on flow visualization of four inlet configuration ducted rocket engine. The complex mixing patterns within the dome head region of the combustors exhibited a strong dependence on dome height, momentum ratios and inlet flow angles. Six combustors have been evaluated. Three of the combustors had the inlet flow inlets at the same axial station. The remaining three had one inlet staggered 1.5 inlet diameters downstream of the upstream inlet flow. All were investigated up to a Reynolds number of 5.5×10^5. The mass flow ratio and momentum ratio were varied between 10 to 60 and 4.58 to 2.58 respectively.

The dump combustors do not contain conventional flame holders. Here the combustion performance depends on recirculation region formed in the dome region.

Major parameters on which mixing and flame holding depends are –

1. Inlet flow angle,
2. Dome height and
3. Momentum ratio.

Higher the inlet flow angle (i.e., 90° > 60° > 45° > 30°) the better is recirculation, mixing & flame holding as the residence time increases. However, dump losses increases with increasing inlet flow angle. For high momentum ratio (i.e. air to fuel momentum ratio), the flow fields follow a passive recirculation regime whereas for low momentum ratio, the fuel jet partially penetrates the inlet flow column & bifurcate into 2 branches. One deflects towards the wall and the other towards the stagnation point of the inlet jets.

For the current study, dump combustor with two inlet configuration with an inlet angle of 40 deg has been used. An analytical model with NASA CEA [16] interface has been developed to predict the combustor performance for the given combustor size and flow rates. NASA Chemical Equilibrium with Applications (CEA) is a computer program for calculation of chemical equilibrium compositions and properties of complex mixtures developed by Gordon and McBride. And, subsequently series of experiments have been carried out by varying different parameters in order to achieve sustained ignition and stable combustion. The details of model & experiments are provided in subsequent sections.

2. Analytical model

To understand the physics of complex systems, it is necessary to predict its performance qualitatively in the early stages of design. This

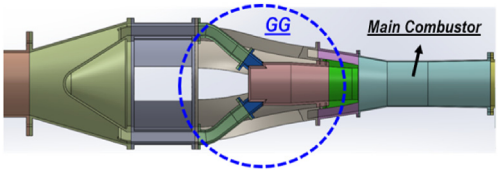

Fig. 2. Dump combustor configuration.

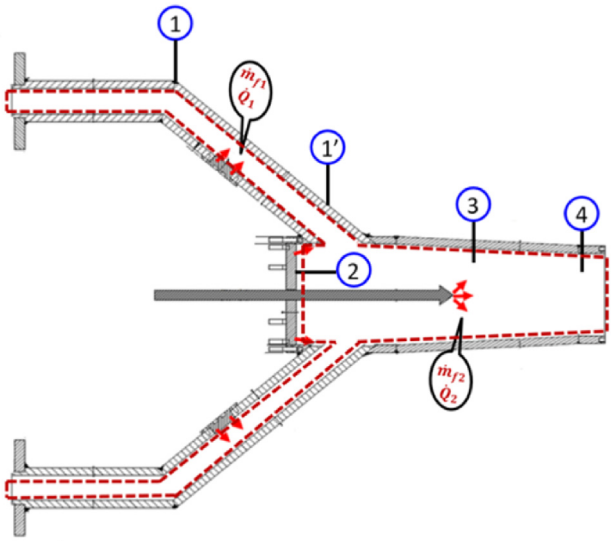

Fig. 3. Dump combustor control volume.

enables the development of concept into reality. Accurate results may be obtained from full scale analysis (CFD Analysis), however it needs higher computational resources, consume large time and also the underlying physics cannot be completely revealed. In this scenario a 1d model developed with experimentally established correlations and reasonable assumptions from basic laws can be highly useful.

One-Dimensional model has been developed to predict the performance of Dump combustor. The control volume considered for the model is shown in Figs. 2 and 3. It is assumed that fuel is injected in two steps i.e.in intake arms and in the combustor as shown for proper mixing of fuel and air and to maintain constant temperature. For model, intake arm equivalent cross-section area is taken for analysis. The equivalent model for the control volume considered is shown in Fig. 4. Here the location descriptions are as follows:

Station1: Intake exit location
Station1': Combustor entry location
Station 2: Injector head location
Station 3: Location after central swirl
Station 4: Upstream of Throat location

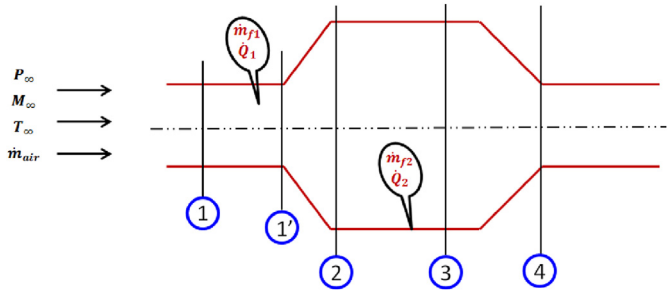

Fig. 4. Equivalent control volume for model analysis.

The physical processes occurring in dump combustors mainly are as follows:

1 – 1': Heat addition @ step 1 (Rayleigh flow)
1 ' – 2: Effect of area variation on Flow properties
2 – 3: Heat addition @ step 2 (Rayleigh flow)
3 – 4: Effect of area variation on Flow properties
4: Choking @ throat

And the model assumptions are as follows:

1. Control volume analysis
2. Steady state one dimensional fluid flow
3. Calorically perfect gas
4. Frictional losses are negligible
5. Stagnation temperature doesn't change with area

Governing equations are developed using conservation of mass, momentum & energy [17–20]. Heat addition is assumed to be a point heat addition and chemical reactions between Fuel and air are calculated using NASA CEA with equilibrium combustion assumption. Chemical species obtained from step1 heat addition is used as oxidiser for step 2 fuel addition. The two main processes involved are Rayleigh flow and flow with area change. It can be observed that the heat addition takes place in Rayleigh flow.

Total pressure & static temperature at station 1 is given by,

$$P_{01} = RF_p \cdot P_{00} \tag{1}$$

$$T_1 = RF_t \cdot T_0 \tag{2}$$

Here, recovery factor is estimated and provided by intake calculations.

Mach number at intake exit is given by,

$$\dot{m}_{air} = A_1 \cdot M_1 \cdot P_{01} \cdot \left(\frac{\gamma}{R \cdot T_{01}}\right)^{0.5} \left(1 + \frac{\gamma - 1}{2} \cdot M_1^2\right)^{\frac{-(\gamma+1)}{2\cdot(\gamma-1)}} \tag{3}$$

Here, A_1, M_1, P_{01}, T_{01}, γ, R are area, Mach number, total pressure, temperature, specific heat ratio & universal gas constant respectively.

Static pressure & total temperature at intake exit are given using gas dynamic relations for stagnation condition,

$$P_1 = \frac{P_{01}}{\left(1 + \frac{\gamma-1}{2} \cdot M_1^2\right)^{\frac{\gamma}{(\gamma-1)}}} \tag{4}$$

$$T_{01} = T_1 \cdot \left(1 + \frac{\gamma - 1}{2} \cdot M_1^2\right) \tag{5}$$

Flow properties between 1 & 1' are given using Rayleigh heat addition relations. The stream thrust per unit area by using momentum conservation equation is given by,

$$P_1 \cdot (1 + \gamma \cdot M_1^2) = P_{1p} \cdot (1 + \gamma_1 \cdot M_{1p}^2) \tag{6}$$

Continuity equation for the flow of a perfect gas in a duct is given by,

$$\dot{m} = \rho \cdot A \cdot V = A \cdot p \cdot M \left(\frac{\gamma}{R \cdot t}\right)^{\frac{1}{2}} \tag{7}$$

For a constant area duct, equation reduces to,

$$\frac{p_{1n} M_1}{\sqrt{t_1}} = \frac{p_{1pn} M_{1p}}{\sqrt{t_{1p}}} \tag{8}$$

Total temperature change in a Rayleigh heat addition is given by using stagnation state relation,

$$\frac{T_{01}}{T_{01p}} = \frac{t_1 \cdot \left(1 + \frac{\gamma - 1}{2} \cdot M_1^2\right)}{t_{1p} \cdot \left(1 + \frac{\gamma_1 - 1}{2} \cdot M_{1p}^2\right)} \tag{9}$$

This equation can be modified using continuity relation in terms of Mach number & temperature as given below,

$$\frac{T_{01}}{T_{01p}} = \frac{M_1^2 \cdot (1 + \gamma_1 \cdot M_{1p}^2)^2 \cdot \left(1 + \frac{\gamma - 1}{2} \cdot M_1^2\right)}{M_{1p}^2 \cdot (1 + \gamma \cdot M_1^2)^2 \cdot \left(1 + \frac{\gamma_1 - 1}{2} \cdot M_{1p}^2\right)} \tag{10}$$

The above relation is used to find flow Mach number after heat addition process is completed at location 1'. For a fixed inlet flow condition, Mach number variation due to heat addition & temperature rise for a subsonic flow can never exceed sonic value i.e.

$$\frac{T_{01}}{T^*} = \frac{2 \cdot M_1^2 \cdot (1 + \gamma_1) \cdot \left(1 + \frac{\gamma - 1}{2} \cdot M_1^2\right)}{(1 + \gamma \cdot M_1^2)^2} \leq 1 \tag{11}$$

At station 1p,

$$\frac{T_{0P}}{T^*} = \frac{T_{01}}{T^*} \cdot \frac{T_{01p}}{T_{01}} \tag{12}$$

Based on the flow Mach number, properties are calculated using stagnation state relations.

Between station 1' & 2, effect of area change is considered for flow parameters estimation. Continuity equation between 1' & 2 is given by,

$$\rho_{1p} \cdot U_{1p} \cdot A_{1p} = \rho_2 \cdot U_2 \cdot A_2 \tag{13}$$

Stream thrust relation using momentum conservation equation between 1' & 2 is given by,

$$A_{1p} \cdot (P_{1p} + \rho_{1p} \cdot U_{1p}^2) + P_{1p} \cdot (A_2 - A_{1p}) = A_2 \cdot (P_2 + \rho_2 \cdot U_2^2) \tag{14}$$

Stagnation temperature relation for station2,

$$T_{02} = T_2 + \frac{U_2^2}{2 \cdot C_p} \tag{15}$$

Total temperature is assumed to be constant as flow is considered to be inviscid i.e. T01p = T02.

Ideal gas relation is given by,

$$P_2 = \rho_2 \cdot R_1 \cdot T_2 \tag{16}$$

Using the above four relations, properties at station 2 are calculated. Between station 2 & 3, flow properties are estimated using the similar relations used for station 1 & 1'. Between station 3 & 4, flow properties are estimated using similar relations used for station 1' & 2.

The model input for one of the simulated case is given in Table 1 and model output is plotted in Figs. 5–7. Entry air temperature is 806 K.

From Fig. 5, it can be observed that first rise in temperature occurs due to combustion in intake arm. Second rise in temperature occurs because of combustion between injected fuel in step 2 and gas products coming from intake arm. Total temperature remains constant after that and Static temperature falls because of flow acceleration in the converging duct.

From Fig. 6, it can be observed that pressure is constant in intake arm. First rise in pressure occurs because of step increase in area at the entry of main combustor. After combustion in second step, pressure starts falling because of decreasing area.

From Fig. 7, it can be observed that flow Mach number decreases at entry to main combustor due to step rise in duct flow area. And it starts rising, when duct area starts converging and reaches sonic value at the throat. This is exactly what happens when flow is subsonic. Flow accelerates in converging area.

Table 1
Model inputs.

Parameters	Value
Air flow rate	3.536 kg/s
Fuel flow rate	0.836 kg/s
Step1	0.204 kg/s
Step2	0.632 kg/s
Fuel initial temperature	298 K
Gama	1.4
R	287 kJ/kg
Intake exit conditions	
Total pressure	3.8 bar
Static pressure	3.6 bar
Static temperature	806K

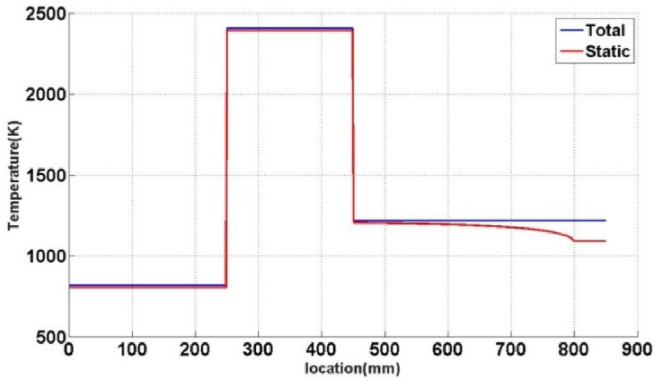

Fig. 5. Predicted axial variation of total & static temperature in dump combustor.

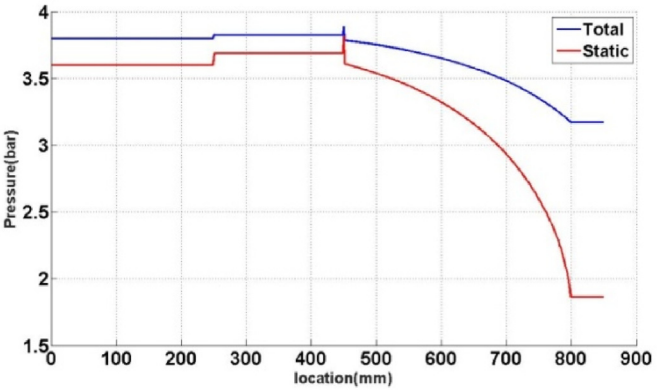

Fig. 6. Predicted axial variation of total & static pressure in dump combustor.

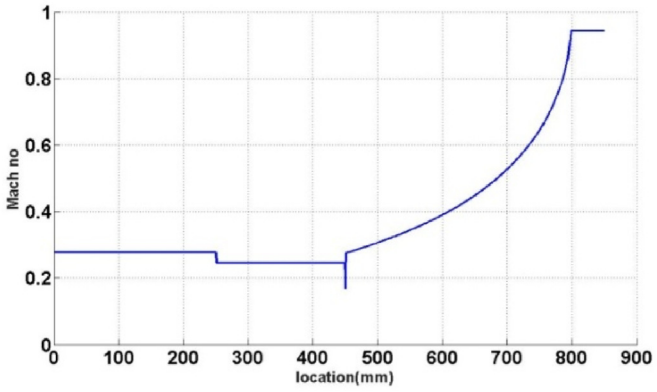

Fig. 7. Predicted axial variation of flow Mach number in dump combustor.

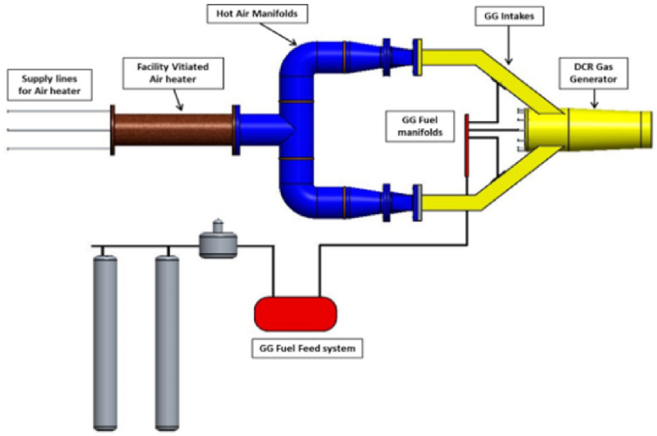

Fig. 8. Test set up layout.

3. Experimental studies

Experimental testing on dump combustor has been carried out in a connect pipe mode facility. The test layout is shown in Fig. 8. Fuel is supplied through fuel feed system. Combustor entry air flow condition is simulated using vitiated air heater. Heated air flows through two intake arms and gets dumped in dump combustor. Instrumented combustor hardware is shown in Fig. 9. There are 3 sets of injectors. Two sets of similar type plain orifice injectors are located in the intake arm and the second set of single swirl type is located in dump combustor. The location of injectors is shown in Fig. 10. A fraction of fuel is injected near the combustor wall in order to cover it by fuel film. The mechanism of liquid film evaporation & boiling is different and has been studied extensively by Tyurenkova et al. [21,22]. They have assumed fuel gasification and gas phase chemical reacting in a diffusion flame. Regression rate of the material surface in the turbulent and laminar flow regimes has been carried out for a hybrid rocket motor. An analytical model of film cooling for liquid rocket engine [23] can also be used to study the wall cooling mechanism. This model has been used for preliminary work. A detailed analysis will be carried out subsequently as the current focus was to establish consistent ignition & stable combustion in gas generator.

Instrumentation locations are shown in Fig. 11 and details are given in Table 2. Data sampling rate was 2 kHz and bandwidth was 1 kHz.

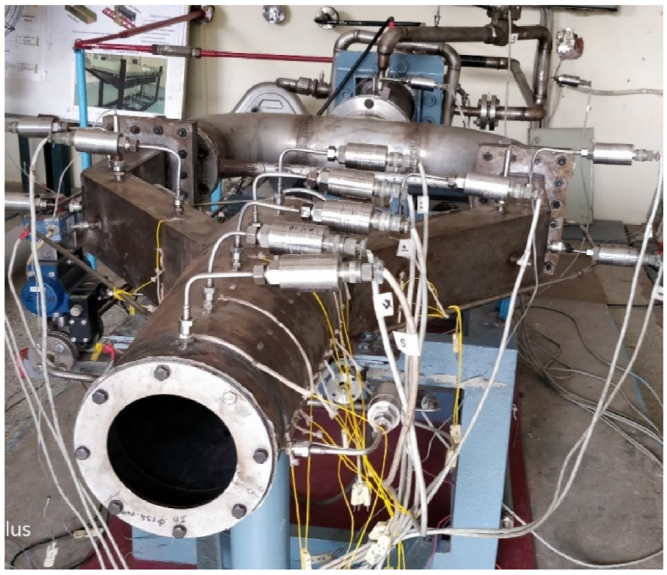

Fig. 9. Instrumented Combustor hardware.

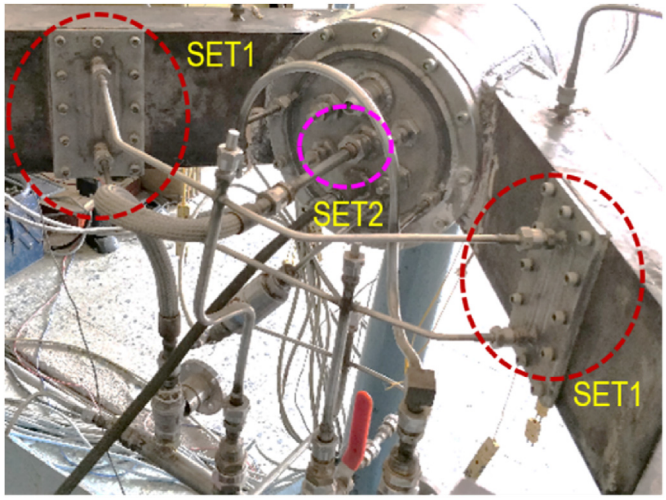

Fig. 10. Injector location in combustor.

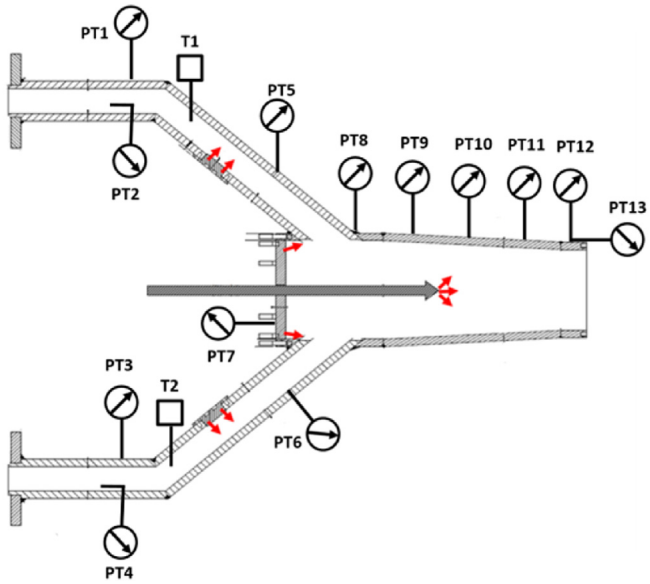

Fig. 11. Pressure & temperature sensor locations in combustor.

Table 2
Instrumentation details.

S No	Instrumentation
1	Air Inlet1 Entry Static Pr. (PT1)
2	Air Inlet1 Entry Total Pr. (PT2)
3	Air Inlet2 Entry Static Pr. (PT3)
4	Air Inlet2 Entry Total Pr. (PT4)
5	Air Exit1 Static Pr. (PT5)
6	Air Exit2 Static Pr. (PT6)
7	Injector Head Pr. (PT7)
8	GG1 Pr. (PT8)
9	GG2 Pr. (PT9)
10	GG3 Pr. (PT10)
11	GG4 Pr. (PT11)
12	Noz1 Pr.(PT12)
13	Noz2 Pr.(PT13)
14	Intake Air Temperature (T1)
15	Intake Air Temperature (T2)
16	Turbine flow meter

The uncertainties in instrumentation measurement are given in Table 3. Each type sensors are pre-calibrated before each test. End to end

Table 3
Uncertainties in measurement.

	Sensors	Type	Make	Uncertainty (± % of full scale)
1	Pressure sensor	Resistance type strain gauge sensors	Sensotech/Honeywell	± 0.2524
2	Temperature sensor	B - type for 600K to 1800 K K-type for RT to 1200 K	Omega	± 1
3	Flow rate sensor	Turbine flow meters	Flow Technologies	± 0.5
4	Data acquisition system	…	National Instruments	± 0.07
5	Signal conditioning unit	…	…	± 0.01
6	Power supply unit	…	…	± 0.016

Table 4
Test firing sequence (Time in Seconds).

	System	ON	OFF
1	Air	0	40
2	Oxygen	4	18
3	Heater Spark igniter	5	9
4	Main Hydrogen	7	18
5	Fuel	9	18
6	GG Spark igniter	11	16
7	GG Pyro (Manual)	13	16

calibration is carried out before each test using dry runs and following a standard operating procedure in order to ensure accuracy & correctness of measure data. The test firing sequence in unit of second is given in Table 4. Ignition is initiated using spark igniter & pyro igniter firing.

Test matrix is tabulated in Table 5. In run1 combined injection of fuel from intake as well as central swirl was done. Total fuel flow rate simulated was 700 g/s approximately. However, there was no ignition. In 2nd run, H_2 from heater was allowed to enter combustion chamber unburnt and heater combustion was initiated once the ignition in combustor was sustained. Sustained ignition was achieved. In 3rd run, injectors in intake arm were only switched on then pyro was fired, sustained ignition was achieved. Combustion happened at equivalence ratio 1 in intake. In 4th run, staged fuel injection was carried out. Injectors in intake arm were switched on first and then pyro was fired. After achieving ignition, central swirl was switched ON and ignition sustained in the combustor. Run 1 to 4 were carried out with total fuel flow rate of ~700 g/s except run3 which was with ~360 g/s mass flow rate of fuel. Run 5 & 6 were carried out with total fuel flow rate of ~800 g/s. However, no ignition occurred in combustor. Equivalence ratio in intake was ~1.2.

So, next set up test was planned with lower equivalence ratio of the order of 0.8–0.9 in the intake arm. Fuel feed system was recalibrated to achieve the desired equivalence ratio and fuel flow rate in the system. In run 7, staged fuel injection was carried out with equivalence ratio of ~0.85 in the intake arm and total fuel flow rate of ~800 g/s. Central swirl was switched on once ignition occurred in the GG. Run 8 & 9 were carried out with simultaneous fuel injection from intake arm as well as central swirl. Pyro was fired next and sustained ignition was achieved in the combustor. Test data plots are shown for run 8 case from Figs. 12–17. Pressure plots are shown from air heater chamber to exit of gas generator. Fuel (Jet-A) feed line pressures are also shown. Heater mass flow rates as well as Jet-A flow rates have also been plotted. Ground testing of combustor for run 8 is shown in Fig. 17. Yellow flame at combustor exit shows highly fuel rich burning of fuel and bluish flame in the plume shows its reaction with ambient air.

Table 5
Test matrix.

S NO.	Configuration	Remarks
RUN1	Fuel injection simultaneously (~700 g/s) 1. Intake injection (~220 g/s) 2. Film cooling injection(~120 g/s) 3. Central swirl injection(~360 g/s) 4. 100 DQ pyro for ignition initiation	No ignition
RUN2	Fuel injection simultaneously (~700 g/s) 1. Intake injection 2. Film cooling injection 3. Central swirl injection 4. 100 DQ pyro for ignition initiation 5. Heater ignition after 3 s pyro firing	Ignition occurred. H_2 from the heater aided in ignition
RUN3	Staged fuel injection (~360 g/s) 1. Intake + Film cooling injection 2. 100 DQ pyro for ignition initiation 3. No – Central swirl injection	Ignition Occurred
RUN4	Staged fuel injection (~700 g/s) 1. Intake + Film cooling injection 2. 100 DQ pyro for ignition initiation 3. Central swirl injection	Ignition Occurred
RUN5&6	Staged fuel injection (~800 g/s) 1. Intake + Film cooling injection 2. 100 DQ pyro for ignition initiation 3. Central swirl injection	No ignition Intake eqv.ratio~1.2
RUN7	Staged fuel injection (~800 g/s) 1. Intake + Film cooling injection 2. 100 DQ pyro for ignition initiation 3. Central swirl injection	Ignition Intake eqv.ratio ~0.85
RUN8&9	Combined fuel injection (~800 g/s) 1. Intake + Film cooling inj. + Central swirl inj. 2. 100 DQ pyro for ignition initiation	Ignition

4. Results and discussion

Test data has been analyzed. Intake entry total & static pressures data are given in Table 6. Average flow Mach number at intake exit is less than 0.3 for reactive cases. Average pressure has been considered for flow Mach number estimation. Mach number is estimated assuming stagnation condition for flow. Average heater & intake entry temperature is given in Table 7. Heater average temperature is of the order of 1160 K and intake entry temperature is of the order of 810 K for reactive cases.

Heater mass flow rate & Jet-A flow rates are given for each run in Table 8. Average total mass flow rate is of the order of 3.5 kg/s except run7 where it was slightly higher. Total mass flow rate consists of Air, O_2 & H_2 and mass fraction of each component is of the order of 91.3,8 & 0.7% respectively. Equivalence ratio for intake arm & its global value is also given in Table 8. Equivalence ratio is calculated in the following ways:

$$\phi = \frac{\left(\frac{O}{F}\right)_{stoich}}{\left(\frac{O}{F}\right)_{actual}} \quad (17)$$

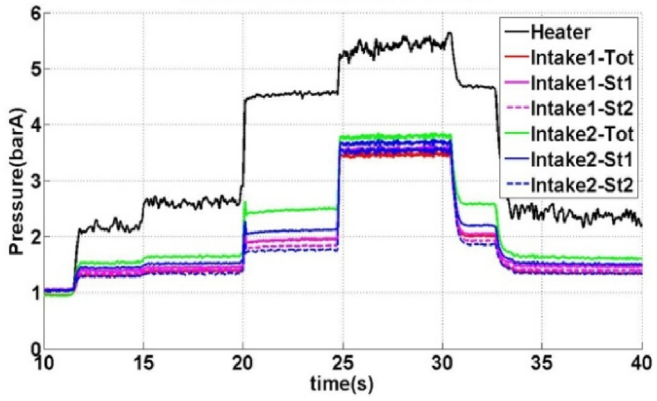

Fig. 12. Pressure plot from heater to intake arm.

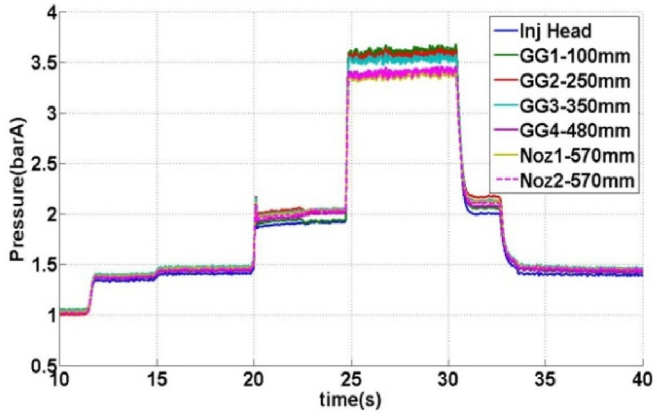

Fig. 13. Axial pressure plot in combustor from head end to nozzle exit.

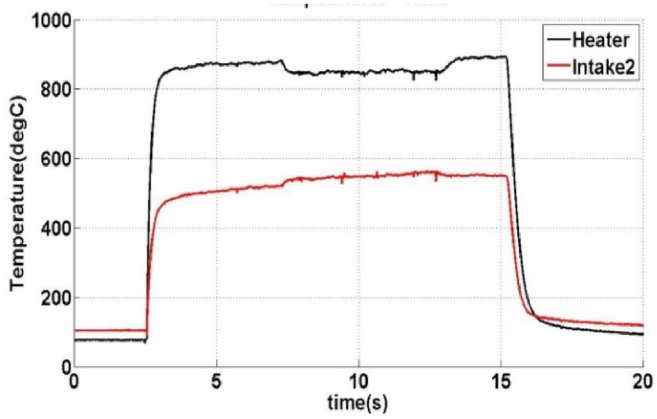

Fig. 14. Air temperature in heater and intake arm.

Here, stoichiometric O/F ratio for Jet-A fuel & air is 14.66.

For Cstar calculation, combustor achieved pressure from test data is used and combustor throat diameter is 134 mm. The achieved Cstar for all the runs is given in Table 9. For an equivalence ratio of 3.5, theoretical Cstar for chemical equilibrium is 1058.1 m/s and combustion efficiency achieved is of the order of 98% for this ratio. Cstar is calculated in the following ways:

$$Cstar = \frac{P_{static} \cdot A_t}{mdot} \tag{18}$$

Combustion product species for equilibrium condition is plotted as a function of equivalence ratio using NASA CEA in Fig. 19. For equivalence ratio of the order of 3.5, major species are CO, H2, & C. These are

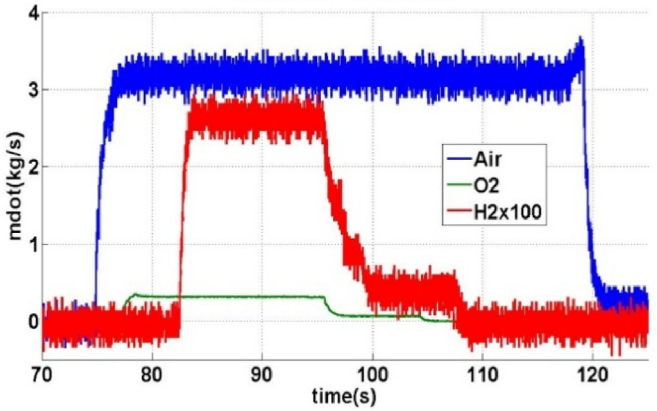

Fig. 15. Heater mass flow rates.

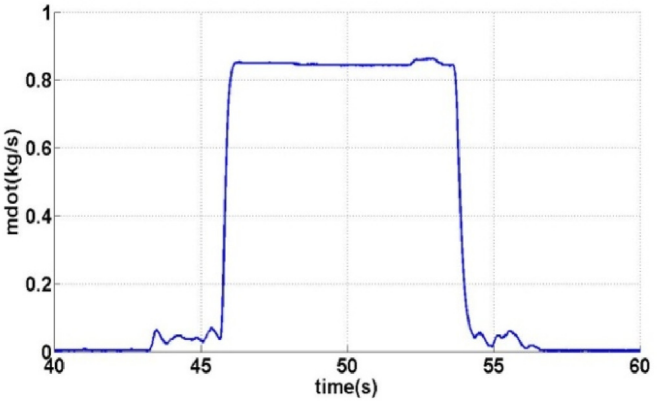

Fig. 16. Jet-A fuel total flow rate in combustor.

Fig. 17. Ground testing of combustor.

Table 6
Intake arm pressures & Mach number.

S No.	**Entry Total Pr (bar)**	Entry **Static Pr (bar)**	Exit **Static Pr (bar)**	M
RUN1	2.4	2.0	1.7	0.72
RUN2	2.4	2.0	1.7	0.72
RUN3	3.8	3.7	3.6	0.28
RUN4	3.6	3.4	3.3	0.35
RUN5	2.4	2.0	1.7	0.72
RUN6	2.4	2.0	1.7	0.72
RUN7	3.7	3.6	3.5	0.28
RUN8	3.7	3.6	3.5	0.28
RUN9	3.8	3.6	3.5	0.34

partially cracked fuel which will undergo secondary combustion in supersonic combustor.

Total 9 runs were taken for the test. As mentioned earlier, the test objective was to achieve sustained ignition. Sustained ignition was achieved for 700 g/s & 800 g/s fuel flow rates. Equivalence ratio

Table 7
Heater outlet & intake entry temperatures.

S No.	Heater Temperature (K)		Intake Entry Temperature(K)	
	Test	Average	Test	Average
RUN1	1133–1180	1156.5	757–824	790.5
RUN2	1095–1164	1129.5	760–787	773.5
RUN3	1143–1178	1160.5	758–819	773.5
RUN4	1128–1173	1150.5	750–833	791.5
RUN5	1136–1171	1153.5	773–838	805.5
RUN6	1140–1177	1158.5	773–833	803.0
RUN7	1166–1181	1173.5	798–821	809.5
RUN8	1156–1161	1158.5	798–827	812.5
RUN9	1144–1157	1150.5	791–820	805.5

Table 8
Achieved flow rates & equivalence ratio of fuel & air.

S NO.	**mdot-air (kg/s)**	Fuel flow rates (kg/s)		Equivalence ratio	
		Intake + FC	Total	Intake arm	Total
RUN1	3.489	0	0.713	–	3.00
RUN2	3.484	–	–	–	–
RUN3	3.476	0.361	–	1.03	–
RUN4	3.495	0.366	0.694	1.04	2.91
RUN5	3.515	0.416	0.813	1.20	3.40
RUN6	3.505	0.414	0.808	1.20	3.40
RUN7	3.726	0.366	0.900	0.80	3.54
RUN8	3.546	0.330	0.845	0.84	3.50
RUN9	3.536	0.330	0.836	0.85	3.46

Table 9
Achieved Cstar based on pressure data.

S No.	Pressure (bar)	Cstar (m/s)
RUN1	1.9	605.5
RUN2	1.9	730.2
RUN3	–	–
RUN4	3.2	1022.9
RUN5	1.9	587.8
RUN6	1.9	589.9
RUN7	3.36	972.6
RUN8	3.4	1036.8
RUN9	3.4	1041.4

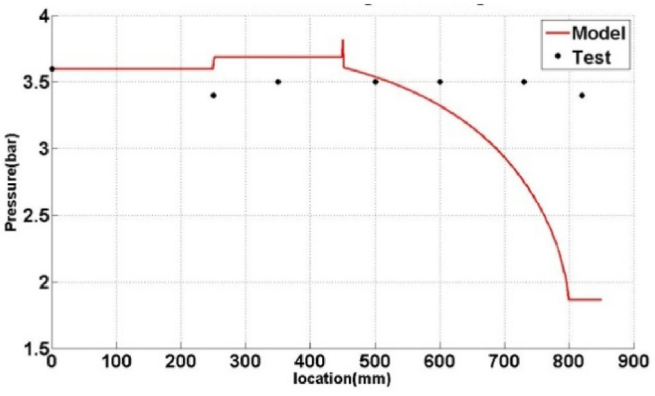

Fig. 18. Comparison of model static pressure with test data.

required in the intake for sustained ignition was of the order 1 for 700 g/s flow rate and 0.8–0.9 for 800 g/s flow rate. There was no ignition for equivalence ratio of 1.2 for 800 g/s flow rate as it can be seen from test data for run 5&6.

In Fig. 18, comparison of static pressure with test results is shown. There is a deviation in pressure between model & test when the duct

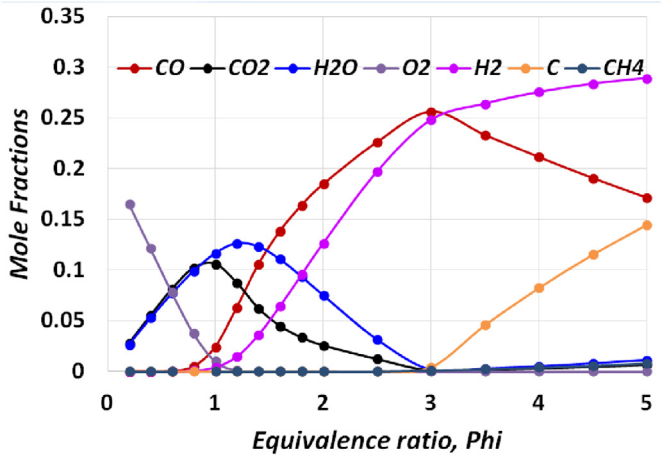

Fig. 19. Combustion products as a function of equivalence ratio using NASA CEA.

starts converging. However, in the model ideal mixing & combustion has been assumed and properties are taken from NASA CEA. In the actual test, finite rate combustion is occurring and presence of other partially cracked products of Jet-A is also possible. The model gives the qualitative picture of process occurring in combustor.

5. Conclusions

The performance and flow field parameters of a dump combustor are investigated through experiments and analytical model using MATLAB. The developed analytical model & extensive experimental data shows that sustained ignition is achieved for a particular equivalence ratio range and fuel flow rates.

Ideal combustion and mixing is assumed in the model which can be improved to reduce the deviation between test results and model data by incorporating reduced order finite rate chemistry model. Also, the stages of liquid droplets breakup, evaporation and mixing with oxidant in heated flow will be added at later stage of study. Detailed & accurate results will be obtained from full scale analysis using CFD.

Resources

This work is supported by Defence Research & Development Laboratory, Hyderabad, India.

Declaration of competing interest

The authors declare that they have no known competing financial interests or personal relationships that could have appeared to influence the work reported in this paper.

References

[1] F.S. Billig, P.J. Waltrup, R.D. Stockbridge, The integral-rocket, dual combustion ramjet: a new propulsion concept, AIAA (1979) 79–7044.
[2] J. Paul, Waltrup, Liquid-fueled supersonic combustion ramjets: a research perspective, J. Propul. Power 3 (6) (1987).
[3] P.J. Waltrup, The dual combustor ramjet: a versatile propulsion system for hypersonic tactical missile applications, AGARD, Airbreathing Propulsion for Missiles and Projectiles, vol. 11, 1992, pp. 5–20 N93-17607.
[4] Edward T. Curran, Scramjet engines: the first forty years, J. Propul. Power 17 (6) (2001).
[5] Ronald S. Fry, A century of ramjet propulsion technology evolution, J. Propul. Power 20 (1) (2004).
[6] Jianguo Tan, Jiping Wu, Zhenguo Wang, Experimental and numerical investigations on flow fields and performance of dual combustion ramjet, Proc IMechE Part G: J. Aero. Eng. 228 (6) (2013).
[7] Jianguo Tan, Yi Wang, Freejet experimental investigation on performance of dual combustion ramjet, J. Propul. Power 31 (1) (2015).

[8] Jong-Ryul Byun, Chul Park, Joon Kwon Oh, Experimental study of combustor–isolator interactions in a dual-combustion ramjet, J. Propul. Power 31 (2) (2015).
[9] V.B. Betelin, N.N. Smirnov, V.F. Nikitin, V.R. Dushin, A.G. Khusnirenko, V.A. Nerchenko, Evaporation and ignition of droplets in combustion chambers modeling and simulation, Acta Astronaut. 70 (2012) 23–35.
[10] N.N. Smirnov, V.B. Betelin, A.G. Khusnirenko, V.F. Nikitin, V.R. Dushin, V.A. Nerchenko, Ignition of fuel sprays by shock wave mathematical modeling and numerical simulation, Acta Astronaut. 87 (2013) 14–29.
[11] Nickolay N. Smirnov, Valeriy F. Nikitin, Vladislav R. Dushin, Yuri G. Filippov, Valentina A. Nerchenko, Javad Khadem, Combustion onset in non-uniform dispersed mixtures, Acta Astronaut. 115 (2015) 94–101.
[12] F.D. Stull, R.R. Craig, G.D. Streby, Investigation of a dual inlet side dump combustor using liquid fuel injection, J. Propul. Power 1 (1) (1985) 83–88.
[13] S.P. Vanka, R.R. Craig, F.D. Stull, Mixing, Chemical Reaction and Flow Field Development in Ducted Rockets, (1985) AIAA-85-1271.
[14] S.P. Vanka, R.R. Craig, F.D. Stull, Mixing, chemical reaction, and flow field development in ducted rockets, J. Propul. Power 2 (4) (1986).
[15] C.M. Brophy, C.W. Hawk, Flow visualization of four-inlet ducted rocket engine configurations, J. Flow Visual. Image Process. 3 (1) (1996).
[16] Gordon Mcbride, Computer Program for Calculation of Complex Chemical Equilibrium Compositions and Applications, NASA reference publication, 1996.
[17] Ascher H. Shapiro, The dynamics & thermodynamics of compressible fluid flow, vol 1, 1953.
[18] Maurice J. Zucrow, Joe D. Hoffman, Gas dyamics 1 (1976).
[19] Heiser and Pratt, Hypersonic Air Breathing Propulsion, AIAA education Series.
[20] Philip G. Hill, Carl R. Peterson, Mechanics and Thermodynamics of Propulsion, second ed., (1992).
[21] Veronika Tyurenkova, Nickolay Smirnov, Mariya Smirnova, Mathematical modeling of burning surface in parallel flow of oxidant, MATEC Web of Conferences 209 (2018) 00007.
[22] V.V. Tyurenkova, M.N. Smirnova, Material combustion in oxidant flows: self-similar solutions, Acta Astronaut. 120 (2016) 129–137.
[23] Avanish Kumar, V. Venkateswarlu, P. Satyaprasad, M. Raghavendra Rao, Development of Film Cooled Thruster for Rocket Application, ASME GT INDIA Conference, 2019, p. 2320.

Aerospace Science and Technology 106 (2020) 106185

Contents lists available at ScienceDirect

Aerospace Science and Technology

www.elsevier.com/locate/aescte

Numerical studies and validation of combustor and annular isolator interactions of hydrocarbon based axisymmetric dual combustion ramjet

M. Raghavendra Rao [a,*], G. Amba Prasad Rao [b], B.V.N. Charyulu [a], Harmeet Singh [a]

[a] Directorate of Liquid Propulsion, Defence Research & Development Laboratory (DRDL), Hyderabad, India
[b] Department of Mechanical Engineering, National Institute of Technology (NIT), Warangal, India

ARTICLE INFO

Article history:
Received 12 May 2020
Received in revised form 31 July 2020
Accepted 31 August 2020
Available online 8 September 2020
Communicated by Kai Liu

Keywords:
Dual Combustion Ramjet
Annular isolator
Scramjet
Turbulence model
Shock train

ABSTRACT

Combustor Intake interactions study is very important for design of Ramjet/Scramjet propulsion systems. High Combustion-induced back pressures make the shock train propagate upstream further and interfere the flow of inlet and the scramjet would unstart. The study has more relevance especially for the propulsion systems like Dual Combustion Ramjet (DCR) due to its wider range operation of Mach number. In this paper, numerical simulation of flow field in an axisymmetric scramjet/ramjet combustor with annular isolator is carried out. Configuration chosen for simulation is Dual Combustion Ramjet, which has a dump subsonic combustor, main supersonic Combustor and an annular isolator. Objective of the work is to evolve a CFD procedure for combustor-isolator interaction and validation of the model with experimental data. Geometry of model DCR is taken from literature for simulations and studies are carried out for Isolator inlet Mach No. 1.79 and 2.23. Favre Averaged equations are solved using Commercial code–ANSYS FLUENT. Premixed composition of air and Kerosene is introduced into dump combustor. Reactive flow is modelled using 7 species and 4 step chemistry. Numerical simulations have been carried out with various turbulence models namely k–ε (Standard), (RNG) k–ε, $k\omega$-Standard, $k\omega$-SST and combustor wall pressures were compared with experimental results. Error in estimation of starting location of Shock train, Maximum Pressure, Average pressure in combustor is compared. (RNG) k–ε predicted shock train location with an error difference of 5% compared to k–ε (Standard). Further, effect on shock train position in isolator with change in gas generator equivalence ratio is also studied for free stream Mach numbers 4 and 5. Shock train moves upstream in Isolator with increase in gas generator equivalence ratio. Various parameters such as Wall static Pressure, Shock train location, length and static pressure along shock train centre, Velocity profile and Combustion efficiency are compared for reactive flow turbulence models.

1. Introduction

Extensive research has been carried out in the field of scramjet engines [1,2] to achieve sustained hypersonic cruise speeds. Unlike subsonic ramjets, fluid flow and combustion inside scramjet engine combustor is supersonic. Due to high speed flow, fuel residence time is of the order of 1 ms which is comparable to ignition delay of most fuels [3]. Performance of scramjet depends on good mixing between fuel and air and minimum pressure loss in combustor. Use of heavy hydrocarbon fuel makes the combustion with low residence time difficult and the use of fixed geometry scramjet designed for specific operating conditions poses problems during off design operation. It is difficult to obtain suitable match of geometry for intake and combustor for large operating range. For a fixed geometry configuration, pressure rise in the combustor depends strongly on fuel control which leads to movement of shock train towards the intake for lower Mach number flight regime leading to intake unstart.

For a typical dual mode hypersonic cruise mission, vehicle is boosted to Mach 4 using a solid rocket booster and then air breathing propulsion takes over. After accelerating to the hyper-

* Corresponding author.
E-mail addresses: ragvzm@gmail.com (M. Raghavendra Rao), mrrao@drdl.drdo.in (G. Amba Prasad Rao).

https://doi.org/10.1016/j.ast.2020.106185
1270-9638/

Nomenclature

ρ	Density
P	Pressure
M	Mach No.
x	Coordinate
u	Velocity
e	Total energy per unit mass
h	Enthalpy
τ	Stress
δ_{ij}	knorker delta
ϕ	Equivalence ratio
Y	Species mass fraction
D	Diffusion coefficient
S	Source term
λ	Thermal conductivity

Subscript

∞	Free stream
SI	Scram Inlet
t	Turbulent
k	Species
gg	Gas Generator

Abbreviations

DMSJ	Dual Mode Scramjet
DCR	Dual Combustion Ramjet
GG	Gas Generator

sonic Mach number (M5 or more), scramjet engine takes over. Hydrocarbon fuel based hypersonic mission is usually operated from 4 to 6 Mach numbers. At lower Mach number, flow inside combustor is subsonic and engine operates in ramjet mode. As vehicle Mach number reaches Mach 6, it is inefficient to operate with subsonic flow [3] in combustor and engine will deliver better performance when operated in scramjet mode. Two concepts are studied worldwide to enhance the performance of engine at off design operation: The Dual Mode Scramjet (DMSJ) and Dual Combustion Ramjet (DCR). In DMSJ, same combustor is used to operate as ramjet (subsonic Combustion) and scramjet (supersonic combustion) [4]. Dual mode scramjets usually have cavity or strut as flame holding devices. Transition of ramjet to scramjet mode is studied numerically by references [5–11]. Zhi-wei Huang et al. [12–17] have numerically studied flame holding with struts, cavity and pilot jet flame with various fuels such as hydrogen, kerosene, ethylene, *n*-heptane. Tian et al. [18] have studied scramjet combustor numerically and experimentally and found the effect of various fuel injection locations on thermal choking position. Malsur Dharavath et al. [19] have carried out simulations on flight size scramjet combustor with ethylene fuel and studied effect of equivalence ratio on combustion and mixing. Jichao Hu et al. [20] have studied wall injection in scramjet combustion experimentally.

DCR concept was first introduced by Billig [21]. DCR is a combination of two ramjet cycles, one with subsonic combustion and another with supersonic. Fig. 1 shows the schematic of axisymmetric DCR. It is more suitable for accelerating flight vehicle between the Mach number ranges of 4 to 6. A typical DCR has a Gas Generator (GG) where entire fuel is injected and operates at fuel rich condition. Flow coming to intake undergoes external compression and then divided into two streams, one goes to gas generator and other goes to main combustor. An annular isolator is essential to avoid interactions between main combustion chamber and intake. Combustion in gas generator produces low molecular products and increases the static pressure. These gases when mix with supersonic air undergoes complete combustion. This pilot flame with low molecular products and enriched radicals enhances ignition and sustained combustion capability in supersonic flow as compared to direct injection of heavy [22,23]. Development of 1-D model provides the preliminary understanding of the system and its characteristics qualitatively. Raghavendra Rao et al. [24] developed a one-dimensional (1-D) mathematical model with NASA CEA interface to predict and compare the test performance of DCR gas generator performance. Numerous tests in connect pipe mode have been carried out using Jet-A fuel and by varying the throat area of gas generator for Mach 4 conditions to establish condition suitable for consistent ignition and sustained combustion with highly fuel rich equivalence ratio. 1-D model and experimental data were correlated. However, CFD studies give more detailed flow field information for such complex reactive systems.

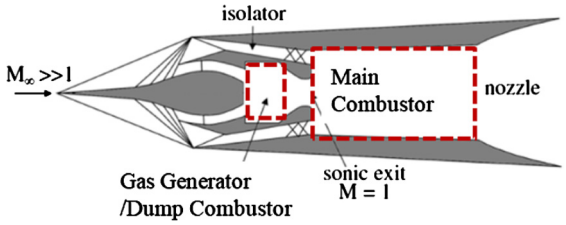

Fig. 1. Schematic of dual combustion Ramjet [1].

As compared to DMSJ, DCR combustion is less investigated. J.A. Schetz et al. [25] have evolved a modular approach to carry out calculations for DCR. Double flame sheet model with chemical equilibrium was adopted in this approach. Liwei Zhang et al. [26] have studied coaxial flow and used LES code to study the effect of splitter plate thickness on flame stabilization and mixing in dual combustion ramjet. According to the research, higher plate thickness leads to better combustion. Jeong Yeol Choi et al. [27] have studied turbulent combustion in DCR with high resolution scheme. Two combustion modes were observed which includes lifting turbulent flame by mixing layer and local thermal choked combustion. Further effect of divergence angle on combustion was studied. Tan et al. [28] investigated flow field in actual dual combustor experimentally and numerically with main focus on combustion efficiency and thrust increment as function of equivalence ratio.

Shock train generates in the isolator to decelerate the supersonic flow with sufficient strength. If the combustion-induced back pressures were big enough to make the shock train propagate upstream further and interfere the flow of inlet, the scramjet would unstart which should be prevented. During the operation of scramjet, the shock train constantly varies its length and structure to match the upstream and downstream conditions. The quality of outflow at the isolator exit has great impacts on the combustion performance since the violent oscillation of shock train may lead to flame oscillation or even flame out. Combustor Intake interactions knowledge is very important for design of Ramjet/Scramjet propulsion systems.

Isolator is a critical component which does not allow shock train to interact with combustion chamber. Worldwide many researchers have numerically studied isolator and shock train phenomena. Zhang et al. [29] numerically investigated and compared effect of isolator shock train with back pressure and combustion. It was found that shock train movement is due to back pressure but is also affected by high temperature which entrains through boundary layer. This temperature shrinks and stretches shock train.

Wei Huang et al. [30] studied three-dimensional scramjet isolator and position of shock train with varying back pressure and increase in divergence angle of isolator. With increase in divergence angle of isolator, it is observed that shock wave transition takes place from oblique shock to normal shock and back to oblique shock. Fei Xing et al. [31] have proposed use of bleed slot for reducing load on isolator. This reduces total pressure loss but also has reducing effect on combustion efficiency. Yubao He et al. [32] have suggested reduction of subsonic region by ejecting cracked gas. This leads to increase on total momentum and suppresses pressure gradient.

Jong-Ryul et al. [33] carried out experiments to study isolator interaction with combustion chamber and evolved correlation for estimating wall static pressure. Experiments simulated flight Mach numbers from 4 to 5, altitude from 20 to 25 km. Isolator entrys Mach No. are 1.8, 2.0, 2.23 for flight Mach No. 4, 4.5, 5 respectively. Liquid hydrocarbon fuel is injected in gas generator at different equivalence ratio varying from 0.0 to 3.0 for all above mentioned conditions. With change in equivalence ratio pressure increase in the combustor and to match pressure combustor pressure, pre-combustion shock train is established in isolator. With increase in equivalence ratio shock train in isolator moves upstream. During study it is concluded that shock train is less affected by isolator inlet Mach number. Experimental work was also compared with existing empirical correlations of Waltrup and Billig's correlation and Stockbridge's correlation. Correlations did not match with experiments for annular isolator. New correlation for DCR is proposed and additional term of equivalence ratio is introduced which was missing in previous correlations.

Stockbridge et al. [34] have carried out similar experiments to evaluate isolator wall pressure rise in annular duct with non-reacting setup. Back pressure is built by blockage of the exit. Numerical simulation was done by using Fluent to solve RANS equations and a two-equation shear stress transport (SST) k–ω model was used as turbulence simulation for predicting the wall pressure distribution of the transverse injection. It was observed that at lower equivalence ratio, weak combustion heat release led to absence of shock train in isolator and increase in static pressure of isolator entrance led to the whole pressure rise. But at higher equivalence ratio, a reverse trend was observed in the pressure variation in isolator and combustor. Lesser the incoming Mach number, shorter was length of the shock train and pressure peak lifted.

Detailed studies of the effect of backward oscillations are carried out by many researchers [35–37]. Wenxin Hou et al. [35] investigated experimentally on shock train self-excited oscillation influenced by background waves occurring within an isolator in a direct-connect wind tunnel using high-speed schlieren technique and high-frequency pressure measurements. Top-Large-Separation, Bottom-Large-Separation, and transition mode of shock train self-excited oscillations were studied. To understand the differences of shock train unsteady behaviours in different modes, the distributions of intermittent region and zero-crossing frequency were compared. For the shock train in a uniform incoming flow and for the shock train influenced by background waves, the Strouhal number range is predicted. It was found that the wall pressure gradient caused by background waves influences the unsteadiness of shock train self-excited oscillation.

Wen Shi et al. [36] investigated the forced oscillations of shock train caused by sinusoidal back pressure perturbations with different amplitudes and frequencies in a hypersonic inlet equipped with translating cowl. Numerical simulations conducted with the application of dynamic mesh method reveal that under sinusoidal back pressure perturbations, the shock train oscillates and propagates upstream as the cowl moves downstream rather than crosses the shock-impact points abruptly with significant migration distance, compared to the result obtained under constant back pressure. Effect of back pressure perturbations on forced oscillations, number of shock impact points crossed by shock train in one cycle and there by the shock train structures variation was studied. In another study, Wen Shi et al. [37] have carried out numerical investigations to study the path dependence characteristic of shock train with the application of dynamic mesh method. Based on the paths of shock train leading edges, it is discovered that the behaviour of shock train is highly related to the variable background waves. The results also reveal that the path dependence characteristic embodies in the abrupt motions, average velocities of shock train, structures of shock train and oscillations. It is concluded that the discrepancies of critical internal contraction ratios that lead to the hysteresis loops in the paths of shock train leading edges; the structures and average velocities of shock train in opposite directions of translating cowl are different in each loop. The shock train would oscillate around the separation bubble, which intensifies the unsteadiness of shock train behaviour.

Lot of research is focused towards rectangular scramjet combustor with strut or cavity flame holding. Very less literature is available on supersonic combustor with gas generator/Pilot flame. Numerical investigation of isolator has been a well-studied for rectangular scramjet combustor but for annular isolator with axisymmetric combustor is still unexplored to that extent. CFD can be a great tool in designing such system as it will reduce developmental efforts.

Present paper evolves CFD procedure to carry out numerical simulations for hydrocarbon fuelled axisymmetric DCR. Various turbulence models such *as k–ε, k–ε (RNG), k–ω and k–ω* (*SST*) are evaluated and numerical procedure has been validated with experimental data. Geometry of model DCR is taken from literature for simulations and studies are carried out for isolator inlet Mach No. 1.79 and 2.23. Favre averaged equations are solved using Commercial code–ANSYS FLUENT. Premixed composition of air and Kerosene is introduced into dump combustor. Reactive flow is modelled using 7 species and 4 step chemistry. Error in estimation of starting location of Shock train, Maximum Pressure, Average pressure in combustor is compared. Effect of gas generator equivalence ratio on combustor pressure and shock train in isolator is also studied.

2. Experimental setup

For the present numerical study experimental setup of Jong-Ryul Byun et al. [33] is taken. The schematic of setup is shown in Fig. 2. In this, DCR experimental set-up was designed with a gas generator, an isolator, and a main combustor. In flight, free stream air is compressed by shock waves in the inlet and then enters main combustor and gas generator. Experiments are conducted in connect pipe mode, where air is heated by a vitiated heater using CH_4 and air. Additional oxygen is added to maintain 21% of O_2 by mole fraction in vitiated air. Heated air gets split in two streams. One stream enters annular plenum and other enters gas generator. Air through Plenum chamber is accelerated to supersonic speeds by annular nozzle and enters isolator from where it goes to main combustor. Air which enters gas generator mixes with Liquid Hydrocarbon Fuel, which enters through fuel injection port. A supersonic nozzle in Gas Generator accelerates the flow to Mach number 1.53. As total pressure and total temperature of air to main combustor and gas generator is same, throat areas of annular nozzle and gas generator are designed such that air splits in the specified ratio of 3:1.

From this literature, two test conditions are chosen for comparison as given in Tables 1 and 2. The experiments were carried for flight Mach numbers from 4.0 to 5.0 for altitude of 20 to 25 km.

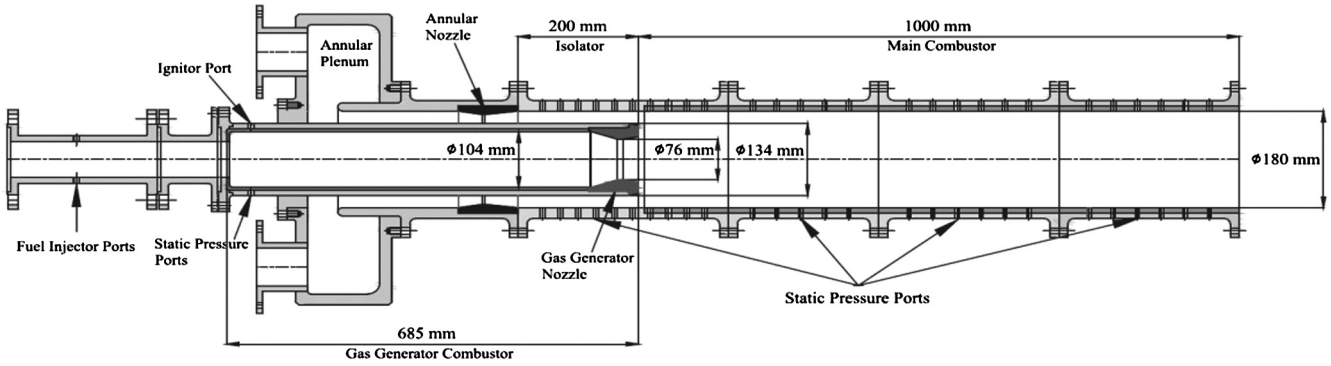

Fig. 2. Schematic of test setup for DCR [33].

Table 1
Test condition for air flow.

Condition	M_∞	M_{SI}	T_t (K)	P_t (kPa)	Total Mass flow rate (kg/s)	Air split ratio
1	4	1.79	925	556	7.71	3
2	5	2.23	1120	610	5.28	2.98

Table 2
Fuel equivalence ratio.

Condition	M_∞	M_{SI}	ϕ_{gg}
1	4	1.79	0.74, 1.24, 2.84
2	5	2.23	1.44, 1.60, 2.64

But Jong-Ryul Byun et al. [33] have considered few more cases in terms of flight Mach number and equivalence ratio.

3. Numerical method

3.1. Governing equations

The Cartesian form of governing equations is given as follows

I. Continuity

$$\frac{\partial}{\partial t}(\rho) + \frac{\partial}{\partial x_i}(\rho u_i) = 0 \tag{1}$$

II. Momentum

$$\frac{\partial}{\partial t}(\rho u_i) + \frac{\partial}{\partial x_i}(\rho u_i u_j) = -\frac{\partial P}{\partial x_i} + \frac{\partial}{\partial x_i}(\tau_{ij}) \tag{2}$$

III. Energy

$$\frac{\partial}{\partial t}(\rho e_{total}) + \frac{\partial}{\partial x_i}(\rho h_{total} u_j) = -\frac{\partial}{\partial x_i}(\tau_{ij} u_i - q_i) \tag{3}$$

τ_{ij} is the stress tensor, q_i is the heat flux

$$\tau_{ij} = (\mu + \mu_t)\left[\frac{\partial u_i}{\partial x_j} + \frac{\partial u_j}{\partial x_i} - \frac{2}{3}\delta_{ij}\frac{\partial u_k}{\partial x_k}\right] - \frac{2}{3}\rho k \delta_{ij}$$

IV. Species transport equation

$$\frac{\partial(\rho Y_k)}{\partial t} + \frac{\partial}{\partial x_i}(\rho u_i Y_k) = -\frac{\partial}{\partial x_i}\left(\rho D_k \frac{\partial Y_k}{\partial x_i}\right) + \dot{\omega}_k \tag{4}$$

$k = 1, 2, \ldots, N$ are the Reacting species.

The flow in combustor has large variations of density, Favre averaging of Navier-Stokes equation is used for solution. In this set of equations density fluctuations are negligible but mean density variation is considered. Thermally perfect gas is assumed.

3.2. Turbulence modelling

As the equations being solved are time averaged, additional terms of Reynold stresses ($-\rho\overline{u_i' u_j'}$) are generated. Turbulence closure is achieved by considering Reynold shear stress related to average velocity gradient by turbulent viscosity, a property of flow. All the turbulence models selected uses Boussinesq model which suggest that like Newton's law of viscosity (shear stress is proportional to shear strain), Reynolds stresses are proportional to mean deformation rate given by

$$\tau_{ij} = -\rho\overline{u_i' u_j'} = \mu_t\left(\frac{\partial \overline{u}_i}{\partial x_j} + \frac{\partial \overline{u}_j}{\partial x_i}\right) - \frac{2}{3}\rho k \delta_{ij} \tag{5}$$

$k = \frac{1}{2}(\overline{u'^2} + \overline{v'^2} + \overline{w'^2})$.

There are different models which can be used for evaluating turbulent viscosity. The common assumption of these models is that the turbulence to be isotropic. For turbulence closures various models such as k–ε, k–ω SST and, k–ε RNG are applied. Turbulence models considered for present analysis are k–ε (Standard wall function) [38], (RNG) k–ε [39], k–ω (Standard) [40], k–ω-SST [41]. Luo et al. [42] suggested that k–ε RNG is most suitable strut based scramjet combustor. Tan et al. [28] have also applied same turbulence model for (DCR) combustor study and found good match with experiments.

a) *k–ε*

The standard two equation model is developed by Launder and Spalding [38]. k is defined as turbulent kinetic energy and ε is dissipation rate. The equations involved are

$$\frac{\partial(\rho k)}{\partial t} + \frac{\partial}{\partial x_i}(\rho k u_i) = \frac{\partial}{\partial x_j}\left[\left(\mu + \frac{\mu_t}{\sigma_k}\right)\frac{\partial k}{\partial x_j}\right] + G_k + G_b - \rho\varepsilon - Y_M + S_k \tag{6}$$

$$\frac{\partial(\rho\varepsilon)}{\partial t} + \frac{\partial}{\partial x_i}(\rho\varepsilon u_i) = \frac{\partial}{\partial x_j}\left[\left(\mu + \frac{\mu_t}{\sigma_k}\right)\frac{\partial \varepsilon}{\partial x_j}\right] + C_{1\varepsilon}\frac{\varepsilon}{k}(G_k + C_{3\varepsilon}G_b) - C_{2\varepsilon}\rho\frac{\varepsilon^2}{k} + S_\varepsilon \tag{7}$$

where, G_K, G_b represent generation of turbulent kinetic energy due to mean velocity gradient and buoyancy respectively. Y_M is Dilatation Dissipation Term to account for compressibility effects in the flow. S_k, S_ε are user defined Source terms. C_μ, σ_k, σ_ε, $C_{1\varepsilon}$, $C_{2\varepsilon}$ are empirical constants.

Turbulent viscosity is given by

$$\mu_t = \frac{\rho C_\mu k^2}{\varepsilon}$$

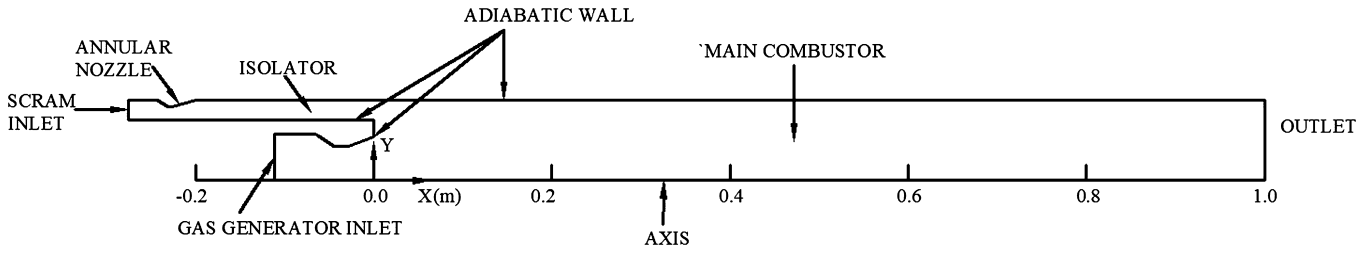

Fig. 3. Flow domain and boundaries for numerical simulation.

b) RNG - *k–ε*

The RNG procedure removes small scales of motion by expressing their effect in terms of large scale motions and modified viscosity.

$$\frac{\partial(\rho k)}{\partial t}+\frac{\partial}{\partial x_i}(\rho k u_i)=\frac{\partial}{\partial x_j}\left[(\mu_{eff})\alpha_k\frac{\partial k}{\partial x_j}\right]+G_k+G_b-\rho\varepsilon-Y_M+S_k \tag{8}$$

$$\frac{\partial(\rho\varepsilon)}{\partial t}+\frac{\partial}{\partial x_i}(\rho\varepsilon u_i)=\frac{\partial}{\partial x_j}\left[(\mu_{eff})\alpha\frac{\partial\varepsilon}{\partial x_j}\right]+C_{1\varepsilon}\frac{\varepsilon}{k}(G_k+C_{3\varepsilon}G_b)-C_{2\varepsilon}\rho\frac{\varepsilon^2}{k}-R+S_\varepsilon \tag{9}$$

$\mu_{eff}=\frac{\rho C_\mu k^2}{\varepsilon}$, C_μ, $C_{1\varepsilon}$, $C_{2\varepsilon}$ are empirical constants.

Following are the major differences between RNG k–ε and k–ε standard turbulence model:

1. α_ε, α_k are evaluated using analytical equations
2. Dissipation rate equation in standard k–ε model is considered to be reason for poor results in large deformation flows. R_ε is added as an additional term in dissipation equation. For weak and moderate strained flows R_ε term is positive. The net numerical result obtained by using RNG is same as standard $k\varepsilon$. But for large strained flows R_ε is negative which increases dissipation rate and reduces turbulent kinetic energy, Hence reduction in turbulent viscosity.

c) *k–ω*

To evaluate dynamic turbulent viscosity, one velocity scale and one length scale is required. In the previous discussion of k–ε model, velocity scale is $\sqrt{k}$ and length scale is $k^{\frac{3}{2}}/\varepsilon$. In $k\omega$ model velocity scale is $\sqrt{k}$ whereas for length scale another variable ω, which is the frequency of turbulence is considered

$$\mu_t=\frac{\rho k}{\omega}$$

$$\frac{\partial(\rho k)}{\partial t}+\frac{\partial}{\partial x_i}(\rho k u_i)=\frac{\partial}{\partial x_j}\left(\Gamma_k\frac{\partial k}{\partial x_j}\right)+G_k-Y_k+S_k \tag{10}$$

$$\frac{\partial(\rho k)}{\partial t}+\frac{\partial}{\partial x_i}(\rho k u_i)=\frac{\partial}{\partial x_j}\left(\Gamma_\omega\frac{\partial k}{\partial x_j}\right)+G_\omega-Y_\omega+S_\omega \tag{11}$$

G_k, G_ω are generation due to velocity gradient. Y_k, Y_ω are dissipation terms and S_k, S_ω are source terms for k and ω.

d) *k–ω* (SST)

Menters [41] SST model is blend of k–ε model and $k\omega$ model. k–ω model performs well near the wall but poor away from wall. It also gets affected by free stream variations. On the other hand k–ε model is not accurate with adverse pressure gradient boundary condition but gives good results away from wall. A blending function is used to have smooth transition of models.

Production limiter is an important feature of SST model, which avoids building up of turbulent kinetic energy in stagnation region. With production limiter results are better in wake region and adverse pressure gradient.

e) Standard wall function

For high Reynolds number the standard k–ε model does not need to be solved up to the wall boundary. The universal behaviour of flow near wall can be considered. For Y^+ between 30 to 500 log law is valid and given by

$$u^+=\frac{U}{u_\tau}=\frac{1}{\kappa}\ln(EY^+) \tag{12}$$

u_τ is friction velocity given by $\sqrt{\tau_w/\rho}$, where Von Karman's constant $\kappa=0.41$, and wall roughness parameter is $E=9.8$.

3.3. Combustion modelling

The reaction rate is determined by chemical kinetic mechanism of Kerosene/Air. It is impossible to apply complete reaction mechanism due to large computation time and single step global reaction over predicts the temperature therefore, a reduced mechanism is applied. Reaction mechanism used by Watanabe et al. [43] and Tan et al. [28] has been used for carrying simulation with kerosene based fuels.

Reaction Mechanism

$$C_{12}H_{23}+6O_2\rightarrow 12CO+11.5H_2 \tag{R1}$$

$$H_2+0.5O_2\rightarrow H_2O \tag{R2}$$

$$CO+0.5O_2\rightarrow CO_2 \tag{R3}$$

$$CO+H_2O\rightarrow CO_2+H_2 \tag{R4}$$

The finite rate/eddy dissipation model is widely used for combustion modelling. Combustion is dependent on mixing and kinetics. For Finite rate/eddy dissipation model if turbulence is low, mixing is slow and it becomes the limiting factor. If turbulence is fast but kinetics is slow then kinetics is limiting factor.

The chemical rate is calculated gas generator incomplete combustion takes place and

$$r=AT^b e^{-\frac{E_a}{RT}} \tag{13}$$

where r is reaction rate coefficient, A Pre-exponential factor, b temperature exponent, E_a is activation energy.

3.4. Solving procedure

A density based solver with 2nd order spatially accurate ROE-FLUX difference splitting scheme is applied. Commercial solver Fluent 13 is used for carrying out simulations (Fig. 3).

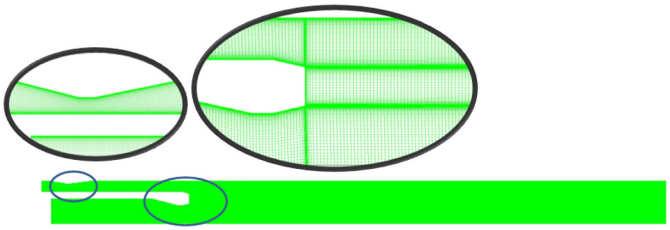

Fig. 4. Grid for simulation.

3.5. Boundary condition

At gas generator inlet and scramjet inlet, mass flow boundary condition as given in Table 1 is applied to maintain the achieved air split ratio for simulation. Total temperature, mass fraction of species is specified. Mixing and evaporation is not accounted in this paper. Premixed mixture is assumed to enter gas generator. All surfaces are assumed to be adiabatic.

Vitiation effect is not considered and therefore only air is assumed to enter from scram inlet. For simulating different Mach number conditions, scram inlet nozzle expansion ratio is changed.

4. Grid structure

Simulations are carried on axisymmetric grid as shown in Fig. 4. Grid independence study is carried out for reacting flow with flow condition 1 ($M_{SI} = 1.79$, $\phi_{gg} = 2.84$) as given in Table 1. RNG k–ε turbulence model with standard wall function is used. Y^+ value along combustor wall and isolator wall is shown in Fig. 5. Grid Independence study is done in two steps. In first step grid is refined in the isolator region, mixing region and gas generator outlet region. Grid near wall is kept unchanged in all grid refinements. Three grids with ratio 1:2:4 are studied. Coarse grid has 0.1 million nodes, Moderate has 0.2 million and fine Grid has 0.4 million nodes. Grid convergence index (GCI) suggested by Roache [44].

$$GCI = \frac{F_s \left| \frac{(f_2 - f_1)}{f_1} \right|}{r^p - 1} \tag{14}$$

where f is the parameter selected for convergence. In present study it is wall static pressure. Subscript 1 and 2 correspond to fine grid and moderate grid. Value of $F_s = 1.25$, $r = 2$, $p = 2$ as suggested by Roache. Maximum error between medium and fine grid is within 2.5%. This analysis indicates that the grid is adequate to capture most of features of the flow and the solution is grid independent. Fig. 6 shows the wall static pressure obtained from three grids. In second step adaptive grid is studied. Moderate grid (0.2 million nodes) is refined based on static pressure gradient. Fig. 7 shows grid refinements for three levels.

5. Results and discussion

Jong-Ryul Byun et al. [33] has performed connect pipe mode experiments on annular isolator with DCR combustor. Isolator entry Mach No. considered are 1.8, 2.0, 2.23 for flight Mach No. 4, 4.5, 5 respectively. Liquid hydrocarbon is injected in gas generator at different equivalence ratio varying from 0.0 to 3.0 for all above mentioned conditions. With change in equivalence ratio pressure increase in the combustor and to match pressure combustor pressure, pre-combustion shock train is established in isolator. With increase in equivalence ratio shock train in isolator moves upstream. From the these experimental studies, two test conditions as given in Tables 1 and 2 are chosen for comparison purpose of validation of the numerically predicted values. The numerical experiments

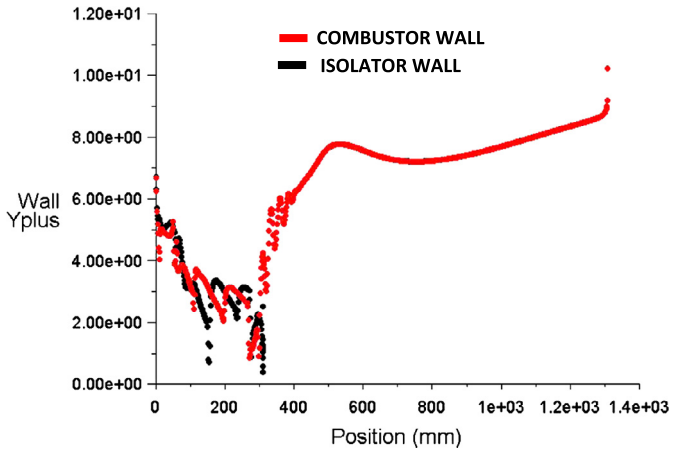

Fig. 5. Y^+ along combustor wall and isolator wall.

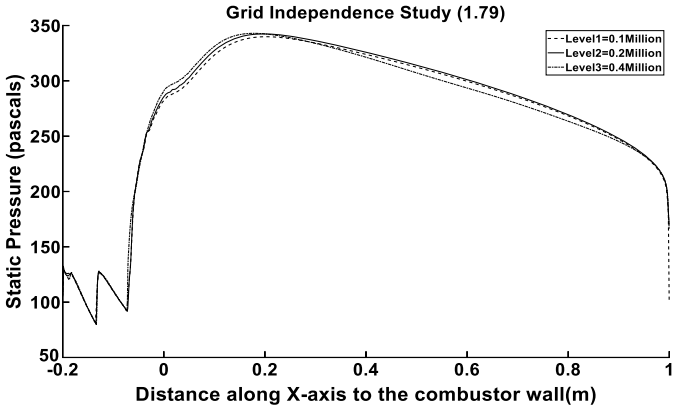

Fig. 6. Wall static pressure for different grids ($M = 1.79$, $\phi = 2.84$).

were carried for flight Mach numbers from 4.0 and 5.0 for altitude of 20 to 25 km. Simulations are carried out in two parts. In first step, numerical procedure is evolved which includes grid independence studies and various turbulence models evaluated for reactive and non-reactive case. These simulations are carried out for conditions given in Table 1.

In part two effect of gas generator equivalence ratio on isolator shock train location, pressure rise and combustion efficiency is studied (Fig. 8).

Fig. 9 shows the schematic of flow field in the combustor. Pressure rise takes place due to combustion in main combustor and to match pressure rise shock train is formed. S_t is the total shock train. This shock train exists in the isolator and moves upstream with rise in pressure. S_o is the length of shock train inside isolator. S_d is shock train length in main combustor.

Fig. 10 shows Mach No., Static pressure, total temperature Contours for M4 condition and equivalence ratio in gas generator, $\phi_{gg} = 2.84$. Different nozzles are used to accelerate flow to achieve required Mach numbers. Nozzle end initiates a weak oblique shock train.

Pressure rise in combustor takes place due to heat addition. Rim dividing supersonic flow and gas generator acts as flame holder. Flame is stabilized when local velocity of flow is equal to normal flame propagation velocity. Two counter rotating recirculation zones are created; one is driven by flow coming out of gas generator and other coming from intake. The static pressure rise (shown in Fig. 10) is observed much before the flame holder. This is due to shock train formed to match the pressure rise due to combustion. This shock train is often referred as pre combustion shock train.

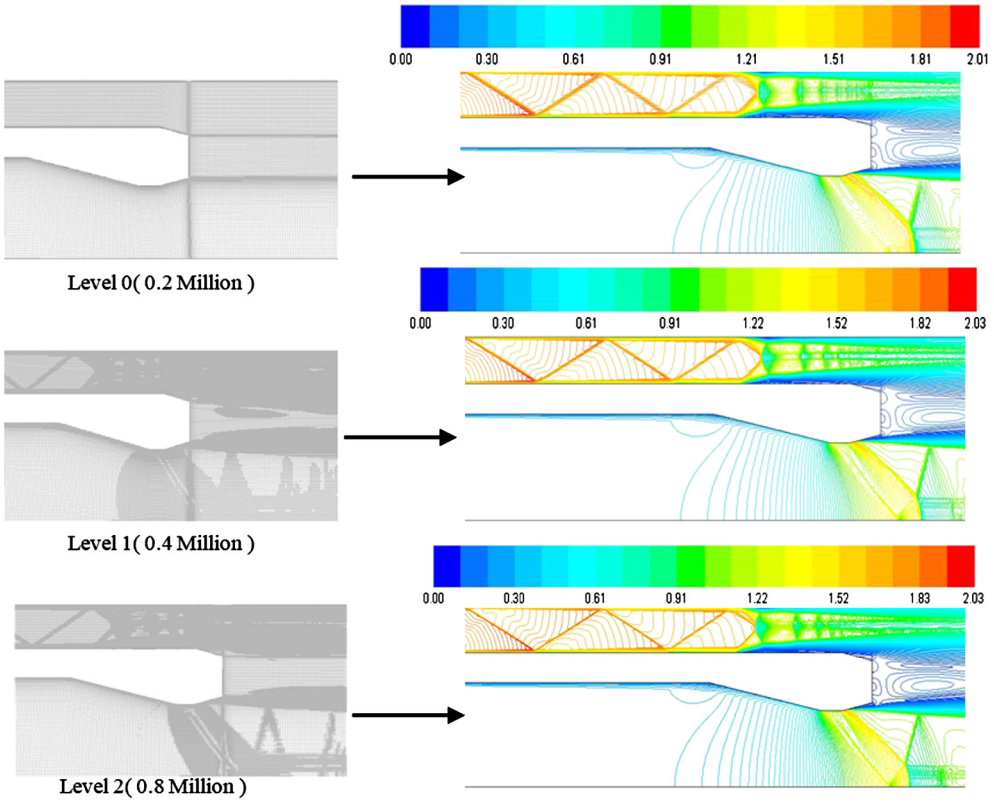

Fig. 7. Simulation result for different grids ($M = 1.79$, $\phi = 2.84$). (For interpretation of the references to color in this figure, the reader is referred to the web version of this article.)

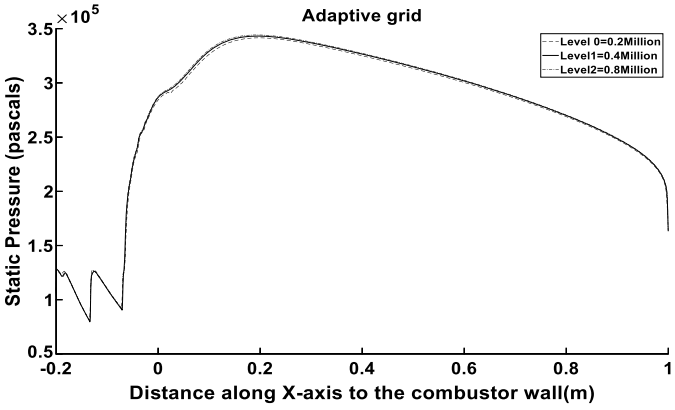

Fig. 8. Wall static pressure for adaptive grids ($M = 1.79$, $\phi_{gg} = 2.84$).

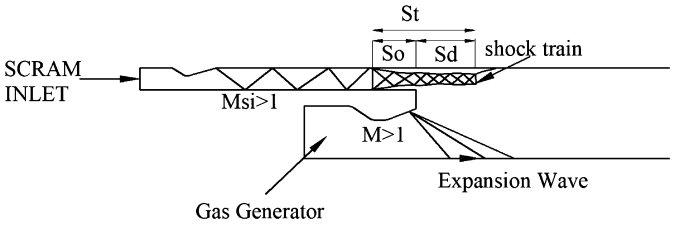

Fig. 9. Schematic of flow field in combustor.

Flow coming out of gas generator is expanded by the gas generator nozzle. Oblique shock train is formed to match the combustor pressure. These shock waves hit the mixing layer and enhance shear layer mixing. An adverse effect of shock is loss in total pressure. The flow in the combustor gets chocked due to heat addition. This can be observed by flow $M = 1$ in the combustor. As equivalence ratio is high in gas generator, cracked, incomplete combustion products of combustion come out of gas generator. It can be seen from temperature contours gas generator outlet flow when mixes with supersonic air stream, complete combustion takes place and temperature raises up to 2600 K at end of combustor.

5.1. Study with turbulence model

Simulation is carried out at two conditions. One is at Mach 4 free stream condition for which isolator inlet Mach number (M_{SI}) is 1.79. Other condition is for Mach 5 free stream condition and isolator inlet Mach number (M_{SI}) is 2.23. Gas generator equivalence ratio (ϕ_{gg}) of M4 condition is 2.84 and of M5 condition is 2.64.

5.1.1. Non-reactive

Pressure rise and fall trend shown in Fig. 11 is due to oblique shock wave reflections from wall. Two shock wave trains are seen in Fig. 12. One is starting from the isolator side and another from gas generator side. Flow from gas generator and isolator are under expanded and refraction wave is formed as flow comes out to the main combustor. The pressure drop in wall static pressure clearly reveals the presence of expansion waves and phenomena is well captured by simulations as results are in close match with experiments. Static wall pressure achieved during the simulation is over estimated as compared to experiments.

5.1.2. Reactive flow field

Normal shock train is characterised by increasing and decreasing pressure. Due to formation of Mach discs, flow becomes subsonic. Flow is again accelerated due to boundary layer shape of

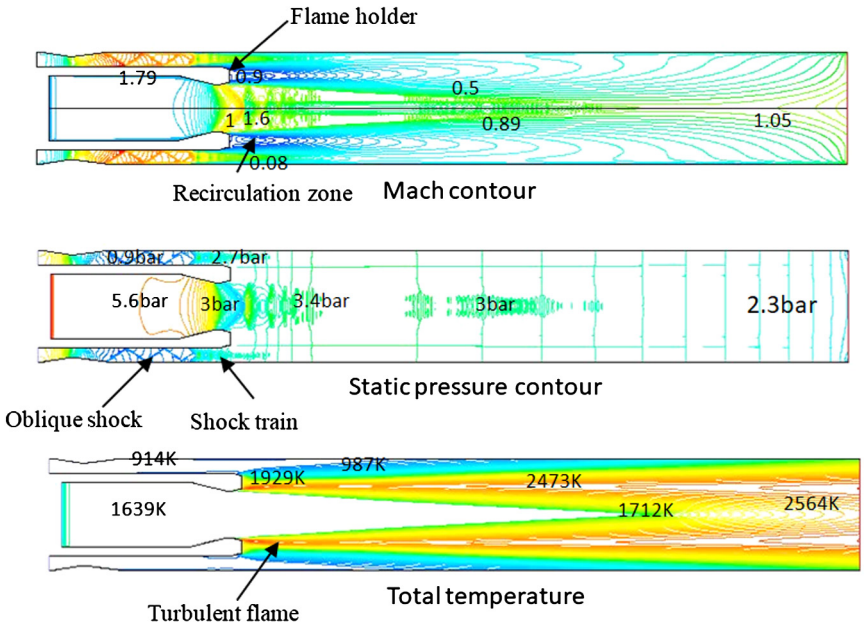

Fig. 10. Mach No., static pressure, total temperature contours for M4 condition ($\phi_{gg} = 2.84$).

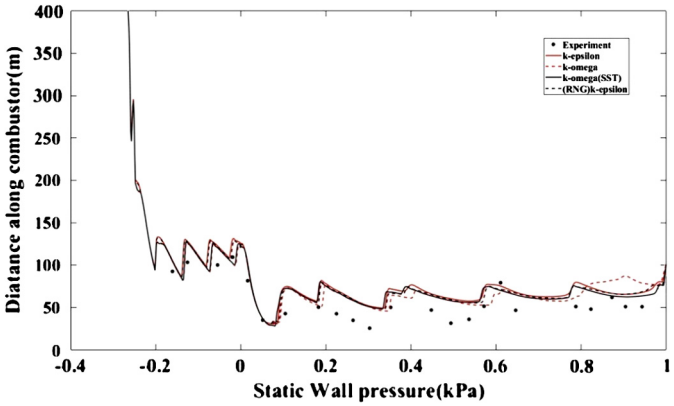

Fig. 11. Wall static pressure comparison with experiments for turbulence models condition ($M_{SI} = 1.79$, $\phi_{gg} = 2.84$).

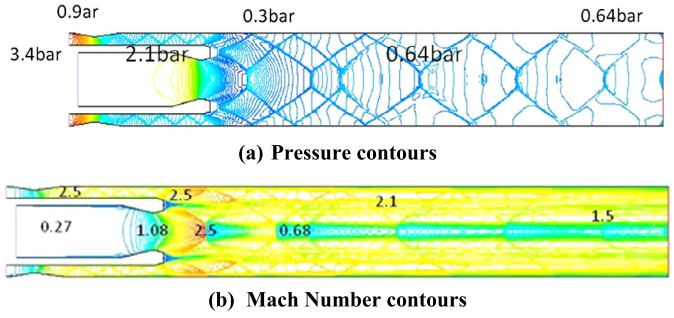

Fig. 12. (a) Pressure contours, (b) Mach contours for non-reactive flow for flow condition.

contraction and expansion leading to another Mach disc. This phenomenon is depicted in Fig. 13.

For reactive flow turbulence models are compared for following parameters

a) Wall static Pressure, Shock train location, length and static pressure along shock train centre
b) Velocity profile and Combustion efficiency

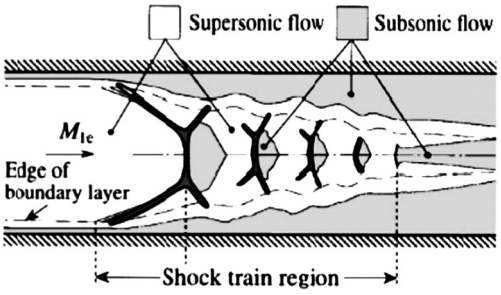

Fig. 13. Shock train structure in a duct.

Wall static pressure:

Flow field can be indirectly represented by the pressure distribution and can be used to validate numerical approach. Fig. 14, Fig. 15 show comparison of wall static pressure with experiments for various turbulence models for condition 1 ($\phi_{gg} = 2.84$) and condition 2 ($\phi_{gg} = 2.64$) respectively.

For both conditions, simulation with turbulence model RNG, SST, $k\varepsilon$ is able to match experimental result quantitatively and qualitatively. $k\omega$ does not match with experimental results at all. For both conditions error is predicted wall pressure is evaluated along the length of combustor. Error in simulated wall static pressure with respect to experiment along length is shown in Fig. 16. As seen in Figs. 14, 15 shock starting position is not captured accurately by any model, therefore error for first three points error is high but subsequently error value has reduced below 10% as seen in error plot.

RNG has captured the pressure rise part much better as compared to other models up to 0.3 m length. For pressure rise RNG predictions are better than compared to other models. SST and $k\varepsilon$ (standard) has larger error in starting prediction but error reduces along length. For capturing pressure rise phenomena RNG is better model for both conditions. $k\omega$ Standard is very much away from experiment and is not suitable for carrying simulations. Simulation of flow condition 2 shows large shock pressure oscillation. These pressure oscillations are usually observed at the centre line but when flow separates and attaches back to wall, these oscillations are observed. Experiment might have not captured this

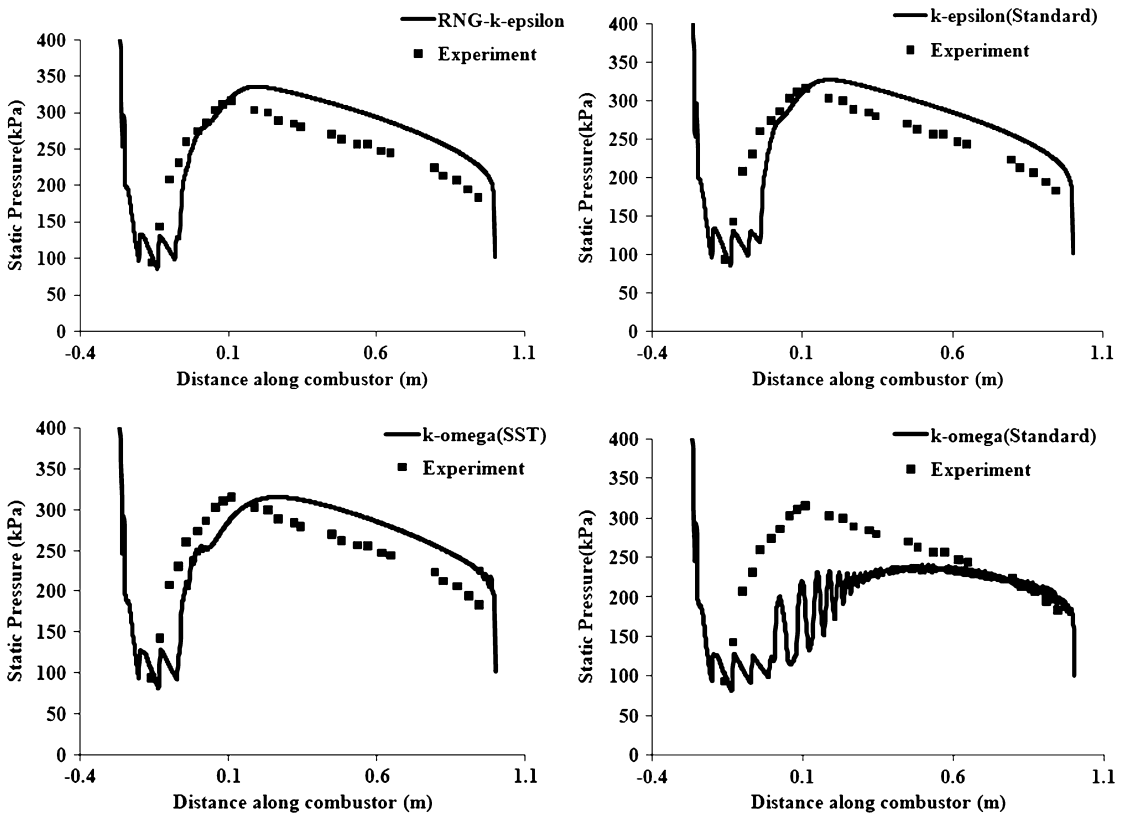

Fig. 14. Wall static pressure compassion with experiments for various turbulence models (Condition 1: $M_\infty = 4$, $M_{SI} = 1.79$).

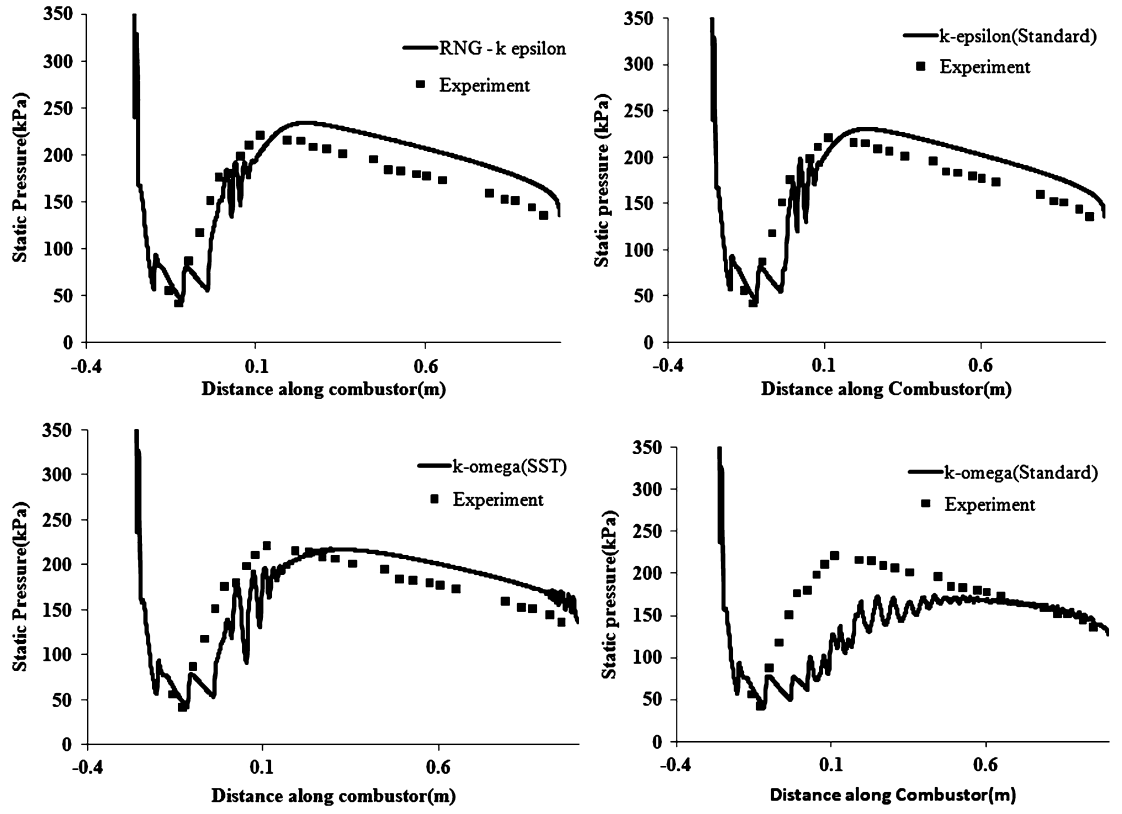

Fig. 15. Wall static pressure compassion with experiments for various turbulence models (Condition 2: $M_\infty = 5$, $M_{SI} = 2.23$).

Table 3
Average wall pressure and shock stating length for condition 1 ($M_{SI} = 1.79$, $\phi = 2.84$).

Parameter	Experiment	RNG-$k\varepsilon$ (error)	$k\varepsilon$ (error)	SST (error)	$k\omega$ (error)
Avg. static pressure (kPa)	248	274 (+10.48)	263 (+6%)	261.58 (+5.5%)	196.2 (−20.8%)
Shock train (S_t)	0.27	0.258 (5%)	0.23 (−15%)	0.304 (+12%)	0.371 (28%)
S_o	0.16	0.08	0.041	0.074	0.013
S_d	0.117	0.178	0.19	0.23	0.35

Table 4
Average wall pressure and shock stating length for condition 2 ($M_{SI} = 2.23$, $\phi = 2.64$).

Parameters	Experiment	RNG-$k\varepsilon$ (error)	$k\varepsilon$ (error)	SST (error)	$k\omega$ (error)
Avg. static pressure (kPa)	166.6	185.8 (+11%)	183.0 (+10%)	174.3 (+4%)	134.0 (−19%)
S_t (m)	0.24	0.263 (+9%)	0.28 (+16%)	0.34 (+41%)	0.451 (+87%)
S_o (m)	0.13	0.043	0.038	0.04	0
S_d	0.11	0.22	0.24	0.3	0.451

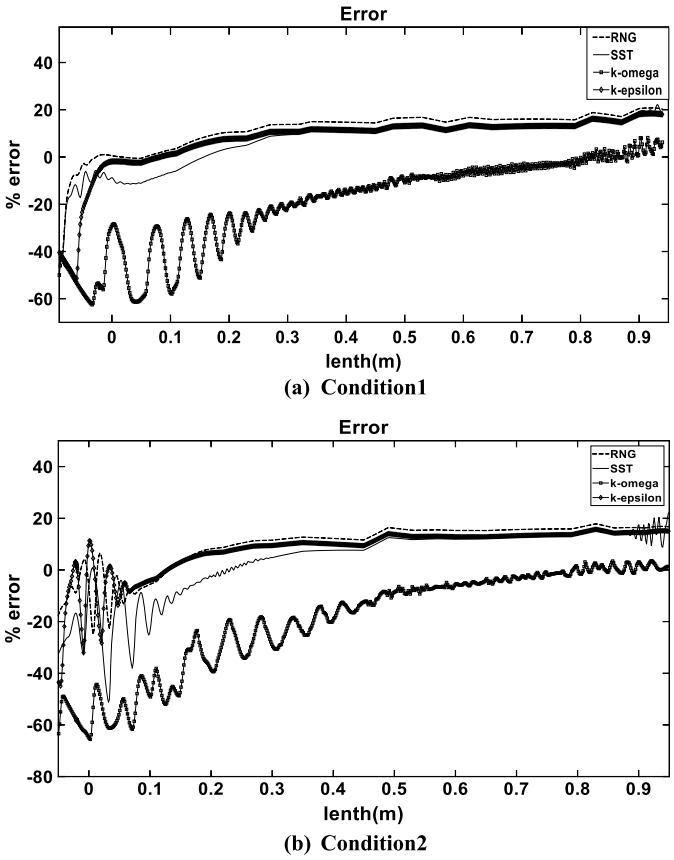

Fig. 16. Estimated error of wall pressure along the length of combustor.

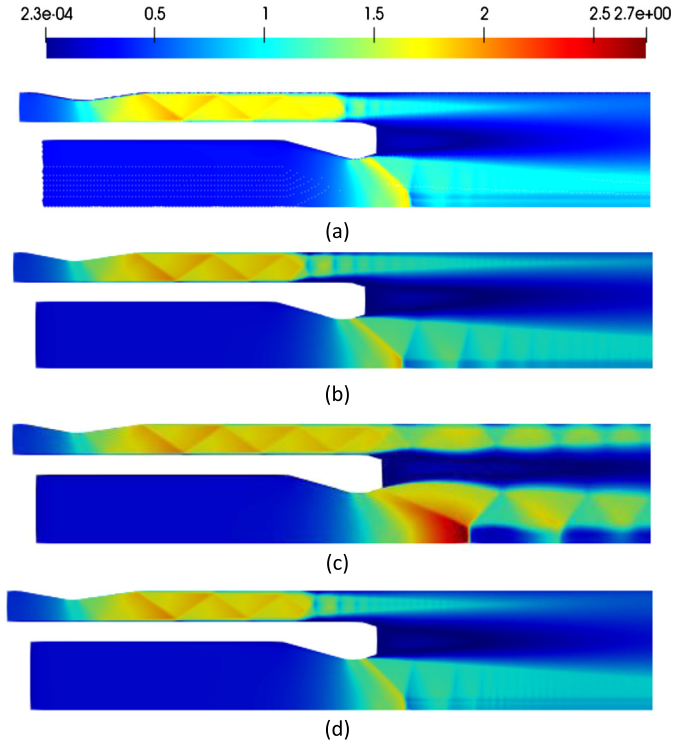

Fig. 17. Mach contours for turbulence models, a) RNG, b) k–ε, c) k–ω, d) k–ω (SST) combustor simulations.

phenomenon due to low number of pressure measurement points and time averaging of data.

If isolator length is insufficient then intake interacts with combustor leading to intake unstart and higher isolator length adds weight. It is very important to predict accurate point of shock train as it decides the length of Isolator to design isolator with optimum length. Four parameters are compared i.e. Average wall static pressure, shock train length (S_t), Shock train length inside isolator (S_o), Shock train length inside main combustor (S_d), which are given in Table 3, Table 4. CFD could not predict shock train starting position exactly and error is 80 mm and 87 mm for conditions 1 and 2 respectively. Average pressure error is low for SST model in both conditions. Shock train length is predicted with less error by RNG. Even though shock train length is captured accurately but still stating location has error more than acceptable.

Fig. 17 shows Mach No. contours of different turbulent models. Other than $k\omega$ standard remaining have similar flow pattern. $k\omega$ standard predicts very poor mixing and therefore large stretched recirculation zone is observed. Normal shock train is clearly visible with RNG, $k\varepsilon$ and SST. SST has captured the shock train formed at centre of combustor much better as compared to other models. Difference is starting position for each model is clearly visible in the Mach contours. Normal shock train is formed. For RNG, $k\varepsilon$ flow does not reattach to boundary, whereas flow simulated by SST model shows reattachment. Therefore, pressure rise by SST model shows oscillations. Fig. 18 shows shock train along line AA. For condition 1 shock train starting point is same but beyond $x = 0.25$ m both data start diverging. It is observed that shock train region is high when predicted by SST as compared to RNG, $k\varepsilon$.

Velocity profile and combustion efficiency:

Velocity profile and combustion efficiency are other two parameters for turbulence model comparison. Combustion products and total temperature are used to define the combustion efficiency. CO_2 is selected product for evaluating combustion efficiency [28].

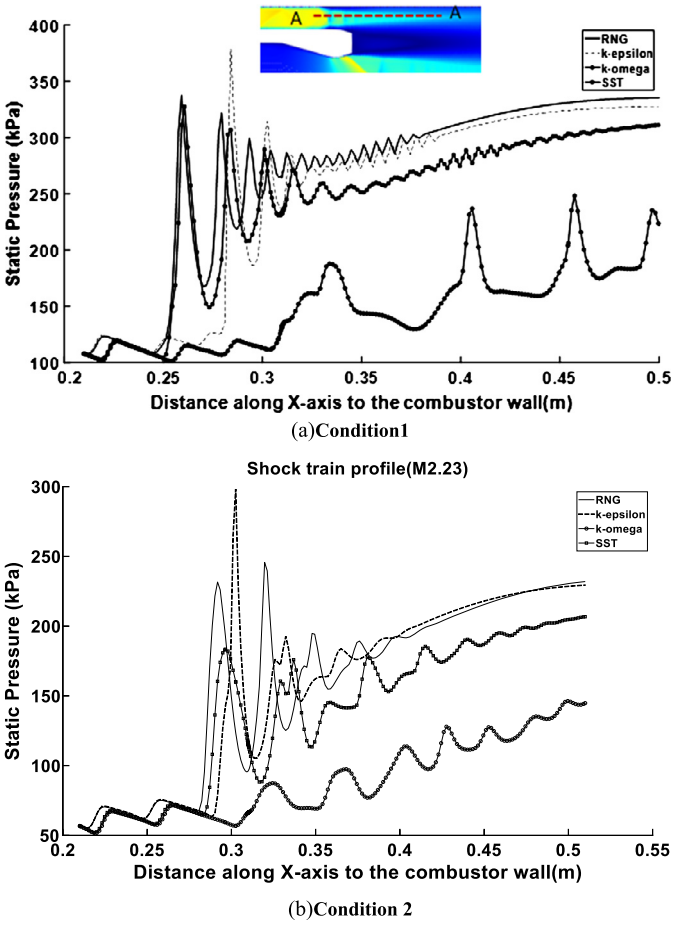

Fig. 18. Static pressure along line 'AA' for various turbulence models. ('AA' is given in the inset picture of Fig. 18(a).)

$$\text{Combustion efficiency} = \frac{m_{CO_2,x}}{m_{CO_2\ \text{ideal}}}$$

$m_{CO_2,x}$ is the concentration of CO_2 at distance 'x' from gas generator exit. $m_{CO_2\ \text{ideal}}$ is concentration of CO_2 evaluated using NASA CEC with inlet flow condition.

Fig. 19 gives combustion efficiency evaluated by different turbulence models for condition 1. Combustion efficiency increases along length shows mixing and combustion. RNG predicts highest combustion efficiency. The effect high combustion efficiency can also be observed in static pressure plot where RNG predicted Maximum wall static pressure more than other models. One point worth noting is combustion efficiency has not reached a plateau and this indicates increment in combustor length is required for further combustion to take place. These values refer to the experimental set up configuration, which is mainly designed to study the annular isolator-combustor interactions. A flight worthy scramjet engine will have higher combustion efficiency.

Fig. 20 shows the velocity profile for condition 1 and 2. Velocity of flow coming out of centre is high as the flow is supersonic, whereas flow coming out of isolator less due to normal shock train formed to adjust the pressure. Recirculation zone where flame holding take place can be observed, as flow has low velocity in that region. Low velocity region formed at centre is due to shock train formed at exit of gas generator to adjust the pressure.

5.2. Effect of equivalence ratio on combustion and shock train

Fig. 21 shows the comparison of Wall static pressure for various equivalence ratio conditions condition 1 as per Table 1. Simulations results are in good match with experimental results. For lean flow in gas generator no pressure is developed. Pressure increasing with increase in equivalence ratio is well captured by simulations. Fig. 22 shows effect on total temperature for condition 1 ($M = 4$). Fig. 23 shows Mach contours for different equivalence ratio. As gas generator equivalence ratio ϕ_{gg} is increased, pressure in the supersonic combustor increases. To balance the increase in pressure shock train becomes strong and advance towards upstream in the isolator. This phenomenon is well captured in the simulations. As compared to scramjet combustor where subsonic flow occurs near cavity, in DCR subsonic combustion occurs in front portion of combustor where maximum pressure rise takes place. Total temperature is indicative parameter of extent of combustion. As the Equivalence ratio is near one in gas generator, most of combustion takes place inside GG. The flow coming out of GG has product of complete combustion. As the equivalence ratio reaches near three in GG, complete combustion cannot take place due to fuel rich condition and combustion products are cracked products of combustion.

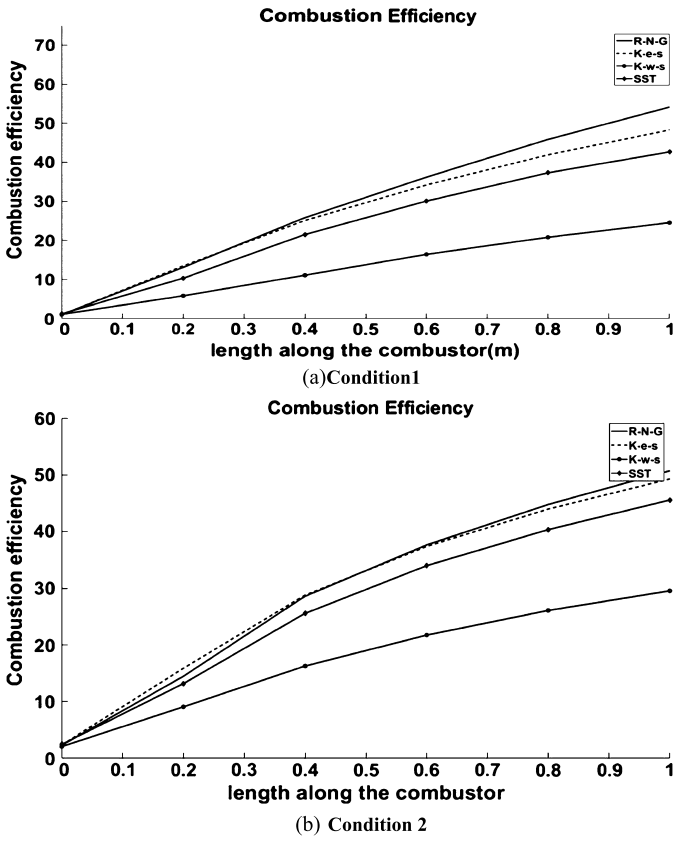

Fig. 19. Combustion efficiency evaluated along combustor with various turbulence models.

Fig. 24 shows wall static pressure for condition 2 with different equivalence ratio. Simulation is in good agreement with experiments. Pressure oscillations are observed in the region of shock train.

6. Summary and conclusions

Numerical investigation of annular isolator and interaction with combustor carried out. CFD procedure validated with experimental results. Reaction mechanism with 4 steps and 7 species is used for modelling chemistry. Main objective of work is to simulate shock train in Isolator for two inlet conditions ($M_{SI} = 1.79,\ 2.23$) with different equivalence ratios.

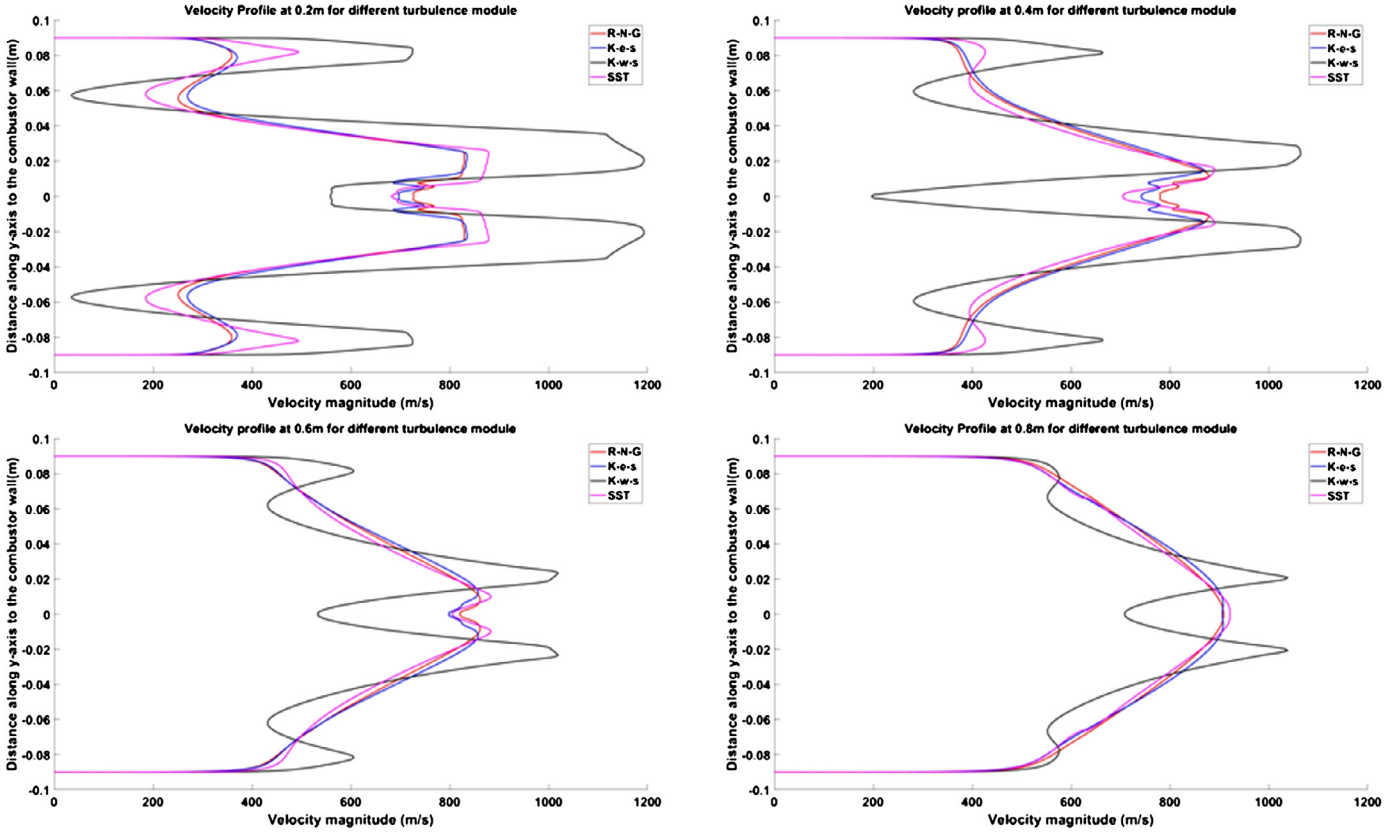

(a) Condition 1

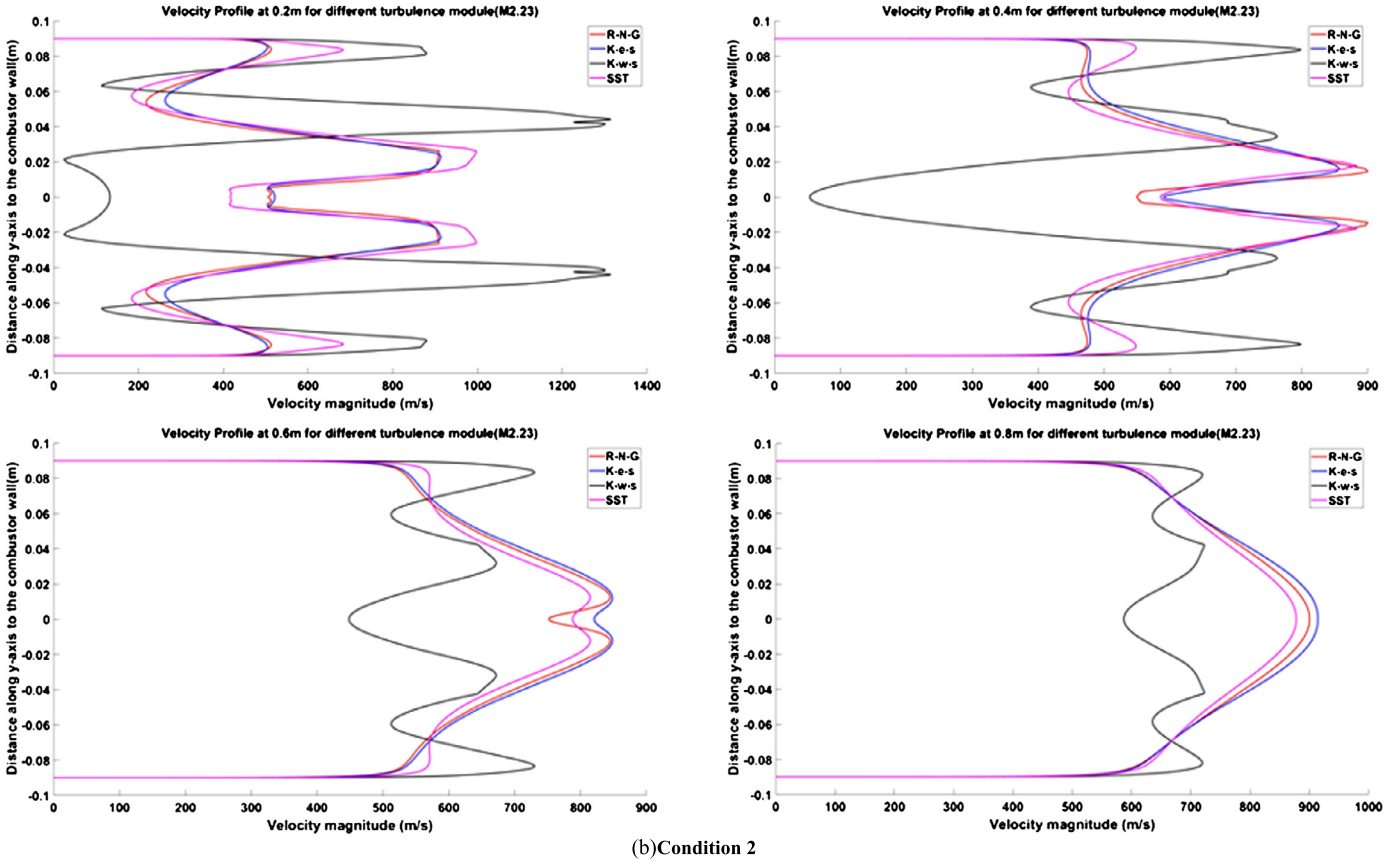

(b)Condition 2

Fig. 20. Velocity profiles with various turbulence models.

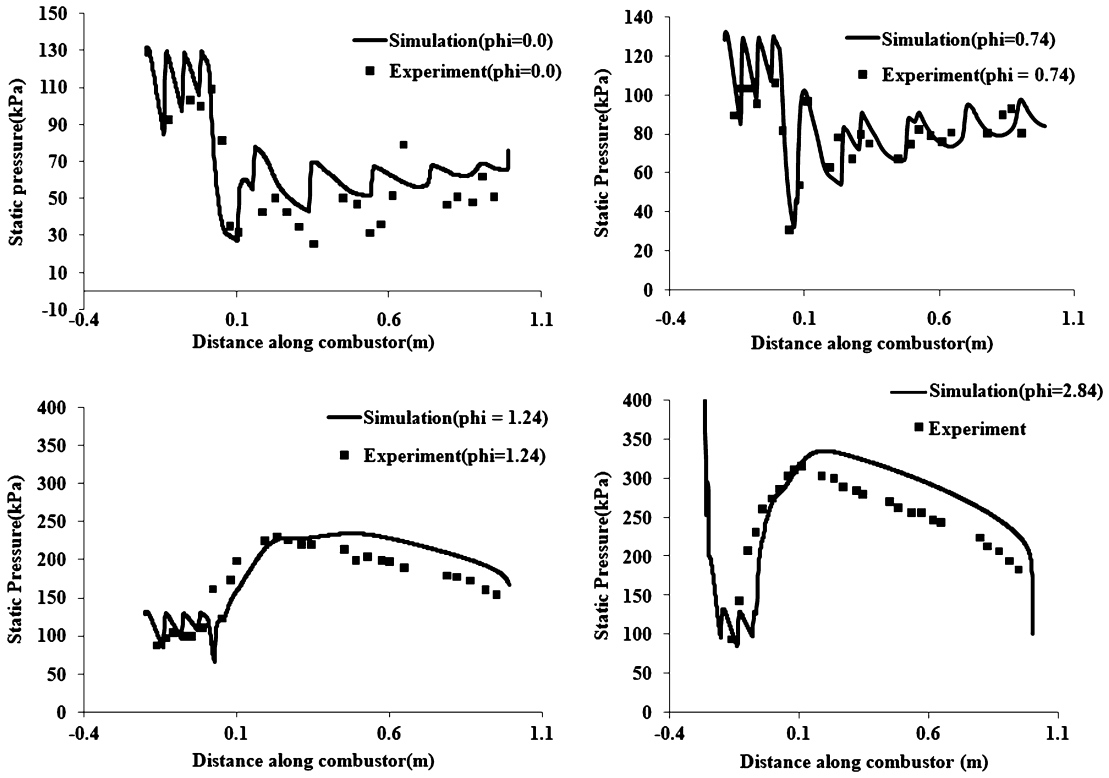

Fig. 21. Wall static pressure along combustor length for condition 1 with different equivalence ratios for condition 1.

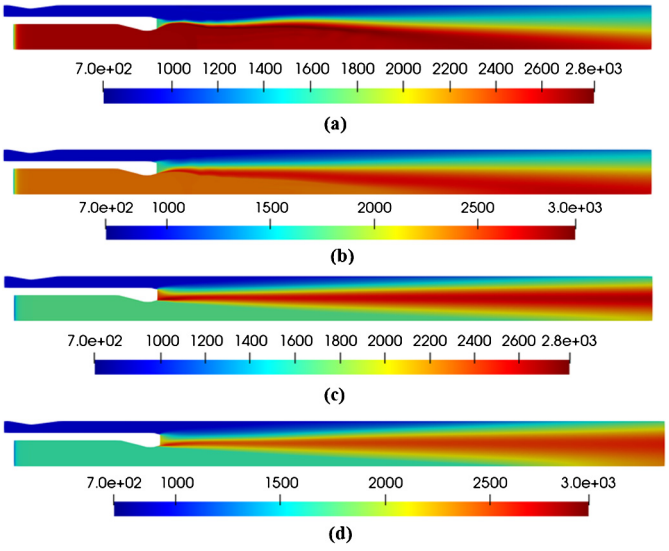

Fig. 22. Total temperature contours for different equivalence ratio (a) $\phi_{gg} = 0.74$, (b) $\phi_{gg} = 1.24$, (c) $\phi_{gg} = 2.84$, (d) $\phi_{gg} = 3.05$.

1. Grid independence study is done with reactive flow in two steps i.e. First step is refinement of selected region such as Isolator, Main combustor, gas generator. Grid Convergence index is used for identifying grid capable to capture phenomena. Moderate Grid with 0.2 million is subsequently refined using grid adaption method with pressure gradients. No significant improvement in wall static pressure is observed.
2. Various turbulence models such as RNG k–ε, $k\varepsilon$ (standard), $k\omega$ (standard), SST-$k\omega$ are studied to find best suitable for flows with shock train and combustion in mixing shear layer. Wall static pressure along wall is compared for all models with experimental results. Starting position of shock train is not well captured, therefore large errors are observed in first 3 points

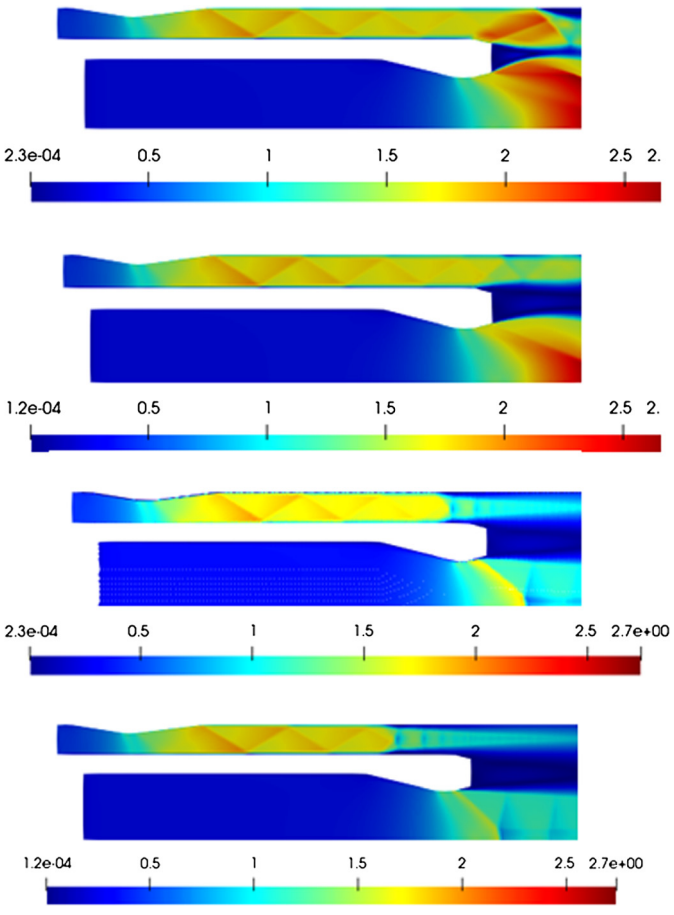

Fig. 23. Mach contours for different equivalence ratio (a) $\phi_{gg} = 0.74$, (b) $\phi_{gg} = 1.24$, (c) $\phi_{gg} = 2.84$, (d) $\phi_{gg} = 3.05$.

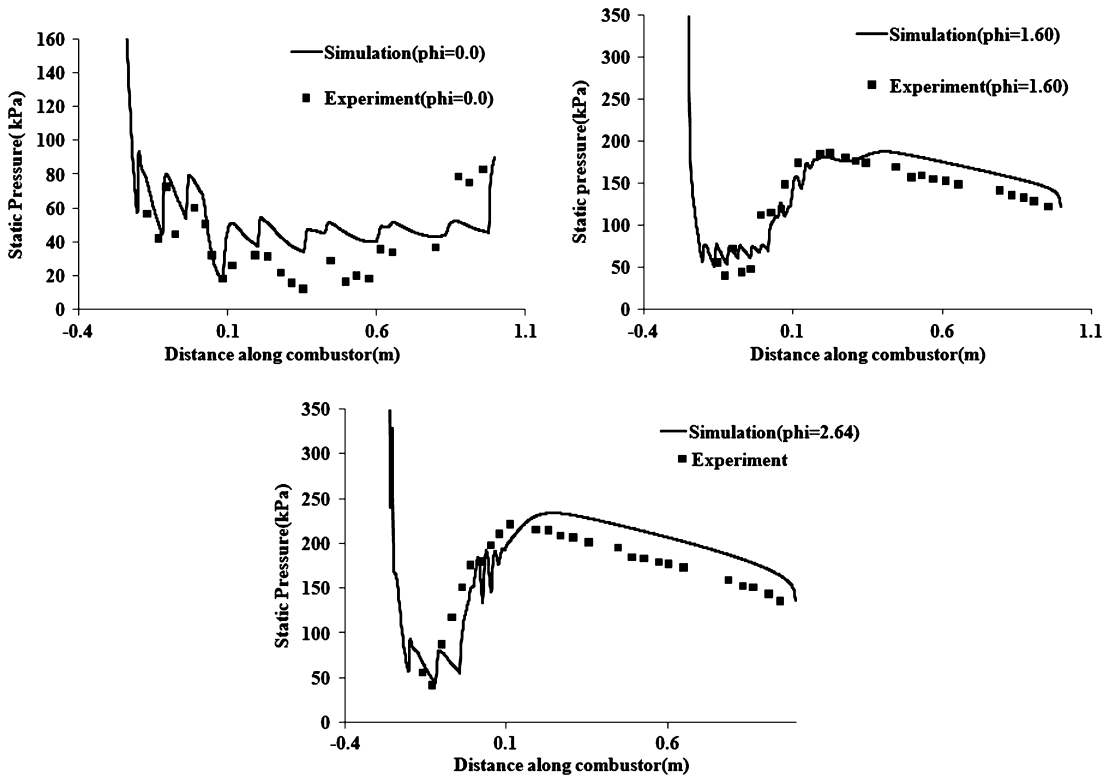

Fig. 24. Wall static pressure along combustor length for different equivalence ratio for condition 2.

but subsequently error reduces. (RNG) $k\varepsilon$ shows best match during pressure rise i.e. capturing of shock train but beyond maximum pressure SST and $k\varepsilon$ shows better match. SST $k\omega$ predicts average pressure with least error. $k\omega$ standard could not predict phenomena properly. Combustion efficiency calculated based on composition of CO_2 is also compared. RNG predicts the highest combustion efficiency.

3. Effect of varying Gas Generator (GG) equivalence ratio is studied. Numerical simulation has good match with experiments. It is observed that when GG equivalence ratio is near one, complete combustion takes place in GG itself and no heat is added in main combustor, hence no pressure rise. The operating GG equivalence ratio should greater than 0.74 for combustion to take place in main combustor for isolator inlet Mach No = 1.79. It is observed in most localised regions flow is subsonic in main combustor. Shock train movement in the isolator with change in equivalence ratio is well captured. To keep the flow supersonic divergent angle to be given as this will avoid thermal choking. Parametric studies of effect of gas generator pressure, isolator angle, GG exit nozzle Mach No. will be studied.

Declaration of competing interest

The authors declare that they have no known competing financial interests or personal relationships that could have appeared to influence the work reported in this paper.

Acknowledgements

We acknowledge our computation facility, D.R.D.L., Hyderabad, India for extending their resources for carrying out simulations.

References

[1] E.T. Curran, Scramjet engines: the first forty years, J. Propuls. Power 17 (6) (2001) 1138–1148, https://doi.org/10.2514/2.5875.

[2] P.J. Waltrup, M.E. White, F. Zarlingo, E.S. Gravlin, History of U.S. navy ramjet, scramjet, and mixed-cycle propulsion development, J. Propuls. Power 18 (1) (2002) 14–27, https://doi.org/10.2514/2.5928.

[3] Ronald S. Fry, A century of ramjet propulsion technology evolution, J. Propuls. Power 20 (2004) 27–58, https://arc.aiaa.org/doi/abs/10.2514/1.9178.

[4] F.S. Billig, Research on supersonic combustion, J. Propuls. Power 9 (1993) 499–514, https://doi.org/10.2514/3.23652.

[5] Xu Zhang, Lianjie Yue, Tinglong Huang, Qifan Zhang, Xinyu Zhang, Numerical investigation of mode transition and hysteresis in a cavity-based dual-mode scramjet combustor, Aerosp. Sci. Technol. 94 (2019) 105420, https://doi.org/10.1016/j.ast.2019.105420.

[6] Chenlin Zhang, Juntao Chang, Jingxue Ma, Wen Bao, Daren Yu, Jingfeng Tang, Effect of Mach number and equivalence ratio on the pressure rising variation during combustion mode transition in a dual-mode combustor, Aerosp. Sci. Technol. 72 (2018) 516–524, https://doi.org/10.1016/j.ast.2017.11.042.

[7] Chenlin Zhang, Juntao Chang, Shuo Feng, Wen Bao, Daren Yu, Investigation of performance and mode transition in a variable divergence ratio dual-mode combustor, Aerosp. Sci. Technol. 80 (2018) 496–507, https://doi.org/10.1016/j.ast.2018.07.025.

[8] Junlong Zhang, Juntao Chang, Jicheng Ma, Youyin Wang, Wen Bao, Investigations on flame liftoff characteristics in liquid-kerosene fueled supersonic combustor equipped with thin strut, Aerosp. Sci. Technol. 84 (2019) 686–697, https://doi.org/10.1016/j.ast.2018.11.017.

[9] Ruifeng Cao, Yue Lu, Daren Yu, Juntao Chang, Study on influencing factors of combustion mode transition boundary for a scramjet engine based on one-dimensional model, Aerosp. Sci. Technol. 96 (2020) 105590, https://doi.org/10.1016/j.ast.2019.105590.

[10] Wubingyi Shen, Yue Huang, Yancheng You, Lizhe Yi, Characteristics of reaction zone in a dual-mode scramjet combustor during mode transitions, Aerosp. Sci. Technol. 99 (2020) 105779, https://doi.org/10.1016/j.ast.2020.105779.

[11] Chenlin Zhang, Juntao Chang, Junlong Zhang, Wen Bao, Daren Yu, Effect of continuous Mach number variation of incoming flow on ram–scram transition in a dual-mode combustor, Aerosp. Sci. Technol. 76 (2018) 433–441, https://doi.org/10.1016/j.ast.2018.02.027.

[12] Zhi-wei Huang, Guo-qiang He, Fei Qin, Xiang-geng Wei, Large eddy simulation of flame structure and combustion mode in a hydrogen fueled supersonic combustor, Int. J. Hydrog. Energy 40 (31) (2015) 9815–9824, https://doi.org/10.1016/j.ijhydene.2015.06.011.

[13] Zhi-wei Huang, Guo-qiang He, Shuai Wang, Fei Qin, Xiang-geng Wei, Lei Shi, Simulations of combustion oscillation and flame dynamics in a strut-based supersonic combustor, Int. J. Hydrog. Energy 42 (12) (2017) 8278–8287, https://doi.org/10.1016/j.ijhydene.2016.12.142.

[14] Zhiwei Huang, Huangwei Zhang, Investigations of autoignition and propagation of supersonic ethylene flames stabilized by a cavity, Appl. Energy 265 (2020) 114795, https://doi.org/10.1016/j.apenergy.2020.114795.
[15] Zhiwei Huang, Majie Zhao, Huangwei Zhang, Modelling n-heptane dilute spray flames in a model supersonic combustor fueled by hydrogen, Fuel 264 (2020) 116809, https://doi.org/10.1016/j.fuel.2019.116809.
[16] Zhiwei Huang, Guo-qiang He, Fei Qin, Dong-gang Cao, Xiang-geng Wei, Lei Shi, Large eddy simulation of combustion characteristics in a kerosene fueled rocket-based combined-cycle engine combustor, Acta Astronaut. 127 (2016) 326–334, https://doi.org/10.1016/j.actaastro.2016.06.016.
[17] Zhi Wei Huang, Guo-Qiang He, Fei Qin, Rui Xue, Xiang-Geng Wei, Lei Shi, Combustion oscillation study in a kerosene fueled rocket-based combined-cycle engine combustor, Acta Astronaut. 129 (2016) 260–270, https://doi.org/10.1016/j.actaastro.2016.09.024.
[18] Ye Tian, Baoguo Xiao, Shunping Zhang, Jianwen Xing, Experimental and computational study on combustion performance of a kerosene fuelled dual-mode scramjet engine, Aerosp. Sci. Technol. 46 (2015) 451–458.
[19] Malsur Dharavath, P. Manna, Debasis Chakraborty, Numerical exploration of mixing and combustion in ethylene fueled scramjet combustor, Acta Astronaut. 117 (2015) 305–318.
[20] Jichao Hu, Juntao Chang, Wen Bao, Qingchun Yang, John Wen, Experimental study of a flush wall scramjet combustor equipped with strut/wall fuel injection, Acta Astronaut. 104 (1) (2014) 84–90.
[21] F.S. Billig, P.J. Waltrup, R.D. Stockbridge, Integral rocket dual combustion ramjet: a new propulsion concept, J. Spacecr. Rockets 17 (5) (1980) 416–424, https://doi.org/10.2514/3.57760.
[22] M.B. Colket III, L.J. Spadaccini, Scramjet fuels autoignition study, J. Propuls. Power 17 (2) (2001) 315–323, https://doi.org/10.2514/2.5744.
[23] P. Puri, F.-H. Ma, J.-Y. Choi, V. Yang, Ignition characteristics of cracked JP-7 fuel, Combust. Flame 142 (4) (2005) 454–457, https://doi.org/10.1016/j.combustflame.2005.06.001.
[24] M. Raghavendra Rao, G. Amba Prasad Rao, Avanish Kumar, Experimental validation of liquid hydrocarbon-based fuel rich gas generator for high speed propulsion systems, Acta Astronaut. 174 (2020) 180–188, https://doi.org/10.1016/j.actaastro.2020.05.009.
[25] J.A. Schetz, F.S. Billig, S. Favin, Flow field analysis of a scramjet combustor with a coaxial fuel jet, AIAA J. (1982) 1268–1274.
[26] Liwei Zhang, Jeong Yeol Choi, Vigor Yang, Supersonic combustion and flame stabilization of coflow ethylene and air with splitter plate, J. Propuls. Power 31 (5) (2015).
[27] Jeong Yeol Choi, Vigor Yang, High resolution numerical study on the supersonic turbulent flame structures and dynamics in dual combustion ramjet, in: 50th AIAA/ASME/SAE/ASEE Joint Propulsion Conference.
[28] J. Tan, J. Wu, Z. Wang, Experimental and numerical investigation on flow fields and performance of dual combustion ramjet, J. Aerosp. Eng. 228 (6) (May 2014) 920–929.
[29] Chenlin Zhang, Juntao Chang, Meng Meng Liu, Shuo Feng, Wen Shi, Wen Bao, Effect of heat release on movement characteristics of shock train in an isolator, Acta Astronaut. 133 (2017) 185–194.
[30] Wei Huang, Zhen-guo Wang, Mohamed Pourkashanian, Lin Ma, Derek B. Ingham, Shi-bin Luo, Jing Lei, Jun Liu, Numerical investigation on the shock wave transition in a three-dimensional scramjet isolator, Acta Astronaut. 68 (11–12) (2011) 1669–1675.
[31] Fei Xing, Can Ruan, Yue Huang, Xiaoyuan Fang, Yufeng Yao, Numerical investigation on shock train control and applications in a scramjet engine, Aerosp. Sci. Technol. 60 (2017) 162–171.
[32] Yubao He, Hongyan Huang, Daren Yu, Investigation of boundary-layer ejecting for resistance to back pressure in an isolator, Aerosp. Sci. Technol. 56 (2016) 1–13.
[33] Jong-Ryul Byun, Chul Park, Oh Joon Kwon, Experimental study of combustor–isolator interactions in a dual-combustion ramjet, J. Propuls. Power (Nov 2014), https://doi.org/10.2514/1.B35391.
[34] R.D. Stockbridge, Experimental investigation of shock wave/boundary-layer interactions in an annular duct, J. Propuls. Power 5 (3) (1989) 346–352, https://doi.org/10.2514/3.23159.
[35] Wenxin Hou, Juntao Chang, Zongqi Xie, Youyin Wang, Linke Wu, Wen Bao, Behavior and flow mechanism of shock train self-excited oscillation influenced by background waves, Acta Astronaut. 166 (2020) 29–40, https://doi.org/10.1016/j.actaastro.2019.09.032.
[36] Wen Shi, Juntao Chang, Junlong Zhang, Jicheng Ma, Ziao Wang, Wen Bao, Numerical investigation on the forced oscillation of shock train in hypersonic inlet with translating cowl, Aerosp. Sci. Technol. 87 (2019) 311–322, https://doi.org/10.1016/j.ast.2019.02.022.
[37] Wen Shi, Juntao Chang, JiCheng Ma, Youyin Wang, Lin Gao, Wen Bao, Path dependence characteristic of shock train in a 2D hypersonic inlet with variable background waves, Aerosp. Sci. Technol. 86 (2019) 650–658, https://doi.org/10.1016/j.ast.2019.02.001.
[38] B.E. Launder, D.B. Spalding, Lectures in Mathematical Models of Turbulence, Academic Press, London, England, 1972.
[39] S.A. Orszag, V. Yakhot, W.S. Flannery, F. Boysan, D. Choudhury, J. Maruzewski, B. Patel, Renormalization group modeling and turbulence simulations, in: International Conference on Near-Wall Turbulent Flows, Tempe, Arizona, 1993.
[40] D.C. Wilcox, Turbulence Modeling for CFD, DCW Industries, Inc., La Canada, California, 1998.
[41] F.R. Menter, Two-equation eddy-viscosity turbulence models for engineering applications, AIAA J. 32 (1994) 1598–1605.
[42] S. Luo, W. Huang, H. Qin, et al., Investigation of turbulent models for the flow field from a typical strut-based scramjet combustor, in: Proceedings of ASME Turbo Expo, Vancouver, Canada, 6–9 June 2011, ASME, New York, 2011, pp. 25–31, paper No. GT-2011-45078.
[43] H. Watanabe, Y. Suwa, Y. Matsushita, et al., Spray combustion simulation including soot and NO formation, Energy Convers. Manag. 48 (2007) 2077–2089.
[44] P.J. Roache, Error base for CFD, AIAA Paper No: 2003-0408, 2003.

ACKNOWLEDGEMENTS

I take the opportunity to express my heartfelt adulation and gratitude to my supervisors, **Dr. G. Amba Prasad Rao** Professor, Mechanical Engineering Department, National Institute of Technology, Warangal and **Dr. B.V.N.Charyulu**, Scientist 'G', Defence Research & Development Laboratory (D.R.D.L), Hyderabad for their unreserved guidance, constructive suggestions, thought provoking discussions and unabashed inspiration in nurturing this research work. It has been a benediction for me to spend many opportune moments under the guidance of the perfectionists at the acme of professionalism. The present work is a testimony to their alacrity, inspiration and ardent personal interest, taken by them during the course of this thesis work in its present form.

I wish to sincerely thank institute authorities, **Prof. N.V. Ramana Rao, Director**, National Institute of Technology, Warangal and other top officials who gave me an opportunity to carry out research work.

I also sincerely thank **Prof. A. Kumar,** Head, Mechanical Engineering Department, National Institute of Technology, Warangal for his continuous support towards carrying out research work.

I wish to express my sincere and wholehearted thanks and gratitude to my DSC member **Dr. K. Madhu Murthy,** Professor in the Department of Mechanical Engineering for his kind help, criticism of my work, valuable suggestions and for his support and co-operation.

I sincerely thank DSC member **Dr. A. Veeresh Babu,** Associate Professor in Mechanical Engineering Department for continuous review of my work and also taking a course during my course work. I thank **Dr. Y. Pydi Setty,** Professor Emeritus from Department of Chemical Engineering for his kind help, encouragement and valuable suggestions for successful completion of research work.

I wish to convey my heartfelt thanks to Director, Defence Research and Development Laboratory, Hyderabad, for his timely suggestions, support and for providing necessary department facilities and services during successful completion of research work. He has given impetus to hypersonic technology and accorded necessary resources to pursue this research in our laboratory.

I sincerely thank my inspiring colleagues **Shri Avanish Kumar & Shri Harmeet Singh**, Scientists of Propulsion group of D.R.D.L for their consistent support, participating in the technical discussions and co-authoring the papers published in reputed international journals.

My sincere and special thanks to scientists of the Scramjet test facility of D.R.D.L and their staff for their excellent support for conducting the experiments and their active participation. It is impossible for me to acquire such valuable experimental data without the support and help from our Ground instrumentation team's participation and involvement in all the experiments conducted at D.R.D.L.

I thank all the industries who have contributed in developing the full scale hardware needed for testing the DCR propulsion system.

Heartfelt thanks to **Dr. T. Karthikeya Sharma,** Assistant Professor Department of Mechanical Engineering, NIT Andhra Pradesh for his kind help, timely suggestions during this research work. I also like to express my sincere thanks to all my friends and colleagues specially to **Late Dr. J.V.S. Moorthy, Dr. M. Vinod Babu and many others** for their help during my work.

Words are inadequate to express my thanks to all my family members, my wife Smt M. Saradamani Acharya, my son Dr. M. Dhruva Kartik and my daughter Ms. M.Sriya Dhanvi for extending their support and giving me sufficient time to focus on my research work.

I want to express my sincere thanks to all those who directly or indirectly helped me at various stages of this work.

My sincere thanks to NIT, Warangal and its professors, staff and many others frontier workers of this country who helped in running the institution in efficient manner in the pandemic situation and enabling us to progress in our respective fields without any hurdle.

Above all, I express my indebtedness to the **almighty** for all his blessing and kindness.

(M. Raghavendra Rao)